Amyloid Fibril Based Bionanotechnologies

A thesis submitted in partial fulfilment of the requirements for the Degree of Doctor of Philosophy in Biochemistry

2016

Manmeet Kaur

University of Canterbury

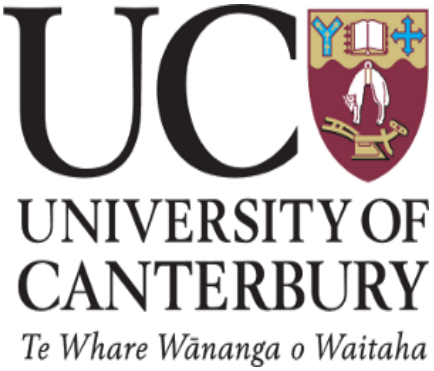

Acknowledgements

First and foremost I would like to thank my senior supervisor, Juliet, for your consistent support, patience, and encouragement. Your smile and enthusiasm was contagious and motivational, I could not ask for more from a supervisor. To Luigi, thank you for everything, I have learnt so much from you. You have been a tremendous mentor for me. I am also very grateful to Madhu, for introducing me to the world of research. Big thanks also to Laura for providing much needed support and expert advice.

Next, I must thank my TEM expert, Jackie, for the fantastic laboratory support, the many TEM images, and for showing a genuine interest in my results. Thanks must go to everyone in the school of biological sciences who helped me during my PhD. In particular, Manfred, Dave, Ashley, and Moritz. Thanks to Matt for help with posters, to Catherine (University of Auckland) for SEM assistance.

Thank you to all of the members of Juliet's lab group – past and present. The group has been a source of friendships as well as good advice and collaboration. Particular thanks to Amy, Jenny, and Karima for your help in the lab, and many insightful discussions and suggestions. Thanks to Steph, for always being there for coffee and chats.

Waffa, I cannot imagine the last three years without your friendship and encouragement. Thank you for being a great and supportive friend. Thank you also to Nadishka and Smitha, for making university a fun place to be. Looking forward to have some more fun times outside of university, Smitha!

My dear family, Mum, Dad, Nav, and Rajeshwari; thank you for your love and unparalleled support. Tej, thank you for being the best brother and friend anyone could ask for.

Table of Contents

Chapter One: Introduction

Chapter Two – Stability and cytotoxicity of PNFs

Chapter Three – Characterisation of crystallin amyloid PNFs

Chapter Four – Glutaraldehyde-based crosslinking of PNFs

Part C – PNFs in biomedical applications

Chapter Six – Summary and Future work

Chapter Seven – Experimental

Abbreviations

µA	*microAmpere*
Å	*Ångstrom*
AAO	*anodic aluminium oxide*
ACN	*acetonitrile*
AFM	*atomic force microscopy*
Ag	*silver*
Au	*gold*
AU	*absorbance units*
Au/GOX	*GOX adsorbed on Au electrode*
Au/GOX-CPNFs	*CPNFs with physically adsorbed GOX, attached onto Au electrode*
Au/GOX-CPNFs-SH	*reduced-CPNFs with adsorbed GOX, attached onto Au electrode*
Au/GOX-GA-CPNFs	*GOX crosslinked via GA onto CPNFs, attached onto Au electrode*
Au/WPNFs-GA-Enz	*dual-functionalised whey PNFs, attached onto Au electrode*
Au/β-gal-GA-CPNFs	*β-gal crosslinked via GA onto CPNFs, attached onto Au electrode*
APTS	*3-aminopropyl triethoxysilane*
BMOE	*bis-(maleimido) ethane*
BSA	*bovine serum albumin*
CA	*current amplification*
CD	*circular dichroism*
CGtase	*cyclodextrin glucanotransferase*
CNTs	*carbon nanotubes*
CPNFs	*crystallin protein nanofibrils*
CPs	*crystallin proteins*
CR	*congo red*
CV	*cyclic voltammetry*
CVS	*crystal violet staining*
D. rerio	*Danio rerio*
dH_2O	*deionised water*
DME	*dimethoxyethane*
DMEM	*Dulbecco's Modified Eagle Medium*
DMSO	*dimethyl sulfoxide*
DNA	*deoxyribonucleic acid*
DSC	*N,N'-disuccinimidyl carbonate*
DNPH	*2, 4-dinitrophenylhydrazine*
DNS	*3,5-dinitrosalicyclic acid*
DTNB	*dithio-bis-(2-nitrobenzoic acid)*
DTT	*dithiothreitol*
E.coli	*Escherichia coli*
EC	*Enzyme Commission number*
Enz	*enzymes (GOX + β-gal)*
epPCR	*error prone polymerase chain reaction*
ERAD	*endoplasmic reticulum associated protein degradation*
EtOH	*ethanol*
EDTA	*ethylenediaminetetraacetic acid*
FA	*formaldehdye*
FBS	*foetal bovine serum*
FcOH	*ferrocenemethanol*
FF	*diphenylalanine*

FTIR	*fourier transform infrared microscopy*
GA	*glutaraldehyde*
Glu	*glucose*
GnRH	*gonadotropin releasing hormone*
GOX	*glucose oxidase*
H_2O_2	*hydrogen peroxide*
HCl	*hydrogen chloride*
HCN	*hydrogen cyanide*
Hec-Ia	*human endometrial adenocarcinoma cell line*
HEPES	*N-2-hydroxyethylpiperazine-N-2-ethane sulfonic acid*
HEWL	*hen egg white lysozyme*
HSA	*human serum albumin*
HNT	*halloysite nanotubes*
h	*hour (s)*
IE	*immobilisation efficiency (%)*
iPrOH	*isopropanol*
IRM	*infrared microspectroscopy*
kDa	*kiloDalton*
KI	*potassium iodide starch test*
L	*Litre (s)*
LOD	*Limit of detection*
M	*Molar*
MEM	*Minimal Essential Medium Eagle*
MES	*2-(N-morpholino)ethanesulfonic acid*
MG	*methylglyoxyl*
mg	*milligram (s)*
min	*minutes*
mL	*millilitre (s)*
mM	*milli Molar*
MOFs	*metal-organic frameworks*
MPH-GFP	*methyl parathion green fluorescent protein*
MTT	*3-(4,5-dimethylthiazol-2-yl)-2,5-diphenyltetrazolium bromide)*
MW	*molecular weight*
MWCNTs	*multi-walled carbon nanotubes*
NaBH3CN	*sodium cyanoborohydride*
$NaBH_4$	*sodium borohydride*
NaCl	*sodium chloride*
NaCN	*sodium cyanide*
$NaHCO_3$	*sodium bicarbonate*
NADP	*nicotinamide adenine dinucleotide phosphate*
NADPH	*nicotinamide adenine dinucleotide phosphate-oxidase*
NADH	*nicotinamide adenine dinucleotide*
NHS	*N-hydroxysuccinimide ester*
NCs	*nanocomposites*
NFs	*nanofibrils*
NIH-3T3	*mouse embryo fibroblast cell line*
NMs	*nanostructured materials*
NPs	*nanoparticles*
NTs	*nanotubes*
O-CPNFs	*oxidised-crystallin PNFs*
ONPG	*o-nitrophenyl-β-galactosidase*
OPA	*o-phthaldialdehyde*
OPH	*organophosphate hydrolase*
PBS	*phosphate buffered saline, pH-7.4*
PDB	*Protein data bank*

PDMS	*polydimethylsiloxane*
PEDOT	*poly(3,4-ethylenedioxythiophene)polystyrene sulfonate*
PGA	*polyglycolic acid*
PLA	*polylactic acid*
PMMA	*poly(methyl methacrylate)*
PNFs	*protein nanofibrils*
PniPAM	*poly(N-isopropylacrylamide)*
PNTs	*protein/peptide nanotubes*
Pt	*platinum*
PVDF	*polyvinylidene fluoride*
PVOH	*poly(vinyl alcohol)*
PAN	*polyacrylonitrile*
PAS	*periodic acid-Schiff's base reaction*
PLGA	*poly-lactic glycolic acid*
PEG	*polyethylene glycol*
RFU	*relative fluorescence units*
Rpm	*rotations per minute*
SATA	*N-succinimidyl S-acetylthioacetate*
SATP	*N-succinimidyl-S-acetylthiopropionate*
SAXS	*small angle X-ray scattering*
SDS-PAGE	*sodium dodecyl sulfate polyacrylamide gel electrophoresis*
SEM	*scanning electron microscopy*
SsNMR	*solid state nuclear magnetic resonance*
STAB	*sodium triacetoxyborohydride*
Sulfo-SMCC	*succinimidyl trans-(maleimidylmethyl)cyclohexane-1-carboxylate*
SWCNTs	*single-walled carbon nanotubes*
TCEP	*tris(2-carboxyethyl)phosphine*
TCP	*tissue culture plate*
TEM	*transmission electron microscopy*
THF	*tetrahydrofuran*
ThT	*thioflavin T*
TiO_2	*titanium oxide*
TNB	*2-nitro-5-thiobenzoic acid*
Tris	*tris(hydroxymethyl)aminomethane(pH 8.0-9.0)*
UA	*uranyl acetate*
UAA	*unnatural aminoacid*
UV	*ultraviolet*
V	*Volts*
WPI	*whey protein isolate*
WPNFs	*whey protein nanofibrils*
WPNFs-GA-Enz	*dual-functionalised (GOX + β-gal) whey protein nanofibrils*
Wt	*weight*
WST	*water soluble tetrazolium salts*
α	*alpha*
β	*beta*
β-Gal	*β-galactosidase*
β-Lg	*β-lactoglobulin*
°C	*degree Celsius*
μ	*micro*
1D	*one dimensional*
2D	*two dimensional*
3D	*three dimensional*

Abstract

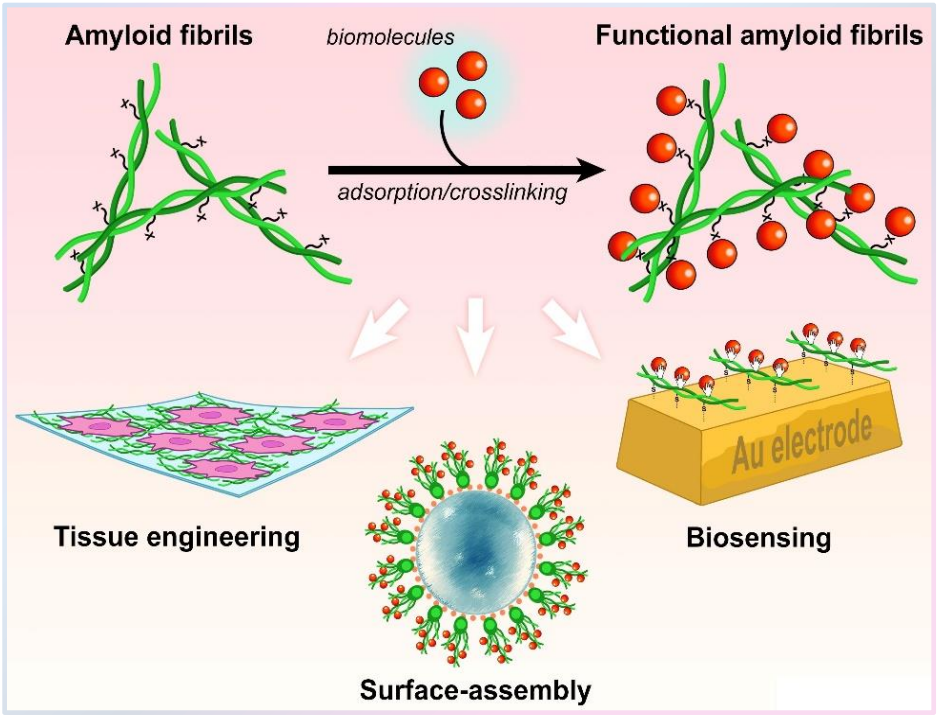

Amyloid protein nanofibrils (PNFs) are self-assembling, misfolded structures formed by many proteins when exposed to denaturing conditions. PNFs offer several attractive features for utilisation in the creation of new bionanomaterials, such as nanometre dimensions, strength and stability, and ease of functionalisation through amino acid residues. However, if amyloid PNFs are to be used in bionanotechnology, then methods need to be developed to utilise inexpensive, crude proteins instead of pure protein preparations. This research focuses on utilising PNFs obtained from a low cost source, including fish eye lens crystallins, and whey protein isolate to develop novel PNF-based nanoscaffolds, with potential applications in bionanotechnology.

To ensure that crystallin PNFs can be effectively used as a versatile bionanoscaffold, biocompatibility and stability studies were done using cell viability and Thioflavin T dye binding assays, Transmission electron microscopy, and Infrared microspectroscopy. Crystallin PNFs were shown to be stable over all the conditions studied (pH and temperature extremes, presence of proteases and solvents), and showed no evidence of cytotoxicity. The results obtained from IR microspectroscopy illustrated the long-term (up to 3 years) structural integrity of crystallin PNFs. To obtain PNF-based functional nanoscaffolds, several enzymes of industrial relevance were successfully immobilised onto the crystallin PNFs *via* a versatile glutaraldehyde-based crosslinking approach. Dual-functionalised PNFs were also obtained by co-immobilising enzymes onto the whey PNF scaffold. The functional PNF-based nanoscaffolds provided a significant increase in thermostability and reusability of industrial enzymes relative to the free enzyme in solution under the same conditions.

To demonstrate that PNF-based scaffolds can be potentially used for creating active bionanomaterials, electrochemistry, surface-assembly, and cell attachment and proliferation experiments were done. Electrochemistry studies demonstrated that functionalised PNFs can be successfully used to develop single enzyme-, or dual enzyme-based biosensing elements, for glucose and lactose analysis. Surface-assembly studies established that PNF scaffold provides more surface area for biomolecule immobilisation, and can be used to create PNF-based active surfaces. The use of PNF-based scaffold for cellular growth resulted in improved attachment and proliferation of fibroblasts, suggesting a role for PNFs obtained from crude protein sources in the biomedical field. This work demonstrated the potential of PNFs obtained from crude proteins to develop functional nanoscaffolds with broad applications. The described work contributes to the existing knowledge of PNF-based bionanomaterials, and is very significant for the technological development and future applications of PNF-based materials in bionanotechnology.

This thesis has contributed to the following publications:

Kaur Manmeet, Jackie Healy, Madhusudan Vasudevamurthy, Moritz Lassé, Ljiljana Puskar, Mark J. Tobin, Celine Valery, Juliet A. Gerrard, and Luigi Sasso. "*Stability and cytotoxicity of crystallin amyloid nanofibrils*." ***Nanoscale*** 6, no. 21 (2014): 13169-13178.

Kaur Manmeet, Sarah Roberts, Jackie Healy, Laura Domigan, Madhusudan Vasudevamurthy, Juliet A. Gerrard, and Luigi Sasso. "*Crystallin Nanofibrils: A Functionalisable Nanoscaffold with Broad Applications Manufactured from Waste*." ***ChemPlusChem*** 80, no. 5 (2015): 810-819.

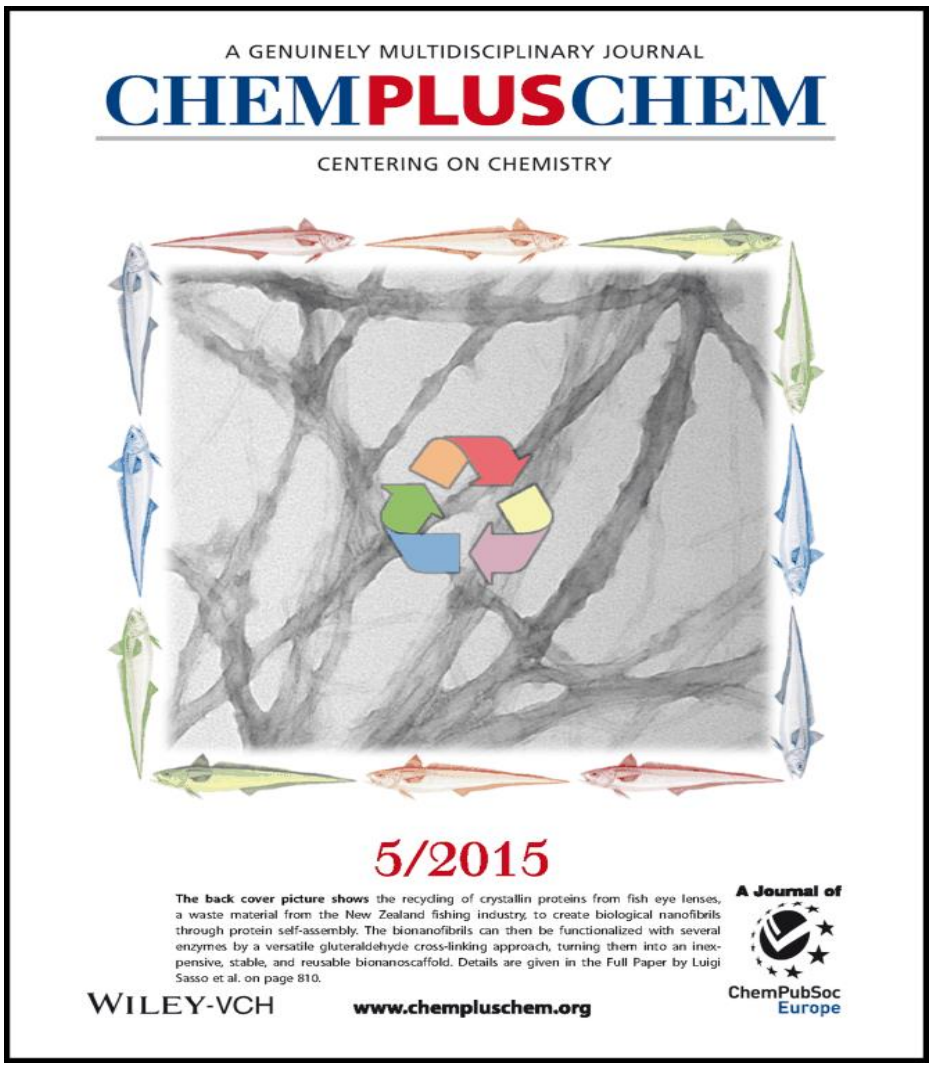

Chapter One

Introduction

1.1. Context

Amyloid protein nanofibrils (PNFs) are highly stable, insoluble protein aggregates with a β-sheet rich structure, formed by many proteins when subjected to denaturing conditions. Amyloid PNFs have been associated with the pathology of a range of diseases known as the amyloidoses. Recent findings have also shown the existence of functional amyloid fibril in nature that play a role in the host organism's survival. From the perspective of nanotechnology, amyloid fibrils are highly suited to incorporation within biomaterials because of their robust material properties, and nanoscaffold capability.

Enzymes have been extensively used in the production of food, pharmaceuticals, and other biologically important products. Several enzymes used in industrial processes have low stability and are quite expensive, but when they are immobilised to an adequate support, the biocatalyst can be used numerous times, thereby lowering costs, and improving enzyme performance. This thesis aims to explore the advantageous properties of amyloid PNFs obtained from cheap, and readily available native proteins to act as a nanoscaffold for the immobilisation of important industrial enzymes - with the goal to create a functional bionanomaterial. The use of amyloid fibrils as a cellular scaffold with potential applications in tissue engineering is also explored.

This chapter provides a background on amyloid fibril structure, their formation, the properties that make them useful for bionanotechnology, and various different applications of amyloid PNFs in bionanotechnologies. It will also discuss industrial catalysts, their limitations, and different immobilising strategies, to provide a context for the work described.

1.2. Industrial catalysts and limitations

In the drive towards green chemistry, the role of biocatalysts is of great significance as they are highly efficient and specific, biodegradable, have the ability to catalyse reactions under mild conditions (physiological pH and temperature), and generate less waste [1], making them both economically and environmentally more attractive than traditional organic synthesis [2]. The end use market for industrial enzymes is extremely wide-spread with numerous industrial commercial applications [3]. The global enzymes market is estimated to rise by 7% to $8.0 billion in 2015 [4]. The increased demand for industrial enzymes is driven by a growing need for sustainable solutions.

However, most of the enzymes utilised in industrial settings suffer from a serious drawback of high production cost, poor stability and limited reusability [5]. Many enzymes are soluble in an aqueous environment, and may require separation from the product after the enzymatic reaction [6]. Additionally, industrial enzymes are prone to inhibition in the presence of industrial solvents, chemicals, and at times from side and end products of the enzyme's own reaction [7]. Thus, often for a given biocatalytic process the native enzyme does not meet the requirements for large-scale application, and its properties need to be optimised or modulated.

Substantial developments in many different scientific areas, such as enzyme engineering [8], biochemical engineering, involving development of novel bioreactor systems coated with composite materials with applications in biocatalysis [9, 10], or immobilisation techniques [11], have been made to overcome the limitations of native enzymes as biocatalysts.

1.3. Enzyme immobilisation

Immobilised enzymes are of particular interest, as immobilisation imparts stability and also allows the reuse and recovery of the biocatalyst, thus improving both technical performance and economy of industrial processes [12]. Additionally, immobilisation can be applied to any natural or engineered enzyme to further improve its catalytic performance, thus, enzyme engineering and immobilisation can be used in tandem. The term immobilised enzymes refers to "enzymes physically confined or localised in a certain defined region of space with retention of their catalytic activities, and which can be used repeatedly and continuously" [13]. The progress in immobilisation of enzymes has been summarised in several excellent reviews [14-18]. The enzymes can be attached to the support via interactions ranging from reversible physical adsorption and ionic linkages to stable covalent bonds. A schematic representation of various immobilisation strategies used is shown in **Figure 1.1**.

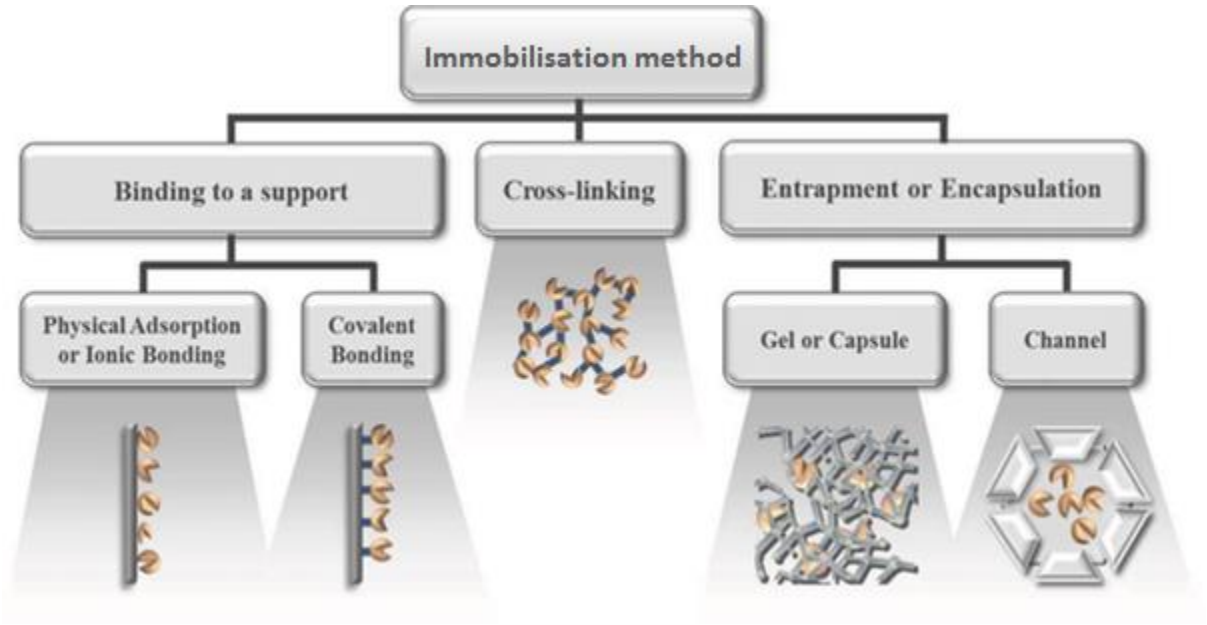

Figure 1.1. *Schematics of the different enzyme immobilisation techniques. Taken from Hwang and Gu (2013)[19].*

The various approaches used for immobilising enzymes can be categorised in two general classes: the chemical and physical methods [20]. Physical methods involve weaker interactions, such as hydrogen bonding, van-der Waals forces, hydrophobic interactions, ionic binding, and affinity binding of the enzyme with the supporting material [21], or mechanical containment/entrapment of enzyme within the support [20]. In the chemical method, enzymes are immobilised to the scaffold *via* a covalent bond. The covalent bond formation is typically between amino acid residues found on the surface of the enzyme and active functional groups found on the scaffold. In general, bond formation involves the following side chains of amino acids: lysine (ε-amino groups), cysteine (thiol groups), aspartic and glutamic acids (carboxylic acid groups) [12].

Three of the most commonly used techniques for immobilising enzymes include physical adsorption, entrapment/encapsulation, and crosslinking or covalent binding [21]. All three methods have been extensively reviewed [5, 12, 20, 21].The physical adsorption method is one of the cheapest and simplest enzyme immobilisation methods available and, in most cases, the catalytic activity of the enzyme is completely preserved [22]. The driving force causing the enzyme binding to the scaffold is usually due to a combination of weak forces [23]. A comparative analysis of the literature reports on the recent trends in the immobilisation of the enzymes by adsorption is presented in Krajewska *et al.* (2014) [24].

Table 1.1. *The advantages and disadvantages of three principle techniques used for immobilising enzymes [25, 26].*

Immobilisation method	Advantages	Disadvantages
Physical adsorption	*Cheap, simple and rapid immobilisation reaction, no conformational changes of the enzyme and complete preservation of enzymatic activity.*	*Leaching of enzymes from the support during the catalytic reaction due to changes in reaction conditions (e.g. temperature, pH) or through mechanical shear forces.*
Encapsulation/entrapment	*Can be used for impure enzyme preparations, different enzymes can be co-immobilised with minimal conformational changes of the enzyme.*	*Limited application as only porous or sol-gel supports can be used, leaching of entrapped enzymes during the process.*
Covalent binding	*Multipoint covalent binding of enzyme to the support, easy availability of wide range of crosslinkers, and established methods for functionalising/modifying supports.*	*Functionalisation or modification of support surface is necessary, reduction or even loss of catalytic activity resulting from conformational restrictions/changes of the enzyme.*

Entrapment/encapsulation of enzymes is another simple and mild immobilisation technique. In entrapment, the enzyme is trapped within the confines of an insoluble matrix, whereas encapsulation refers to the formation of a membrane like physical barrier around the enzyme [17]. Encapsulation is an excellent immobilisation method to avoid any negative influence on the structure of an enzyme [26]. Many encapsulation methods have been developed, the sol-gel method being the most prominent and widely used technique [27]. In the case of crosslinking, enzymes are irreversibly attached to the scaffold *via* a covalent bond, with the help of a crosslinking reagents or crosslinkers [11, 28]. The covalent bond formation is typically between amino acid residues found on the surface of the enzyme and active functional groups found on the carrier or scaffold. The advantages and disadvantages of all the three commonly used immobilisation methods are detailed in **Table 1.1.**

Each immobilisation technique has its own advantages and disadvantages and a universally applicable method of enzyme immobilisation is not available [25]. Immobilisation of enzymes has been largely achieved using a trial and error approach, and several important factors need to be considered in order to achieve high loading of enzyme, with high retention of activity, and enhanced operational stability and durability. Several different factors, such as concentration, temperature and pH of the reaction, can influence the outcome of enzyme immobilisation and need to be considered when selecting appropriate immobilisation conditions. Some general factors to be taken into account while selecting and optimising an enzyme immobilisation technique are shown in **Table 1.2.**

Table 1.2. *Critical factors for the development of the optimised immobilisation protocol. Modified from Hartmann et al. (2013) [25].*

Factors	Examples
Carrier	*Composition, morphology, surface area, porosity, dimensions, functional groups, stability against solvent, cost and availability.*
Enzyme	*Purity, available functional groups, conformational flexibility, active site, stability towards reaction conditions, such as pH, solvents, temperature, size, molecular weight.*
Immobilisation process	*Immobilisation strategy, such as adsorption, crosslinking, or encapsulation, Immobilising conditions (pH, temperature, solvents, buffers, additives), reusability, costs of enzyme and carrier, toxicity, stability.*

Several modified/unmodified supports have been assessed for their efficiency for enzyme immobilisation [11, 18]. During the last decade, the newly emerging field of nanobiocatalysis has demonstrated its potential applications in enzyme stabilisation. Nanobiocatalysis is a sub-field of biocatalysis, which explores more advanced nanostructured materials for the role of enzyme carrier [29].

The use of nanomaterials in enzyme immobilisation could achieve not only a much higher enzyme loading capacity, and a significantly enhanced mass transfer efficiency, but also excellent stabilisation [29, 30].

1.4. Nanomaterials and nanobiocatalysis

Nanostructured materials (NMs) can be defined as any material that has structured components with at least one dimension less than 100 nm [31]. The synthesis, characterisation and processing or manipulation of such NMs are all part of a rapidly growing field referred to as nanotechnology [32]. Methods used to generate NMs are commonly characterised as "top-down" and "bottom-up" methods depending on the processes involved in creating nanoscale structures [33]. A top-down approach corresponds to methods that are controlled by external experimental parameters to create NMs/nanodevices with the desired shapes and characteristics, starting with patterns made on a large scale and reducing them to the required values before forming nanostructures [34]. The various top-down techniques for producing nanomaterials include photolithography, scanning beam lithography, molding, and printing. In contrast, bottom-up approaches seek to have molecular or atomic components built up into more complex nanoscale assemblies, in some cases through smart use of self-organisation [34, 35].

Different physical and biological bottom-up self-assembly processes have been reported in recent years to direct the assembly of nanoscale functional blocks into hierarchically ordered structures, and are reviewed by Thiruvengadathan *et al.* (2013) [36]. Recent research undertaken to synthesise functional NMs has highlighted the need and advantages in synergistically combining top-down fabrication methods with bottom-up self-assembly. For a comprehensive review on prominent nanofabrication tools and techniques used for developing novel and efficient functional NMs/nanostructured devices see [33, 35]. Many robust NMs with properties tailored to their applications as enzyme scaffolds, such as nanoparticles (NPs), nanotubes (NTs), nanoporous media, and nanofibres (NFs) have been developed. **Figure 1.2** shows images of the three nanostructures - NPs, NTs, and NFs, as observed under microscope.

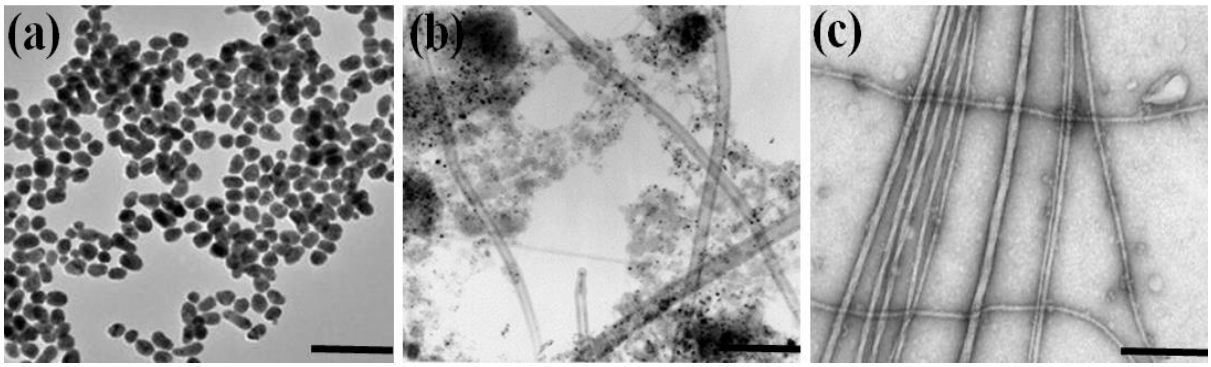

Figure 1.2. *A representative TEM (transmission electron microscopy) images of (a) gold nanoparticles [37], (b) carbon nanotubes [38], and (c) crystallin protein nanofibrils (Taken as detailed in section 7.1.3). Scale bar is 200 nm.*

Several nanobiocatalysis reviews have eloquently explained the different types of nanomaterials used for enzyme immobilisation, each with its characteristic pros and cons [30, 39-41]. Some examples of nanostructured supports that have been successfully employed for enzyme immobilisation are listed in **Table 1.3.**

1.4.1. Nanoparticles (NPs)

NPs are defined as particles ranging in size from 1-100 nm, that may not exhibit size-related properties and differ significantly from those observed in fine particles or bulk materials [42]. There exists a huge variety of different types of NPs ranging from carbon-based structures, such as spherical fullerenes, to the ones derived from natural materials, such as liposomes, gelatines, and alginates [43]. Additionally, NPs can be obtained from polymers [44], silicates or metals [45], such as gold, copper or silver NPs [46].

NPs provide an ideal solution to the usually contradictory issues encountered in the optimisation of immobilised enzymes: minimum diffusional limitation, maximum surface area per unit mass, and high enzyme loading [47]. Recently, special interest has been given to magnetic NPs as they can be removed easily from the reaction medium, using an external magnetic field, for example silica-encapsulated nanomagentic particles used for β-lactamase immobilisation [48].

1.4.2. Nanotubes (NTs)

Nanotubes have distinct inner and outer surfaces, and large inner volumes (relative to the dimensions of the tube), and therefore can be modified differentially with any desired biomolecule, ranging in size from small molecules through to proteins. The three main types of nanotubes used in bionanotechnology based applications are carbon nanotubes (CNTs), peptide/protein nanotubes (PNTs), and template-synthesised nanotubes [49]. CNTs are further categorised as single- (SWCNTs) or multi-walled CNTs (MWCNTs) based on the number of graphitic layers surrounding the central tubule. SWCNTs are attractive for their higher surface area for enzyme interaction, but MWCNTs are preferred for their easier dispersibility and lower cost [50]. CNTs exhibit extraordinary mechanical, electrical, and thermal properties and have been extensively explored for several potential applications, such as biosensors, drug delivery systems, tissue engineering, and as multifunctional coating materials [51]. However, more work needs to be done towards defect free, cheap mass-production of CNTs [52]. The chemical inertness, and toxicological concerns associated with CNTs also limits their versatility and suitability [53].

The application of self-assembled hollow nanotubes synthesised from synthetic peptides in bionanotechnology is robust, practical, and affordable due to their advantages of reproducibility, relatively simple large-scale production, monodispersity, and simpler experimental methods [54]. Different types of peptide nanotubes are categorised on the basis of the peptide structure from which they are designed, such as, cyclic PNTs, dipeptide-based PNTs, or coiled coil PNTs [55].

Some of the challenges hindering peptide NTs synthesis and applications includes control during synthesis, stability in liquid environments, manipulation and conductivity [56, 57]. In contrast, the template synthesis method offers control in both size and shape. In template synthesis, nanoporous membranes act as templates for the synthesis of nanostructures of the desired material [58]. Hard templates used for template synthesis of NTs possess well-confined voids of uniform diameter, and NTs are prepared within cylindrical and monodisperse channels, pores, or connected hollow spaces of a nanopore membrane or other solid surface [49]. Template-synthesised NTs can be created from a wide variety of tube materials including proteins, silica, carbon, chitiosan/alginate, DNA [59].

Table 1.3. *Some examples of different type of nanoscaffolds utilised for enzyme immobilisation.*

Nanomaterial used	Type of nanoscaffolds	Immobilised enzymes
NPs	*Copper chelated magnetic mesoporous silica NPs; zinc oxide NPs; Au and Ag NPs*	*Laccase [60];β-galactosidase [61]; alcohol dehydrogenase and NADPH* bioconjugates [62]*
NTs	*MWCNTs*; halloysite NTs (HNTs); SWCNTs**	*Glucose oxidase [63]; laccase [64], and lipase [65]; His-tagged NADH* oxidase [66]*
Nanoporous media	*Nanoporous silica, nanoporous alumina; MOFs*- zeolitic imidazolate framework 90 (ZIF-90)*	*Horseradish peroxidase [67], and lipase [68]; alcohol oxidase [69]; catalase [70]*
NFs	*Copolymer (styrene and maleic anhydride) fibres; polyaniline, polystyrene, and cellulose NFs; PNFs*	*Horseradish peroxidase, and glucose oxidase [71]; lactase [72]; glucose oxidase [73]; and organophosphate hydrolase [74]*
Nanocomposites (NCs)/Hybrid nanomaterials	*Polyaniline- Ag NCs; chitosin-halloysite hybrid NTs; polyvinyl alcohol(PVOH)-silica hybrid films; PVOH-amyloid PNFs hybrid films*	*α-Amylase [75]; horseradish peroxidase [76]; glucose oxidase [77],[78]*

**NADPH - Nicotinamide adenine dinucleotide phosphate-oxidase; NADP - Nicotinamide adenine dinucleotide phosphate; SWCPNTs – Single-walled carbon nanotubes; MWCNTS – Multi-walled carbon nanotubes; MOFs - Metal organic framework.*

The template synthesis method also allows distinct surface chemistries on the inside and outside [58]. Initially, while nanotubes are still embedded within the template, the inner surface is accessible for functionalisation, and the outer surface becomes available only once the nanostructures have been released by dissolving the template [59].

However, nanocatalysis-based applications of synthesised polymer-based nanotubes are currently limited by the fact that these structures do not maintain their shape indefinitely [79, 80]. By far, porous anodic aluminium oxide (AAO) is the most preferred template, as it is relatively low cost, and provides large versatility with a long range ordered arrangement of homogenous pores availability [81].

1.4.3. Nanoporous media

Materials having pores with diameters below 100 nm are considered as nanoporous materials. Several organic/inorganic materials with well-defined pore sizes, surface chemistries, and functionalities have been developed, such as zeolites, silica or alumina, activated charcoal, block co-polymers (polylactide, polystyrene, or polyacrylonitrile) [82].

Nanoporous materials with pore sizes ranging from 2-50 nm have received a lot of attention as a nanoscaffold owing to their controlled pore structure, mechanical stability, and high surface area, and ease of functionalisation *via* simple physical adsorption methods [29, 82]. Typical disadvantages of these materials include continuous leaching of physically adsorbed enzyme molecules from nanoporous media [29]. Another challenge is to tailor-design materials for specific properties and functions [83]. Current research efforts in this field have been driven by the rapidly growing emerging applications of these materials in enzyme immobilisation, energy storage, and environmental applications [84-87].

1.4.4. Nanofibres (NFs)

Nanofibres are defined as long fibrillar structures with a diameter equal to or less than 100 nm, and are characterised by high specific surface area, flexibility, and superior directional strength [88]. Current fibre fabricating processes includes nanolithography [89], thermally induced phase separation [90], molecular self-assembly [91], and bio-fabrication alternatives [92]. Electrospinning has been regarded as the most promising approach to produce continuous nanofibres [93], and several different synthetic/natural polymers, proteins, and peptides have been used for generating nanofibres, such as poly(methyl methacrylate) (PMMA), polylactic acid (PLA) and polyacrylonitrile (PAN), chitosin, gelatin, silk, and collagen [94]. Although electrospun NFs have potential application in many fields such as energy devices, high temperature filtration, and efficient catalysis, it remains a challenge to understand the structure and performance of NFs. Furthermore, the performance and range of electrospun nanofibres have been limited due to the limited variety of organic electrospun NFs, and friability issues for inorganic electrospun NFs [93].

Self-assembly of nanofibres holds promise as a low-cost, high-yield technique with a wide range of scientific and technological applications. Self-assembly is the spontaneous, bottom up organisation of molecules into ordered structures by using specific interaction, that may arise due to the intrinsic properties of the individual elements within the system or under the influence of applied external forces [36]. Many proteins and peptides serve as potential sources of self-assembled NFs.

Amyloid fibrils are a well-investigated example of self assembled polypeptides, and have been shown to be very versatile materials with potential applications in various fields [95]. In addition to the above mentioned nanomaterials, a relatively new class of materials, "hybrid nanomaterials" is also gaining attention in the field of catalysis for achieving specific physical and catalytic properties [19, 96-98]. Hybrid materials are unique conjugates of organic/inorganic nanostructure, or can also be obtained by combining different nanocomponents/nanostructures **(Table 1.3)**.

1.5. Amyloid PNFs

Amyloid fibrils are a highly stable, insoluble form of proteins or polypeptides formed by the assembly of normally soluble protein or peptide monomers into intermolecular hydrogen bonded β-sheets [99, 100]. Amyloid, originally meaning starch-like, refers to the protein deposits that were reminiscent of starch when first observed by Rudolph Virchow in 1854 [101, 102]. Later, in 1859, Friedreich and Kekule demonstrated that amyloid deposits were made of protein, leading to the study of amyloid deposits as a class of proteins with a propensity to undergo changes in conformation that result in fibril formation [102]. Apart from their association with protein misfolding diseases such as Huntington's, Parkinson's, Alzheimer's, Type II diabetes, and Creutzfeld-Jacob disease [103, 104], amyloid structures are also naturally found in many functional roles [105-107]. Prominent examples of such functional amyloid materials include bacterial coatings [108], regulation of melanin synthesis [109, 110], natural adhesins [111], and structures for the storage of peptide hormones [112]. The presence of functional amyloid, along with a proposal that, if the correct conditions are found, amyloid fibril formation is a generic property of all proteins [99], elicited a lot of interest in the possibility of utilising *in vitro*-prepared fibrils as novel bionanomaterials.

1.5.1. Amyloid fibril formation - protein folding and misfolding

Once synthesised at the ribosome, proteins have to attain their native folded confirmation in order to function effectively. Protein folding is quite complex and susceptible to errors, resulting in the formation of several intermediate misfolded states as illustrated in **Figure 1.3.** To prevent and address protein misfolding problems, cells have protein quality control systems, which includes chaperones, and proteasomes. Chaperones play vital roles in helping proteins become folded in the first place or in aiding misfolded proteins to regain their correct conformation whereas, once a misfolded protein cannot be properly refolded, proteasome-, autophagy- or endoplasmic reticulum-associated protein degradation (ERAD) systems are deployed to degrade any misfolded proteins. The protein folding and unfolding process is thermodynamically driven [113] and is also governed by the external conditions, such as pH, temperature, pressure [114, 115], molecular crowding [116], and entropy [117].

Depending on the conditions, proteins can adopt any of the possible competing conformational states - unfolded peptide chains, partially folded intermediate states/aggregates, or completely folded native forms **(Figure 1.3)**.

The protein aggregation literature is extensive and various recent reviews describe our current understanding of the aggregation process [118-120]. In order to form amyloid fibrils, proteins need to undergo partial unfolding to form an intermediate conformational state. Partial unfolding can be induced by exposing the protein to denaturing conditions *(in vitro)*, such as high temperature and pressure, low pH, or the presence of organic solvents. In these denaturing conditions, non-covalent interactions such as hydrogen bonding can still occur within the polypeptide, which stabilise the amyloid fibril structure [121]. Many polypeptides can achieve the amyloid folding motif as a nearly ubiquitous alternative folded state, despite having different amino acid sequences and native conformations [122]; however, different proteins have different propensities for forming amyloid fibrils. Amyloid fibril forming tendency is governed by many factors, such as hydrophobicity, net charge, propensity of constituent amino acid residues to form β-sheets, and the presence of aromatic residues in the polypeptide [123].

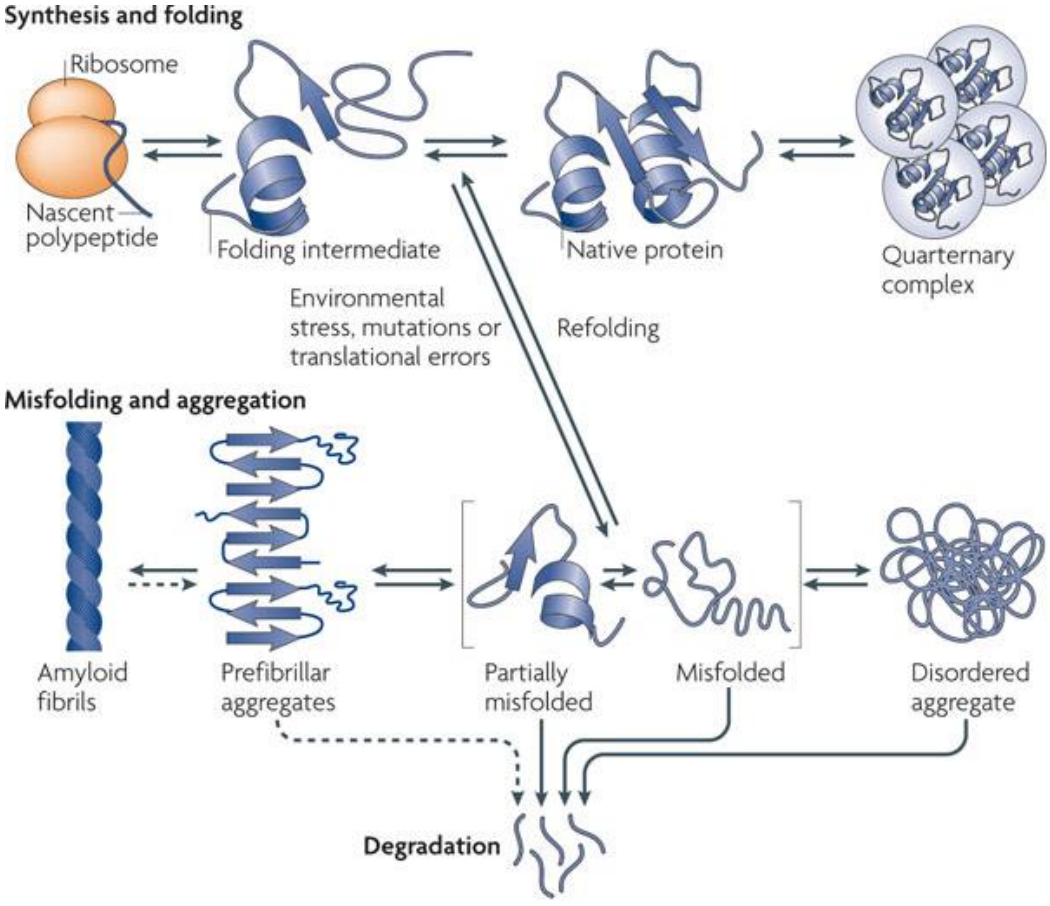

Figure 1.3. *The process of protein folding, misfolding, and aggregation. Taken from Tyedmers et al. (2010) [124].*

1.5.2. Mechanism of amyloid fibrillation

Fibrillation is universally recognised as a nucleation-dependent polymerisation reaction [99, 125], with few exceptions [126], and is commonly depicted as a sigmoidal-shaped growth curve [127] **(Figure 1.4)**.

The typical fibril formation process consists of three distinct phases characterised by protein misfolding, nucleation, and fibril elongation [128]. In the initial phase, called the "lag phase", protein monomers associate and may attain a critical concentration of oligomers to form fibril nuclei. Nucleus formation is thermodynamically unfavorable, and requires a series of association steps of monomers, thereby, is a rate-limiting step [129]. At the end of the nucleus phase, larger ordered structures with intrinsic fibrillar (β-sheet) structures, termed as protofibrils are formed [130, 131]. The next phase is the "growth or elongation phase" in which further addition of monomers to the nucleus results in rapid growth or formation of fibrillar structures (ordered aggregates).

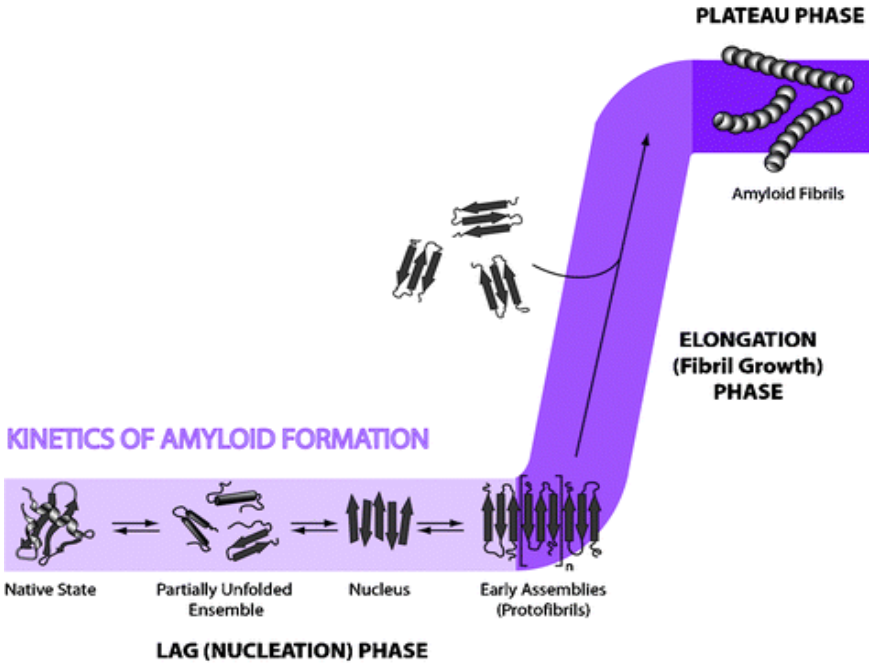

Figure 1.4. *Nucleation-dependent fibrillation process. Taken from Wilson et al. (2008) [132].*

The formation of protofibrils (initial stable pre-fibrillar structures) is a precursor to mature amyloid fibril development in the (next phase) "saturation phase" **(Figure 1.4)**. In the elongation phase, fibrils can be formed either by longitudinal addition, in which individual peptides are added to the end of each β-sheet, or by lateral addition, in which the fibril grows by adding an already-formed β-sheet to its side. Both mechanisms seem to contribute equally in the formation of mature amyloid fibrils [133]. The rate of the fibrillation process is influenced by the addition of seeded molecules (pre-formed fibrils) [130, 134], by the presence of foreign surfaces [135, 136], by deamidation [137] and acetylation [138], or by mechanical agitation [139].

Although nucleation-dependent formation of amyloid fibrils is considered the main mechanism for the growth of fibrils, there are some unanswered questions to be explored, such as nature of the nucleus or amyloid aggregates [140], growth of amyloid nuclei [141], and the concentration dependence of the fibrillation process [142].

1.5.3. Amyloid fibril structure

Irrespective of the native structure and nature of the proteins used for generating amyloid fibrils, amyloid and amyloid-like fibrils all exhibit a similar X-ray diffraction fingerprint -"the cross β-sheet pattern"[102, 143] as shown in **Figure 1.5.** The cross β-sheet pattern has two major features common in all the fibrillar structures: β-strands which lie perpendicular to the fibril axis, and β-sheet filaments running parallel to the fibril axis, formed by polypeptide backbones folding upon themselves at 4.8 Å (meridonial reflection), and interweaving β-strands at a distance of 10-11 Å (equatorial reflection) depending on the side-chain composition of the β-sheets [144].

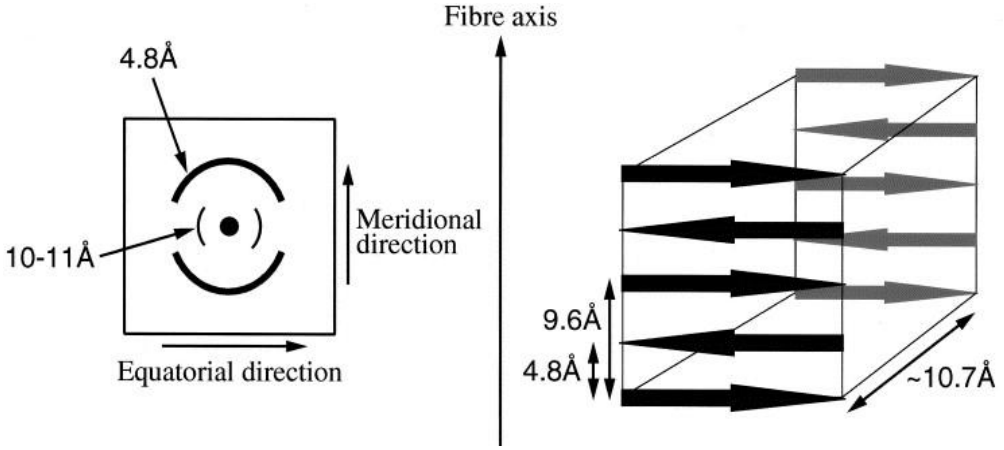

Figure 1.5. *This shows a schematic of a characteristic cross β-sheet diffraction pattern, in which intermolecular β-sheets extend over the length of the fibril such that each β-strand within the β-sheets runs perpendicular to the fibril axis. Taken from Serpell (2000) [145].*

With the help of X-ray diffraction [143, 146], small angle X-ray scattering (SAXS) [147], atomic force microscopy (AFM) [130, 148], electron microscopy (EM) techniques [149-151], solid-state nuclear magnetic resonance (ssNMR) [152, 153], and birefringence and spectroscopic assays [154, 155], vital information about the size (widths in the range of 2–10 nm and lengths from 1 up to 10 μm) [73], unbranched morphology, and the characteristic "cross-β" fibril comprising protofilaments has been attained [102]. The basic unit of amyloid fibrils is known as a protofilament, which itself is made up of a number of intertwined β-sheets as shown in **Figure 1.6**.

The protofilament structure of amyloid fibrils is conserved across a range of proteins, although the way the protofilaments associate with each other can differ [145]. Mostly mature amyloid PNFs consists of 2-6 protofilments, where these protofilaments wind around each other in a rope-like manner to form a super coiled rope-like structure [156]. In addition to the rope like arrangement, protofilaments in a fibril can also arrange into a ribbon-like lateral-packing arrangement to form long ribbons, as has been demonstrated using β-lactoglobulin (β-lg) PNFs [157, 158] **(Figure 1.6)**.

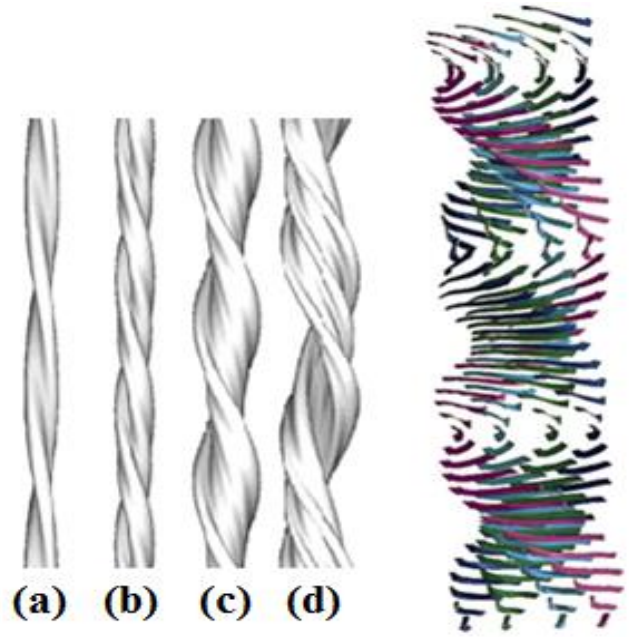

Figure 1.6. *Surface representation of 3-D maps of the four different protofilament structure for insulin fibril structures (left), (a) - a pair of filaments, (b) - the four protofilament compact fibrils, (c) - the six protofilament fibrils, and (d) - the twisted ribbon. Right - molecular model of the common core protofilament structure (four β-sheets illustrated here) in a generic amyloid fibril, as determined using synchrotron X-ray diffraction on amyloid fibrils. Figures taken from Jiminez et al. (2002)[156]; and Finke et al. (2009) [119], respectively.*

1.6. Defining characteristics

A number of techniques exist for the characterisation of amyloid fibrils, with the main ones being the binding of the histological dyes Congo red (CR) and Thioflavin T (ThT); fibrillar morphology by AFM, and transmission electron microscopy (TEM); and β-sheet secondary structure determination by Fourier transform infrared (FTIR) spectroscopy, and X-ray fibre diffraction [154]. X-ray fibre diffraction is one of the main methods used for amyloid fibril characterisation, where the amyloid fibril structures give characteristic diffraction patterns as discussed in section 1.6.3. In this thesis, the histological dye ThT, and TEM were used extensively. ThT was chosen as it is widely used to test for the presence of amyloid fibrils and because it is known to work reliably with the model amyloid forming protein, insulin.

1.6.1. ThT binding of amyloid PNFs

Thioflavin T is a benzothiozole dye with a high affinity for proteins containing β-sheet content and is the most widely used "gold standard" for selectively staining and identifying amyloid fibrils *ex vivo*, *in vitro*, and in animal model studies [155, 159, 160]. Unbound ThT dye has fluorescence excitation (from 385 nm to 450 nm), which on binding to β-sheet structure undergoes a characteristic spectral shift resulting in enhanced fluorescence emission (from 445 nm to 482 nm). This spectral shift is used to differentiate bound ThT and unbound ThT and consequently the presence of amyloid structures [160].

The main advantages of the ThT method are its simplicity, low ThT interaction with pre-fibrillar structures (folded or unfolded intermediates/monomers), minimal impact on the fibrillation process, and that the method can be used to assess the amyloid formation both *in vitro* and *in vivo* [161]. A large number of studies have examined the binding mode of ThT for amyloid fibrils [159, 160, 162, 163]. The β-sheet structured cavities and channels found in amyloid fibrils have been proposed to be the binding locations of ThT [159, 164, 165].

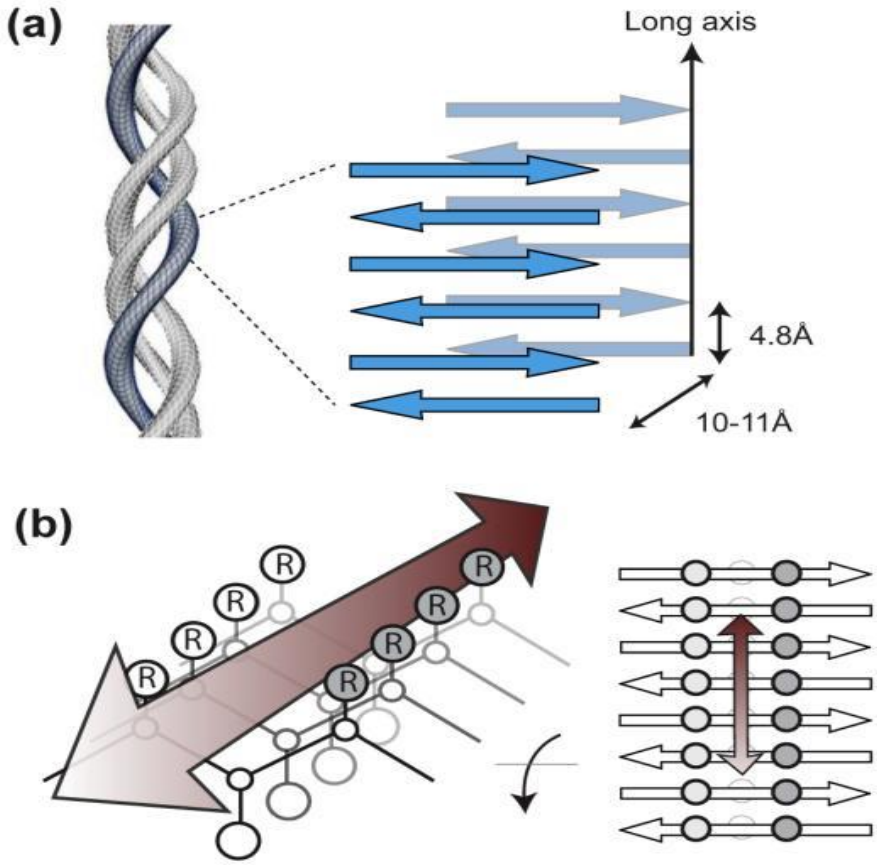

Figure 1.7. *The directional binding of ThT for amyloid fibrils, where (a) shows a common cross-β structure of amyloid fibrils and a structural rationale for fibril-ThT interactions, and (b) schematic representation of channel model binding of ThT along surface side-chain grooves running parallel to the long axis of the fibril β-sheet structure. Taken from Biancalana et al. [160].*

The binding is highly directional, with the ThT long axis parallel to the elongation axis of the fibrils **(Figure 1.7)** and can be characterised by features such as ThT accessibility, binding stoichiometry, and affinity. In the same direction run channels (channel like motifs formed by the neighbouring rows of cross-strand chains, along the solvent exposed surface of fibrils) on the β-sheet of the amyloid fibrils, suggesting that these channels are the possible binding site of the dye [160, 165] as shown in **Figure 1.7**. In addition to the characterisation of the ThT binding site, the molecular form of ThT binding is crucial for understanding the binding mechanism [163]. Conflicting reports claims that the molecular form of ThT on binding to the amyloid fibrils is either monomeric [165, 166], dimeric [167] or a micelle [159].

1.6.2. TEM

TEM is a useful technique to detect and distinguish fibril like morphology from other types of protein aggregates [154, 168]. Under the TEM it is possible to observe unbranched long fibrillar structures or higher-order assemblies of fibrils such as association of at least two strands to form a flat ribbon-like fibrils [169]. Negatively stained TEM images of amyloid PNFs are shown in **Figure 1.8.** TEM images can be used for obtaining both qualitative and quantitative information, such as length and width of fibrils, smoothness of the surface, number of protofilaments, and the periodicity of fibril twists [156, 168].

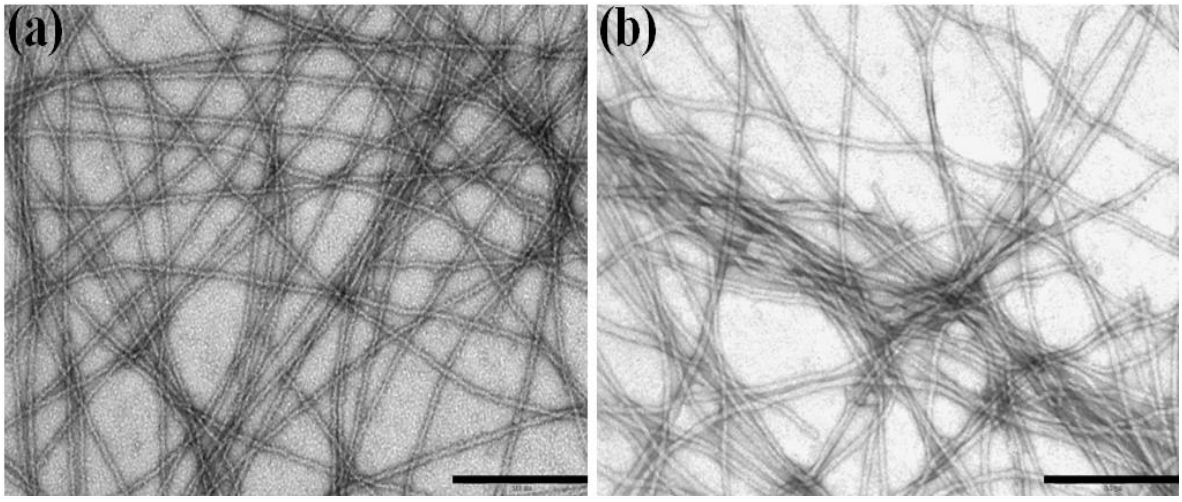

***Figure 1.8**. TEM image of amyloid (taken as detailed in section 7.1.3), (a) whey PNFs, and (b) crystallin PNFs, showing the presence of unbranched, long fibrillar structures with smooth surface. Scale bar is 200 nm.*

The grids for amyloid fibril detection can be made of copper or nickel with 200–400 unit mesh spacing and are usually negatively stained using 2% uranyl acetate prepared in deionised water (dH_2O) [154]. Negative staining provides good contrast, protects the sample from radiation damage and preserves morphology [168].

1.6.3. FTIR

A protein's FTIR spectrum consists of two prominent features, the amide I (~ 1650 cm^{-1}) and amide II (~ 1540 cm^{-1}) bands, where the former arise primarily from the C=O stretching vibration and the latter is attributed to the N-H bending and C-N stretching vibrations of the peptide backbone. Different secondary structures, such as α-helix, β-sheet, and β-turn, exhibit characteristic frequencies and intensities in the amide I band region as shown in **Figure 1.9**. Therefore, the FTIR spectrum of a protein is routinely used to characterise protein secondary structures in solution as well as in the solid state [170].

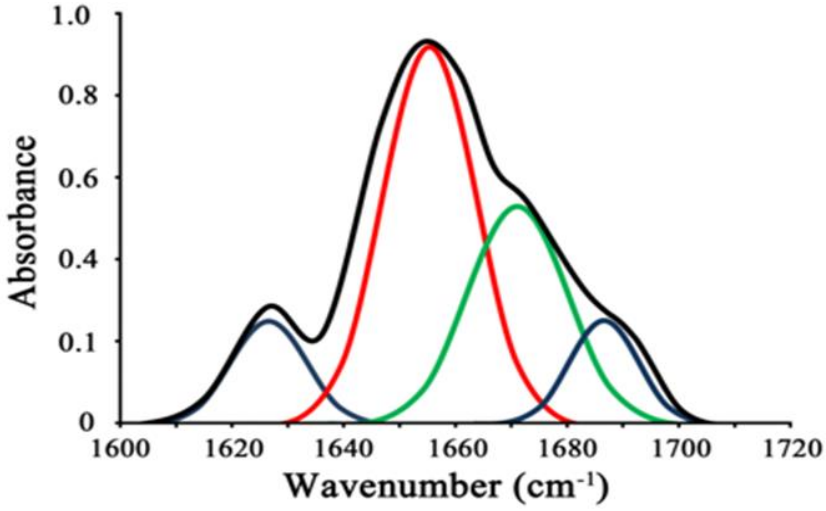

Figure 1.9. *A schematic representation of amide I region of FTIR spectrum (1700-1600 cm^{-1}), showing spectrum peaks corresponding to different secondary structures including β-sheet (blue), random coil (green), and α-helix (red), and experimental band-shape (black). Modified from Walther et al. (1996) [171].*

FTIR is usually used in combination with other biophysical techniques, such as circular dichroism (CD), and electron microscopy (EM) to study protein aggregation or fibrillation processes [172]. Amyloid fibrils have a spectral signature frequency peak between 1611 and 1630 cm^{-1}, while for native β-sheet proteins it extends from 1630 to 1643 cm^{-1} [173].

1.7. *In vitro* amyloid fibrillation

A large number of proteins that are not known to form fibrils in disease or nature have been induced to form fibrils *in vitro*, these include bovine insulin [127], human serum albumin (HSA) [174], hen egg white lysozyme (HEWL) [175], ovalbumin and bovine serum albumin (BSA) [176], β-lg [177], whey protein isolate (WPI) [178], fish lens crystallins [179], and wheat glutenin proteins [180]. However, most research in the field of bionanotechnology has focused on pure, well-defined amyloid-protein systems or *de novo*-designed peptides [74, 181-185]. In this thesis, three different amyloid-forming proteins were used, bovine insulin, crude crystallin proteins, and WPI, each possessing different interesting properties.

1.7.1. Bovine insulin – a model amyloid forming protein

Bovine insulin was used as a model amyloid-forming protein in this study, since it is extremely well characterised [127, 156, 172, 186-188]. With the size of a polypeptide, but having all the structural features of a large protein, insulin has been one of the most extensively studied proteins [189]. The polypeptide hormone insulin has a mainly helical native structure, with its two polypeptide chains linked by two inter-chain and one intra-chain disulfide bonds [190]. *In vitro*, insulin is readily converted to well-defined fibrillar structures by incubation at low pH and high temperatures [172, 188].

There is a large amount of literature available on bovine insulin amyloid PNFs, including detail of their morphology [127, 156], mechanism and kinetics of their formation [147, 172, 186, 191], and potential applications in bionanotechnology [74, 181, 192-194]. An illustrative schematic of insulin fibrillation process is shown in **Figure 1.10.**

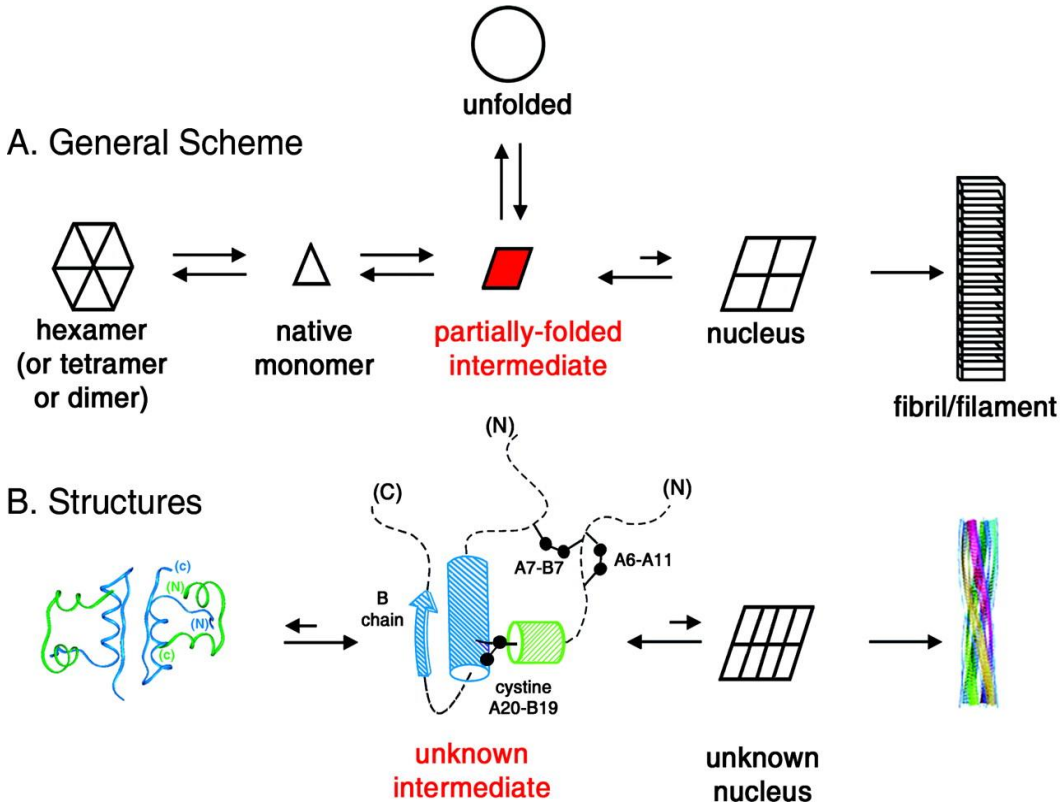

Figure 1.10. *Schematic mechanism of fibrillation process (A) represents a general fibril kinetic mechanism, and (B) shows representative insulin structures. Native protein structure (far left) under denaturing conditions disassemble, leading to an equilibrium between native and partially folded monomers (open triangle and red trapezoid, respectively). The partial unfolded or intermediate state may unfold completely as an off-pathway event* (*open circle*) *or aggregate to form a nucleus, followed by pre-fibrillar and consecutively fibrillar state* (*far right*). *(B) A crystal structure of the native insulin dimer (PDB 1GUJ), and proposed insulin fibrillation model. The α-chain is shown in green, and blue represents the β-chain. Cylinders and arrow indicate temperature-stable substructure (residues B9-B26 and A16-A20). Dashed lines indicate disordered regions, and balls represent the three disulfide bonds. Taken from Hua et al. (2004) [195].*

1.7.2. The industrially relevant (low cost) amyloid forming protein sources

The other amyloid fibril-forming proteins used includes WPI, and fish eye lens crystallin proteins (CPs). Amyloid fibrils formed from crude fish eye CPs and WPI were considered, since if amyloid fibrils are to be used successfully in bionanotechnology, there is a need for production of amyloid fibrils from a readily available and inexpensively sourced protein [100].

(a) Crystallins

The healthy eye lens is transparent and functions to focus light on to the retina [196]. The crystallins are highly organised (supramolecular β-sheet structure) and stable proteins present within the lens [197]. The α-, β-, and γ- crystallins are the major structural proteins within the eye lens, and are responsible for its exceptional stability and transparency [198]. Previous studies have shown that the inherent stability of the β-sheet supramolecular structure adopted by the crystallins in the eye lens, and the chaperone ability of α-crystallin must be crucial for preventing protein aggregation *in vivo* [196, 199]. However, any disruption to the native crystallin structure can lead to protein aggregation, leading to the development of cataract [198].

Due to their ability to aggregate leading to the formation of amyloid fibrils both *in vitro* and *in vivo* [200], crystallin proteins have the potential to be of use in the creation of protein nanomaterials [201]. Previous work has reported the synthesis of amyloid PNFs from crude crystallin protein mixtures, extracted from bovine lenses obtained from the abattoir [200], and from fish eye lenses [179]. CPs extracted from hoki (*Macruronus novaezelandiae*) fish eye lenses were used in this research to prepare crystallin PNFs, by methods adopted from Healy *et al*. (2012) [179]. Fish eye lens crystallins were preferred mainly due to their ready availability from the seafood industry, and the fact that they are perceived safer than bovine products in the wake of bovine spongiform encephalopathy outbreaks. Additionally, previous work in our lab has shown that the fibril manufacture process from fish eye crystallins can be scaled up to produce large quantities of fibrils [202]. The main focus of this research was to characterise crystallin PNFs obtained from hoki fish eye lenses in terms of their applicability to bionanotechnological applications, and to create a functional crystallin fibril nanoscaffold by incorporating enzymatically active components.

(b) WPI

Whey proteins are reported to form a wide range of assemblies (fibrils, ribbons, spherulites, or spherical particles) depending on the conditions applied on heating [203]. Whey proteins from bovine milk have gained considerable attention as a fibril forming globular protein in the food sector [204]. In this study, an industrial grade WPI was used as an amyloid forming protein source, because of its relevance for practical applications. Commercial WPI, amongst other whey ingredients, are produced from whey obtained from cheese manufacturing.

The main proteins in WPI are β-lg (70-80%), BSA and α-lactalbumin [205]. β-Lg was found to be the only protein that is incorporated into WPI fibrils, when they were formed by heating at pH 2 and low ionic strength [206]. β-Lg predominantly exists as dimer under physiological conditions, but dissociates to monomer at about pH 2-3, preserving its native structure [207]. A representative crystal structure of bovine β-lg is shown in **Figure 1.11**. Given the small molecular weight of 18.4 kDa [208], and globular nature, it has proven to be a well-suited model system for studying fibrillar protein aggregation [203, 209, 210].

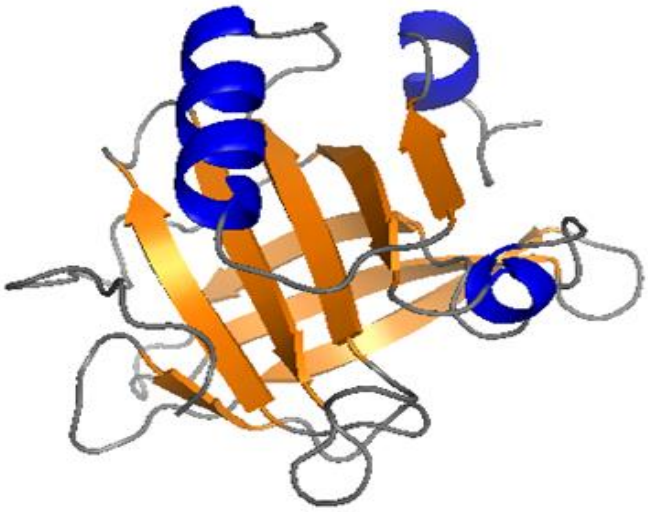

Figure 1.11. *PyMOL image of the native structure of bovine β-lg. In this ribbon representation, the β-sheets are shown in orange, the α-helices in blue, and the disordered loops are shown in grey. This image was constructed using PyMOL from PDB file 2BLG.*

The literature available on obtaining β-lg fibrils by heating at 80 °C, pH 2 and low ionic strength for 10-24 h is extensive [203, 211-213]. The contributions of the Loveday group have been particularly important in the understanding of whey amyloid fibrillation, and factors influencing the process, such as pH, temperature, presence of salts and cations [214-217]. In this work, whey protein nanofibrils (WPNFs) were prepared from the commercially available whey protein isolate powder, using in-house methods, as published in Sasso *et al.* (2014) [73].

1.8. Amyloid fibrils and bionanotechnology

Over the past decade, amyloid fibrils have attracted burgeoning interest in bionanotechnology due to them possessing a number of desirable properties suitable for many different applications in this field [100, 123, 193, 218-221]. The unique properties that make amyloid fibrils attractive for nanotechnological purpose include: (i) spontaneous formation of amyloid fibrils by any protein/peptides under certain denaturing conditions [121, 222], *via* a nucleation-dependent polymerisation process, where pre-formed amyloid fibrils can act as seed to form fibrils/accelerate the kinetics of fibril formation [95, 187, 223, 224]; (ii) high mechanical strength and stability comparable to silk and steel [225, 226], and the ability to self-assemble providing a bottom-up approach to material design [123, 227]; (iii) ability to form highly ordered amyloid fibril structures, such as gels, and films, in the micro or macroscale [183, 228, 229]. (iv) ease of production and functionalisation of amyloid fibrils for specific applications [73, 181, 230-232], due to intrinsic side chain chemistry from their amino acid composition; (v) low cost production and large surface area due to nanometre size range [102]; (vi) structural compatibility with other materials, and reversibility depending upon the conditions [78, 182, 233].

1.8.1. Applications of amyloid PNFs

The research focus in the amyloid fibril field is broadening to include new horizons in nanotechnology. Amyloid fibrils have been identified as a novel nanomaterial and several applications are under scrutiny, with the most promising ones using amyloid fibril as potential nanowires for electronics, as functional templates and liquid crystals, as nanoscaffolds for enzyme immobilisation, for the production of amyloid-based gels in cell adhesion and wound-healing, and as drug delivery systems [185]. In the past ten years amyloid fibrils have been explored for a multitude of different bionanotechnology applications, some of which are listed in **Table 1.4.**

The main focus of this research was to demonstrate the potential of amyloid fibrils obtained from readily available sources as a novel nanoscaffold by immobilising enzymes. Amyloid fibrils have been used as nanoscaffold for enzyme immobilisation **(Table 1.4)**, resulting in enhanced activity, improved stability and reusability of the enzymes. As stated before, the dimensions of amyloid PNFs, and readily available surface chemistry for adding functional groups makes amyloid fibrils an ideal choice for nanocatalysis applications. Two commonly used methods for creating functional PNFs or for immobilising enzymes onto amyloid PNFs are:

(i) Attaching functionalities before fibrillation, such as creation of fusion proteins, where the protein of interest is rationally conjugated to an amyloidogenic sequence, followed by exposure to the fibril forming conditions, thereby, resulting in the fabrication of functional PNFs. A few examples of functional amyloid PNFs obtained by the fusion method include green fluorescent protein, barnase, carbonic anhydrase, glutathione-S-transferase [234], and cytochrome b562 functionalised PNFs [235].

(ii) Attaching or adding functional groups onto the mature fibrils, after fibrillation. This method relies on the availability of the different amino acid side chains onto the surface of mature PNFs. The chemistry of available amino acid residues can be exploited to attach biomolecules of interest to fibrils either *via* physical adsorption, crosslinking, or covalent attachment. Organophosphate hydrolase (OPH) and GOX have both been covalently attached to PNFs in this manner, making functional fibrils that could be used in bioremediation, antimicrobial films, and biosensing [73, 74, 78, 181].

In this work, functional amyloid PNFs were obtained by attaching important industrial enzymes onto the PNFs, post-fibrillation, using physical adsorption, and a covalent crosslinking approach. To understand the potential of PNFs to act as a versatile nanoscaffold, a diverse range of industrially relevant enzymes including GOX, β-galactosidase (β-gal), pectinase, α-amylase, and laccase were studied. In addition to crystallin PNFs, PNFs obtained from whey fibrils were investigated for potential applications in bionanotechnologies.

Table 1.4. *Summary of different biotechnologies utilising amyloid fibrils obtained from various amyloid forming proteins/peptides.*

Applications	References
Amyloid nanowires	*A hybrid Au-Ag nanowire fabricated from amyloid fibrils of wild-type Sup35p [230]; Electronically active luminescent nanowire derived from insulin amyloid fibrils decorated with conjugated polymers [236, 237]; Insulin amyloid PNFs coated with polymer alkoxysulfonate (PEDOT) [238]; Ag-nanowires obtained from lysozyme amyloid fibrils with hollow channels filled with silver [239]; Insulin amyloid fibrils integrated organic solar cells [240]; Ultrathin Pt nanowires obtained by using insulin amyloids as a template [192]; Bi-functional protein nanowires obtained from Sup35p amyloid fibrils for immunoassays [241]; Functional nanowires obtained from amyloid peptides via bio-mineralisation [227]; β-Lg amyloid-directed TiO_2 nanowires for photovoltaics [242].*
Drug delivery, cell growth, and tissue engineering	*Self-assembled amyloid fibrils from gonadotropin-releasing hormone (GnRH) analogues as stable drug depots [243]; Lysozyme amyloid networks for cell growth and spreading [232]; Functionalised transthyrethrin peptide amyloids for 3T3(mouse fibroblasts) cell adhesion and proliferation [244]; Amyloid peptide hydrogels for wound healing [245].*
Functional amyloids, and bio or nanosensing	*Organophosphate hydrolase immobilised insulin amyloids for bioremediation [74]; GOX-functionalised insulin fibrils [181]; Multi-functionalisation of whey amyloids [73]; α-synuclein amyloid hydrogels with entrapped horseradish peroxidase [229]; Cytochrome b562 fused SH3 amyloids with affinity for metalloporphyrins [235]; A fluorescent molecular biosensor for methyl parathion (pesticide) detection by fusing the methyl parathion hydrolase enzyme and green fluorescent protein mutant (MPH-GFP) to Sup35 amyloids [246].*
Novel hybrid materials for diverse applications	*Amyloid peptide-polymer (PEG) conjugates as drug delivery systems [247]; β-Lg and gold platelets nanocomposite films with fluorescent, conductive and sensing properties [248];Graphene-amyloid based biodegradable nanocomposites [182]; MWCNTs and β-lg amyloid hybridised pH responsive hydrogels [249]; Temperature responsive poly(*N-*isopropylacrylamide) (PNiPAM) coated β-lg amyloid hydrogels [233]; Insulin amyloid-PVOH composite films with antibacterial properties [78, 181].*

1.9. Thesis objectives

Amyloid fibrils have the potential of making an enormous impact in future technologies because of the many advantages they provide as a protein nanomaterial. However, if amyloid PNFs are to be used for commercial applications, then methods will be required to utilise inexpensive, crude proteins.

This prompted a study to investigate synthesis of amyloid PNFs from crude crystallin proteins - crude extracts obtained from fish eye lenses of *Macruronus novaezelandie* (Hoki) or from bovine lenses, and β-lg which offer a cheap and readily available source of fibril-forming protein material. Successful immobilisation of industrially important enzymes onto PNFs can lead to the creation of cheap and readily available protein-based highly efficient matrices.

In the first instance this thesis focuses on considering practical issues, such as stability of crystallin PNFs in different solutions, over a range of pH and temperature, and to understand the behaviour of these fibrils under different conditions, so as to ensure that they can be effectively used as a versatile bionanoscaffold. Due to the association of amyloid fibrils with neurodegenerative diseases, the potential toxicity of crystallin PNFs was also investigated. The next section of this thesis involves characterisation of crystallin PNFs in order to evaluate the availability of functional groups on the surface of crystallin PNFs, which can be potentially used for functionalisation. Different immobilisation methods were employed to create a functional crystallin PNF scaffold.

Previously, different studies have used insulin amyloid PNFs for immobilising enzymes, however, it is for the first time that crystallin PNFs were investigated as a versatile nanoscaffold for active biocatalysts. Finally, the last part of this thesis focus on using developed functional amyloid PNFs in bionanotechnologies. Electrochemistry and surface-assembly experiments were performed to illustrate that amyloid PNFs can be potentially used for creating active bionanomaterials. Both crystallin and whey PNFs were also investigated for their suitability as a biomaterial with potential to be used as substrates for the attachment and proliferation of cells.

1.10. Thesis overview

Chapter 2 is an investigation into the stability of amyloid fibrils formed from the three protein sources used in this thesis: bovine insulin, WPI, and crude fish crystallins. The main aim of this research was to explore crystallin PNFs as a novel bionanomaterial, therefore, the stability and cytotoxicity study was primarily focused on the crystallin PNFs. The results from infrared microspectroscopy (IRM) study to understand the long-term structural integrity of crystallin PNFs is also described in this chapter.

Chapter 3 focuses on the characterisation of crystallin protein nanofibrils (PNFs) in terms of the availability of amino acid groups, which were then investigated for functionalising crystallin PNFs. Detailed information of the enzymes used in this thesis, and different immobilisation methods studied for creating functional crystallin PNFs is provided in this chapter.

Chapter 4 presents a versatile glutaradehyde-based crosslinking approach to obtain functional crystallin amyloid fibrils with potential applications in bionanotechnology. The results from stability and reusability studies performed on the functionalised crystallin PNFs are presented in this chapter.

Chapter 5 details an investigation into the use of amyloid fibrils:

(a) *in the construction of a biosensing element for glucose and lactose detection*. This entails the creation of PNF-based biosensing elements using GOX-, and β-gal-functionalised fibrils, electrochemical characterisation of amyloid fibrils, and the biosensing capabilities of an electrode modified with functionalised amyloid PNFs.

(b) *in the creation of surface-assembled PNFs as a novel nanomaterial.* Surfaces with amyloid PNFs attached *via* adsorption or covalent crosslinking were characterised by a range of methods. As a proof of principle, the surface-assembled amyloid PNFs nanoscaffold was functionalised with a biotechnologically important biocatalyst, leading to the generation of active bionanomaterials.

(c) *as a cellular growth scaffold*. PNFs were blended with other biocompatible fibrous protein - silk to obtain silk:PNF blend films, and studied for their suitability as a biomaterial with applications in tissue engineering. Blend films were characterised using scanning electron microscopy (SEM), optical transmittance, wet contact angle analysis, and *in vitro* degradation, and investigated further as a scaffold for cell growth and proliferation.

Chapter 6 summarises the major findings of this thesis, and future directions to be pursued from this work.

Chapter 7 outlines the experimental techniques used throughout this body of work.

1.11. References

[1] R. Schoevaart, M. Wolbers, M. Golubovic, M. Ottens, A. Kieboom, F. Van Rantwijk, L. Van der Wielen, R. Sheldon, Preparation, optimisation, and structures of cross-linked enzyme aggregates (CLEAs), *Biotechnology and Bioengineering*, 87 (2004) 754-762.

[2] J.A. Tao, R.J. Kazlauskas, *Biocatalysis for green chemistry and chemical process development*, John Wiley & Sons, New York, (2011).

[3] S. Li, X. Yang, S. Yang, M. Zhu, X. Wang, Technology prospecting on enzymes: Application, marketing and engineering, *Computational and Structural Biotechnology Journal*, 2 (2012) 1-11.

[4] S. Dewan, *Enzymes in industrial applications: Global markets, Market Research Report. Wellesley*, MA: BCC Research, (2011).

[5] R.A. Sheldon, Enzyme immobilisation: The quest for optimum performance, *Advanced Synthesis & Catalysis*, 349 (2007) 1289-1307.

[6] S. D'souza, Immobilised enzymes in bioprocess, *Current Science*, 77 (1999) 69-79.

[7] B. Krajewska, Application of chitin- and chitosan-based materials for enzyme immobilisation: A review, *Enzyme and Microbial Technology*, 35 (2004) 126-139.

[8] U. Bornscheuer, G. Huisman, R. Kazlauskas, S. Lutz, J. Moore, K. Robins, Engineering the third wave of biocatalysis, *Nature*, 485 (2012) 185-194.

[9] D. Fiedler, A. Thron, U. Soltmann, H. Böttcher, New packing materials for bioreactors based on coated and fibre-reinforced biocers, *Chemistry of Materials*, 16 (2004) 3040-3044.

[10] M.N. Kumar, A.-I. Gialleli, J.B. Masson, P. Kandylis, A. Bekatorou, A.A. Koutinas, M. Kanellaki, Lactic acid fermentation by cells immobilised on various porous cellulosic materials and their alginate/poly-lactic acid composites, *Bioresource Technology*, 165 (2014) 332-335.

[11] R.A. Sheldon, S. van Pelt, Enzyme immobilisation in biocatalysis: Why, what and how, *Chemical Society Reviews*, 42 (2013) 6223-6235.

[12] B.M. Brena, F. Batista-Viera, Immobilisation of enzymes, *Immobilisation of enzymes and cells*, (2006) 15-30.

[13] E. Katchalski-Katzir, Immobilised enzymes - learning from past successes and failures, *Trends in Biotechnology*, 11 (1993) 471-478.

[14] R. DiCosimo, J. McAuliffe, A.J. Poulose, G. Bohlmann, Industrial use of immobilised enzymes, *Chemical Society Reviews*, 42 (2013) 6437-6474.

[15] S. Nisha, S. Arun Karthick, N. Gobi, A review on methods, application and properties of immobilised enzyme, *Chemical Science Review and Letters*, 1 (2012) 148-155.

[16] A.A. Khan, M.A. Alzohairy, Recent advances and applications of immobilised enzyme technologies: A review, *Research Journal of Biological Sciences*, 5 (2010) 565-575.

[17] L. Cao, Introduction: *Carrier-bound immobilised enzymes: Principles, application and design*, Wiley-VCH: Weinhem, Germany, (2005) 1-52.

[18] S. Datta, L.R. Christena, Y.R.S. Rajaram, Enzyme immobilisation: An overview on techniques and support materials, *3 Biotech*, 3 (2013) 1-9.

[19] E.T. Hwang, M.B. Gu, Enzyme stabilisation by nano/microsised hybrid materials, *Engineering in Life Sciences*, 13 (2013) 49-61.

[20] N.R. Mohamad, N.H.C. Marzuki, N.A. Buang, F. Huyop, R.A. Wahab, An overview of technologies for immobilisation of enzymes and surface analysis techniques for immobilised enzymes, *Biotechnology & Biotechnological Equipment*, 29 (2015) 205-220.

[21] C. Spahn, S.D. Minteer, Enzyme immobilisation in biotechnology, *Recent Patents on Engineering*, 2 (2008) 195-200.

[22] N.R. Mohamad, N.A. Buang, N.A. Mahat, Y.Y. Lok, F. Huyop, H.Y. Aboul-Enein, R.A. Wahab, A facile enzymatic synthesis of geranyl propionate by physically adsorbed *Candida rugosa* lipase onto multi-walled carbon nanotubes, *Enzyme and microbial technology*, 72 (2015) 49-55.

[23] M.J. Moehlenbrock, S.D. Minteer, *Enzyme Stabilisation and Immobilisation*: *Methods and Protocols*, Human Press, New York, (2011), 1-7.

[24] T. Jesionowski, J. Zdarta, B. Krajewska, Enzyme immobilisation by adsorption: A review, *Adsorption*, 20 (2014) 801-821.

[25] M. Hartmann, X. Kostrov, Immobilisation of enzymes on porous silicas-benefits and challenges, *Chemical Society Reviews*, 42 (2013) 6277-6289.

[26] U. Hanefeld, L. Gardossi, E. Magner, Understanding enzyme immobilisation, *Chemical Society Reviews*, 38 (2009) 453-468.

[27] D. Avnir, T. Coradin, O. Lev, J. Livage, Recent bio-applications of sol–gel materials, *Journal of Materials Chemistry*, 16 (2006) 1013-1030.

[28] G.T. Hermanson, *Bioconjugate techniques*, Academic press, USA, (2013).

[29] J. Kim, J.W. Grate, P. Wang, Nanobiocatalysis and its potential applications, *Trends in Biotechnology*, 26 (2008) 639-646.

[30] K. Min, Y.J. Yoo, Recent progress in nanobiocatalysis for enzyme immobilisation and its application, *Biotechnology and Bioprocess Engineering*, 19 (2014) 553-567.

[31] P. Iqbal, J.A. Preece, P.M. Mendes, *Supramolecular Chemistry: From Molecules to Nanomaterials*, John & Wiley Sons, New York, (2012).

[32] M.J. Pitkethly, Nanomaterials–the driving force, *Materials Today*, 7 (2004) 20-29.

[33] B.D. Gates, Q. Xu, M. Stewart, D. Ryan, C.G. Willson, G.M. Whitesides, New approaches to nanofabrication: Molding, printing, and other techniques, *Chemical Reviews*, 105 (2005) 1171-1196.

[34] D. Mijatovic, J. Eijkel, A. Van Den Berg, Technologies for nanofluidic systems: Top-down vs. bottom-up - a review, *Lab on a Chip*, 5 (2005) 492-500.

[35] A. Biswas, I.S. Bayer, A.S. Biris, T. Wang, E. Dervishi, F. Faupel, Advances in top–down and bottom-up surface nanofabrication: Techniques, applications & future prospects, *Advances in Colloid and Interface Science*, 170 (2012) 2-27.

[36] R. Thiruvengadathan, V. Korampally, A. Ghosh, N. Chanda, K. Gangopadhyay, S. Gangopadhyay, Nanomaterial processing using self-assembly-bottom-up chemical and biological approaches, *Reports on Progress in Physics*, 76 (2013) 066501.

[37] D.E. Owens III, J.K. Eby, N.A. Peppas, Metal-Polymer Nanocomposites for Therapeutic and Imaging Applications, Abstract submitted at: *American Institute of Chemical Engineering Meeting, (2006).*

[38] G.G. Tibbetts, G.P. Meisner, C.H. Olk, Hydrogen storage capacity of carbon nanotubes, filaments, and vapor-grown fibres, *Carbon*, 39 (2001) 2291-2301.

[39] S.A. Ansari, Q. Husain, Potential applications of enzymes Immobilised on/in nano materials: A review, *Biotechnology Advances*, 30 (2012) 512-523.

[40] M.N. Gupta, M. Kaloti, M. Kapoor, K. Solanki, Nanomaterials as matrices for enzyme immobilisation, *Artificial Cells, Blood Substitutes, and Biotechnology*, 39 (2011) 98-109.

[41] M.L. Verma, M. Puri, C.J. Barrow, Recent trends in nanomaterials immobilised enzymes for biofuel production, *Critical Reviews in Biotechnology*, (2014) 1-12.

[42] C. Buzea, I.I. Pacheco, K. Robbie, Nanomaterials and nanoparticles: Sources and toxicity, *Biointerphases*, 2 (2007) MR17-MR71.

[43] W.H. De Jong, P.J. Borm, Drug delivery and nanoparticles: Applications and hazards, *International Journal of Nanomedicine*, 3 (2008) 133.

[44] J.P. Rao, K.E. Geckeler, Polymer nanoparticles: Preparation techniques and size-control parameters, *Progress in Polymer Science*, 36 (2011) 887-913.

[45] S.-H. Wu, C.-Y. Mou, H.-P. Lin, Synthesis of mesoporous silica nanoparticles, *Chemical Society Reviews*, 42 (2013) 3862-3875.

[46] S. Iravani, Green synthesis of metal nanoparticles using plants, *Green Chemistry*, 13 (2011) 2638-2650.

[47] H. Jia, G. Zhu, P. Wang, Catalytic behaviors of enzymes attached to nanoparticles: The effect of particle mobility, *Biotechnology and Bioengineering*, 84 (2003) 406-414.

[48] S.C. Tsang, C.H. Yu, X. Gao, K. Tam, Silica-encapsulated nanomagnetic particle as a new recoverable biocatalyst carrier, *The Journal of Physical Chemistry B*, 110 (2006) 16914-16922.

[49] C.R. Martin, P. Kohli, The emerging field of nanotube biotechnology, *Nature Reviews Drug Discovery*, 2 (2003) 29-37.

[50] W. Feng, P. Ji, Enzymes immobilised on carbon nanotubes, *Biotechnology Advances*, 29 (2011) 889-895.

[51] M.F. De Volder, S.H. Tawfick, R.H. Baughman, A.J. Hart, Carbon nanotubes: Present and future commercial applications, *Science*, 339 (2013) 535-539.

[52] A. Eatemadi, H. Daraee, H. Karimkhanloo, M. Kouhi, N. Zarghami, A. Akbarzadeh, M. Abasi, Y. Hanifehpour, S.W. Joo, Carbon nanotubes: Properties, synthesis, purification, and medical applications, *Nanoscale Research Letters*, 9 (2014) 1-13.

[53] H.M. Caicedo, L.A. Dempere, W. Vermerris, Template-mediated synthesis and bio-functionalisation of flexible lignin-based nanotubes and nanowires, *Nanotechnology*, 23 (2012) 105605.

[54] X. Gao, H. Matsui, Peptide-based nanotubes and their applications in bionanotechnology, *Advanced Materials*, 17 (2005) 2037-2050.

[55] I.W. Hamley, Peptide nanotubes, *Angewandte Chemie International Edition*, 53 (2014) 6866-6881.

[56] J. Castillo-León, K.B. Andersen, W.E. Svendsen, *Self-assembled peptide nanostructures for biomedical applications: Advantages and challenges*, INTECH Open Access Publisher, (2011).

[57] K.B. Andersen, J. Castillo-Leon, M. Hedström, W.E. Svendsen, Stability of diphenylalanine peptide nanotubes in solution, *Nanoscale*, 3 (2011) 994-998.

[58] J. Hulteen, A general template-based method for the preparation of nanomaterials, *J*ournal of Materials Chemistry, 7 (1997) 1075-1087.

[59] J.L. Perry, C.R. Martin, J.D. Stewart, Drug-Delivery strategies by using template-synthesised nanotubes, *Chemistry-A European Journal*, 17 (2011) 6296-6302.

[60] F. Wang, C. Guo, L.-r. Yang, C.-Z. Liu, Magnetic mesoporous silica nanoparticles: Fabrication and their laccase immobilisation performance, *Bioresource Technology*, 101 (2010) 8931-8935.

[61] Q. Husain, S.A. Ansari, F. Alam, A. Azam, Immobilisation of *Aspergillus oryzae* β galactosidase on zinc oxide nanoparticles *via* simple adsorption mechanism, *International Journal of Biological Macromolecules*, 49 (2011) 37-43.

[62] G.A. Petkova, K. Záruba, P. Žvátora, V. Král, Gold and silver nanoparticles for biomolecule immobilisation and enzymatic catalysis, *Nanoscale Research Letters*, 7 (2012) 1-10.

[63] J. Shi, J.C. Claussen, E.S. McLamore, A. ul Haque, D. Jaroch, A.R. Diggs, P. Calvo-Marzal, J.L. Rickus, D.M. Porterfield, A comparative study of enzyme immobilisation strategies for multi-walled carbon nanotube glucose biosensors, *Nanotechnology*, 22 (2011) 355502.

[64] C. Chao, J. Liu, J. Wang, Y. Zhang, B. Zhang, Y. Zhang, X. Xiang, R. Chen, Surface modification of halloysite nanotubes with dopamine for enzyme immobilisation, *ACS Applied Materials & Interfaces*, 5 (2013) 10559-10564.

[65] H. Wang, X. Zhao, S. Wang, S. Tao, N. Ai, Y. Wang, Fabrication of enzyme-immobilised halloysite nanotubes for affinity enrichment of lipase inhibitors from complex mixtures, *Journal of Chromatography A*, 1392 (2015) 20-27.

[66] L. Wang, L. Wei, Y. Chen, R. Jiang, Specific and reversible immobilisation of NADH oxidase on functionalised carbon nanotubes, *Journal of Biotechnology*, 150 (2010) 57-63.

[67] H. Ikemoto, Q. Chi, J. Ulstrup, Stability and catalytic kinetics of horseradish peroxidase confined in nanoporous SBA-15, *Journal of Physical Chemistry C*, 114 (2010) 16174-16180.

[68] A. Buthe, *Entrapment of enzymes in nanoporous sol–gels*, Springer US (2011), 223-237.

[69] M. Kjellander, K. Götz, J. Liljeruhm, M. Boman, G. Johansson, Steady-state generation of hydrogen peroxide: kinetics and stability of alcohol oxidase immobilised on nanoporous alumina, *Biotechnology Letters*, 35 (2013) 585-590.

[70] F.-K. Shieh, S.-C. Wang, C.-I. Yen, C.-C. Wu, S. Dutta, L.-Y. Chou, J.V. Morabito, P. Hu, M.-H. Hsu, K.C.-W. Wu, Imparting functionality to biocatalysts *via* embedding enzymes into nanoporous materials by a *de novo* approach: Size-selective sheltering of catalase in metal–organic framework microcrystals, *Journal of the American Chemical Society*, 137 (2015) 4276-4279.

[71] W.J. Cloete, C. Adriaanse, P. Swart, B. Klumperman, Facile immobilisation of enzymes on electrospun poly (styrene-alt-maleic anhydride) nanofibres, *Polymer Chemistry*, 2 (2011) 1479-1481.

[72] L. Jin, Y. Li, X. Ren, J. Lee, Immobilisation of lactase onto various polymer nanofibres for enzyme stabilisation and recycling, *Journal of Microbiology and Biotechnology*, (2015).

[73] L. Sasso, S. Suei, L. Domigan, J. Healy, V. Nock, M. Williams, J. Gerrard, Versatile multi-functionalisation of protein nanofibrils for biosensor applications, *Nanoscale*, 6 (2014) 1629-1634.

[74] J.K. Raynes, F.G. Pearce, S.J. Meade, J.A. Gerrard, Immobilisation of organophosphate hydrolase on an amyloid fibril nanoscaffold: towards bioremediation and chemical detoxification, *Biotechnology Progress*, 27 (2011) 360-367.

[75] M.J. Khan, Q. Husain, S.A. Ansari, Polyaniline-assisted silver nanoparticles: A novel support for the immobilisation of α-amylase, *Applied Microbiology and Biotechnology*, 97 (2013) 1513-1522.

[76] R. Zhai, B. Zhang, Y. Wan, C. Li, J. Wang, J. Liu, Chitosan–halloysite hybrid-nanotubes: Horseradish peroxidase immobilisation and applications in phenol removal, *Chemical Engineering Journal*, 214 (2013) 304-309.

[77] U. Lad, G.M. Kale, R. Bryaskova, Glucose oxidase encapsulated polyvinyl alcohol–silica hybrid films for an electrochemical glucose sensing electrode, *Analytical Chemistry*, 85 (2013) 6349-6355.

[78] S.P. Rao, S.J. Meade, J.P. Healy, K.H. Sutton, N.G. Larsen, M.P. Staiger, J.A. Gerrard, Amyloid fibrils as functionalisable components of nanocomposite materials, *Biotechnology Progress*, 28 (2012) 248-256.

[79] E. Mabrouk, D. Cuvelier, F. Brochard-Wyart, P. Nassoy, M.-H. Li, Bursting of sensitive polymersomes induced by curling, *Proceedings of the National Academy of Sciences of the United States of America*, 106 (2009) 7294-7298.

[80] P. Kohli, C. Martin, Template-synthesised nanotubes for biotechnology and biomedical applications, *Journal of Drug Delivery Science and Technology*, 15 (2005) 49-57.

[81] J. Martín, J. Maiz, J. Sacristan, C. Mijangos, Tailored polymer-based nanorods and nanotubes by" template synthesis": From preparation to applications, *Polymer*, 53 (2012) 1149-1166.

[82] Q. Xu, *Nanoporous materials: Synthesis and applications*, 4, 4 World Scientific, (2013).

[83] G.Q. Lu, X.S. Zhao, T.K. Wei, *Nanoporous materials: Science and engineering*, Imperial College Press, (2004).

[84] R.E. Morris, P.S. Wheatley, Gas storage in nanoporous materials, *Angewandte Chemie International Edition*, 47 (2008) 4966-4981.

[85] J. Jiang, R. Babarao, Z. Hu, Molecular simulations for energy, environmental and pharmaceutical applications of nanoporous materials: From zeolites, metal–organic frameworks to protein crystals, *Chemical Society Reviews*, 40 (2011) 3599-3612.

[86] S. Sotiropoulou, V. Vamvakaki, N.A. Chaniotakis, Stabilisation of enzymes in nanoporous materials for biosensor applications, Biosensors and Bioelectronics, 20 (2005) 1674-1679.

[87] K.J. Stine, K. Jefferson, O.V. Shulga, Nanoporous gold for enzyme immobilisation, Enzyme Stabilisation and Immobilisation, Springer2011, pp. 67-83.

[88] F.K. Ko, Y. Wan, Introduction to nanofibre materials, Cambridge University Press2014.

[89] D. Wouters, U.S. Schubert, Nanolithography and Nanochemistry: Probe-Related Patterning Techniques and Chemical Modification for Nanometer-Sized Devices, Angewandte Chemie International Edition, 43 (2004) 2480-2495.

[90] J. Zhao, W. Han, M. Tu, S. Huan, R. Zeng, H. Wu, Z. Cha, C. Zhou, Preparation and properties of biomimetic porous nanofibrous poly (l-lactide) scaffold with chitosan nanofibre network by a dual thermally induced phase separation technique, *Materials Science and Engineering: C*, 32 (2012) 1496-1502.

[91] F. Jiang, S. Han, Y.-L. Hsieh, Controlled defibrillation of rice straw cellulose and self-assembly of cellulose nanofibrils into highly crystalline fibrous materials, *RSC Advances*, 3 (2013) 12366-12375.

[92] C. Luo, S.D. Stoyanov, E. Stride, E. Pelan, M. Edirisinghe, Electrospinning versus fibre production methods: From specifics to technological convergence, *Chemical Society Reviews*, 41 (2012) 4708-4735.

[93] X. Shi, W. Zhou, D. Ma, Q. Ma, D. Bridges, Y. Ma, A. Hu, Electrospinning of nanofibres and their applications for energy devices, *Journal of Nanomaterials*, 2015 (2015).

[94] D.B. Khadka, D.T. Haynie, Protein-and peptide-based electrospun nanofibres in medical biomaterials, *Nanomedicine: Nanotechnology, Biology and Medicine*, 8 (2012) 1242-1262.

[95] S. Mankar, A. Anoop, S. Sen, S.K. Maji, Nanomaterials: Amyloids reflect their brighter side, *Nano Reviews*, 2 (2011).

[96] V. Polshettiwar, R. Luque, A. Fihri, H. Zhu, M. Bouhrara, J.-M. Basset, Magnetically recoverable nanocatalysts, *Chemical Reviews*, 111 (2011) 3036-3075.

[97] O. Parlak, A. Tiwari, A.P. Turner, A. Tiwari, Template-directed hierarchical self-assembly of graphene based hybrid structure for electrochemical biosensing, *Biosensors and Bioelectronics*, 49 (2013) 53-62.

[98] D. Aili, M.M. Stevens, Bioresponsive peptide–inorganic hybrid nanomaterials, *Chemical Society Reviews*, 39 (2010) 3358-3370.

[99] F. Chiti, C.M. Dobson, Protein misfolding, functional amyloid, and human disease, *Annual Review of Biochemistry*, 75 (2006) 333-366.

[100] S.H. Waterhouse, J.A. Gerrard, Amyloid fibrils in Bionanotechnology, *Australian Journal of Chemistry*, 57 (2004) 519-523.

[101] R.A. Kyle, Amyloidosis: A convoluted story, *British Journal of Haematology*, 114 (2001) 529-538.

[102] J.D. Sipe, A.S. Cohen, Review: History of the amyloid fibril, *Journal of Structural Biology*, 130 (2000) 88-98.

[103] T.P. Knowles, M. Vendruscolo, C.M. Dobson, The amyloid state and its association with protein misfolding diseases, *Nature Reviews Molecular Cell Biology*, 15 (2014) 384-396.

[104] D. Eisenberg, M. Jucker, The amyloid state of proteins in human diseases, *Cell*, 148 (2012) 1188-1203.

[105] S. Jarvis, A. Mostaert, *The functional fold: Amyloid structures in nature*, CRC Press, (2012).

[106] D.M. Fowler, A.V. Koulov, W.E. Balch, J.W. Kelly, Functional amyloid–from bacteria to humans, *Trends in Biochemical Sciences*, 32 (2007) 217-224.

[107] L.P. Blanco, M.L. Evans, D.R. Smith, M.P. Badtke, M.R. Chapman, Diversity, biogenesis and function of microbial amyloids, *Trends in Microbiology*, 20 (2012) 66-73.

[108] M.F. Gebbink, D. Claessen, B. Bouma, L. Dijkhuizen, H.A. Wösten, Amyloids-a functional coat for microorganisms, *Nature Reviews Microbiology*, 3 (2005) 333-341.

[109] D.M. Fowler, A.V. Koulov, C. Alory-Jost, M.S. Marks, W.E. Balch, J.W. Kelly, Functional amyloid formation within mammalian tissue, *PLoS Biology*, 4 (2006) 100.

[110] J.F. Berson, A.C. Theos, D.C. Harper, D. Tenza, G. Raposo, M.S. Marks, Proprotein convertase cleavage liberates a fibrillogenic fragment of a resident glycoprotein to initiate melanosome biogenesis, *Journal of Cell Biology*, 161 (2003) 521-533.

[111] P. Larsen, J.L. Nielsen, M.S. Dueholm, R. Wetzel, D. Otzen, P.H. Nielsen, Amyloid adhesins are abundant in natural biofilms, *Environmental microbiology*, 9 (2007) 3077-3090.

[112] S.K. Maji, M.H. Perrin, M.R. Sawaya, S. Jessberger, K. Vadodaria, R.A. Rissman, P.S. Singru, K.P.R. Nilsson, R. Simon, D. Schubert, Functional amyloids as natural storage of peptide hormones in pituitary secretory granules, *Science*, 325 (2009) 328-332.

[113] Q. Zhao, Nature of protein dynamics and thermodynamics, *Reviews in Theoretical Science*, 1 (2013) 83-101.

[114] A.L. Fink, Protein aggregation: Folding aggregates, inclusion bodies and amyloid, *Folding and Design*, 3 (1998) R9-R23.

[115] V.N. Uversky, J. Li, A.L. Fink, Evidence for a partially folded intermediate in α-synuclein fibril formation, *Journal of Biological Chemistry*, 276 (2001) 10737-10744.

[116] Y. Wang, M. Sarkar, A.E. Smith, A.S. Krois, G.J. Pielak, Macromolecular crowding and protein stability, *Journal of the American Chemical Society*, 134 (2012) 16614-16618.

[117] T.R. Jahn, S.E. Radford, Folding versus aggregation: Polypeptide conformations on competing pathways, *Archives of Biochemistry and Biophysics*, 469 (2008) 100-117.

[118] C. Frieden, Protein aggregation processes: In search of the mechanism, *Protein Science*, 16 (2007) 2334-2344.

[119] A.M. Morris, M.A. Watzky, R.G. Finke, Protein aggregation kinetics, mechanism, and curve-fitting: A review of the literature, *Biochimica et Biophysica Acta (BBA)-Proteins and Proteomics*, 1794 (2009) 375-397.

[120] S.I. Cohen, M. Vendruscolo, C.M. Dobson, T.P. Knowles, From macroscopic measurements to microscopic mechanisms of protein aggregation, *Journal of Molecular Biology*, 421 (2012) 160-171.

[121] F. Chiti, P. Webster, N. Taddei, A. Clark, M. Stefani, G. Ramponi, C.M. Dobson, Designing conditions for in vitro formation of amyloid protofilaments and fibrils, *Proceedings of the National Academy of Sciences of the United States of America*, 96 (1999) 3590-3594.

[122] J.-C. Rochet, P.T. Lansbury, Amyloid fibrillogenesis: Themes and variations, *Current Opinion in Structural Biology*, 10 (2000) 60-68.

[123] S.L. Gras, Amyloid Fibrils: From Disease to Design. New biomaterial applications for self-assembling cross-β fibrils, *Australian Journal of Chemistry*, 60 (2007) 333-342.

[124] J. Tyedmers, A. Mogk, B. Bukau, Cellular strategies for controlling protein aggregation, *Nature Reviews Molecular Cell Biology*, 11 (2010) 777-788.

[125] Y. Liang, D.G. Lynn, K.M. Berland, Direct observation of nucleation and growth in amyloid self-assembly, *Journal of the American Chemical Society*, 132 (2010) 6306-6308.

[126] H. Ecroyd, T. Koudelka, D.C. Thorn, D.M. Williams, G. Devlin, P. Hoffmann, J.A. Carver, Dissociation from the oligomeric state is the rate-limiting step in fibril formation by κ-casein, *Journal of Biological Chemistry*, 283 (2008) 9012-9022.

[127] L. Nielsen, R. Khurana, A. Coats, S. Frokjaer, J. Brange, S. Vyas, V.N. Uversky, A.L. Fink, Effect of environmental factors on the kinetics of insulin fibril formation: Elucidation of the molecular mechanism, *Biochemistry*, 40 (2001) 6036-6046.

[128] C.-C. Lee, A. Nayak, A. Sethuraman, G. Belfort, G.J. McRae, A three-stage kinetic model of amyloid fibrillation, *Biophysical Journal*, 92 (2007) 3448-3458.

[129] J.T. Jarrett, P.T. Lansbury, Seeding "one-dimensional crystallisation" of amyloid: A pathogenic mechanism in Alzheimer's disease and scrapie?, *Cell*, 73 (1993) 1055-1058.

[130] J.D. Harper, C.M. Lieber, P.T. Lansbury, Atomic force microscopic imaging of seeded fibril formation and fibril branching by the Alzheimer's disease amyloid-β protein, *Chemistry & Biology*, 4 (1997) 951-959.

[131] M. Fändrich, Oligomeric intermediates in amyloid formation: Structure determination and mechanisms of toxicity, *Journal of Molecular Biology*, 421 (2012) 427-440.

[132] M.R. Wilson, J.J. Yerbury, S. Poon, Potential roles of abundant extracellular chaperones in the control of amyloid formation and toxicity, *Molecular Biosystems*, 4 (2008) 42-52.

[133] C. Iannuzzi, R. Maritato, G. Irace, I. Sirangelo, Misfolding and amyloid aggregation of apomyoglobin, *International Journal of Molecular Sciences*, 14 (2013) 14287-14300.

[134] M.R. Krebs, D.K. Wilkins, E.W. Chung, M.C. Pitkeathly, A.K. Chamberlain, J. Zurdo, C.V. Robinson, C.M. Dobson, Formation and seeding of amyloid fibrils from wild-type hen lysozyme and a peptide fragment from the β-domain, *Journal of Molecular Biology*, 300 (2000) 541-549.

[135] M. Mahmoudi, F. Quinlan-Pluck, M.P. Monopoli, S. Sheibani, H. Vali, K.A. Dawson, I. Lynch, Influence of the physiochemical properties of superparamagnetic iron oxide nanoparticles on amyloid β protein fibrillation in solution, *ACS Chemical Neuroscience*, 4 (2013) 475-485.

[136] R. Vácha, S. Linse, M. Lund, Surface effects on aggregation kinetics of amyloidogenic peptides, *Journal of the American Chemical Society*, 136 (2014) 11776-11782.

[137] E.B. Dunkelberger, L.E. Buchanan, P. Marek, P. Cao, D.P. Raleigh, M.T. Zanni, Deamidation accelerates amyloid formation and alters amylin fibre structure, *Journal of the American Chemical Society*, 134 (2012) 12658-12667.

[138] D. Morshedi, A. Ebrahim-Habibi, A.A. Moosavi-Movahedi, M. Nemat-Gorgani, Chemical modification of lysine residues in lysozyme may dramatically influence its amyloid fibrillation, *Biochimica et Biophysica Acta (BBA)-Proteins and Proteomics*, 1804 (2010) 714-722.

[139] A. Tiiman, A. Noormägi, M. Friedemann, J. Krishtal, P. Palumaa, V. Tõugu, Effect of agitation on the peptide fibrillisation: Alzheimer's amyloid-β peptide 1-42 but not amylin and insulin fibrils can grow under quiescent conditions, *Journal of Peptide Science*, 19 (2013) 386-391.

[140] G.-B. Bhak, Y.-J. Choe, S.-R. Paik, Mechanism of amyloidogenesis: Nucleation-dependent fibrillation versus double-concerted fibrillation, *BMB Reports*, 42 (2009) 541-551.

[141] J. Zhang, M. Muthukumar, Simulations of nucleation and elongation of amyloid fibrils, *Journal of Chemical Physics*, 130 (2009) 035102.

[142] W.-F. Xue, S.W. Homans, S.E. Radford, Systematic analysis of nucleation-dependent polymerisation reveals new insights into the mechanism of amyloid self-assembly, *Proceedings of the National Academy of Sciences of the United States of America*, 105 (2008) 8926-8931.

[143] M. Sunde, L.C. Serpell, M. Bartlam, P.E. Fraser, M.B. Pepys, C.C. Blake, Common core structure of amyloid fibrils by synchrotron X-ray diffraction, *Journal of Molecular Biology*, 273 (1997) 729-739.

[144] M. Fändrich, On the structural definition of amyloid fibrils and other polypeptide aggregates, *Cellular and Molecular Life Sciences*, 64 (2007) 2066-2078.

[145] L.C. Serpell, Alzheimer's amyloid fibrils: Structure and assembly, *Biochimica et Biophysica Acta (BBA)-Molecular Basis of Disease*, 1502 (2000) 16-30.

[146] A.E. Langkilde, K.L. Morris, L.C. Serpell, D.I. Svergun, B. Vestergaard, The architecture of amyloid-like peptide fibrils revealed by X-ray scattering, diffraction and electron microscopy, *Biological Crystallography*, 71 (2015).

[147] B. Vestergaard, M. Groenning, M. Roessle, J.S. Kastrup, M. Van De Weert, J.M. Flink, S. Frokjaer, M. Gajhede, D.I. Svergun, A helical structural nucleus is the primary elongating unit of insulin amyloid fibrils, *PLoS Biology*, 5 (2007) e134.

[148] J. Adamcik, R. Mezzenga, Study of amyloid fibrils *via* atomic force microscopy, *Current Opinion in Colloid & Interface Science*, 17 (2012) 369-376.

[149] L.R. Volpatti, M. Vendruscolo, C.M. Dobson, T.P. Knowles, A clear view of polymorphism, twist, and chirality in amyloid fibril formation, *ACS Nano*, 7 (2013) 10443-10448.

[150] E. Takai, G. Ohashi, R. Ueki, Y. Yamada, J.-I. Fujita, K. Shiraki, Scanning electron microscope imaging of amyloid fibrils, *American Journal of Biochemistry & Biotechnology*, 10 (2014) 31.

[151] J.L. Jimenez, J.I. Guijarro, E. Orlova, J. Zurdo, C.M. Dobson, M. Sunde, H.R. Saibil, Cryo-electron microscopy structure of an SH3 amyloid fibril and model of the molecular packing, *The EMBO Journal*, 18 (1999) 815-821.

[152] R. Tycko, Solid state NMR studies of amyloid fibril structure, *Annual Review of Physical Chemistry*, 62 (2011) 279.

[153] G. Comellas, C.M. Rienstra, Protein structure determination by magic-angle spinning solid-state NMR, and insights into the formation, structure, and stability of amyloid fibrils, *Annual Review of Biophysics*, 42 (2013) 515-536.

[154] M.R. Nilsson, Techniques to study amyloid fibril formation *in vitro*, *Methods*, 34 (2004) 151-160.

[155] S.G. Bolder, L.M. Sagis, P. Venema, E. van der Linden, Thioflavin T and birefringence assays to determine the conversion of proteins into fibrils, *Langmuir*, 23 (2007) 4144-4147.

[156] J.L. Jiménez, E.J. Nettleton, M. Bouchard, C.V. Robinson, C.M. Dobson, H.R. Saibil, The protofilament structure of insulin amyloid fibrils, *Proceedings of the National Academy of Sciences of the United States of America*, 99 (2002) 9196-9201.

[157] J. Adamcik, J.-M. Jung, J. Flakowski, P. De Los Rios, G. Dietler, R. Mezzenga, Understanding amyloid aggregation by statistical analysis of atomic force microscopy images, *Nature Nanotechnology*, 5 (2010) 423-428.

[158] J. Adamcik, R. Mezzenga, Proteins fibrils from a polymer physics perspective, *Macromolecules*, 45 (2011) 1137-1150.

[159] R. Khurana, C. Coleman, C. Ionescu-Zanetti, S.A. Carter, V. Krishna, R.K. Grover, R. Roy, S. Singh, Mechanism of Thioflavin T binding to amyloid fibrils, *Journal of Structural Biology*, 151 (2005) 229-238.

[160] M. Biancalana, S. Koide, Molecular mechanism of Thioflavin T binding to amyloid fibrils, *Biochimica et Biophysica Acta (BBA)-Proteins and Proteomics*, 1804 (2010) 1405-1412.

[161] E.V. Hackl, J. Darkwah, G. Smith, I. Ermolina, Effect of acidic and basic pH on Thioflavin T absorbance and fluorescence, *European Biophysics Journal*, 44 (2015) 249-261.

[162] A.I. Sulatskaya, I.M. Kuznetsova, K.K. Turoverov, Interaction of thioflavin T with amyloid fibrils: Stoichiometry and affinity of dye binding, absorption spectra of bound dye, *Journal of Physical Chemistry B*, 115 (2011) 11519-11524.

[163] M. Groenning, Binding mode of Thioflavin T and other molecular probes in the context of amyloid fibrils-current status, *Journal of Chemical Biology*, 3 (2010) 1-18.

[164] R. Sabaté, I. Lascu, S.J. Saupe, On the binding of Thioflavin T to HET-s amyloid fibrils assembled at pH 2, *Journal of Structural Biology*, 162 (2008) 387-396.

[165] M.R. Krebs, E.H. Bromley, A.M. Donald, The binding of Thioflavin T to amyloid fibrils: localisation and implications, *Journal of Structural Biology*, 149 (2005) 30-37.

[166] E. Voropai, M. Samtsov, K. Kaplevskii, A. Maskevich, V. Stepuro, O. Povarova, I. Kuznetsova, K. Turoverov, A. Fink, V. Uverskii, Spectral properties of Thioflavin T and its complexes with amyloid fibrils, *Journal of Applied Spectroscopy*, 70 (2003) 868-874.

[167] M. Groenning, L. Olsen, M. van de Weert, J.M. Flink, S. Frokjaer, F.S. Jørgensen, Study on the binding of Thioflavin T to β-sheet-rich and non-β-sheet cavities, *Journal of Structural Biology*, 158 (2007) 358-369.

[168] S.L. Gras, L.J. Waddington, K.N. Goldie, Transmission electron microscopy of amyloid fibrils, Protein Folding, Misfolding, and Disease, *Methods and Protocols*, (2011) 197-214.

[169] C.S. Goldsbury, G.J. Cooper, K.N. Goldie, S.A. Müller, E.L. Saafi, W. Gruijters, M.P. Misur, A. Engel, U. Aebi, J. Kistler, Polymorphic fibrillar assembly of human amylin, *Journal of Structural Biology*, 119 (1997) 17-27.

[170] Y. Jiang, C. Li, X. Nguyen, S. Muzammil, E. Towers, J. Gabrielson, L. Narhi, Qualification of FTIR spectroscopic method for protein secondary structural analysis, *Journal of Pharmaceutical Sciences*, 100 (2011) 4631-4641.

[171] F.J. Walther, R. David-Cu, C. Leung, R. Bruni, J. Hernández-Juviel, L.M. Gordon, A.J. Waring, A synthetic segment of surfactant protein A: Structure, *in vitro* surface activity, and *in vivo* efficacy, *Pediatric Research*, 39 (1996) 938-946.

[172] M. Bouchard, J. Zurdo, E.J. Nettleton, C.M. Dobson, C.V. Robinson, Formation of insulin amyloid fibrils followed by FTIR simultaneously with CD and electron microscopy, *Protein Science*, 9 (2000) 1960-1967.

[173] R. Sarroukh, E. Goormaghtigh, J.-M. Ruysschaert, V. Raussens, ATR-FTIR: A "rejuvenated" tool to investigate amyloid proteins, *Biochimica et Biophysica Acta (BBA)-Biomembranes*, 1828 (2013) 2328-2338.

[174] P. Taboada, S. Barbosa, E. Castro, V. Mosquera, Amyloid fibril formation and other aggregate species formed by human serum albumin association, *Journal of Physical Chemistry B*, 110 (2006) 20733-20736.

[175] A. Cao, D. Hu, L. Lai, Formation of amyloid fibrils from fully reduced hen egg white lysozyme, *Protein Science*, 13 (2004) 319-324.

[176] F.G. Pearce, S.H. Mackintosh, J.A. Gerrard, Formation of amyloid-like fibrils by ovalbumin and related proteins under conditions relevant to food processing, *Journal of Agricultural and Food Chemistry*, 55 (2007) 318-322.

[177] D. Hamada, C.M. Dobson, A kinetic study of β-lactoglobulin amyloid fibril formation promoted by urea, *Protein Science*, 11 (2002) 2417-2426.

[178] C. Akkermans, A.J. van der Goot, P. Venema, E. van der Linden, R.M. Boom, Formation of fibrillar whey protein aggregates: Influence of heat and shear treatment, and resulting rheology, *Food Hydrocolloids*, 22 (2008) 1315-1325.

[179] J. Healy, K. Wong, E.B. Sawyer, C. Roux, L. Domigan, S.L. Gras, M. Sunde, N.G. Larsen, J. Gerrard, M. Vasudevamurthy, Polymorphism and higher order structures of protein nanofibres from crude mixtures of fish lens crystallins: Toward useful materials, *Biopolymers*, 97 (2012) 595-606.

[180] S.H. Mackintosh, S.J. Meade, J.P. Healy, K.H. Sutton, N.G. Larsen, A.M. Squires, J.A. Gerrard, Wheat glutenin proteins assemble into a nanostructure with unusual structural features, *Journal of Cereal Science*, 49 (2009) 157-162.

[181] S.M. Pilkington, S.J. Roberts, S.J. Meade, J.A. Gerrard, Amyloid fibrils as a nanoscaffold for enzyme immobilisation, *Biotechnology Progress*, 26 (2010) 93-100.

[182] C. Li, J. Adamcik, R. Mezzenga, Biodegradable nanocomposites of amyloid fibrils and graphene with shape-memory and enzyme-sensing properties, *Nature Nanotechnology*, 7 (2012) 421-427.

[183] T.P. Knowles, T.W. Oppenheim, A.K. Buell, D.Y. Chirgadze, M.E. Welland, Nanostructured films from hierarchical self-assembly of amyloidogenic proteins, *Nature Nanotechnology*, 5 (2010) 204-207.

[184] B. Dai, D. Li, W. Xi, F. Luo, X. Zhang, M. Zou, M. Cao, J. Hu, W. Wang, G. Wei, Tunable assembly of amyloid-forming peptides into nanosheets as a retrovirus carrier, *Proceedings of the National Academy of Sciences of the United States of America*, 112 (2015) 2996-3001.

[185] C.A. Hauser, S. Maurer-Stroh, I.C. Martins, Amyloid-based nanosensors and nanodevices, *Chemical Society Reviews*, 43 (2014) 5326-5345.

[186] M.R. Nilsson, C.M. Dobson, Chemical modification of insulin in amyloid fibrils, *Protein science*, 12 (2003) 2637-2641.

[187] C. Ha, C.B. Park, Template-directed self-assembly and growth of insulin amyloid fibrils, *Biotechnology and Bioengineering*, 90 (2005) 848-855.

[188] J.L. Whittingham, D.J. Scott, K. Chance, A. Wilson, J. Finch, J. Brange, G.G. Dodson, Insulin at pH 2: structural analysis of the conditions promoting insulin fibre formation, *Journal of Molecular Biology*, 318 (2002) 479-490.

[189] J. Brange, L. Langkjœr, *Stability and Characterisation of Protein and Peptide Drugs*, Springer, (1993), 315-350.

[190] J.P. Mayer, F. Zhang, R.D. DiMarchi, Insulin structure and function, *Peptide Science*, 88 (2007) 687-713.

[191] J. Brange, L. Andersen, E.D. Laursen, G. Meyn, E. Rasmussen, Toward understanding insulin fibrillation, *Journal of Pharmaceutical Sciences*, 86 (1997) 517-525.

[192] L. Zhang, N. Li, F. Gao, L. Hou, Z. Xu, Insulin amyloid fibrils: An excellent platform for controlled synthesis of ultrathin superlong platinum nanowires with high electrocatalytic activity, *Journal of the American Chemical Society*, 134 (2012) 11326-11329.

[193] L.J. Domigan, J.P. Healy, S.J. Meade, R.J. Blaikie, J.A. Gerrard, Controlling the dimensions of amyloid fibrils: Toward homogenous components for bionanotechnology, *Biopolymers*, 97 (2012) 123-133.

[194] Q. Tang, N. Solin, J. Lu, O. Inganäs, Hybrid bioinorganic insulin amyloid fibrils, *Chemical Communications*, 46 (2010) 4157-4159.

[195] Q.-X. Hua, M.A. Weiss, Mechanism of Insulin Fibrillation. The structure of insulin under amyloidogenic conditions resembles a protein-folding intermediate, *Journal of Biological Chemistry*, 279 (2004) 21449-21460.

[196] S. Meehan, Y. Berry, B. Luisi, C.M. Dobson, J.A. Carver, C.E. MacPhee, Amyloid fibril formation by lens crystallin proteins and its implications for cataract formation, *Journal of Biological Chemistry*, 279 (2004) 3413-3419.

[197] J. Harding, *Cataract: Biochemistry, epidemiology and pharmacology*, Chapman and Hall London, (2003).

[198] H. Bloemendal, W. de Jong, R. Jaenicke, N.H. Lubsen, C. Slingsby, A. Tardieu, Ageing and vision: Structure, stability and function of lens crystallins, *Progress in Biophysics and Molecular Biology*, 86 (2004) 407-485.

[199] W.C. Boelens, W.W. Jong, α-Crystallins, versatile stress-proteins, *Molecular Biology Reports*, 21 (1995) 75-80.

[200] M. Garvey, S. Gras, S. Meehan, S. Meade, J. Carver, J. Gerrard, Protein nanofibres of defined morphology prepared from mixtures of crude crystallins, *International Journal of Nanotechnology*, 6 (2009) 258-273.

[201] H. Ecroyd, J.A. Carver, Crystallin proteins and amyloid fibrils, *Cellular and Molecular Life Sciences*, 66 (2009) 62-81.

[202] K.Y. Wong, *Scaling up the production of protein nanofibres*, Master's Thesis, University of Canterbury, (2011).

[203] T. Nicolai, D. Durand, Controlled food protein aggregation for new functionality, *Current Opinion in Colloid & Interface Science*, 18 (2013) 249-256.

[204] F. Guyomarc'h, M.-H. Famelart, G. Henry, M. Gulzar, J. Leonil, P. Hamon, S. Bouhallab, T. Croguennec, Current ways to modify the structure of whey proteins for specific functionalities - a review, *Dairy Science & Technology*, (2014) 1-20.

[205] C. Morr, E. Ha, Whey protein concentrates and isolates: Processing and functional properties, *Critical Reviews in Food Science & Nutrition*, 33 (1993) 431-476.

[206] S.G. Bolder, H. Hendrickx, L.M. Sagis, E. van der Linden, Fibril assemblies in aqueous whey protein mixtures, *Journal of Agricultural and Food Chemistry*, 54 (2006) 4229-4234.

[207] S. Uhrínová, M.H. Smith, G.B. Jameson, D. Uhrín, L. Sawyer, P.N. Barlow, Structural changes accompanying pH-induced dissociation of the β-lactoglobulin dimer, *Biochemistry*, 39 (2000) 3565-3574.

[208] L. Sawyer, β-Lactoglobulin, *Advanced dairy chemistry*, Springer US, (2013) 211-259.

[209] V. Vetri, V. Militello, Thermal induced conformational changes involved in the aggregation pathways of beta-lactoglobulin, *Biophysical Chemistry*, 113 (2005) 83-91.

[210] Y.L. Xiong, K.A. Dawson, L. Wan, Thermal aggregation of β-lactoglobulin: Effect of pH, ionic environment, and thiol reagent, *Journal of Dairy Science*, 76 (1993) 70-77.

[211] L.N. Arnaudov, R. de Vries, H. Ippel, C.P. van Mierlo, Multiple steps during the formation of β-lactoglobulin fibrils, *Biomacromolecules*, 4 (2003) 1614-1622.

[212] W.S. Gosal, A.H. Clark, P.D. Pudney, S.B. Ross-Murphy, Novel amyloid fibrillar networks derived from a globular protein: β-lactoglobulin, *Langmuir*, 18 (2002) 7174-7181.

[213] G.M. Kavanagh, A.H. Clark, S.B. Ross-Murphy, Heat-induced gelation of globular proteins: Gelation kinetics of low pH β-lactoglobulin gels, *Langmuir*, 16 (2000) 9584-9594.

[214] S.M. Loveday, J. Su, M.A. Rao, S.G. Anema, H. Singh, Whey protein nanofibrils: Kinetic, rheological and morphological effects of group IA and IIA cations, *International Dairy Journal*, 26 (2012) 133-140.

[215] S.M. Loveday, J. Su, M.A. Rao, S.G. Anema, H. Singh, Whey protein nanofibrils: The environment–morphology–functionality relationship in lyophilisation, rehydration, and seeding, *Journal of Agricultural and Food Chemistry*, 60 (2012) 5229-5236.

[216] S. Loveday, X. Wang, M. Rao, S. Anema, H. Singh, β-Lactoglobulin nanofibrils: Effect of temperature on fibril formation kinetics, fibril morphology and the rheological properties of fibril dispersions, *Food Hydrocolloids*, 27 (2012) 242-249.

[217] S. Loveday, X. Wang, M. Rao, S. Anema, L. Creamer, H. Singh, Tuning the properties of β-lactoglobulin nanofibrils with pH, NaCl and $CaCl_2$, *International Dairy Journal*, 20 (2010) 571-579.

[218] S.P. Rao, *Amyloid fibrils in bionanomaterials*, PhD Thesis, University of Canterbury, (2008).

[219] R.N. Rambaran, L.C. Serpell, Amyloid fibrils, *Prion*, (2008), 112-117.

[220] P. Taboada, S. Barbosa, J. Juárez, M.A. Meda, V. Mosquera, Amyloid-Like Fibrils: Origin, structure, properties, and potential technological applications, *Proteins in Solution and at Interfaces: Methods and Applications in Biotechnology and Materials Science*, (2013) 233-282.

[221] I. Cherny, E. Gazit, Amyloids: Not only pathological agents but also ordered nanomaterials, *Angewandte Chemie International Edition*, 47 (2008) 4062-4069.

[222] M. Ramírez-Alvarado, J.S. Merkel, L. Regan, A systematic exploration of the influence of the protein stability on amyloid fibril formation *in vitro*, *Proceedings of the National Academy of Sciences of the United States of America*, 97 (2000) 8979-8984.

[223] A. Moshe, M. Landau, D. Eisenberg, Preparation of Crystalline Samples of amyloid fibrils and oligomers, *Protein Amyloid Aggregation: Methods and Protocols*, (2015) 201-210.

[224] K.-i. Yamaguchi, S. Takahashi, T. Kawai, H. Naiki, Y. Goto, Seeding-dependent propagation and maturation of amyloid fibril conformation, *Journal of Molecular Biology*, 352 (2005) 952-960.

[225] B. Choi, G. Yoon, S.W. Lee, K. Eom, Mechanical deformation mechanisms and properties of amyloid fibrils, *Physical Chemistry Chemical Physics*, 17 (2015) 1379-1389.

[226] J.F. Smith, T.P. Knowles, C.M. Dobson, C.E. MacPhee, M.E. Welland, Characterisation of the nanoscale properties of individual amyloid fibrils, *Proceedings of the National Academy of Sciences of the United States of America*, 103 (2006) 15806-15811.

[227] H. Sakai, K. Watanabe, Y. Asanomi, Y. Kobayashi, Y. Chuman, L. Shi, T. Masuda, T. Wyttenbach, M.T. Bowers, K. Uosaki, Formation of functionalised nanowires by control of self-assembly using multiple modified amyloid peptides, *Advanced Functional Materials*, 23 (2013) 4881-4887.

[228] U. Shimanovich, I. Efimov, T.O. Mason, P. Flagmeier, A.K. Buell, A. Gedanken, S. Linse, K.S. Åkerfeldt, C.M. Dobson, D.A. Weitz, Protein microgels from amyloid fibril networks, *ACS Nano*, 9 (2015) 43-51.

[229] G. Bhak, S. Lee, J.W. Park, S. Cho, S.R. Paik, Amyloid hydrogel derived from curly protein fibrils of α-synuclein, *Biomaterials*, 31 (2010) 5986-5995.

[230] T. Scheibel, R. Parthasarathy, G. Sawicki, X.-M. Lin, H. Jaeger, S.L. Lindquist, Conducting nanowires built by controlled self-assembly of amyloid fibres and selective metal deposition, *Proceedings of the National Academy of Sciences of the United States of America*, 100 (2003) 4527-4532.

[231] D. Li, E.M. Jones, M.R. Sawaya, H. Furukawa, F. Luo, M. Ivanova, S.A. Sievers, W. Wang, O.M. Yaghi, C. Liu, D.S. Eisenberg, Structure-based design of functional amyloid materials, *Journal of American Chemical Society*, 136 (2014) 18044-18051.

[232] N.P. Reynolds, M. Charnley, R. Mezzenga, P.G. Hartley, Engineered lysozyme amyloid fibril networks support cellular growth and spreading, *Biomacromolecules*, 15 (2014) 599-608.

[233] C. Li, M.M. Alam, S. Bolisetty, J. Adamcik, R. Mezzenga, New biocompatible thermo-reversible hydrogels from PNiPAM-decorated amyloid fibrils, *Chemical Communications*, 47 (2011) 2913-2915.

[234] U. Baxa, V. Speransky, A.C. Steven, R.B. Wickner, Mechanism of inactivation on prion conversion of the *Saccharomyces cerevisiae* Ure2 protein, *Proceedings of the National Academy of Sciences of the United States of America*, 99 (2002) 5253-5260.

[235] A.J. Baldwin, R. Bader, J. Christodoulou, C.E. MacPhee, C.M. Dobson, P.D. Barker, Cytochrome display on amyloid fibrils, *Journal of the American Chemical Society*, 128 (2006) 2162-2163.

[236] A. Herland, D. Thomsson, O. Mirzov, I.G. Scheblykin, O. Inganäs, Decoration of amyloid fibrils with luminescent conjugated polymers, *Journal of Materials Chemistry*, 18 (2008) 126-132.

[237] H. Tanaka, A. Herland, L.J. Lindgren, T. Tsutsui, M.R. Andersson, Enhanced current efficiency from bio-organic light-emitting diodes using decorated amyloid fibrils with conjugated polymer, *Nano Letters*, 8 (2008) 2858-2861.

[238] M. Hamedi, A. Herland, R.H. Karlsson, O. Inganäs, Electrochemical devices made from conducting nanowire networks self-assembled from amyloid fibrils and alkoxysulfonate PEDOT, *Nano Letters*, 8 (2008) 1736-1740.

[239] M. Malisauskas, R. Meskys, L.A. Morozova-Roche, Ultrathin silver nanowires produced by amyloid biotemplating, *Biotechnology Progress*, 24 (2008) 1166-1170.

[240] S. Barrau, F. Zhang, A. Herland, W. Mammo, M.R. Andersson, O. Inganäs, Integration of amyloid nanowires in organic solar cells, *Applied Physics Letters*, 93 (2008) 023307.

[241] D. Men, Y.-C. Guo, Z.-P. Zhang, H.-p. Wei, Y.-F. Zhou, Z.-Q. Cui, X.-S. Liang, K. Li, Y. Leng, X.-Y. You, Seeding-induced self-assembling protein nanowires dramatically increase the sensitivity of immunoassays, *Nano Letters*, 9 (2009) 2246-2250.

[242] S. Bolisetty, J. Adamcik, J. Heier, R. Mezzenga, Amyloid directed synthesis of titanium dioxide nanowires and their applications in hybrid photovoltaic devices, *Advanced Functional Materials*, 22 (2012) 3424-3428.

[243] S.K. Maji, D. Schubert, C. Rivier, S. Lee, J.E. Rivier, R. Riek, Amyloid as a depot for the formulation of long-acting drugs, *PLoS Biology*, 2 (2008) e17.

[244] S.L. Gras, A.K. Tickler, A.M. Squires, G.L. Devlin, M.A. Horton, C.M. Dobson, C.E. MacPhee, Functionalised amyloid fibrils for roles in cell adhesion, *Biomaterials*, 29 (2008) 1553-1562.

[245] Y. Loo, Y.-C. Wong, E.Z. Cai, C.-H. Ang, A. Raju, A. Lakshmanan, A.G. Koh, H.J. Zhou, T.-C. Lim, S.M. Moochhala, Ultrashort peptide nanofibrous hydrogels for the acceleration of healing of burn wounds, *Biomaterials*, 35 (2014) 4805-4814.

[246] Y. Leng, H.P. Wei, Z.P. Zhang, Y.F. Zhou, J.Y. Deng, Z.Q. Cui, D. Men, X.Y. You, Z.N. Yu, M. Luo, Integration of a fluorescent molecular biosensor into self-assembled protein nanowires: A large sensitivity enhancement, *Angewandte Chemie International Edition*, 122 (2010) 7401-7404.

[247] V. Castelletto, J. McKendrick, I. Hamley, U. Olsson, C. Cenker, PEGylated amyloid peptide nanocontainer delivery and release system, *Langmuir*, 26 (2010) 11624-11627.

[248] C. Li, S. Bolisetty, R. Mezzenga, Hybrid Nanocomposites of gold single-crystal platelets and amyloid fibrils with tunable fluorescence, conductivity, and sensing properties, *Advanced Materials*, 25 (2013) 3694-3700.

[249] C. Li, R. Mezzenga, Functionalisation of multiwalled carbon nanotubes and their pH-responsive hydrogels with amyloid fibrils, *Langmuir*, 28 (2012) 10142-1014

Chapter TWO

Stability and cytotoxicity of protein nanofibrils

2.1. Introduction

This chapter will provide stability information for PNFs under various conditions so as to ensure that they can be effectively used as a versatile bionanoscaffold for different industrial applications. An investigation of PNFs stability at a wide range of pHs, a variety of temperatures, in the presence of industrially related solvents, such as methanol (MeOH), ethanol (EtOH), isopropanol (iPrOH), dimethyl sulfoxide (DMSO) and acetonitrile (ACN), on the exposure to proteolytic enzymes such as bovine trypsin, pepsin and recombinant Proteinase K, and over long periods of storage was carried out. The ThT assay was used to detect the presence of fibrils under given conditions, followed by TEM imaging, to visually confirm the presence of fibrils. The stability and cytotoxicity study was primarily focused on the crystallin PNFs. For comparison, well characterised fibrils obtained from insulin and whey proteins were used. A further study using infrared microspectroscopy (IRM) was done to understand the long-term structural integrity of crystallin PNFs. Apart from stability studies, association of amyloid fibrils with neurodegenerative diseases raises reasonable concerns to the biosafety of crystallin PNFs. Thus, a cytotoxicity study was done to assess the possible crystallin PNF toxicity to cell viability using the human endometrial adenocarcinoma (Hec-1a endometrial) cell line.

2.2. Effect of proteases on PNFs

One of the hallmarks of amyloid fibrils is their high resistance to proteases compared to the natively folded protein [1-3]. To assess the extent of fibril digestion, proteolytic enzymes such as bovine trypsin, pepsin and recombinant Proteinase K were used. Several *in vitro* digestibility assays using pepsin and trypsin have previously been conducted as they are physiologically relevant proteases [4-6]. Proteinase K is a broad-spectrum and highly active protease that has been used extensively to characterise the protease resistance of disease-related amyloid fibrils [7, 8].

The ThT assay was selected as it is well accepted as an indicator of the presence of amyloid fibrils [9, 10]. Upon its incorporation into amyloid fibrils, ThT exhibits a considerable increase in the fluorescence intensity; however, the interaction mechanism between ThT and amyloid fibrils remains to be fully elucidated [11]. It has been suggested that ThT binds parallel to the fibril axis in the grooves between adjacent β-sheets or adjacent protofilaments [12], (see section 1.8, Chapter One). As the ThT assay is known to be sensitive to pH and viscosity [13-15], care was taken to have appropriate ThT control measurements as shown in **Figure 2.1** for each of the (i) buffers, and (ii) solvents used in this work.

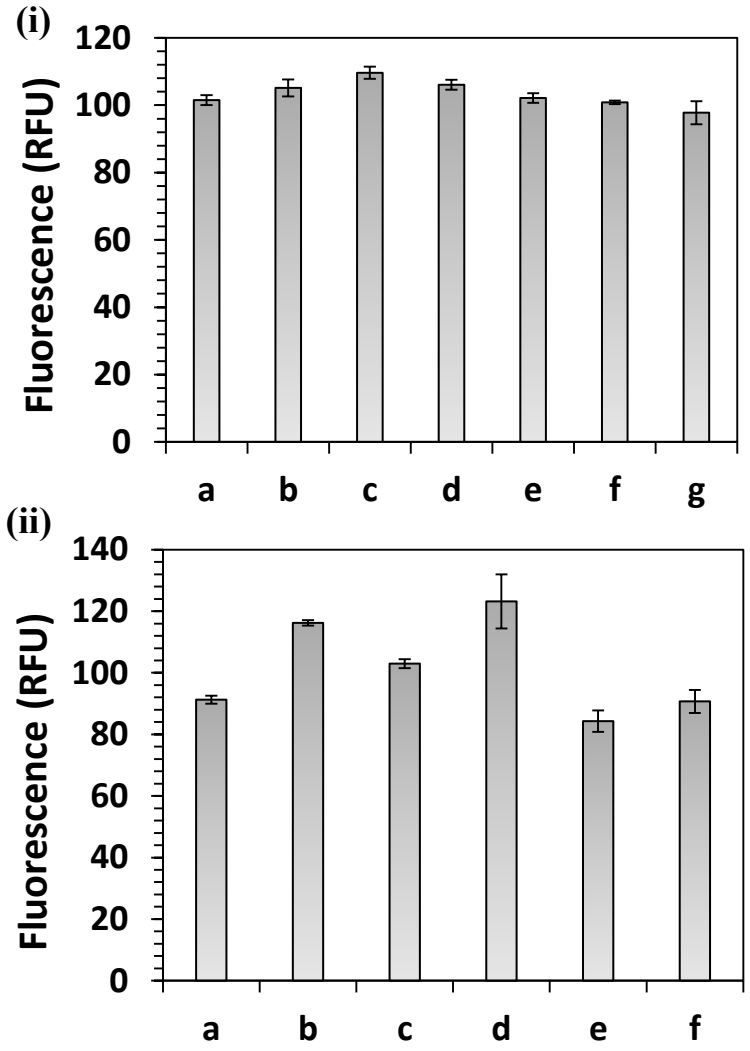

Figure 2.1. (i) *ThT fluorescence of buffers, where (a) 0.1 M sodium acetate, pH-2.0, (b) 0.1 M sodium acetate, pH-4.0, (c) 0.1 M sodium phosphate, pH-6.0, (d) 0.1 M sodium phosphate, pH-7.2, (e) 0.1 M HEPES, pH-8.0, (f) 0.1 M HEPES, pH- 9.0, and (g) sodium borate, pH-11.0.* ***(ii)*** *ThT fluorescence of solvents, where (a) MeOH, (b) EtOH, (c) DMSO, (d) iPrOH, (e) ACN, and (f) dH_2O, used for normalising ThT fluorescence of PNFs. Error bars represent the standard deviation of the mean of three replicates.*

PNFs were formed using in-house methods that had been adapted from the literature, see section 7.2. Briefly, for insulin PNFs (section 7.2.1), 5.8 mg/mL of insulin (obtained from Sigma-Aldrich) was dissolved in 100 mM NaCl, 25 mM HCl (pH 1.6), and sterile filtered [16]. The solution was incubated at 60 °C for 22 h. After heat incubation, the samples were cooled down on ice for 10 min and finally stored at room temperature for 7 days to allow for fibril formation. For whey PNFs (section 7.2.2), aqueous solution of WPI (10 mg/mL) was prepared and stirred for 10 min. The pH was adjusted to 2.0 with 100 mM HCl, using a pH probe. The solutions were left overnight at 4 °C while stirring, and then heated to 80 °C for 20-22 h in a dry bath heater.

After cooling for 10 min on ice, the resulting whey PNF suspensions were kept at room temperature for at least 1 week before proceeding with the experiments [17]. For crystallin PNFs (section 7.2.3), proteins were extracted from fish eye lenses and PNFs were formed from this crude mixture, as previously described [18]. The presence of PNFs was confirmed using the Thioflavin T (ThT) (section 7.1.2) assay, and TEM imaging (section 7.1.3).

For the proteolytic digestion study, pre-formed fibrils (section 7.2), at the final concentration of 10 mg/mL for both whey and crystallin PNFs, and 5.6 mg/mL for insulin PNFs were centrifuged at 12,500 rpm for 10 min using an Eppendorf® Minispin® Plus benchtop centrifuge. The supernatant was removed and the fibrils resuspended in appropriate buffers with and without enzymes, in an enzyme:fibril ratio of 1:20 (w/w). Fibrils in the presence and absence of proteases were incubated at 37 °C for 3 h, taking 200 µL aliquots at various time intervals (0, 20, 60, 180 min) (section 7.3.4). For data analysis, the fibril + buffer fluorescence at each time point was used to normalise the data. For characterisation purposes, the fibrils were negatively stained with uranyl acetate (UA) and analysed by TEM (section 7.1.3) and the degree of fibril digestion was assessed after 3 h by the ThT fluorescence decrease (section 7.1.2).

Insulin PNFs, used as a well characterised standard for comparison, proved to be the most resistant fibrils to proteolysis, followed by crystallin PNFs (in presence of all three proteases), as indicated by a constant ThT fluorescence over the entire duration of the experiment **(Figure 2.2)**. Both insulin and crystallin PNFs displayed high resistance towards protease digestion. However, whey PNFs exhibited different digestion patterns towards different proteases.

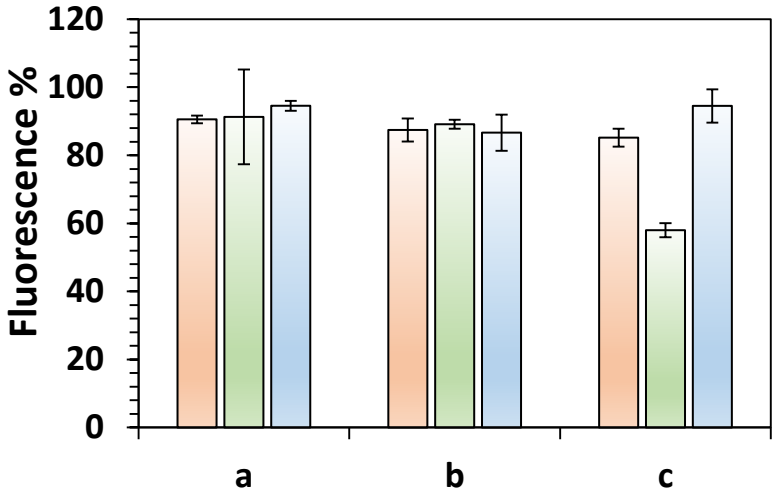

Figure 2.2. *ThT fluorescence of insulin PNFs (red), whey PNFs (green) and crystallin PNFs (blue) in presence of proteolytic enzymes, after 3h incubation at room temperature. ThT fluorescence is represented as % decrease in fluorescence compared to the control sample, where (a) trypsin, (b) pepsin, and (c) Proteinase K. Error bars represent the standard deviation of the mean of three replicates.*

TEM micrographs of fibrils were also obtained following the 3 h digestion in order to assess the change of morphology of the fibrils before and after treatment. Although some enzymatic digestion was present in all samples, there were still considerable amounts of fibrils present after the 3 h digestion by pepsin, trypsin and even by Proteinase K **(Figure 2.3)**, consistent with observations from ThT fluorescence, and also indicates partial digestion of the whey PNFs (shown in Fig. 2.3, sample h), whereas there was still a high fluorescence after 3 h of trypsin and pepsin digestion of the whey PNFs. The general pattern is a slightly higher resistance towards pepsin and trypsin digestion than towards Proteinase K digestion.

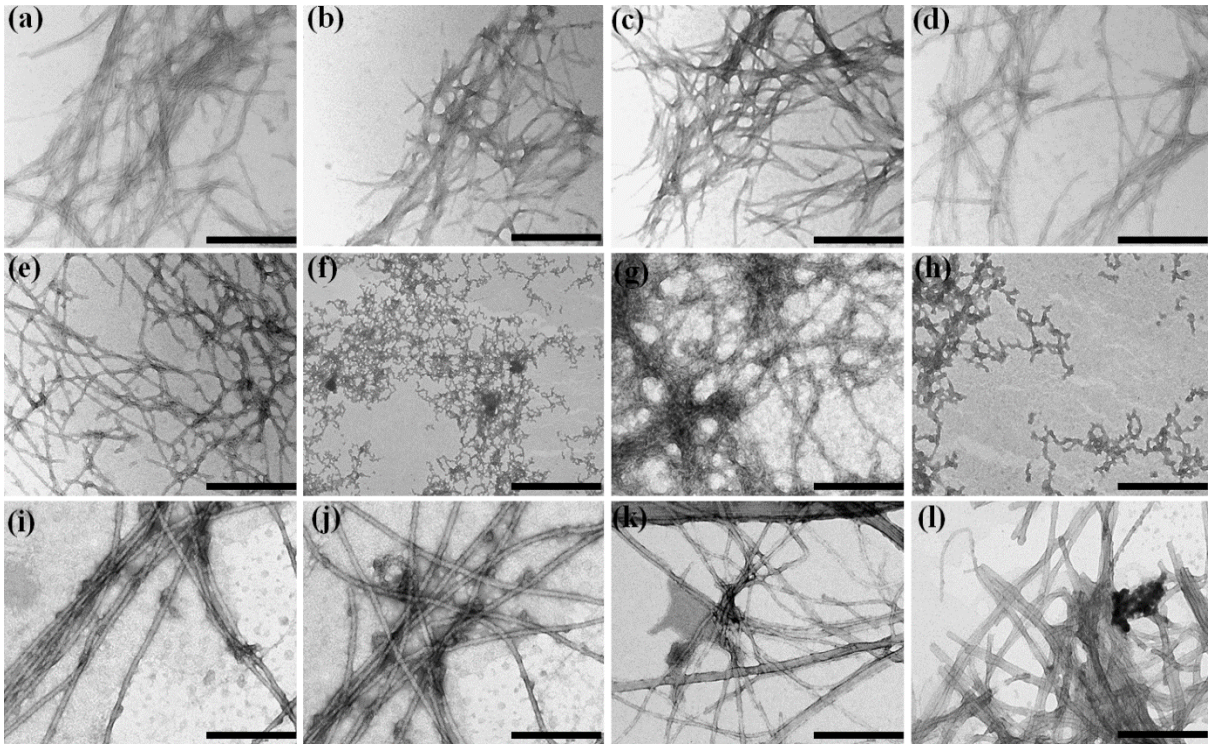

Figure 2.3. *Representative TEM images of PNFs after incubation with proteolytic enzymes.* ***Row 1****: insulin PNFs - (a) control, (b) trypsin, (c) pepsin, and (d) Proteinase K.* ***Row 2****: whey PNFs - (e) control, (f) trypsin, (g) pepsin, and (h) Proteinase K.* ***Row 3****: crystallin PNFs - (i) control, (j) trypsin, (k) pepsin, and (l) Proteinase K. Scale bar is 100 nm.*

2.3. Effect of solvents on PNFs

This part of the study focuses on PNFs resistance to common industrial solution (H_2O) and solvents used especially in cleanroom-based microfabrication: MeOH, EtOH, DMSO, iPrOH, and ACN. After a washing step, fibrils were resuspended in the test solvent (section 7.3.1) and a ThT assay was then carried out (section 7.1.2.) on these samples after a 3 h incubation at room temperature. The influence of different solvents on each of the PNFs used was determined by comparing the decrease in ThT fluorescence to the control sample. For all three types of PNFs, a significant decrease in ThT fluorescence was seen in the samples resuspended in DMSO and ACN, with ACN-incubation exhibiting the largest decrease, as depicted in **Fig. 2.4**, sample c and e.

In the presence of MeOH, EtOH, iPrOH and H_2O, all three types of PNFs exhibited high ThT fluorescence indicating fibril stability in the presence of these solvents. However, in comparison to insulin and crystallin PNFs, whey PNFs in the presence of methanol showed a considerable decrease in ThT fluorescence, which is hypothesised to be due to the fibrils degrading or dissolved. From the ThT fluorescence readings, in all the other solvents used, except DMSO and ACN, crystallin PNFs exhibited maximum stability, followed by insulin PNFs and whey PNFs, without any remarkable difference in ThT fluorescence after 3 h of incubation.

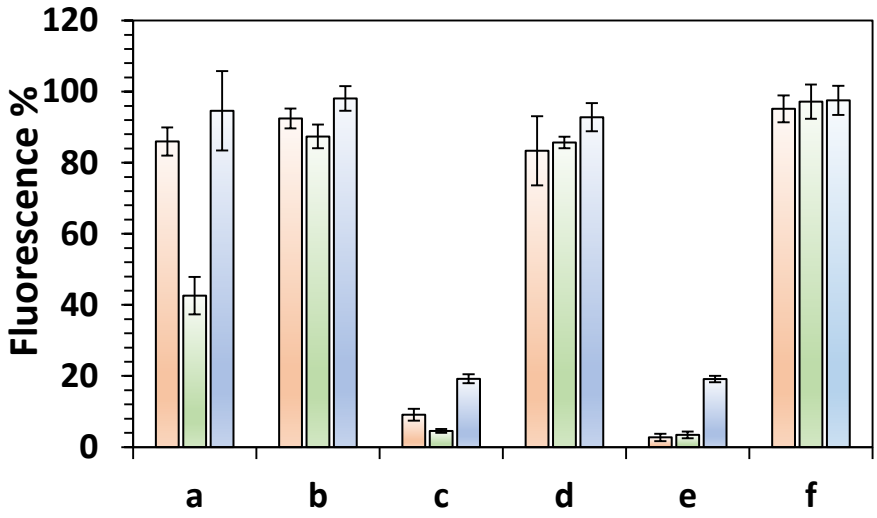

Figure 2.4. *ThT fluorescence of insulin PNFs (red), whey PNFs (green) and crystallin PNFs (blue) resuspended in various solvents, after 3 h incubation. ThT fluorescence is represented as % decrease in fluorescence compared to the control sample, where (a) MeOH, (b) EtOH, (c) DMSO, (d) iPrOH, (e) ACN, and (f) H_2O. Fluorescence values have all had the appropriate control (solvent and H_2O) value subtracted. Error bars represent the standard deviation of the mean of three replicates.*

The high decrease in ThT fluorescence for the samples resuspended in DMSO and ACN was expected, since organic solvents, mainly polar aprotic solvents including DMSO and ACN, have previously been shown to dissolve amyloid fibrils [19]. To validate the observed changes in ThT fluorescence, TEM analysis (section 7.1.3) was carried out to confirm the presence or absence of fibrils in each of the samples, see **Figure 2.5**. For all the three types of PNFs used, resuspension in water yielded PNFs typical of a control fibril preparation indicating that centrifugation and resuspension procedures had not damaged the fibrils, which appeared unchanged **(Figure 2.5. sample g, n, u compared to a, h, o respectively**).

TEM images for the samples of crystallin, insulin and whey PNFs resuspended in EtOH, iPrOH, and MeOH also show the presence of clear fibrils **(Fig. 2.5)**. In the case of ACN and DMSO, for insulin and whey PNFs **(Fig. 2.5 - e, f, and l, m)** no clear fibril morphology can be observed, which could be due to fibrils dissolving, in agreement with the low ThT fluorescence readings.

However, for the crystallin PNFs incubated in DMSO and ACN, TEM images suggest the presence of fibrils but with slightly different morphologies (lack of ordered fibrils structure) **(Fig. 2.5 - s, t)**. The results obtained are in agreement with a similar study done on crystallin PNFs by Domigan *et al.* (2013) [20], who investigated the effect of ACN by resuspending fibrils in 50% ACN. Loss of β-sheet content in amyloid aggregates in presence of DMSO and ACN has been reported previously [21].

The significant decrease in ThT fluorescence and presence of disrupted fibrils in the TEM images for fibrils dissolved in DMSO and ACN could be due to inhibition of hydrophobically driven associations, leading to a lack in extensive self-assembly and disordered fibril structure [22]. Studies have revealed that pure DMSO can cause complete loss of β-sheet structure as it competes with protein carbonyl groups for hydrogen bonding to protein amine groups, leading to the destabilisation of secondary structures [23]. In the case of whey PNFs, TEM images obtained indicated that, in most of the solvents, fibrils are present but different morphologies were observed, illustrating fibril rearrangement in different solvent environments.

The dark aggregates observed in the samples resuspended in solvents could be due to the formation of the stain crystals upon drying of the TEM grids, and are unlikely to be dissolved or fragmented fibrils, as it was also observed for the buffer-only sample **(Fig 2.5 (a) control – with insulin insulin fibril buffer only)**. Uranyl acetate when used as a staining agent can form complexes with various buffers and solvents leading to the formation of different complexes with different charges [24]. Therefore, these dark aggregates are likely to be due to the interaction between solvent/buffer and the stain used for TEM, as this was not observed for the samples with water, **(see Fig. 2.5 – sample g, n, u)**.

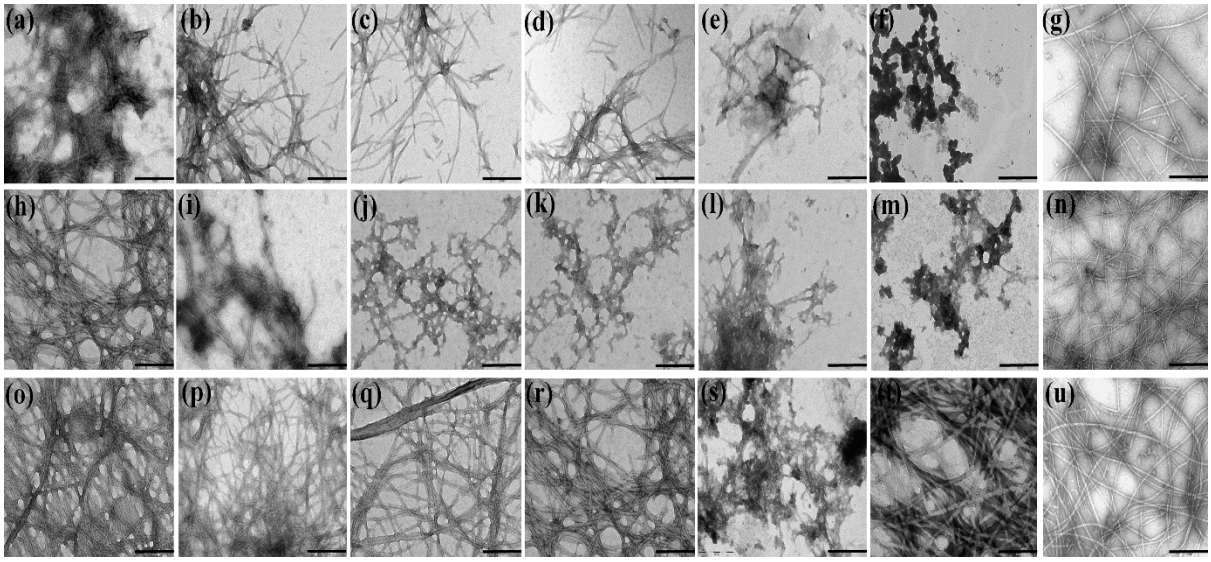

Figure 2.5. *Representative TEM images of PNFs resuspended in solvents.* ***Row 1****: insulin PNFs - (a) control, (b) MeOH, (c) EtOH, (d) iPrOH, (e) DMSO, (f) ACN, and (g)* H_2O. ***Row 2****: whey PNFs - (h) control, (i) MeOH, (j) EtOH, (k) iPrOH, (l) DMSO, (m) ACN, and (n)* H_2O. ***Row 3****: crystallin PNFs - (o) control, (p) MeOH, (q) EtOH, (r) iPrOH, (s) DMSO, (t) ACN, and (u)* H_2O. *Scale bar is 100 nm.*

PNTs obtained from the dipeptide diphenylalanine (FF) have attracted a large amount of attention as platforms for cell culture and biosensing over the last few years [25-27] (as discussed earlier in section 1.6, Chapter One). However, a recent finding of instability of FF tubes in most solvents, including water and phosphate buffer raises some limitations for the use of protein-based materials in the applications involving solvent submersion, such as biosensing [28, 29]. Comparing the stability of crystallin amyloid fibrils with FF nanotubes in various solvents [29], it can be confirmed that crystallin PNFs are significantly more stable in solution than FF nanotubes, and therefore could be a more appropriate choice for biosensing applications. This high stability of crystallin amyloid fibrils could be attributed to the presence of a high proportion of interstrand bridges in the crystallins as compared to other proteins [30].

In general, this comparative study of PNFs obtained from different sources has revealed that crystallin PNFs obtained from crude proteins obtained from fish eye lenses provide fibrils with better stability in a diverse range of solvents compared to PNFs derived from other protein sources.

2.4. Effect of pH and temperature on PNFs

Previous studies have characterised the effect of pH on fibril self-assembly [16, 31, 32]. However, not much literature is available on the long term stability of PNFs at different pH values post-assembly. To study the impact of pH on pre-formed PNFs, a wide range of buffers (section 7.3.2) at both acidic and alkaline pH values were selected. To test the effect of biological pH, 100 mM PBS (pH 7.4), was selected as a commonly used biological buffer solution. Fibril stability differed at varying pH, with crystallin PNFs displaying greater stability at alkaline pH values. For all PNFs, no observable decrease in ThT fluorescence was observed when fibrils were resuspended in solutions with pH values between pH 2.0 and 8.0, as shown in **Figure 2.6**.

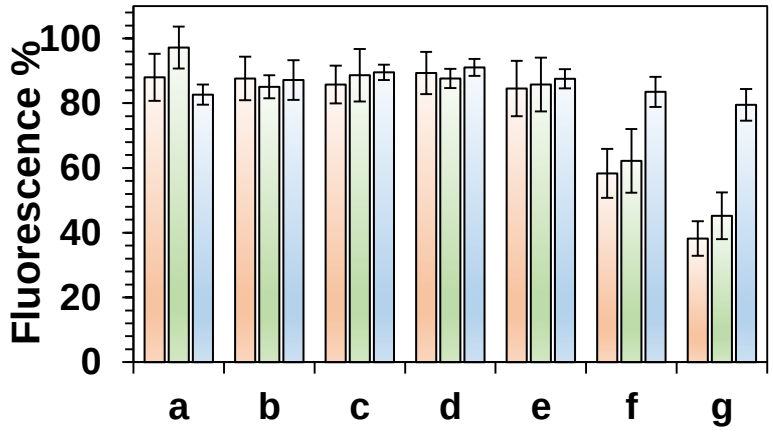

Figure 2.6. *ThT fluorescence of insulin PNFs (red), whey PNFs (green) and crystallin PNFs (blue) at selected pH values, after 24 h incubation. ThT fluorescence is represented as % decrease in fluorescence compared to the control (buffer-only) sample, where a) pH-2.0, (b) pH-4.0, (c) pH-6.0, (d) pH-7.4, (e) pH-8.0, (f) pH-9.0, and (g) pH-11.0. Error bars represent the standard deviation of the mean of three replicates.*

For whey and insulin PNFs between pH 9.0 and 11.0, a considerable decrease in ThT fluorescence was observed, indicating that the fibril structure was disrupted. The results obtained for insulin PNFs (grown under similar pH conditions) are consistent with recent findings [32], demonstrating the dissociation of insulin amyloid fibrils in this pH range using fibril recovery after centrifugal sedimentation. The ThT fluorescence data were supported by examination of the fibrils in each of the buffers by TEM **(Fig. 2.7)**. In agreement with the ThT fluorescence measurements, abundant fibrils were observed between pH 2.0 and pH 8.0, all showing clear fibrils.

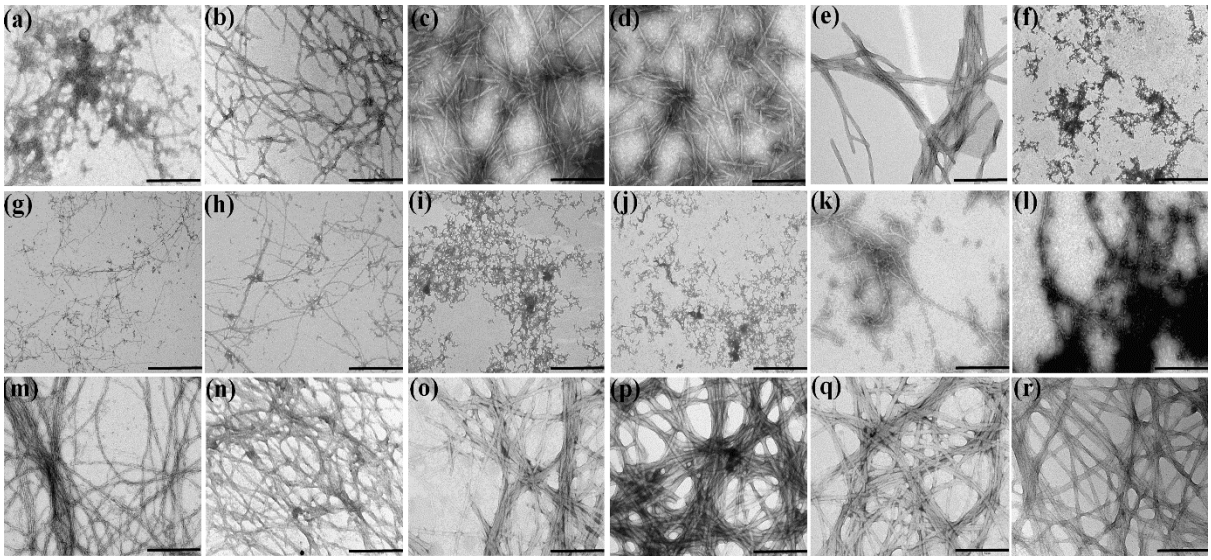

Figure 2.7. *Representative TEM images of fibrils over a wide range of pH.* ***Row 1****: insulin PNFs - (a) pH-2.0, (b) pH-4.0, (c) pH-6.0, (d) pH-8.0, (e) pH-9.0 and (f) pH-11.0.* ***Row 2****: whey PNFs - (g) pH-2.0, (h) pH-4.0, (i) pH-6.0, (j) pH-8.0, (k) pH-9.0 and (l) pH-11.0.* ***Row 3****: crystallin PNFs - (m) pH-2.0, (n) pH-4.0, (o) pH-6.0, (p) pH-8.0, (q) pH-9.0 and (r) pH-11.0. Scale bar is 100 nm.*

For whey and insulin PNFs, fewer fibrils were present at pH 9.0, and no clear fibrils were detected at pH 11.0, confirming their dissociation in this pH range, whereas crystallin PNFs retained morphology over the entire pH range. Although for insulin and whey PNFs no significant decrease in ThT fluorescence was observed for fibrils at below pH 8.0, fibrils at pH 6.0 and 8.0 were morphologically distinct from those at pH 2.0 and 4.0. For insulin fibrils, fibrils at pH 6.0 and 8.0 appear short and discrete whereas for whey fibrils, fibrils at elevated pH values appear aggregated and clumped together **(Fig. 2.7)**. The observation of slightly different morphologies at high pH values was not an unexpected result, as morphological differences have been seen previously with elevated pH in fibrils formed from bovine insulin [33] and from crude bovine crystallins [34].

To study the impact of temperature on pre-formed PNFs, fibrils in the respective buffers used to produce them (section 7.2) were incubated at selected temperatures for 24 h. The range of temperatures was selected according to the optimal temperature range of industrial enzymes, considering the application of protein fibrils as enzyme nanoscaffolds (section 7.3.3).

After a 24 h incubation at the selected temperatures, high ThT fluorescence readings were seen for all the samples as shown in **Figure 2.8 (i)**. In agreement to the ThT results, a high ThT fluorescence readings were obtained for all the samples studied suggesting high stability of pre-formed PNFs at all the given temperature settings used. TEM images of the crystallin fibril samples at all the given temperatures confirmed the presence of fibrils with no major morphological differences as compared to the control, see **Fig. 2.8 (ii)**.

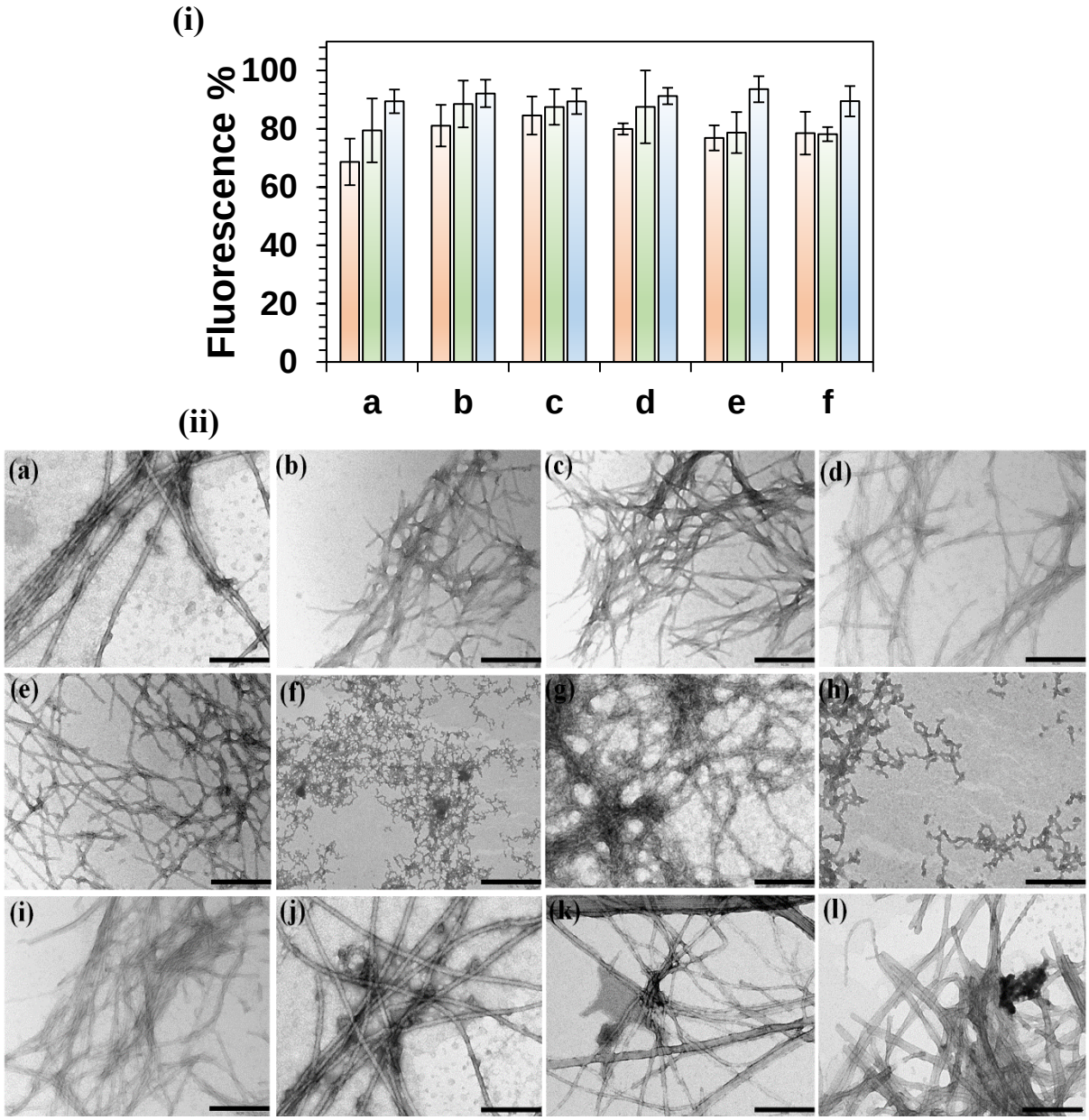

Figure 2.8. (i) *ThT fluorescence of insulin PNFs (red), whey PNFs (green) and crystallin PNFs (blue) after 24 h incubation at a variety of temperatures (°C), where (a) -20, (b) 4, (c) 22, (d) 37, (e) 60, and (f) 80. Fluorescence values represented as % decrease in fluorescence compared to the control sample. Error bars represent the standard deviation of the mean of three replicates.* ***(ii)*** *Representative TEM images of PNFs at variety of temperatures (°C).* ***Row 1****: insulin PNFs at (a) -20, (b) 22, (c) 37, and (d) 80.* ***Row 2****: whey PNFs at (e) -20, (f) 22, (g) 37 and (h) 80.* ***Row 3****: crystallin PNFs at (i) -20, (j) 22, (k) 37, and (l) 80. Scale bar is 100 nm.*

2.5. Effect of crystallin PNFs on Hec-1a cell proliferation

As discussed earlier in section 1.5, Chapter One, there are over 20 diseases, such as Alzheimer's, diabetes (type II), and Parkinson's disease, that are associated with amyloidoses [35-38]. It has been suggested that amyloid fibril related diseases share common amyloid aggregate structures and pathological pathways regardless of the source of protein [39, 40]. Amyloid fibrils generated from non-amyloid proteins have also been reported to be toxic. For example, the amyloid aggregates of the SH3 domain from bovine phosphatidyl-inositol-3'-kinase and the amino-terminal domain of the *E. coli* hypF protein showed toxicity towards mouse embryo fibroblast cell line (NIH-3T3 cells) [41]. Bovine insulin has also been reported to form either toxic rigid fibrils with parallel β-sheet conformation or non-toxic filaments with anti-parallel β-sheet character under reducing conditions [42]. Therefore, it is important to study the biosafety of crystallin PNFs before exploring them for further applications.

Despite extensive studies in recent years [40, 43-47], the identity of the culprits of cytotoxicity associated with amyloidoses still remains unclear [48]. Although non-fibrillar oligomers are the main focus of attention, a significant number of studies have reported that mature amyloid fibrils can also produce a cytotoxic effect [49-51]. For toxicity studies (section 7.4), Hec-1a cells were cultured in Minimum Essential Medium Eagle (MEM) (section 7.4.1) and cell viability (section 7.4.2) was measured in the presence and absence of crude crystallin proteins, mature amyloid fibrils, and sonicated (fragmented) fibrils. These conditions were tested as fibril length may play an important role in cell toxicity [52, 53].

To cause the fragmentation of PNFs, sonication was investigated as it has previously been shown to cause the fragmentation of insulin amyloid fibrils [54, 55]. For fragmenting amyloid fibrils, mature crystallin PNFs were subjected to a range of sonication times (0-40 sec). The resulting solutions were assessed for fragmentation by TEM, and it was found that a sonication time of 20 sec was needed to fragment the crystallin PNFs (section 7.16.1). TEM images for PNFs, before and after sonication are shown in **Figure 2.9**.

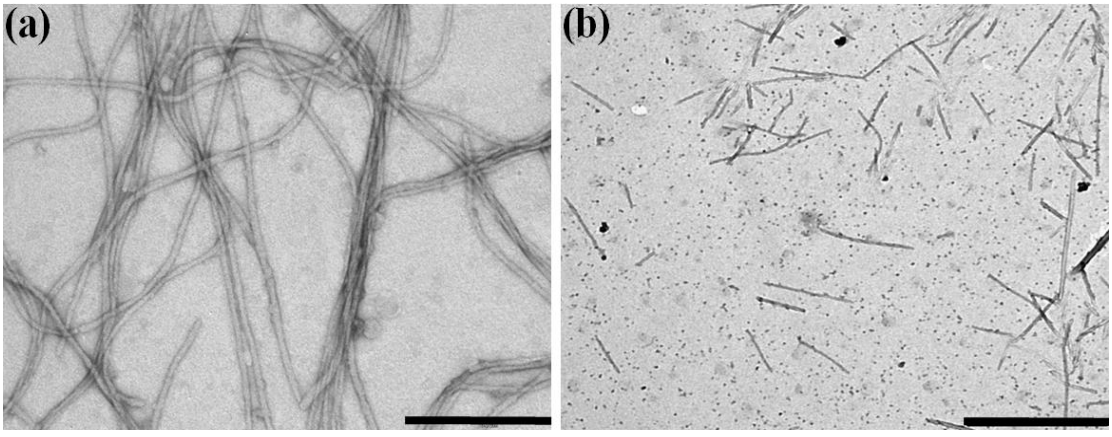

Figure 2.9. *Representative TEM images of crystallin PNFs, where (a) mature fibrils and (b) fragmented fibrils. Scale bar is 200 nm.*

The crystal violet staining (CVS) assay (7.4.3), a method of similar accuracy as WST (water soluble tetrazolium salts) assays, [56, 57] was done to assess the potential toxicity of crystallin PNFs. The CVS assay is a simple and reproducible assay of cytotoxicity [58-60]. In the CVS method, the principle involved to calculate the cell viability is based on the dye taken up by the viable cells in culture after the cells are stained with crystal violet (DNA of the cells is stained), and the resulting colour intensity is then measured spectrophotometrically at 570 nm.

The method of Gillies *et al.* (1986) [61] used to quantify the cell number in monolayer cultures as a function of the amount of the dye taken up by the cells has been extensively used with modifications for a wide number of applications including: to determine cytotoxicity or cell death produced by chemicals or toxins produced by microorganisms [62-64] and to determine cell proliferation [65] or cell viability [66]. Hec-1a cells were incubated with 10 mg/mL concentration of the crude protein, mature fibrils and sonicated fibrils, and the number of viable cells measured by the binding of crystal violet after 24 and 48 h. Even after 48 h incubation in comparison to the control, no substantial difference in the number of viable cells exposed to any of the given treatments was observed as demonstrated in **Figure 2.10.**

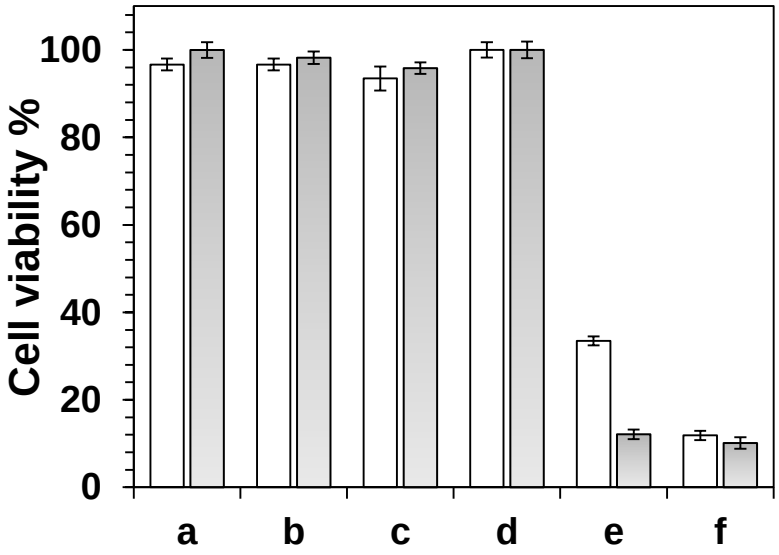

Figure 2.10. *Hec 1a cell viability, in the presence of (a) mature fibrils, (b) fragmented fibrils, (c) crude crystallin protein (10 mg/mL), (d) control - nutrient medium + PBS, (e) 10% DMSO, and (f) no-cell sample. Cell viability is represented as % decrease/increase in number of cells as compared to control (d), nutrient medium is set to 100%. Error bars represent the standard deviation of the mean of three replicates. Blank columns 24 h and filled columns 48 h incubation time.*

A further study was undertaken to assess whether there is any interaction between the cell and the proteins. The cells were pre-incubated in the absence of foetal bovine serum (FBS) to "starve" them overnight prior to the treatments (section 7.4.2). In comparison to the previous experiment there was an increase of cell viability in the presence of fibrils after 48 h incubation as depicted in **Fig. 2.11**. Similar results have been reported earlier for PNFs obtained from non-disease related proteins [67].

The control (buffer + media) shows that the buffer conditions do not change the cell viability. 10% DMSO is toxic to cells and was therefore used as a positive control. The no-cell control also did not show any sign of viability, demonstrating that no contamination was present.

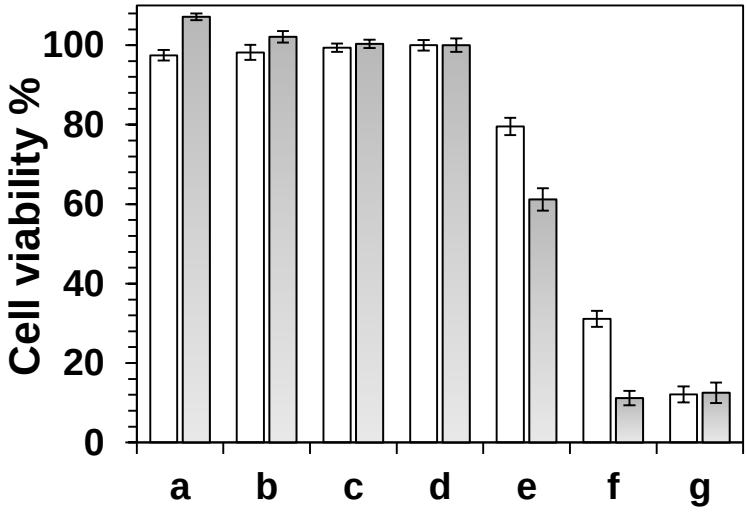

Figure 2.11. *Hec 1a cell viability, in presence of (a) mature fibrils, (b) fragmented fibrils, (c) crude crystallin protein (10 mg/mL), (d) control - nutrient medium + PBS, (e) control - starvation medium + PBS, (f) 10% DMSO, and (g) no-cell sample. Cell viability is represented as % decrease/increase in number of cells as compared to control (d), nutrient medium is set to 100%. Error bars represent the standard deviation of the mean of three replicates. Blank columns 24 h and filled columns 48 h incubation time.*

Our results suggest that Hec-1a cells are not adversely affected by the presence of crystallin amyloid fibrils at the studied concentration. There was also no indication that fragmented (sonicated) fibrils decreased cell viability, in contrast to literature reports [52]. Instead, the *in vitro* studies suggest that the cells can perhaps utilise the fibrillar proteins as a source of nutrients, although the contribution of non-fibrillar protein components requires further investigation [68]. Previous studies have shown that the inherent stability of the β-sheet supramolecular structure adopted by the crystallins in the eye lens and the chaperone ability of α-crystallin must be crucial for preventing protein aggregation *in vivo.* Aoyama *et al.* (1993), have also shown that the presence of α-crystallins in cultured cells leads to an enhanced survival of these cells after a period of stress [69]. Thus, a further investigation is required to investigate that the increased cell viability is due to the maintained chaperone activity of crystallins in the fibrillar structure or due to the non-fibrillar crystallins present in the cell culture.

It is commonly agreed that the toxicity of fibrillar aggregates is caused by membrane disruption [70-73] and is often associated with Ca^{2+} release and oxidative damage [47]. Membrane disruption could be linked directly to the hydrophobicity and flexibility of the amyloid aggregate [47]. Therefore, the potential interaction of fibrils with cell membranes could differ [74], and further studies may be required using different cell lines with altered compositions of cellular membranes (see section 5.22, Chapter Five - attachment and proliferation of mouse fibroblast cells was investigated in the presence of PNFs).

2.6. Long-term storage stability

The long term stability of the crystallin amyloid fold was carried out at the Australian Synchrotron, using the IRM beamline (section 7.5). The analysis was focused on amide I vibrations (1600-1700 cm^{-1}), which are commonly used as conformational markers for peptides and proteins [75]. Amide I vibrations mainly arise from stretching vibrational modes of the backbone carbonyl groups and correspond to different strengths/types of hydrogen bonds in which the backbone carbonyl groups are involved. They can hence be assigned to specific secondary structures [76]. IRM spectra were collected on crystallin fibrils aged for 2 to 37 months kept at room temperature (section 7.5). These were compared to IRM spectra collected for recently formed fibrils kept under the same conditions (less than a month old).

Typical IR absorbance spectrum of amyloid crystallin PNFs, across the whole amide fingerprint region is shown in *Appendix A, Figure A1*. Representative amide I vibrations are shown here as a function of the aging time together with the corresponding second derivative **(Figure 2.12)**, left and right panel respectively. Independent of the aging time, the amide I region exhibited two well-defined infrared absorption peaks at around 1620 cm^{-1} and 1690 cm^{-1} for all the samples, as for the recently formed fibrils **(Fig. 2.12)**. Similar IR amide I vibrations including antiparallel β-sheet, random coil and turn, were previously reported for amyloid fibrils generated from a γD-crystallin domain [77]. In accordance with the literature, this pair of absorption peaks was assigned to extended antiparallel β-sheet networks, which are a hallmark of the amyloid fibril fold [76, 78].

Less defined vibrations could be detected at around 1650 cm^{-1} and 1670-1680 cm^{-1} from the second derivative spectra **(Table 2.1)**. These were assigned to respectively random coil and turn secondary structures [76]. The variation of the type of turn from one sample to another (1 or 2 absorption peaks) is likely due to the variation in content of the types of crystallins [78]. Taken together, the IRM results show that the crystallin fibrils conserve the same conformational features for up to 37 months, when kept in solvent used to prepare the crystallin PNFs at room temperature (section 7.2.3). These features are typical of the amyloid fold and consistent with previous conformational characterisations of γD-crystallin amyloid fibrils [77].

Table 2.1. *IRM amide I vibrations of aged crystallin PNFs (wavenumbers taken from minima in second derivatives of IRM spectra) and corresponding secondary structures.*

Crystallin PNF age (months)	**Antiparallel β-sheet (cm^{-1})**	**Random coil (cm^{-1})**	**Turn (cm^{-1})**	**Antiparallel β-sheet (cm^{-1})**
0	*1619*	*1655*	*1662, 1676*	*1693*
2	*1620*	*1650*	*1663, 1670*	*1693*
5	*1620*	*1650*	*1660, 1676*	*1689*
13	*1618*	*1656*	*1664, 1675*	*1693*
27	*1618*	*1652*	*1672*	*1693*
37	*1621*	*1652*	*1670*	*1692*

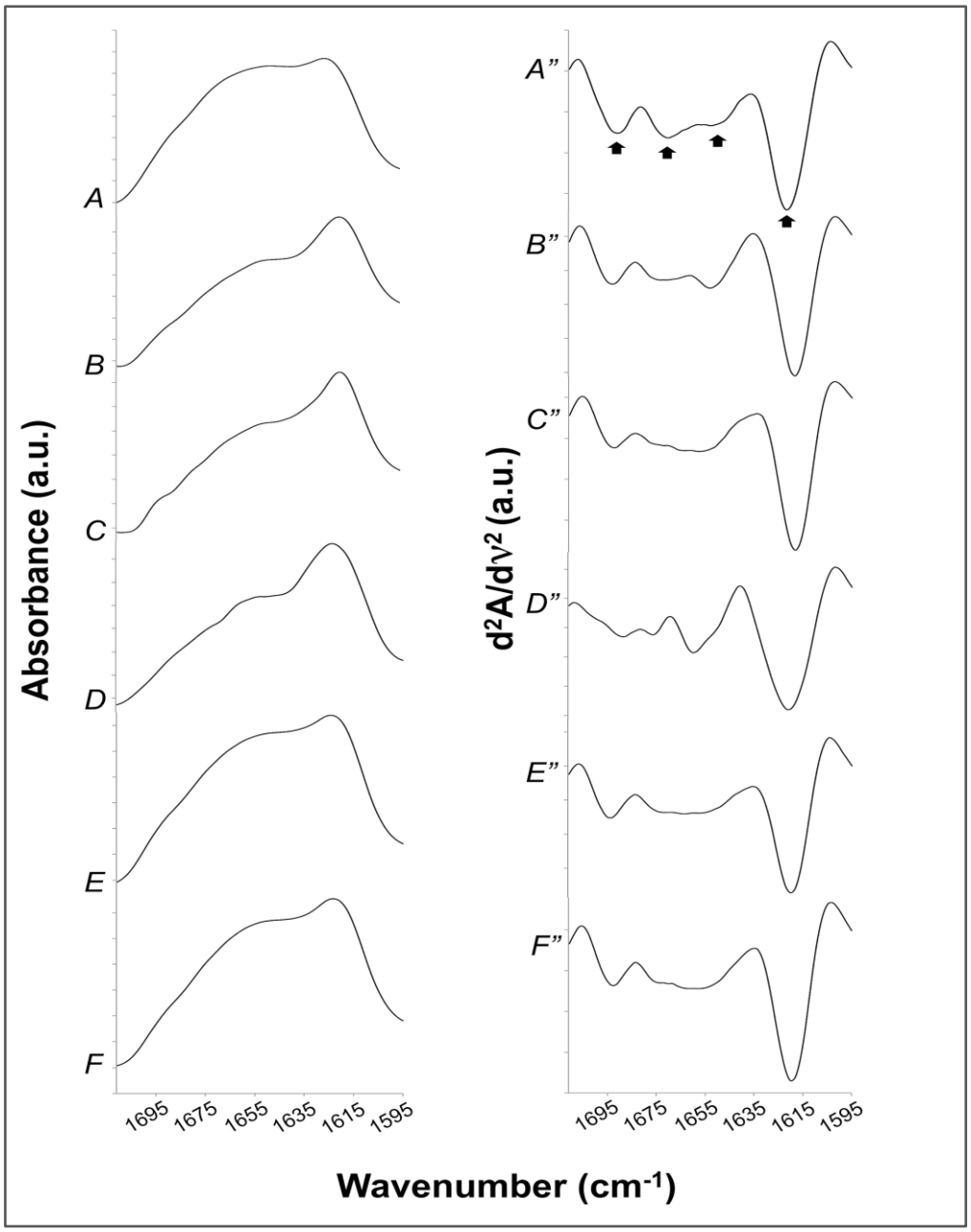

Figure 2.12. *IR absorbance spectra (A, B, C, D, E, F) and 2nd derivative spectra d^2A/dv^2 (A”, B”, C”, D”, E”, F”) of crystallin amyloid PNF samples after long-term storage with periods of A) 37, B) 27, C) 13, D) 5, E) 2 and F) 0 months.*

2.7. Conclusion

Crude crystallin proteins extracted from fish eye lenses have been previously identified as an economically viable source of PNFs, allowing for amyloid fibril production in large quantities at a low cost [18],[78]. This chapter has investigated the suitability of this material as a bionanoscaffold, specifically in terms of stability under a variety of parameters. Crystallin PNFs were shown to be stable across a wide pH range, in a number of industrially relevant solvents, at both low and high temperatures, and in the presence of proteases.

A comparative study, including insulin and whey PNFs suggests that crystallin PNFs obtained from cheap and readily available protein source, offer similar and often improved stability properties. No evidence of cytotoxicity of crystallin PNFs has been found by preliminary cytotoxicity assays using Hec-1a cells. An IRM study illustrates the long-term (up to 3 years) structural integrity of crystallin PNFs. This study supports the use of crystallin PNFs as nanomaterials, particularly in applications such as biosensing and enzyme immobilisation, which require prolonged solvent contact and stability over a wide range of pHs and temperatures.

2.8. References

[1] C. Nordstedt, J. Näslund, L.O. Tjernberg, A. Karlström, J. Thyberg, L. Terenius, The Alzheimer A beta- peptide develops protease resistance in association with its polymerisation into fibrils, *Journal of Biological Chemistry*, 269 (1994) 30773-30776.

[2] C. Selvaggini, L. Degioia, L. Cantu, E. Ghibaudi, L. Diomede, F. Passerini, G. Forloni, O. Bugiani, F. Tagliavini, M. Salmona, Molecular characteristics of a protease-resistant, amyloidogenic and neurotoxic peptide homologous to residues 106-126 of the prion protein, *Biochemical and Biophysical Research Communications*, 194 (1993) 1380-1386.

[3] R.S. Mishra, S. Basu, Y. Gu, X. Luo, W.-Q. Zou, R. Mishra, R. Li, S.G. Chen, P. Gambetti, H. Fujioka, Protease-resistant human prion protein and ferritin are co-transported across Caco-2 epithelial cells: Implications for species barrier in prion uptake from the intestine, *Journal of Neuroscience*, 24 (2004) 11280-11290.

[4] R.M. DeBaun, W.M. Connors, Nutritional assay, Relationship between *in vitro* enzymatic digestibility and *in vivo* protein evaluation of powdered whey, *Journal of Agricultural and Food Chemistry*, 2 (1954) 524-526.

[5] W.C. Thresher, H.E. Swaisgood, G.L. Catignani, Digestibilities of the protein in various foods as determined *in vitro* by an immobilised digestive enzyme assay (IDEA), *Plant Foods for Human Nutrition*, 39 (1989) 59-65.

[6] K. Thomas, M. Aalbers, G. Bannon, M. Bartels, R. Dearman, D. Esdaile, T. Fu, C. Glatt, N. Hadfield, C. Hatzos, A multi-laboratory evaluation of a common *in vitro* pepsin digestion assay protocol used in assessing the safety of novel proteins, *Regulatory Toxicology and Pharmacology*, 39 (2004) 87-98.

[7] J.C. Watts, J. Stöhr, S. Bhardwaj, H. Wille, A. Oehler, S.J. DeArmond, K. Giles, S.B. Prusiner, Protease-resistant prions selectively decrease shadoo protein, *PLoS Pathogens*, 7 (2011) e1002382.

[8] D.W. Colby, R. Wain, I.V. Baskakov, G. Legname, C.G. Palmer, H. Nguyen, A. Lemus, F.E. Cohen, S.J. DeArmond, S.B. Prusiner, Protease-sensitive synthetic prions, *PLoS Pathogens*, 6 (2010) e1000736-e1000736.

[9] M.R. Nilsson, Techniques to study amyloid fibril formation *in vitro*, *Methods*, 34 (2004) 151-160.

[10] H. LeVine 3rd, Thioflavin T interaction with synthetic Alzheimer's disease beta-amyloid peptides: Detection of amyloid aggregation in solution, *Protein science: A publication of the Protein Society*, 2 (1993) 404.

[11] M. Groenning, Binding mode of Thioflavin T and other molecular probes in the context of amyloid fibrils-current status, *Journal of Chemical Biology*, 3 (2010) 1-18.

[12] M. Biancalana, S. Koide, Molecular mechanism of Thioflavin T binding to amyloid fibrils, *Biochimica et Biophysica Acta (BBA)-Proteins and Proteomics*, 1804 (2010) 1405-1412.

[13] R. Sabaté, S.J. Saupe, Thioflavin T fluorescence anisotropy: An alternative technique for the study of amyloid aggregation, *Biochemical and Biophysical Research Communications*, 360 (2007) 135-138.

[14] A.I. Sulatskaya, I.M. Kuznetsova, K.K. Turoverov, Interaction of Thioflavin T with amyloid fibrils: Stoichiometry and affinity of dye binding, absorption spectra of bound dye, *Journal of Physical Chemistry B*, 115 (2011) 11519-11524.

[15] E.V. Hackl, J. Darkwah, G. Smith, I. Ermolina, Effect of acidic and basic pH on Thioflavin T absorbance and fluorescence, *European Biophysics Journal*, 44 (2015) 249-261.

[16] L. Nielsen, R. Khurana, A. Coats, S. Frokjaer, J. Brange, S. Vyas, V.N. Uversky, A.L. Fink, Effect of environmental factors on the kinetics of insulin fibril formation: Elucidation of the molecular mechanism, *Biochemistry*, 40 (2001) 6036-6046.

[17] L. Sasso, S. Suei, L. Domigan, J. Healy, V. Nock, M. Williams, J. Gerrard, Versatile multi-functionalisation of protein nanofibrils for biosensor applications, *Nanoscale*, 6 (2014) 1629-1634.

[18] J. Healy, K. Wong, E.B. Sawyer, C. Roux, L. Domigan, S.L. Gras, M. Sunde, N.G. Larsen, J. Gerrard, M. Vasudevamurthy, Polymorphism and higher order structures of protein nanofibres from crude mixtures of fish lens crystallins: Toward useful materials, *Biopolymers*, 97 (2012) 595-606.

[19] N. Hirota-Nakaoka, K. Hasegawa, H. Naiki, Y. Goto, Dissolution of β_2-microglobulin amyloid fibrils by dimethylsulfoxide, *Journal of Biochemistry*, 134 (2003) 159-164.

[20] L. Domigan, K.B. Andersen, L. Sasso, M. Dimaki, W.E. Svendsen, J.A. Gerrard, J. Castillo-León, Dielectrophoretic manipulation and solubility of protein nanofibrils formed from crude crystallins, *Electrophoresis*, 34 (2013) 1105-1112.

[21] C.-L. Shen, R.M. Murphy, Solvent effects on self-assembly of beta-amyloid peptide, *Biophysical Journal*, 69 (1995) 640-651.

[22] S.W. Snyder, U.S. Ladror, W.S. Wade, G.T. Wang, L.W. Barrett, E.D. Matayoshi, H.J. Huffaker, G.A. Krafft, T.F. Holzman, Amyloid-beta aggregation: Selective inhibition of aggregation in mixtures of amyloid with different chain lengths, *Biophysical Journal*, 67 (1994) 1216.

[23] M. Jackson, H.H. Mantsch, Beware of proteins in DMSO, *Biochimica et Biophysica Acta (BBA)-Protein Structure and Molecular Enzymology*, 1078 (1991) 231-235.

[24] W. Press, M. D.C. Hayat, P*rinciples and techniques of electron microscopy: Biological applications*, Wiley Online Library, (2000).

[25] R.V. Ulijn, A.M. Smith, Designing peptide based nanomaterials, *Chemical Society Reviews*, 37 (2008) 664-675.

[26] M. Yemini, M. Reches, J. Rishpon, E. Gazit, Novel electrochemical biosensing platform using self-assembled peptide nanotubes, *Nano Letters*, 5 (2005) 183-186.

[27] M. Reches, E. Gazit, Controlled patterning of aligned self-assembled peptide nanotubes, *Nature Nanotechnology*, 1 (2006) 195-200.

[28] H. Nezammahalleh, G. Amoabediny, F. Kashanian, M.F. Moghaddam, An investigation on the chemical stability and a novel strategy for long-term stabilisation of diphenylalanine nanostructures in aqueous solution, *Results in Physics*, 5 (2015) 11-19.

[29] K.B. Andersen, J. Castillo-Leon, M. Hedström, W.E. Svendsen, Stability of diphenylalanine peptide nanotubes in solution, *Nanoscale*, 3 (2011) 994-998.

[30] J.N. Sarakatsannis, Y. Duan, Statistical characterisation of salt bridges in proteins, *Proteins: Structure, Function, and Bioinformatics*, 60 (2005) 732-739.

[31] J.P. Schmittschmitt, J.M. Scholtz, The role of protein stability, solubility, and net charge in amyloid fibril formation, *Protein Science*, 12 (2003) 2374-2378.

[32] S.L. Shammas, T.P. Knowles, A.J. Baldwin, C.E. MacPhee, M.E. Welland, C.M. Dobson, G.L. Devlin, Perturbation of the stability of amyloid fibrils through alteration of electrostatic interactions, *Biophysical Journal*, 100 (2011) 2783-2791.

[33] S.P. Rao, *Amyloid fibrils in bionanomaterials*, PhD Thesis, University of Canterbury, (2008).

[34] S. Pilkington, *Incorporating glucose oxidase activity into amyloid fibrils*, Master's Thesis, University of Canterbury, (2009).

[35] G. Husby, T. Stenstad, J.H. Magnus, K. Sletten, B.Y. Nordvåg, G. Marhaug, Interaction between circulating amyloid fibril protein precursors and extracellular tissue matrix components in the pathogenesis of systemic amyloidosis, *Clinical Immunology and Immunopathology*, 70 (1994) 2-9.

[36] T.P. Knowles, M. Vendruscolo, C.M. Dobson, The amyloid state and its association with protein misfolding diseases, *Nature Reviews Molecular Cell Biology*, 15 (2014) 384-396.

[37] J.W. Kelly, Alternative conformations of amyloidogenic proteins govern their behavior, *Current Opinion in Structural Biology*, 6 (1996) 11-17.

[38] H.T. Blumenthal, Amyloidosis: A universal disease of ageing?, *Journals of Gerontology Series A: Biological Sciences and Medical Sciences*, 59 (2004) M361-M369.

[39] C.G. Glabe, Common mechanisms of amyloid oligomer pathogenesis in degenerative disease, *Neurobiology of Ageing*, 27 (2006) 570-575.

[40] R. Kayed, E. Head, J.L. Thompson, T.M. McIntire, S.C. Milton, C.W. Cotman, C.G. Glabe, Common structure of soluble amyloid oligomers implies common mechanism of pathogenesis, *Science*, 300 (2003) 486-489.

[41] M. Bucciantini, E. Giannoni, F. Chiti, F. Baroni, L. Formigli, J. Zurdo, N. Taddei, G. Ramponi, C.M. Dobson, M. Stefani, Inherent toxicity of aggregates implies a common mechanism for protein misfolding diseases, *Nature*, 416 (2002) 507-511.

[42] T. Zako, M. Sakono, N. Hashimoto, M. Ihara, M. Maeda, Bovine insulin filaments induced by reducing disulfide bonds show a different morphology, secondary structure, and cell toxicity from intact insulin amyloid fibrils, *Biophysical Journal*, 96 (2009) 3331-3340.

[43] M. Verma, A. Vats, V. Taneja, Toxic species in amyloid disorders: Oligomers or mature fibrils, *Annals of Indian Academy of Neurology*, 18 (2015) 138.

[44] M. Fändrich, Oligomeric intermediates in amyloid formation: Structure determination and mechanisms of toxicity, *Journal of Molecular Biology*, 421 (2012) 427-440.

[45] M. Stefani, Structural features and cytotoxicity of amyloid oligomers: Implications in Alzheimer's disease and other diseases with amyloid deposits, *Progress in Neurobiology*, 99 (2012) 226-245.

[46] N. Reixach, S. Deechongkit, X. Jiang, J.W. Kelly, J.N. Buxbaum, Tissue damage in the amyloidoses: Transthyretin monomers and nonnative oligomers are the major cytotoxic species in tissue culture, *Proceedings of the National Academy of Sciences of the United States of America*, 101 (2004) 2817-2822.

[47] M. Stefani, C.M. Dobson, Protein aggregation and aggregate toxicity: New insights into protein folding, misfolding diseases and biological evolution, *Journal of Molecular Medicine*, 81 (2003) 678-699.

[48] D. Eisenberg, M. Jucker, The amyloid state of proteins in human diseases, *Cell*, 148 (2012) 1188-1203.

[49] M. Malisauskas, A. Darinskas, V. Zamotin, A. Gharibyan, I. Kostanyan, L. Morozova-Roche, Intermediate amyloid oligomers of lysozyme: Is their cytotoxicity a particular case or general rule for amyloid?, *Biochemistry* (Moscow), 71 (2006) 505-512.

[50] S. Campioni, B. Mannini, M. Zampagni, A. Pensalfini, C. Parrini, E. Evangelisti, A. Relini, M. Stefani, C.M. Dobson, C. Cecchi, A causative link between the structure of aberrant protein oligomers and their toxicity, *Nature Chemical Biology*, 6 (2010) 140-147.

[51] M. Meyer-Luehmann, T.L. Spires-Jones, C. Prada, M. Garcia-Alloza, A. de Calignon, A. Rozkalne, J. Koenigsknecht-Talboo, D.M. Holtzman, B.J. Bacskai, B.T. Hyman, Rapid appearance and local toxicity of amyloid-beta plaques in a mouse model of Alzheimer's disease, *Nature*, 451 (2008) 720-724.

[52] W.-F. Xue, A.L. Hellewell, W.S. Gosal, S.W. Homans, E.W. Hewitt, S.E. Radford, Fibril fragmentation enhances amyloid cytotoxicity, *Journal of Biological Chemistry*, 284 (2009) 34272-34282.

[53] W.-F. Xue, A.L. Hellewell, E.W. Hewitt, S.E. Radford, Fibril fragmentation in amyloid assembly and cytotoxicity: When size matters, *Prion*, 4 (2010) 20-25.

[54] Y. Ohhashi, M. Kihara, H. Naiki, Y. Goto, Ultrasonication-induced amyloid fibril formation of β_2-microglobulin, *Journal of Biological Chemistry*, 280 (2005) 32843-32848.

[55] W. Dzwolak, Insulin amyloid fibrils form an inclusion complex with molecular iodine: A misfolded protein as a nanoscale scaffold, *Biochemistry*, 46 (2007) 1568-1572.

[56] M. Ishiyama, H. Tominaga, M. Shiga, K. Sasamoto, Y. Ohkura, K. Ueno, A combined assay of cell viability and *in vitro* cytotoxicity with a highly water-soluble tetrazolium salt, neutral red and crystal violet, *Biological and Pharmaceutical Bulletin*, 19 (1996) 1518-1520.

[57] D.A. Flick, G.E. Gifford, Comparison of *in vitro* cell cytotoxic assays for tumor necrosis factor, *Journal of Immunological Methods*, 68 (1984) 167-175.

[58] H. Itagaki, S. Hagino, S. Kato, T. Kobayashi, M. Umeda, An *in vitro* alternative to the draize eye-irritation test: Evaluation of the crystal violet staining method, *Toxicology in vitro*, 5 (1991) 139-143.

[59] K. Saotome, H. Morita, M. Umeda, Cytotoxicity test with simplified crystal violet staining method using microtitre plates and its application to injection drugs, *Toxicology in vitro*, 3 (1989) 317-321.

[60] K. Chiba, K. Kawakami, K. Tohyama, Simultaneous evaluation of cell viability by neutral red, MTT and crystal violet staining assays of the same cells, *Toxicology in vitro*, 12 (1998) 251-258.

[61] R. Gillies, N. Didier, M. Denton, Determination of cell number in monolayer cultures, *Analytical Biochemistry*, 159 (1986) 109-113.

[62] L. Harhaji, O. Vuckovic, D. Miljkovic, S. Stosic-Grujicic, V. Trajkovic, Iron down-regulates macrophage anti-tumour activity by blocking nitric oxide production, *Clinical & Experimental Immunology*, 137 (2004) 109-116.

[63] J. Castro-Garza, H.B. Barrios-García, D.E. Cruz-Vega, S. Said-Fernandez, P. Carranza-Rosales, C.A. Molina-Torres, L. Vera-Cabrera, Use of a colorimetric assay to measure differences in cytotoxicity of Mycobacterium tuberculosis strains, *Journal of Medical Microbiology*, 56 (2007) 733-737.

[64] S.W. Rothman, Technique for measuring 50% end points in cytotoxicity assays for *Clostridium difficile* toxins, *Journal of Clinical Pathology*, 39 (1986) 672-676.

[65] D. Zivadinovic, C.S. Watson, Membrane estrogen receptor-alpha levels predict estrogen-induced ERK1/2 activation in MCF-7 cells, *Breast Cancer Research*, 7 (2005) R130-144.

[66] M. Thomas, C.E. Finnegan, K.M.-A. Rogers, J.W. Purcell, A. Trimble, P.G. Johnston, M.P. Boland, STAT1 a modulator of chemotherapy-induced apoptosis, *Cancer research*, 64 (2004) 8357-8364.

[67] M. Lassé, *Does the Protein Aggregation State Affect the Digestibility and Safety of Foods?* PhD Thesis, University of Canterbury, (2013).

[68] H. Bloemendal, W. de Jong, R. Jaenicke, N.H. Lubsen, C. Slingsby, A. Tardieu, Ageing and vision: Structure, stability and function of lens crystallins, *Progress in Biophysics and Molecular Biology*, 86 (2004) 407-485.

[69] A. Aoyama, E. Fröhli, R. Schäfer, R. Klemenz, Alpha B-crystallin expression in mouse NIH 3T3 fibroblasts: Glucocorticoid responsiveness and involvement in thermal protection, *Molecular and Cellular Biology*, 13 (1993) 1824-1835.

[70] J. Janson, R.H. Ashley, D. Harrison, S. McIntyre, P.C. Butler, The mechanism of islet amyloid polypeptide toxicity is membrane disruption by intermediate-sized toxic amyloid particles, *Diabetes*, 48 (1999) 491-498.

[71] C.G. Glabe, R. Kayed, Common structure and toxic function of amyloid oligomers implies a common mechanism of pathogenesis, *Neurology*, 66 (2006) S74-S78.

[72] F. Tofoleanu, N.-V. Buchete, Alzheimer Aβ peptide interactions with lipid membranes: Fibrils, oligomers and polymorphic amyloid channels, *Prion*, 6 (2012) 339-345.

[73] F. Tofoleanu, B.R. Brooks, N.-V. Buchete, Modulation of Alzheimer's Aβ protofilament-membrane interactions by lipid headgroups, *ACS Chemical Neuroscience*, 6 (2015) 446-455.

[74] M. Stefani, Biochemical and biophysical features of both oligomer/fibril and cell membrane in amyloid cytotoxicity, *FEBS Journal*, 277 (2010) 4602-4613.

[75] A. Barth, Infrared spectroscopy of proteins, *Biochimica et Biophysica Acta (BBA)-Bioenergetics*, 1767 (2007) 1073-1101.

[76] W. van Grondelle, S. Lecomte, C. Lopez-Iglesias, J.-M. Manero, R. Cherif-Cheikh, M. Paternostre, C. Valéry, Lamination and spherulite-like compaction of a hormone's native amyloid-like nanofibrils: Spectroscopic insights into key interactions, *Faraday Discussions*, 166 (2013) 163-180.

[77] S.D. Moran, A.M. Woys, L.E. Buchanan, E. Bixby, S.M. Decatur, M.T. Zanni, Two-dimensional IR spectroscopy and segmental 13C labeling reveals the domain structure of human γD-crystallin amyloid fibrils, *Proceedings of the National Academy of Sciences of the United States of America*, 109 (2012) 3329-3334.

[78] M. Garvey, S. Gras, S. Meehan, S. Meade, J. Carver, J. Gerrard, Protein nanofibres of defined morphology prepared from mixtures of crude crystallins, *International Journal of Nanotechnology*, 6 (2009) 258-273

Chapter Three

Characterisation of crystallin amyloid fibrils – Towards functionalisation

3.1. Introduction

This chapter will explore the use of crystallin protein nanofibrils (CPNFs) - synthesised from crude fish eye lens protein extracts of *Macruronus novaezelandie* (Hoki), as a nanoscaffold for the immobilisation of important industrial enzymes. Enzyme immobilisation has widened the scope of industrial enzymes allowing not only reusing of the biocatalyst, with a benefit in terms of costs, but especially improving enzyme performances, leading to higher activity and stability [1]. PNFs in addition to their cheap availability, biocompatibility, self-assembly, and remarkable mechanical strength also offer a high surface-to-volume ratio, resulting in increased immobilisation capacity as compared to conventional 2D supports (as discussed earlier in section 1.9, Chapter One) and thus, are an exciting alternative to the currently used nanoscaffolds for enzyme immobilisation.

In this chapter, a brief introduction about each of the enzymes used, their lysine group availability for crosslinking, and results from the various assays employed for characterising crystallin PNFs are presented. Different assays were used to identify surface-exposed amino acid residues in CPNFs, which can be potentially used for crosslinking. Additionally, results from the different methodologies: reversible immobilisation (physical adsorption), and irreversible immobilisation, involving crosslinking *via* functional groups such as lysine, sulfhydryl, and aldehyde used for functionalising crystallin PNFs will be discussed. In this work, GOX was first used as a model enzyme to test the potential of crystallin PNFs as a nanoscaffold, before expanding to a range of enzymes, such as β-gal, pectinase, α-amylase, and laccase. All of the above enzymes used in this work were purchased commercially as a lyophilised powder from Sigma-Aldrich and were characterised using enzyme-specific activity assays *(as detailed in Appendix B)*. These activity-based assays were then routinely used to characterise functionalised PNFs. The enzymes ranged in size from ~30-180 kDa, included monomeric and dimeric quaternary structures, and are predominantly used in food industry relevant processes (discussed in section 3.2).

3.2. Enzymes used for the immobilisation

3.2.1. Glucose Oxidase (GOX)

GOX (EC 1.1.3.4.) is a dimeric and glycosylated flavoprotein that catalyses the oxidation of glucose to gluconolactone, which spontaneously yields gluconic acid, producing hydrogen peroxide as a side product [2]. GOX is an industrially important enzyme with extensive commercial uses in the chemical, food and beverage, and biotechnology industries [3-5].

The crystal structure of GOX **(Figure 3.1(a))** shows the surface of the enzyme with the lysine residues highlighted in pink. Previous research has shown that due to the presence of glycosylation, from the 24 lysine residues on the surface of the GOX dimer, only 5 are potentially available for crosslinking [6]. GOX is widely used in biosensing applications for the detection and estimation of glucose concentration in industrial and clinical analysis [7, 8]. Other uses include: as an antimicrobial agent for food storage and packaging [9], as a food preservative, by removing oxygen from fruit juices, and from mayonnaise to prevent rancidity; or by removing glucose for improving colour, flavour and shelf life of food products, such as dried egg powder [5], or as a textile bleaching agent [9, 10]. GOX due to its high stability and activity, is considered an ideal enzyme for immobilisation studies [2, 11], and has been successfully immobilised onto various scaffolds [12-14], including insulin PNFs [15, 16], where the resulting GOX-functionalised enzyme scaffold was then incorporated into a model poly(vinyl alcohol) (PVOH) film, and tested on *E.coli* for the antibacterial activity of GOX [15]. GOX was selected for this research as a model enzyme, as it is highly stable under a variety of conditions and its stability has been improved by using different immobilisation techniques [12, 17, 18].

3.2.2. β-Galactosidase (β-gal)

β-Gal (EC 3.2.1.23) is distributed in a wide variety of organisms including animals, plants and microorganisms, and is known to catalyse the conversion of lactose into glucose and galactose [19, 20]. β-Gal based industrial applications include production of lactose-hydrolysed products for lactose-intolerant or lactase-deficient people [21, 22], and as a biosensor for specific lactose determination in the dairy industry [23]. The X-ray crystal is shown in **Figure 3.1(b)**, with the theoretically available lysine residues highlighted in pink.

β-Gal has previously been immobilised to a wide range of supports including magnetic chitosan NPs [24], zinc oxide NPs [25], graphite [26], microporous polyvinylidene fluoride (PVDF) membrane [27], and silicon [28]. A huge amount of research into the immobilised β-gal focuses mainly on the development of biosensors for the detection of lactose [29-33]. Successful co-immobilisation of GOX and β-gal on amyloid fibrils anchored to surfaces could lead to the creation of cheap, reliable and reusable active surface-coating nanomaterials for the production of lactose biosensor (discussed later, Chapter Five).

3.2.3. Pectinase

Pectinases have numerous applications in the food, textile and bionanotechnological processes [34, 35]. These enzymes catalyse degradation of pectin substances either *via* esterification (esterases reactions) or through depolymerisation (hydrolases and lyases) [36]. The crystal structure of pectinase is shown in **Figure 3.1(c)**. Pectinases are an integral part of the fruit industry and are extensively used for clarification of fruit juices and wines by degrading pectin [36-38]. Another important application of pectinase is in the farming industry for the formulation of animal feeds where pectinases are used with other hydrolases to reduce viscosity [39].

To date, several supports, mainly polymers have been used for immobilising pectinase either by physical adsorption, entrapment, multipoint attachment or *via* covalent immobilisation [40-43]. The proteinaceous building blocks of the PNFs nanoscaffold can offer a beneficial environment for pectinase immobilisation, decreasing the enzyme's liability for denaturation.

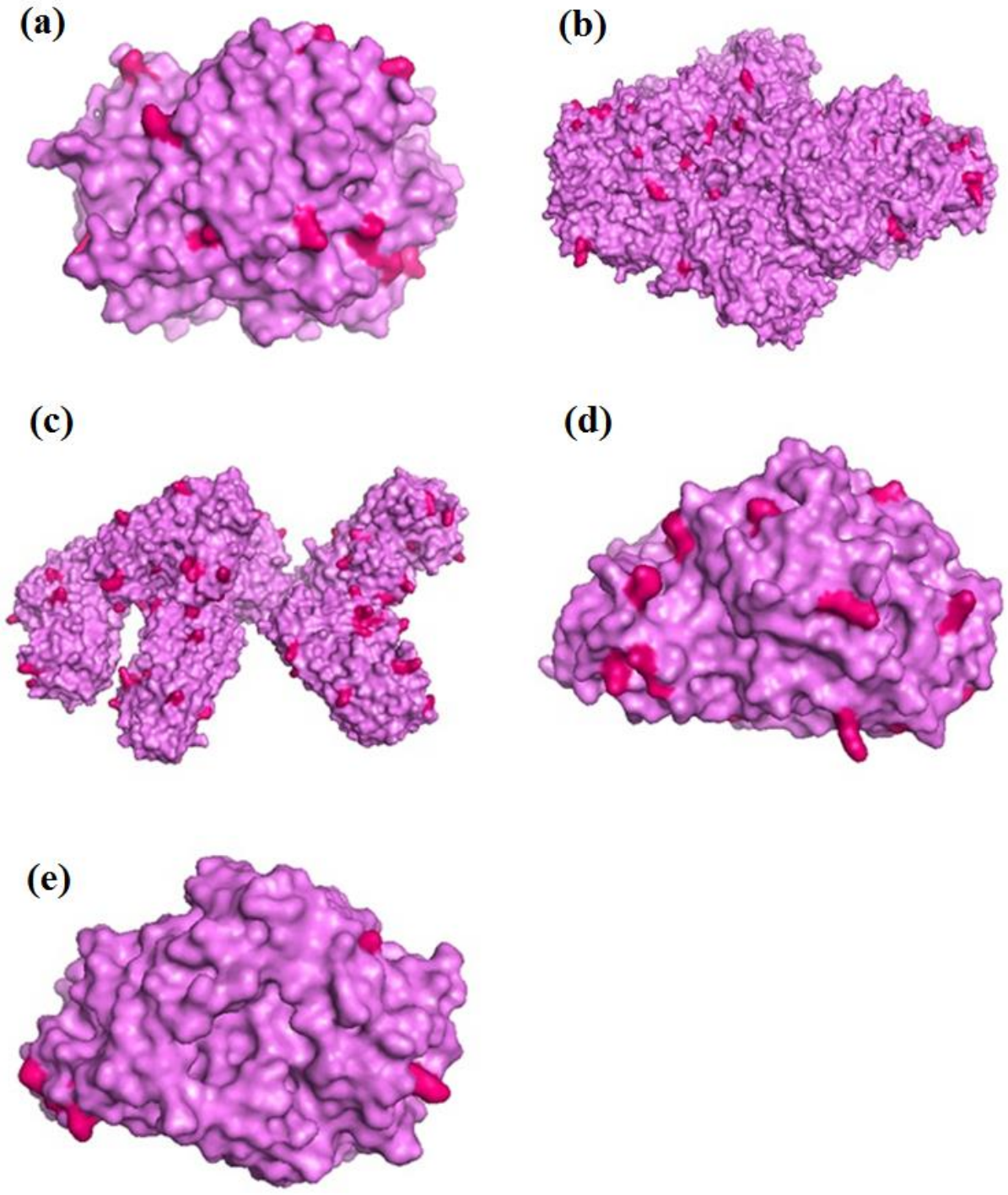

Figure 3.1. *Crystal structure of (a) GOX dimer (PDB ICF3), (b) β-Gal (PDB IPX3), (c) Pectinase (PDB INHC), (d) α-Amylase (PDB 3KWX), and (e) Laccase (PDB 2H5U), showing the surface with the lysine residues coloured in pink, as visualised by using PyMol.*

3.2.4. Amylase

Starch is a very important raw material and a major constituent of food products. However, starch utilisation requires its degradation to maltodextrins, maltose, and glucose which can be achieved by using amylolytic enzymes [44]. Amylases have wide application in starch saccharification and degradation process leading to the production of various useful products, such as sweeteners, gelling agents, and adhesives [45, 46]. Amylases have gained considerable importance due to their wide spectrum applications in various industrial processes such as food, pharmaceutical, and fermentation industry [47]. Some of the main applications include production of glucose syrups, high fructose corn syrups, maltose syrups, reduction of viscosity of sugar syrups and haze formation in fruit juices [48]. In the brewing industries, amylases are extensively used for solubilisation and saccharification of starch for alcohol fermentation [49]. Previous studies have revealed that immobilisation of amylases on water insoluble carriers seems to be the most promising method to obtain stable and reusable forms of enzymes [50-52]. Thus, amyloid fibril nanoscaffolds may provide a support that is beneficial towards amylase activity and stability. The crystal structure of the α-amylase enzyme (EC 3.2.1.1) with potentially available lysine groups for crosslinking, highlighted in pink is shown in **Figure 3.1(d)**.

3.2.5. Laccase

Laccases (EC 1.10.3.2) have gained great importance in enzymatic oxidation techniques due to their high non-specific oxidation ability, and are used extensively for diverse biotechnological applications. The crystal structure of fungal laccase from *Cerrena maxima* showing the surface with the lysine residues coloured in pink is shown in **Figure 3.1(e)**. Some of the major laccase using industries include the textile industry for bleaching and waste water treatment [53, 54], the paper industry for delignification [55] and the biopulping [56], pharmaceutical [57], and food industry [58]. Several laccase substrates, such as phenols, thiol-containing proteins, and fatty acids are important components of various beverages and foods. Modification of all such compounds by laccase may lead to sustainable processes with new functionality, quality improvement, or cost reduction [59]. Laccases have also been applied to eliminate undesirable phenolics responsible for browning, turbidity development and haze formation in beverage industries so to enhance or modify the appearance of clear fruit juices, beer and wine, and also in biosensing [60, 61]. Different methodologies have been reported for laccase immobilisation, such as adsorption, entrapment, encapsulation, and covalent binding. The scope of laccase applications has widened further by immobilisation techniques, as recently reviewed by Fernández-Fernández [62].

All the enzymes studied in this work are important industrial biocatalysts with many possible applications in biotechnological processes. However, there are still many constraints to their application, due to processing conditions such as, extreme pH values, high temperatures, very high ionic strength, presence of surfactants and solvents, huge substrate volumes. All such limitations clearly highlight the need for the choice of very robust catalysts for the process.

3.3. Characterisation of CPNFs as immobilisation scaffolds

In this work, initial attempts were made to immobilise GOX onto crystallin PNFs using the methods of Pilkington *et al.* (2010) [15], who showed that GOX can be covalently immobilised to insulin PNFs using glutaraldehyde (GA). The extent of crosslinking was then assessed by SDS-PAGE (section 7.1.1), which implied that no immobilisation of GOX to the crystallin PNFs was occurring, and that only GOX crosslinked to other GOX molecules (strong band at 160 kDa corresponding to the GOX dimer) was observed despite extensive efforts *(see Appendix C, Figure C1)*. As the established method did not result in successful immobilisation, a number of alternative methods using different lysine residue-based crosslinking molecules, such as formaldehyde (FA), and methylglyoxal (MG) were studied, by altering various variables. A summary of different conditions tried is given in **Table 3.1.**

Table 3.1. *Details of different conditions attempted for immobilisation of GOX to crude crystallin PNFs (GOX - glucose oxidase, CPNFs - crystallin protein nanofibrils, and X - crosslinker), where arrow indicates 15 min incubation time.*

Conditions	Details
Reaction order	*One step reaction:* GOX + CPNFs + X *Two step reaction*: GOX + CPNFs ⟶ X GOX + X ⟶ CPNFs CPNFs + X ⟶ GOX
Total reaction time	30-180 min; 12-24 h
Pre-incubation time	15-60 min
Reaction temperature	25, and 37 °C
Crosslinker	GA, MG, FA, and GA+FA
Crosslinker concentration	GA 10-200 mM, MG and GA 1-4%
Crystallin fibril concentration	2-10 mg/mL
GOX concentration	0.5-2 mg/mL

*******This value is approximate. Fibrils were formed using the standard in-house conditions and then concentrated and resuspended in PBS (pH 7.4) by centrifugation.*

None of the crosslinking conditions detailed in **Table 3.1** were successful, with all resulting in GOX dimer formation. In addition to GOX, several attempts to immobilise other enzymes to the crystallin PNFs using GA were also tried, but successful immobilisation conditions could not be found. Thus, in order to detect lysine residues, as well as N-terminal amines, and to investigate the lack of crosslinking *via* lysine residue-based crosslinkers for crystallin PNFs, the amino group availability of crystallin PNFs was assessed using the *o*-phthaldialdehyde (OPA) assay, and the ninhydrin assay.

3.3.1. Assessment of amino group availability

3.3.1.1. OPA assay

The OPA assay is based on the reaction of *o*-phthaldialdehyde with primary amines, in the presence of a reducing agent, such as 2-mercaptoethanol. When OPA reacts with primary amines it produces a fluorescent isoindole product as shown in **Figure 3.2.**

The fluorescent isoindole produced can then be detected spectrophotometrically at 340 nm. The OPA assay was carried out according to in-house methods [63] (section 7.6.1), with a standard curve (section 7.6.1.1) created using lysine concentrations ranging from 0.2-2.0 mM, *see Appendix D, Figure D1(a).*

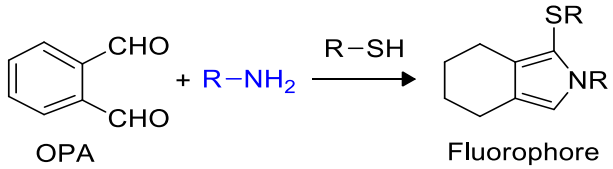

Figure 3.2. *Reaction scheme of OPA reagent with a primary amine, in the presence of a reducing agent, to produce a fluorescent product that can be detected at 340 nm [63].*

3.3.1.2. Ninhydrin assay

The reaction of ninhydrin with primary amino groups to form the purple dye commonly known as Ruhemann's purple was discovered by Siegfried Ruhemann in 1910. The ninhydrin assay functions by reaction of ninhydrin solution (triketohydrindene hydrate), with ϵ-amino groups and N-terminal amines, to produce a purple coloured compound diketohydrindylidenediketohydrindamine (Ruhemann's purple) which can be detected at 570 nm [64] **(Figure 3.3).** The procedure of Moore [65], as modified by Friedman *et al.* (1984) [66], was used according to in-house methods (section 7.6.2), with a standard curve (section 7.6.2.1) constructed using lysine concentrations from 0.2 to 2.0 mM, see *Appendix D, Figure D1(b).*

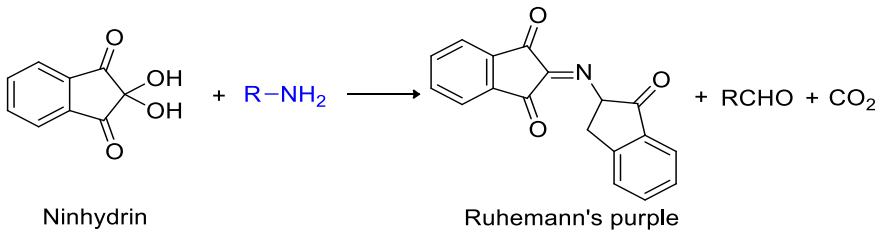

Figure 3.3. *Reaction scheme of ninhydrin reagent with primary amines to produce a fluorescent product, Ruhemann's purple that can be detected at 570 nm [64].*

3.4. Amino group availability assay for PNFs

In order to validate the use of fluorescence-based amino group assays, it is important to calculate a theoretical amino group concentration of the protein. It is not possible to calculate an exact amino group concentration of PNFs, due to the unknown solvent accessibility of particular residues and a lack of information regarding the number of native monomers involved per fibril. Thus, it was decided to validate the use of lysine residue-based assays by using the two assays described above for whey protein isolate (WPI), as it is relatively easy to determine the theoretical amino acid concentration of WPI due to available sequence information.

3.4.1. Amino group availability assay for whey protein, and whey PNFs

Both the OPA, and the ninhydrin assays were done on native whey protein isolate (1 mg/mL) and whey PNFs (formed from 1 mg/mL native whey protein isolate) to validate the use of these assays. The results of these assays are shown in **Table 3.2.**

Table 3.2. *Summary of calculated amino group availabilities of native whey protein isolate and whey PNFs, using the OPA (section 7.6.1) and ninhydrin assays (section 7.6.2). Theoretical amino group composition estimated from β-lg sequence is also given.*

Sample	OPA assay (μM)*	Ninhydrin assay (μM)*	Theoretical (μM)
Native whey protein isolate (1.0 mg/mL)	292±15	287±14	271
*Whey protein nanofibrils (1.0 mg/mL)***	160±10	166±12	N/A

**OPA and ninhydrin assay concentration is calculated from standard curve. As the standard curve was constructed using lysine, therefore values were multiplied by two to obtain amino group concentration.*

***Fibrils were formed at 10 mg/mL concentration and diluted to 1.0 mg/mL after washing and centrifugation to ensure that there aren't any additional free proteins available in the solution.*

The WPI used in this study mainly consists of β-lg, therefore the theoretical amino acid concentration of WPI was determined from the β-lg sequence **(Fig. 3.4).** The β-lg monomer (β-lg occurs as monomer at the pH (2.0) used in this study) has a total of 15 lysine residues, of which 5 lysine groups are accessible at the surface [67, 68]. All other lysine groups on the protein and the N-terminal amine group of the β-lg monomer are partially "buried" within the molecule so they are inaccessible [67]. By comparison with the theoretical amino group concentration of WPI, the amino group availability as ascertained by each of the two assays indicate a very good correlation between the two assays **(Table 3.2)**, suggesting that both assays are suitable to assess the amino group availability of PNFs formed from crude crystallin proteins.

LIVT QTMKGLDIQK VAGTWYSLAM AASDISLLDA QSAPLRVYVE
ELKPTPEGDL EILLQKWENG ECAQKKIIAE KTKIPAVFKI
DALNENKVLV LDTDYKKYLL FCMENSAEPE QSLACQCLVR
TPEVDDEALE KFDKALKALP MHIRLSFNPT QLEEQCHI

Figure 3.4. *Primary sequence of bovine β-lg (PDB 1BEB) showing lysine residues in red.*

3.4.2. Amino group availability assay for crystallin protein, and crystallin PNFs

The theoretical amino group concentration for crystallin proteins is unknown as:

1. Mixtures of crude crystallin proteins were used in this study and it was difficult to determine the initial concentration of each protein involved.

2. The proteins have a heterogeneous population of post translational modifications (discussed in section 3.6).

However, a detailed study of hoki crystallin proteins done by Domigan (2012) [68], revealed that crude crystallin proteins consists of all the three main classes of crystallin proteins named as α-, β-, and γ-crystallins. On comparing the results from Domigan (2012) with the elution profiles for bovine crystallins [69, 70], it was observed that hoki crystallins have higher amounts of γ- and lower amounts of β-crystallins. Both these observations seems to be a common feature of fish crystallin proteins as supported by the literature [71-76].

A sequence study (on γ-crystallins from *D.rerio*) and results from OPA and ninhydrin assays showed that crystallin proteins do have high concentration of amino groups available for crosslinking, and lack of crosslinking suggests the presence of some other interference (results not shown). To understand this, both OPA (section 7.6.1) and ninhydrin (7.6.2) assays were done on the crude crystallin protein solution, the amorphous aggregate removed during fibrillation process, and on the crystallin PNFs obtained after fibrillation (section 7.2.3). Results of these assays are summarised in **Table 3.3.**

Table 3.3. *Summary of calculated (using the OPA and ninhydrin assays) amino group availability of crude crystallin protein solution, amorphous aggregate removed while making fibrils, and crystallin amyloid fibrils. Sample concentration is calculated from standard curve obtained using lysine, therefore values were multiplied by two to obtain amino group concentration.*

Sample	OPA assay (μM)	Ninhydrin assay (μM)
Crude crystallin proteins (10 mg/mL)	286±12	298±9
*Amorphous protein aggregate**	118±10	126±14
Crystallin protein nanofibrils (10 mg/mL)	26±7	32±12

**Removed while fibrillation process, and re-dissolved in extraction buffer. All samples had same concentration and volume.*

Results obtained from the amino group availability studies show that the lysine rich components were getting removed along with the amorphous aggregates during the fibrillation process **(Table 3.3)** as anticipated**.** To ascertain whether there is any variability associated with crude crystallin proteins due to post translational modifications (section 3.6) or batch-to-batch variations, the OPA assay was also done on crude proteins extracted from different batches. Results obtained as shown in **Figure 3.5** verify that there is a difference between the lysine residue group availability of crystallin proteins extracted within the same batch **(Fig. 3.5, sample a and b)** and from the different batches **(Fig. 3.5 sample c)**. The lack of crosslinking *via* amine groups in crystallin PNFs indicates that only few lysine groups are available for crosslinking, and the remaining lysine groups are involved in forming/stabilising or are buried within the amyloid fibril structure, thus, they are not accessible.

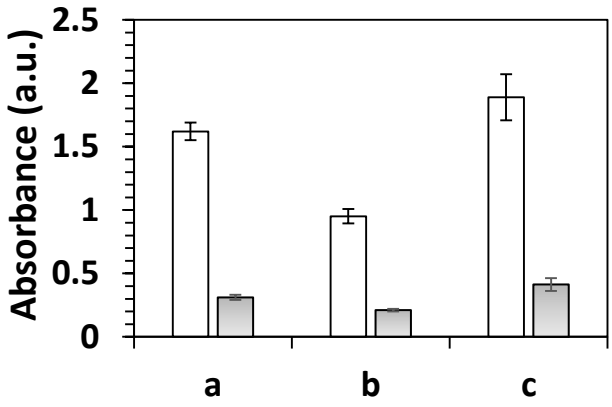

Figure 3.5. *Amino group availability assay as determined by the OPA assay. Blank bar - crude crystallin protein extract, and filled bar - crystallin PNFs prepared from the same batch sample - a and b, and from different batch - sample c. Error bars represent the standard deviation of three replicates.*

The results obtained by using amino group-based assays, suggested that there is insufficient availability of lysine groups in crystallin PNFs for the crosslinking reaction, and in order to achieve effective immobilisation, other methods such as immobilisation *via* other amino acid residues, oxidation of crystallin PNFs or crosslinking *via* polysaccharide chains needs to be utilised. Thus, further work was done to determine the potential functional residues available on the surface of crystallin PNFs, and to develop an efficient method for functionalising crystallin PNFs *via* these functional groups. A schematic representation of the amyloid fibrils with surface amino acid residues available for immobilising enzymes (*via* crosslinking or adsorption) to obtain functionalised PNFs is shown in **Figure 3.6**.

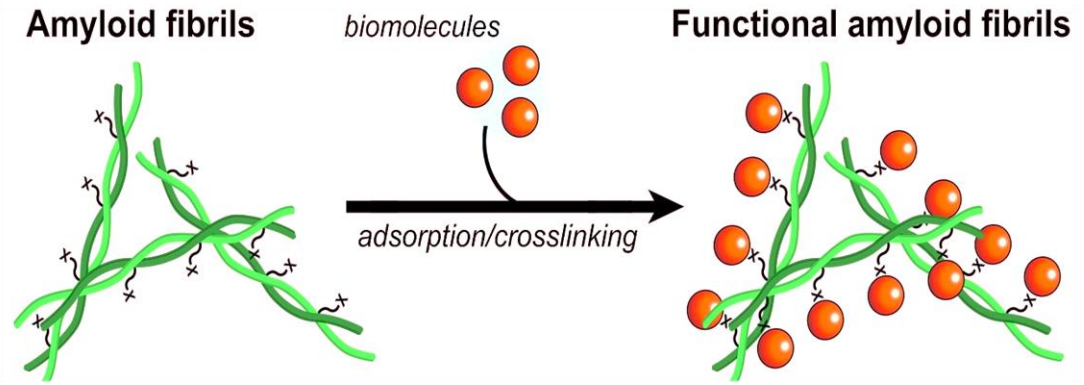

Figure 3.6. *A schematic representation of different amino acid residues studied in this work to obtain functionalised crystallin PNFs, where x- can be lysine, sulfhydryl, or aldehyde residue.*

3.5. Assessment of sulfhydryl/thiol group availability

Sulfhydryl/thiol groups due to their strong nucleophilic nature are very reactive and useful targets for coupling reactions [77].Thus, it was decided to attempt crosslinking *via* sulfhydryl groups using either homo-bifunctional or hetero-bifunctional crosslinkers, such as, bis-(maleimido) ethane (BMOE), and succinimidyl *trans*-(maleimidylmethyl) cyclohexane-1-carboxylate (Sulfo-SMCC). Other advantages of coupling *via* sulfhydryl groups include:

1. **Selective crosslinking**: The rarity of free sulfhydryl groups present in most proteins makes the reaction more selective [77].
2. **Easy to modify**: Sulfhydryl groups in proteins are generally present as disulfide bonds. Thus, free sulfhydryl/thiol groups can be easily generated by reduction of these native disulfide bonds by using reducing agents, such as dithiothreitol (DTT), and Tris-(2-carboxyethyl) phosphine hydrochloride (TCEP); or alternatively thiols can be introduced into a protein by using sulfhydryl-addition reagents, such as 2-iminothiolane (Traut's reagent) [78].
3. **Control over reaction**: Use of hetero-bifunctional crosslinkers for coupling sulfhydryl-reactive groups with amine-reactive groups provides greater flexibility and control over the crosslinking reaction [77].

Some proteins do contain free sulfhydryl groups available for crosslinking, but often it is required to introduce such groups artificially [78]. Hence it was important to evaluate the number of sulfhydryl groups present on the crystallin PNFs which could potentially be used for immobilising enzymes. To assess the availability of sulfhydryl groups in crystallin amyloid fibrils, Ellman's assay was used.

3.5.1. Ellman's assay

Ellman's assay, also known as the dithio-bis-(2-nitrobenzoic acid) DTNB assay, works by reacting DTNB with free sulfhydryl groups to yield a yellow-coloured product, 2-nitro-5-thiobenzoic acid (TNB) which can be detected at wavelengths of 412 nm **(Fig. 3.7)**. Ellman's assay was carried out according to in-house methods (section 7.6.3) [79], with a standard curve created using cysteine concentrations ranging from 0.2–2.0 mM, *see Appendix D, Fig. D1 (c).*

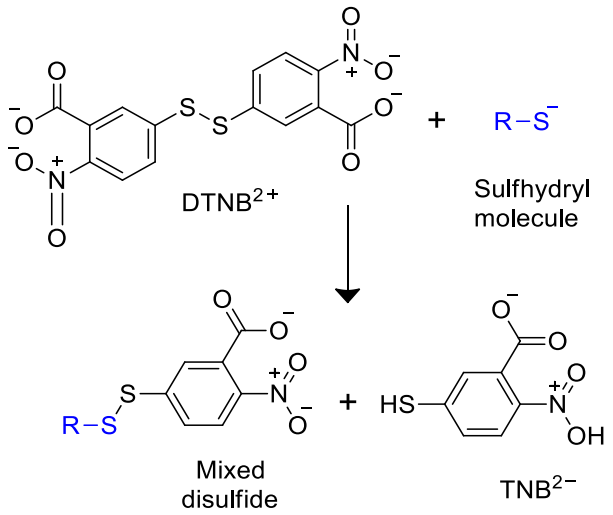

Figure 3.7. *Reaction scheme of Ellman's reagent with free sulfhydryls to produce a measurable yellow-coloured product product, 2-nitro-5-thiobenzoic acid (TNB) that can be detected at 412 nm [80].*

3.5.2. Sulfhydryl group availability of crystallin PNFs

Ellman's assay (section 7.6.3) was used to gain preliminary information about the presence of sulfhydryl groups, before the crosslinking experiments. Both crude crystallin protein solution at 10 mg/mL and crystallin PNFs obtained from this crude protein mixture were studied for sulfhydryl group availability. The results of Ellman's assay as summarised in **Table 3.4**, showed that there is a significant amount of reduction in the available sulfhydryl groups in crystallin PNFs as compared to the crude crystallin protein mixture.

Table 3.4. *Summary of calculated sulfhydryl group availability of crude crystallin protein solution, amorphous aggregate removed while making fibrils, and crystallin PNFs. Sample concentration is calculated from standard curve obtained using cysteine.*

Sample	Ellman's assay value (μM)
Crude crystallin protein solution	289 ± 14
Redissolved protein aggregate	112 ± 8
Crystallin protein nanofibrils	12 ± 6

Fibrils were formed using the standard in-house conditions and then concentrated and resuspended in PBS (pH 7.4) by centrifugation

This result was not unexpected since, a similar result was observed with the amino group availability (section 3.4.2). It is likely that sulfhydryl groups are buried within the fibrillar structure and are not accessible.

Free sulfhydryl groups undergo dimerisation in the presence of atmospheric oxygen to give disulfide bonds, which stabilise secondary and tertiary structures [81-86]. In general free sulfhydryl groups in proteins are protected by a microenvironment to prevent non-native dimer formation [78]. However, in the case of crystallin PNFs, the process of formation of crystallin PNFs is based on the denaturation of crystallin protein and involves disruption of the microenvironment. Thus, it is possible that available sulfhydryl groups are involved in stabilising the fibril structure, resulting in fewer sulfhydryl groups on the surface of crystallin PNFs as compared to the crude crystallin proteins. Lack of abundant free thiol groups on the crystallin PNFs surface suggested that in order to obtain a successful functionalisation of crystallin PNFs *via* sulfhydryl groups, different methodology is required. Two alternative ways studied were (i) use of reducing agents (e.g. dithiothreitol (DTT), and tris(2-carboxyethyl)phosphine (TCEP) to reduce the existing disulfide bonds, or (ii) introducing sufhydryl groups by using chemical reagents, such as 2-iminothiolane (Traut's reagent).

3.5.2.1 TCEP reduction of crystallin PNFs

For reducing sulfhydryl groups, TCEP, a sulfhydryl-free compound, was used. Bond breaker TCEP solution was preferred as TCEP is non-volatile, odourless, and unlike most other reducing agents, resistant to air oxidation [85]. Compared to DTT, TCEP is more stable, effective and water-soluble, and is able to reduce disulfide bonds over a wide range of pHs and temperatures [86, 87].

The reduction was carried out as detailed in section 7.6.4. For characterising free sulfhydryl groups, Ellman's assay was done on the reduced crystallin fibril sample (section 7.6.3). To remove any residual TCEP solution in the treated sample, PNFs were washed and collected by centrifugation, before performing the assay (section 7.6.4).

As shown in **Figure 3.8**, the reduction of crystallin PNFs using TCEP yielded free sulfhydryl groups. As compared to initial sulfhydryl group readings, a significant increase in the assay reading was observed for the fibrils treated with TCEP, suggesting successful reduction of crystallin PNFs with TCEP. These TCEP-treated samples were then used further for crosslinking reactions using Sulfo-SMCC, a sulfhydryl group-based crosslinker, see **Table 3.5 (b)**.

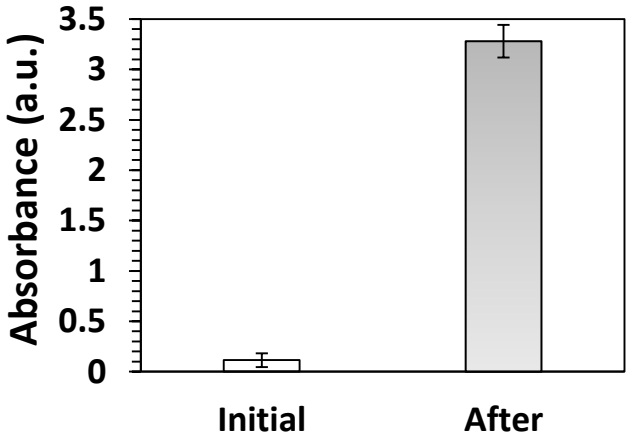

Figure 3.8. *TCEP reduction of crystallin PNFs, where blank bar - initial sulfhydryl group concentration, and filled bar - sulfhydryl group concentration after TCEP reduction. Fibrils were characterised using Ellman's assay, absorbance readings were taken at 412 nm. Error bars represent the standard deviation of the mean of three replicates.*

3.5.2.2. Introducing sulfhydryl groups onto CPNFs, using Traut's reagent

Another approach usually used for crosslinking *via* sulfhydryl groups is to introduce sulfhydryl groups into a protein, by using sulfhydryl-adding reagents. The most commonly encountered and commercially available protein thiolation reagents are those which exhibit reactivity towards amines, such as SATA (N-succinimidyl S-acetylthioacetate), SATP (N-succinimidyl-S-acetylthiopropionate), and Traut's reagent [78].

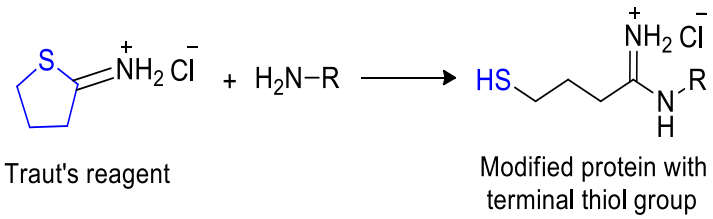

Figure 3.9. *Schematic representation of Traut's reagent reaction with primary amines (-NH_2) to introduce sulfhydryl (-SH) groups [77].*

The results from the lysine-based assays (section 3.4.2) suggest a lack of sufficient amine groups on the crystallin PNFs, thereby, any method involving amine groups cannot be used for functionalising crystallin PNFs. However, as previous work on whey PNFs demonstrated successful thiolation of whey PNFs using Traut's reagent [16], so it was decided to perform Traut's reaction **(Figure 3.9)** on both whey, and crystallin PNFs to further confirm the lack of sufficient amine groups onto the surface of crystallin PNFs. The thiolation of PNFs (section 7.6.5) and availability of sulfhydryl groups on the surface of modified PNFs was characterised *via* Ellman's assay as detailed in section 7.6.3, and is shown in **Figure 3.10**.

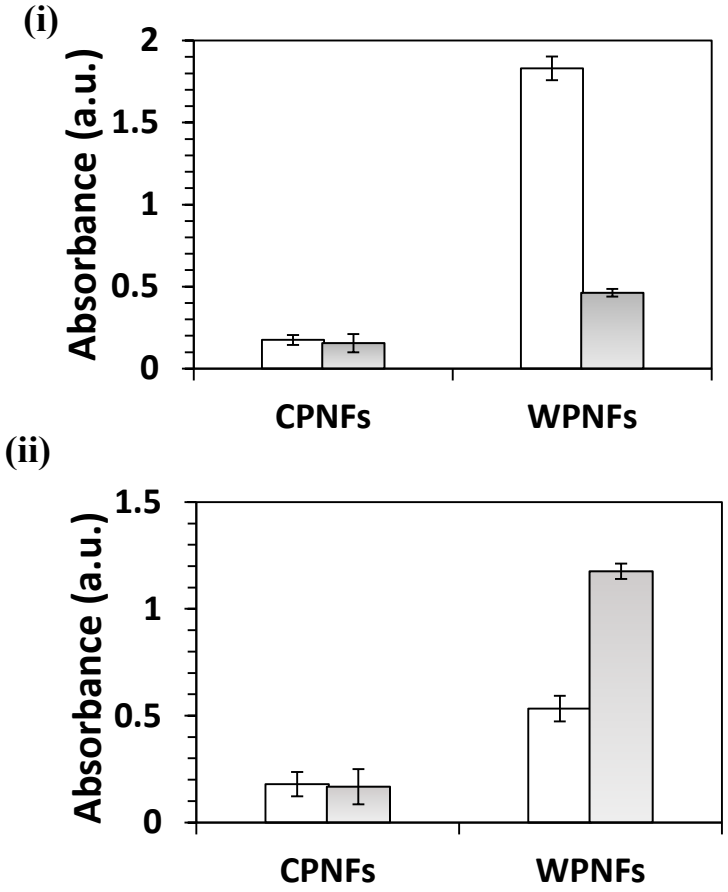

Figure 3.10. (i) *OPA and* ***(ii)*** *Ellman's assay for crystallin amyloid fibrils (CPNFs), and whey protein nanofibrils (WPNFs). Blank bars - initial readings, and filled bars - readings taken after treating with Traut's reagent. Error bars represent the standard deviation of the mean of three replicates.*

As stated earlier, Traut's reagent targets the primary amines present on the surface of the fibrils, therefore, crosslinking of Traut's reagent to the free amino groups of the fibrils was also determined by assessing the decrease in amine-residue group availability, using the OPA assay (section 7.6.1). The addition of Traut's reagent decreases the free amino group concentration on the surface of whey PNFs, **Fig. 3.10(i)**, and increases the amount of free thiol groups on the surface of the whey PNFs as shown in **Fig. 3.10(ii)**. For crystallin PNFs, addition of Traut's reagent did not result in any increase in the amount of free thiol groups, as anticipated due to lack of available amine groups **(Fig 3.10(i))**.

This corroborates the observation that due to the lack of sufficient amine groups on the crystallin PNFs, any method involving amine groups cannot be used for functionalising crystallin PNFs. Traut's reagent reaction chemistry is specific to amines and hence, it worked effectively for whey PNFs.

Inefficient crosslinking *via* both lysine residues and thiols (results summarised in **Table 3.5**) suggested the need for other effective crosslinking methods. Previous work by Domigan (2012), had recommended that the possible glycosylation of the crystallin proteins could be a reason for the observed lack of crosslinking *via* amino groups [68]. In this work, crystallins were tested for presence of glycosylation and the possibility of using oxidised PNFs for creating functional fibril scaffolds was explored.

3.6. Post translational modifications

Several studies have shown that eye lenses grow throughout the lifetime of an individual, and significant changes occur in the structure and function of lenses with aging [88-93]. The major post-translational modifications include phosphorylation, truncation, deamidation, glycosylation, glycation, racemisation, isomerisation, deoxidation, acetylation, and carbamylation [77, 94-96]. The accumulation of all such post translational modifications in the lens proteins, specifically crystallins, is considered to be the major cause of cataract development [97]. The attachment of sugar residues is the most common [98] and complicated post-translational modification that a protein can undergo [99]. The attachment of carbohydrates or extended sugar chains to proteins can be attained both enzymatically (glycosylation), and non-enzymatically (glycation) [77]. Crystallin proteins are one of the important proteins subjected to glycosylation [100], and glycation [101] and are the possible target sites for crosslinking reactions.

Glycation typically involves the addition of a carbohydrate to a protein *via* a reaction between reducing sugars and amine groups of proteins [102]. A reducing sugar may modify protein amine groups, such as those on lysine residues, through Schiff base formation followed by an Amadori rearrangement to give a stable ketoamine product [77] as shown in **Figure 3.11**. The aldehyde group of a reducing sugar first forms a Schiff base linkage with the amine group *via* a nucleophilic addition. The chemically unstable Schiff base then undergoes chemical rearrangement, resulting in the formation of a stable ketoamine (Amadori product).

Amadori adduct formation is slow but much faster than the reverse reaction, leading to accumulation of Amadori glycation products on the protein [103, 104]. This results in a blocked amine containing a sugar derivative [77]. Although most proteins are glycated through their lysine residues [105], other sites for glycation may include side chains of arginine, histidine, tryptophan and cysteine residues [106].

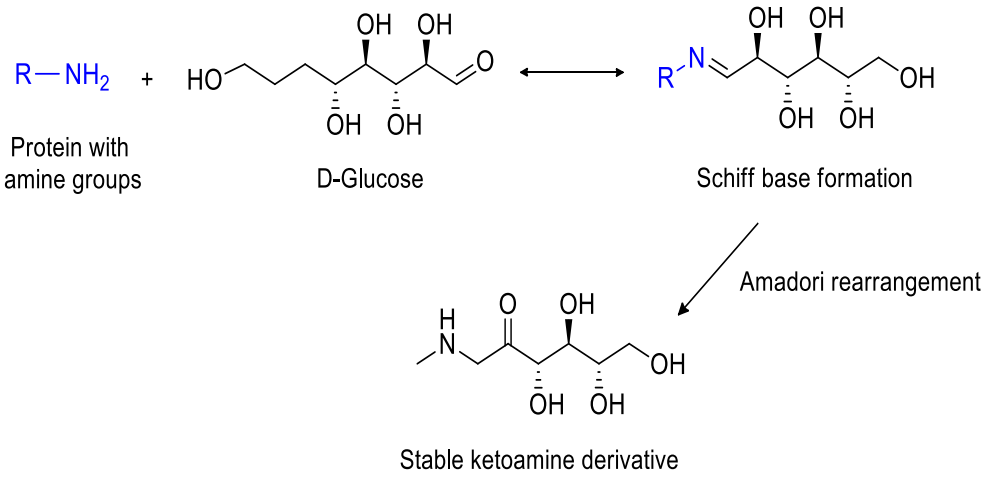

Figure 3.11. *Schematic representation of a reaction between a reducing sugar and amine groups of proteins, such as those on lysine residues. A reducing sugar may modify protein amine groups, through Schiff base formation followed by an Amadori rearrangement to give a stable ketoamine product, Hermanson, (2013) [77].*

In contrast to the glycation, lysine amine groups are not targeted directly in the case of glycosylation but, depending upon the attachment site of carbohydrates, it could hinder access to available amino acid residues of proteins. In glycosylation, one or several carbohydrate chains covalently attach to the amide group of asparagine residues (*N*-linked), or to hydroxyl groups of serine and threonine residues (*O*-linked) of the protein polypeptide chain [98, 107] **(Figure 3.12).**

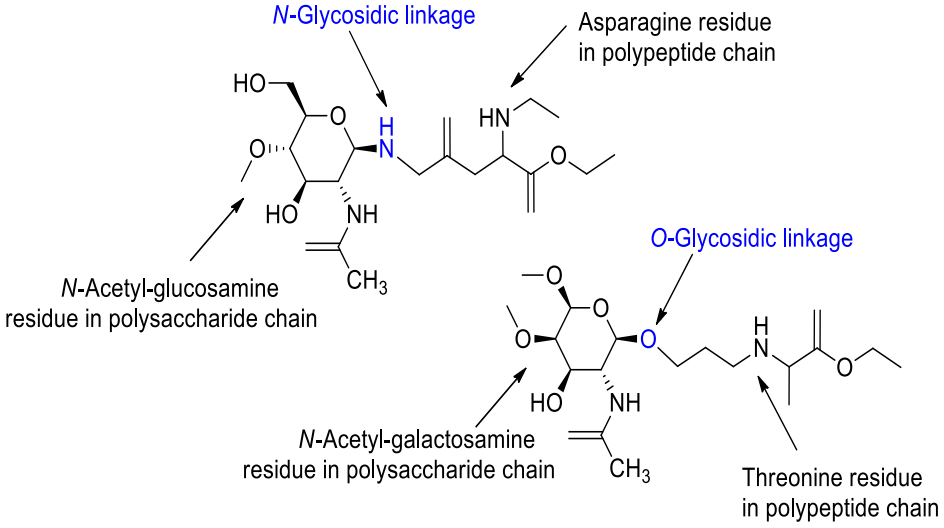

Figure 3.12. *Common attachment sites for carbohydrate chains on glycoproteins, Hermanson, (2013) [77].*

3.7. Crystallin proteins and glycosylation

The presence of carbohydrates in crystallin proteins was investigated by staining SDS-PAGE with Pro-Q Emerald 300 staining solution (Molecular Probes, Invitrogen) (section 7.7), which reacts with periodate-oxidised carbohydrate groups, creating a fluorescent signal on glycoproteins (Molecular Probes, 2007). The detection of glycoproteins using Pro-Q Emerald 300 stain has been reported to be suitable for sensitive direct fluorescence detection of glycoproteins in gels or electroblots [108]. The staining method is based on periodic acid-Schiff's base (PAS) reaction mechanism (discussed in section 3.7.1), and involves oxidation of glycols present in the glycoprotein to aldehydes using periodic acid, followed by staining with Pro-Q Emerald dye. The dye reacts with the aldehydes on the glycoproteins to generate the fluorescent conjugate which can be then visualised with 300 nm UV illumination [109].

Crude crystallin proteins, along with crystallin PNFs were run on an SDS-PAGE (section 7.1.1), and stained for glycoproteins using Pro-Q Emerald 300 staining solution (as detailed in section 7.7.1). GOX was also run as a positive glycoprotein control, as GOX is known to possess a carbohydrate shell [110]. A representative SDS-PAGE stained with Pro-Q Emerald 300 is shown in **Figure 3.13.** Positive staining for glycoproteins was seen for the GOX control (Lane 1), and also for bands containing mixtures of crude crystallin proteins at a final concentration of 5 mg/mL in Lane 2, and 10 mg/mL in Lane 3. Similarly, positive staining was seen for crystallin PNFs which are too large to enter the gel, and so remain in the well at the top of the gel (Lane 4 and Lane 5).

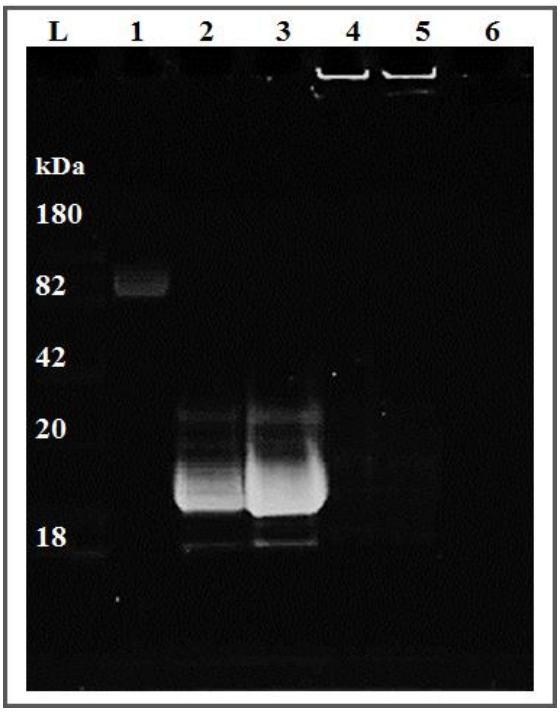

Figure 3.13. *SDS-PAGE gel of crystallin proteins stained for glycoproteins. Lane 1 – Ladder, Lane 2 - GOX (glycoprotein positive control), Lane 3 - crude crystallin protein solution (5 mg/mL), Lane 4 - crude crystallin protein solution (10 mg/mL), Lane 5 - crystallin PNFs (~5 mg/mL), Lane 6 - crude crystallin PNFs (~10 mg/mL).*

From these results, it can be confirmed that fish crystallin proteins do contain carbohydrates, which would at least hinder access to available amino acid residues of crystallin proteins and can be targeted for crosslinking reactions. Positive glycoprotein staining for crystallin proteins as indicated by the presence of the fluorescent bands **(Figure 3.13)** confirmed the presence of carbohydrate moieties in crystallin proteins, which could be potentially used for immobilisation reaction [77].

3.7.1. Periodate oxidation of glycoproteins

To achieve successful crosslinking *via* carbohydrate groups, periodate oxidation of carbohydrate residues was investigated (section 7.7.2). The periodate oxidation reaction also known as the Malaprade reaction [78], involves treatment of the glycoprotein with periodic acid or its salt in aqueous solution, such as sodium metaperiodate [111]. The reaction of sodium metaperiodate oxidises the vicinal diols in the glycoprotein and usually cleaves adjacent hydroxyl groups in sugar residues to create amine reactive aldehyde groups as shown in **Figure 3.14**. The aldehydes obtained contain a highly electron-deficient carbon atom and are prone to nucleophilic attack, thus are an excellent target for the crosslinking reactions [112].

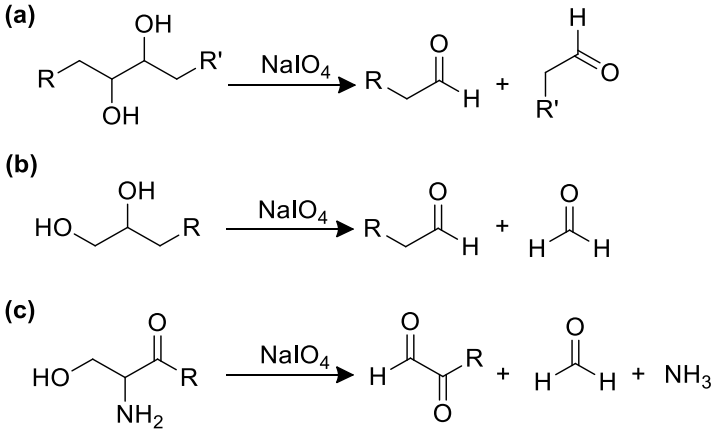

Figure 3.14. *Schematic representation of the oxidative cleavage of carbohydrates. Sodium metaperiodate can oxidise (a) internal diol groups, (b) terminal diol groups or (c) terminal hydroxylamine groups to yield aldehyde groups, Hermanson (2013) [77].*

3.7.2. Periodate oxidation of crude crystallin proteins

In order to investigate the effect of the sodium metaperiodate treatment, glycoprotein staining (section 7.7.1) was done on the crude crystallin proteins. Crude crystallin protein mixture was treated with different concentrations of sodium metaperiodate for 1 h, at 26 °C, in dark conditions (section 7.7.2) to prevent over oxidation and decomposition of periodate, leading to the production of more reactive species [113]. The oxidation reaction was done at pH 4.5, as the optimum pH for periodate oxidation reaction is considered to be between pH 3-5 [113].

To assess the extent of oxidation, crude crystallin proteins (~10 mg/mL) after treatment with sodium metaperiodate was run on the SDS-PAGE (section 7.1.1), and stained with Pro-Q Emerald 300 staining solution (section 7.7.1). A representative SDS-PAGE is shown in **Figure 3.15**. Positive staining for glycoproteins was seen for the crude crystallin proteins (control-Lane 1).

With the increasing concentration of sodium metaperiodate - 10 mM (Lane 2), 20 mM (Lane 3), 30 mM (Lane 4), 40 mM (Lane 5), and 50 mM (Lane 6) - a decrease in glycoprotein stained protein band on gel, and appearance of new bands in the well (Lane 5, 6, and 7) was observed, confirming the presence of oxidised proteins. This presence of a new band suggests the formation of protein aggregates, proposing that with higher concentrations of sodium metaperiodate, more aldehyde groups are generated. The presence of aldehyde groups in large amounts can lead to a number of intramolecular interactions [114] and aggregation of protein is either due to the amine to aldehyde or aldehyde to aldehyde linkages.

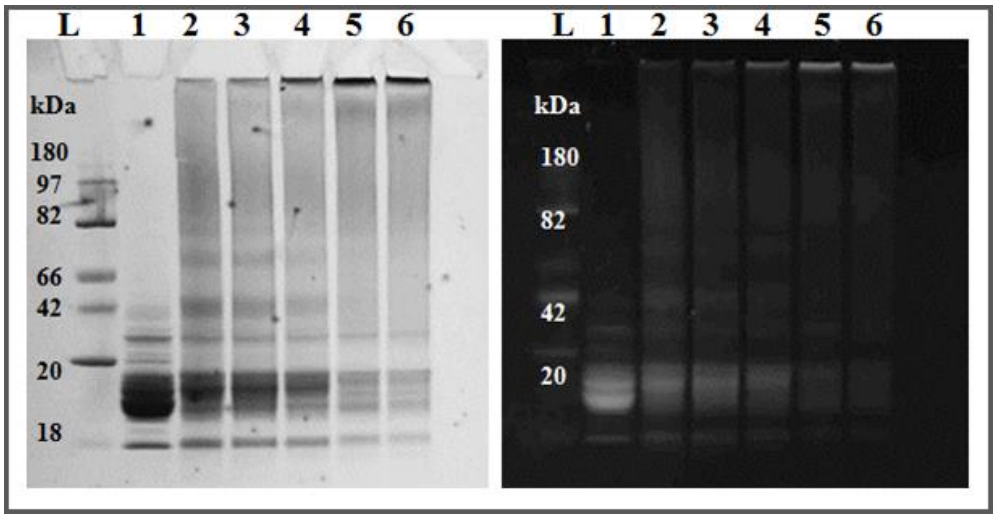

Figure 3.15. *SDS-PAGE gel of crystallin proteins (CPs) stained for proteins (left-hand image), and glycoproteins (right-hand image) after treatment with sodium metaperiodate. From left to right - Lane 1 - Ladder; Lane 2 - crude crystallin proteins-only; Lane 3 - CP + 10 mM sodium metaperiodate; Lane 4 - CP + 20 mM sodium metaperiodate; Lane 5 - CP + 30 mM sodium metaperiodate; Lane 6 - CP + 40 mM sodium metaperiodate; and Lane 7 - CP + 50 mM sodium metaperiodate.*

This intramolecular crosslinking of oxidised glycoproteins in the presence of multiple aldehyde and hydroxyl groups is well reported in literature [115], [116]. The appearance of new glycoprotein stained bands after treating crude crystallin protein mixture with sodium metaperiodate (Lane 2-Lane 6), compared to the untreated crystallin proteins (Lane 1) on the gel, confirms that the sodium metaperiodate treatment was effective for producing reactive aldehyde groups, which can be further targeted for immobilisation reactions.

3.7.3. Periodate oxidation of crystallin PNFs

Oxidation of crystallin PNFs was obtained by the same method used for crude crystallin protein mixtures.

The results obtained from crude crystallin protein treatment with sodium metaperiodate suggested that a final concentration of 30 mM sodium metaperiodate was effective to yield carbonyl groups, and higher concentrations may result in aldehyde-amine or aldehyde-aldehyde linkages. Therefore, a final 30 mM concentration was used for oxidising crystallin PNFs (section 7.7.3). Crystallin PNFs at ~10 mg/mL concentration were treated with 30 mM of sodium metaperiodate solution prepared in sodium acetate buffer, pH 4.5 and incubated for 2 h at room temperature. Considering that the availability of carbohydrate moieties can be different in fibrillar structures compared to the crude proteins in solution, thereby, incubation time of 180 min was preferred instead of 60 min used for crystallin protein solution to ensure that the reaction is complete with aliquots taken at regular intervals. As stated earlier during gel electrophoresis, due to size restrictions, PNFs remain in the well at the top of the gel, thus glycoprotein staining could not be used for confirming oxidation of crystallin PNFs. Alternatively, the 2, 4-dinitrophenylhydrazine (DNPH) assay was used to characterise aldehyde groups in oxidised crystallin PNFs.

(a) DNPH assay to evaluate the oxidation reaction: The DNPH assay of carbonyl groups provides a convenient technique for detecting and quantifying oxidative modification of proteins [117]. DNPH reacts with protein carbonyls *via* a nucleophilic addition-elimination reaction to produce a bright orange or yellow hydrazine product, as illustrated in **Figure 3.16**.

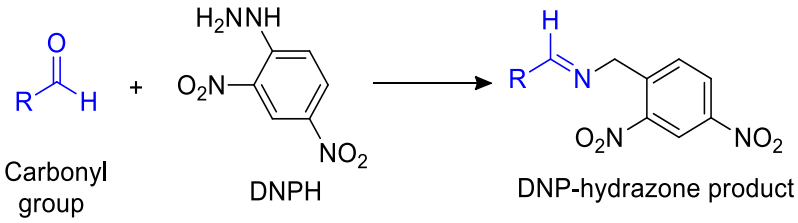

Figure 3.16. *Schematic representation of DNPH reaction with protein carbonyl groups, producing a protein-DNP hydrazine product (yellow to orange solid) that can be detected spectrophotometrically [117].*

In order to eliminate any unreacted sodium metaperiodate, treated fibrils were washed, centrifuged, and the pellet was re-suspended in PBS (pH 7.4). Initially, carbonyl group quantification was done as described by Levine *et al*. (1990) [117], and absorbance measurements of hydrazine derivatives of carbonyl groups formed by reaction with DNPH were made at a wavelength of 370 nm. As unbound DNPH itself absorbs at the same wavelength (370 nm) and could interfere with the results [117], care was taken to eliminate any residual DNPH.

To remove any unreacted DNPH, extensive organic solvent washing of crystallin PNFs was done before taking measurements but still high background absorbance measurements were obtained, and is a common drawback for the DNPH assay [117]. Another approach usually used to remove any unbound DNPH from protein samples is *via* gel filtration [118]. However, gel filtration method was not feasible for PNFs, due to the size restrictions and thus a new method as described by Mesquita *et al.* (2014) (section 7.8) was used [119].

In this method, addition of NaOH to the reaction shifts the maximum absorbance of hydrazine derivatives of carbonyl group in oxidised protein from 370 to 450 nm and eliminates the interference of free DNPH [119].

(b) DNPH assay to characterise oxidised crystallin PNFs: The DNPH assay was done for periodate oxidised crystallin PNFs (section 7.8) and the absorbance was measured at 450 nm. The increase in absorbance at 450 nm for treated fibrils as compared to the untreated fibrils due to the formation of hydrazine derivatives of carbonyl groups, confirms that 30 mM sodium metaperiodate is effective in yielding carbonyl groups on the surface of oxidised crystallin fibrils, see **Figure 3.17(i).** Also, the DNPH assay was done on samples taken at different time intervals. The results obtained as shown in **Figure 3.17(ii)**, indicate an increase in carbonyl groups over the time period of 2 h. The presence of carbonyl groups was detected after 30 min of the reaction, which further increased after 60 min of the reaction and reached a maximum within 120 min. Interestingly, there is a drop in absorbance for the sample taken at 180 min. This decrease over the longer duration is due to the formation of multiple aldehyde groups which are prone to a number of intermolecular reactions, thereby converting oxidised carbohydrate moieties into more stable forms [105].

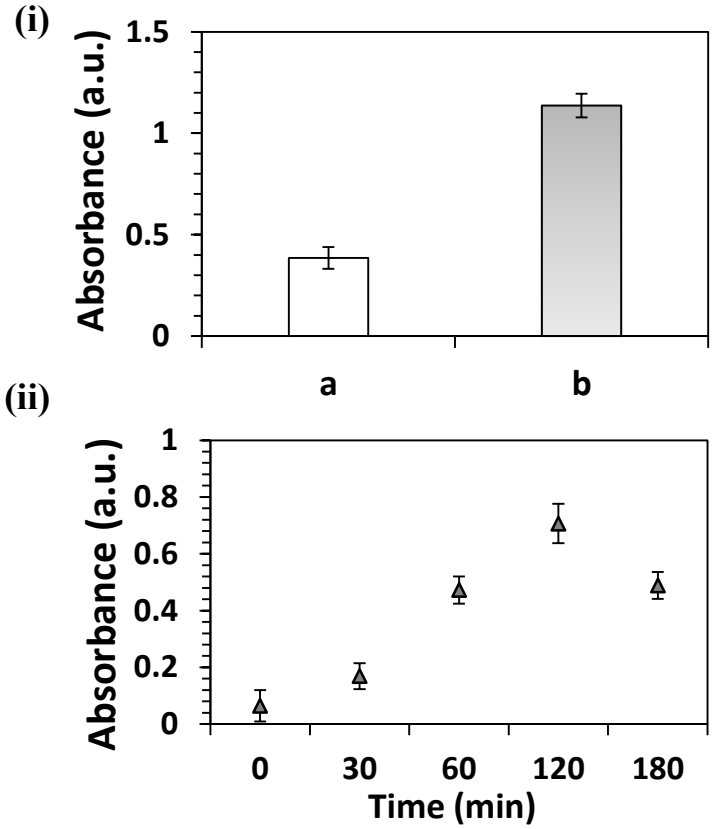

Figure 3.17. (i) *Carbonyl group availability assay for crude crystallin amyloid fibrils (CPNFs), before and after sodium metaperiodate treatment, absorbance was measured at 450 nm, where sample a - carbonyl group availability of untreated CPNFs, and sample b - carbonyl group availability of CPNFs after sodium metaperiodate treatment (oxidised CPNFs).* ***(ii)*** *Carbonyl group availability characterised by the DNPH assay for deglycosylate/oxidised crystallin amyloid fibrils (CPNFs), over the time period of 2 h, absorbance measured at 450 nm. Error bars represent the standard deviation of the mean of three replicates.*

After the periodate oxidation method development, the oxidation conditions chosen for crystallin PNFs were: a final concentration of ~10 mg/mL crystallin PNFs; with 30 mM final concentration of sodium metaperiodate solution; incubated for 120 min, at 26 °C in dark conditions. The oxidised crystallin PNFs were investigated further for immobilisation experiments **(Table 3.5, c and d)**. For functionalising oxidised crystallin PNFs, aldehyde group-based crosslinking methods were studied. Aldehydes are electrophilic in nature due to the presence of electron-deficient carbon groups and thus are highly reactive towards nucleophilic functional groups, such as primary amines.

3.8. Aldehyde group-based crosslinking reaction

The reaction of an aldehyde with an amine proceeds with the formation of α-hydroxyamine intermediate, followed by spontaneous dehydration to form an imine or Schiff base **(Figure 3.18)**. This leads to the formation of a conjugate between the carbohydrate moiety of one protein and the amine groups of another protein. In this work, oxidised crystallin PNFs provides the carbohydrate group (aldehyde) and immobilisation of the enzymes was achieved by targeting their amine groups either *via* direct coupling reaction or reductive amination reaction.

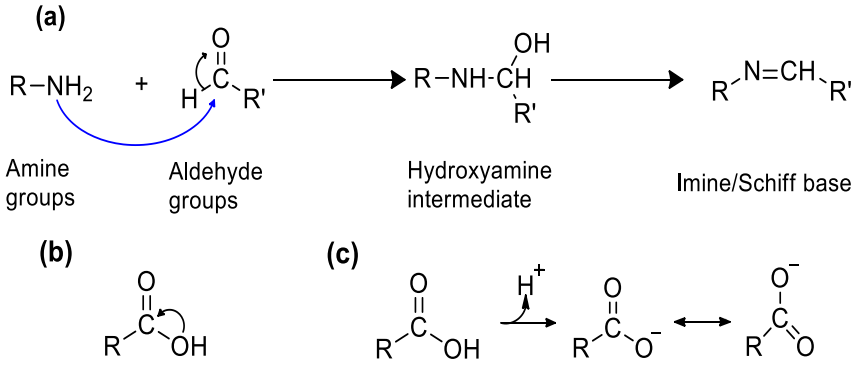

Figure 3.18. *Schematic representation of direct coupling reaction of carbonyl groups with amine groups (a) the α-hydroxyamine intermediate formation followed by spontaneous dehydration to form an imine or Schiff base. However, carboxylate anion is a very poor target for nucleophilic attack, (b) the mesomeric effect from the hydroxyl group increases the electron density around the carbon, and (c) the likely predominance of the anionic carboxylate formation (around pH 5.5-6.5) prevent direct coupling reaction of aldehyde with amine [78].*

3.8.1 Direct coupling reaction

The aldehyde groups generated by the sodium metaperiodate oxidation (section 7.7.3) of crystallin PNFs can be coupled to the available amine groups on the surface of the enzyme *via* a direct reaction, generating an imine or Schiff base, **Figure 3.18 (a)**. However, Schiff bases formed with amines are highly unstable and rapidly hydrolyses (reverses) in aqueous solution, [120], [121], and it is common practice to reduce the Schiff base to generate a secondary amine linkage (stable alkylamine linkage) instead, *via* a reductive amination reaction [122].

3.8.2 Reductive amination reaction

Reductive amination is usually fast and is very efficient method for obtaining stable secondary and tertiary amines [123]. In reductive amination, the Schiff base linkage obtained by the direct coupling of aldehyde with an amine is reduced to a stable, irreversible secondary amine bond by using a reducing agent as illustrated in **Figure 3.19**. The transformation of carbonyl groups to amines can be obtained either by direct reductive amination reaction or by indirect reaction. In the direct reductive amination reaction **(Figure 3.19, *scheme 1*)**, both the conversion of a carbonyl compound to the intermediate imine and reduction of the intermediate imines formed to obtain stable amine linkages is carried on simultaneously in one step reaction only, in the presence of a suitable reducing agent. On the other hand, indirect reductive amination **(Figure 3.19, *scheme 2*)** is a stepwise reaction, in which intermediate imine/Schiff base are formed first by the reaction between a carbonyl group and the primary amine. This intermediate is then reduced with a suitable reducing agent to obtain a stable amine.

Scheme 1.

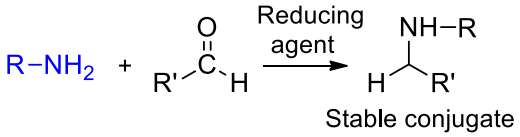

Scheme 2.

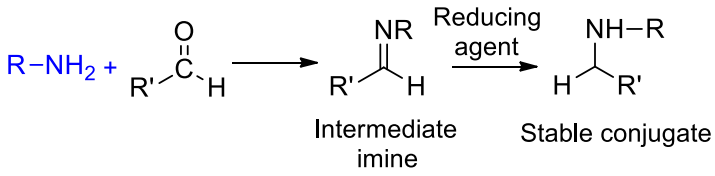

Figure 3.19. *Schematic representation of the reductive amination reaction.* ***Scheme 1*** *- shows direct reductive amination, when the carbonyl compound and the amine are mixed with the proper reducing agent without prior formation of the imine intermediate.* ***Scheme 2*** *- shows indirect reductive amination, a stepwise reaction which involves the preformation of the intermediate imine followed by its reduction in a separate step, adapted from Cho and Kang, (2005) [124].*

Several reducing agents and variety of methods [125-130] have been successfully used for the reductive amination reactions. Care should be taken while using a reducing agent depending upon if the reductive amination reaction is to be carried on directly or indirectly. For direct reductive amination, reducing agents that are more reactive towards intermediate imines than the carbonyl groups, and are stable under mild acidic conditions, such as sodium cyanoborohydride ($NaBH_3CN$), and sodium triacetoxyborohydride ($NaBH(OCOCH_3)_3$ (STAB) should be used [131], see **Table 3.5 (d)**.

3.9. Conclusion

The use of different amino acid availability assays for characterising crystallin PNFs was demonstrated. After successfully characterising crystallin PNFs for the available amino residues, different immobilisation methods were used to functionalise crystallin PNFs, including physical adsorption, crosslinking *via* amine-thiol groups, and aldehyde-based cross-linking approach. GOX was successfully immobilised onto the crystallin PNFs *via* both physical adsorption and amine-thiol linking. The oxidised CPNFs were also successfully functionalised by GOX, and β-gal *via* indirect reductive amination, in the presence of STAB. However, none of these methods was consistent **(Table 3.5)**, and thus a modified GA-based method in search of a reliable crosslinking approach was studied further (Chapter Four).

Table 3.5. *A brief summary of various crosslinking methods used for functionalising crystallin PNFs, with all the variables considered, and success rate for each of the crosslinking reaction, where ✓✓ - good immobilisation efficiency, ✓ - poor immobilisation efficiency, and X - no immobilisation.*

(a) Physical adsorption

Details	Conditions/Variables	Success/Comments
Crystallin PNFs *(10 mg/mL) were directly added to the enzyme (GOX)(section 7.9.1.1)*	***Reaction:*** *CPNFs + GOX (2 mg/mL)* *CPNFs + GOX (1 mg/mL)* *CPNFs + GOX (0.5 mg/mL)* ***Time (h):*** *6-24* ***Temperature (°C):*** *26, and 4*	***Success rate:*** ✓ ✓ ✓ *24 h reaction at 4°C.* ***Comment:*** *N/A for other enzymes*

(b) TCEP reduced PNFs: physical adsorption, and crosslinking via Sulfo-SMCC

Details	Conditions/Variables	Success/comments
Crystallin PNFs *were treated with TCEP(section 7.6.4), and TCEP treated CPNFs (10 mg/mL) were then added to the enzyme (GOX) - physical adsorption (section 7.9.1.2) or* ***Crosslinking via Sulfo-SMCC*** *(section 7.9.2)*	***Reaction:*** *CPNFs + GOX (2 mg/mL)* *CPNFs + GOX (1 mg/mL)* *CPNFs + GOX (0.5 mg/mL)* ***Crosslinker:*** *+ Sulfo-SMCC** ***Time (h):*** *24* ***Temperature (°C):*** *4*	***Success rate:*** ✓✓ ✓✓ ✓✓ *24 h reaction at 4°C.* ***X*** ***Comment:*** *N/A for other enzyme, and reproducibility issues due to inefficient TCEP reduction.*

****Sulfo-SMCC*** *is a highly reactive hetero-bifunctional crosslinker, with two distinct reactive groups: an amine-reactive N-hydroxysuccinimide (NHS ester) and a sulfhydryl-reactive maleimide group [77]. NHS esters react with primary amines at pH 7-9 to form stable amide bonds and maleimides react with sulfhydryl groups at pH 6.5-7.5 to form stable thio-ether bonds. Sulfo-SMCC chemistry is compatible with sulfhydryl residues, and was used to functionalise PNFs via sulfhydryl and amine residues of PNFs, and enzymes respectively, in order to overcome the problems faced due to the lack of lysine group availability of crystallin PNFs.*

(c) Direct coupling reaction

Details	Conditions/Variables	Success/Comments
***Crystallin PNFs** were treated with sodium metaperiodate (section 7.7.3), and **oxidised CPNFs (10 mg/mL)** were then added to the enzyme (GOX)(section 7.9.3)*	***Reaction:*** *O-CPNFs + GOX (2 mg/mL)* ***Time (h):*** *2* ***Temperature (℃):*** *26*	***Success rate:*** ✗ ***Comment:*** *Rapid hydrolysis of Schiff bases formed resulting in inefficient crosslinking***

*****Direct coupling reaction**: It is well reported in the literature that Schiff bases formed with amines rapidly hydrolysis (reverses) in aqueous solution and for achieving a successful conjugation, it is customary to reduce the Schiff base to a stable alkylamine linkage, known as reductive amination reaction [122].*

(d) Reductive amination reaction: In the presence of reducing agents

Details	Conditions/Variables	Success/Comments
*Crystallin PNFs were treated with sodium metaperiodate (section 7.7.3), and **oxidised CPNFs (10 mg/mL)** were then added to the enzyme (GOX) in the presence of Sodium borohydride **(section 7.9.4.1)*** ***(i)** either added directly - I step reaction* ***(ii)** or after 15 min incubation of the enzyme with CPNFs - II step reaction.*	***Reaction:*** *In the presence of $NaBH_4$ or H_3BO_3 activated $NaBH_4$ O-CPNFs + GOX (2 mg/mL) I step reaction II step reaction* ***Time (h):*** *1-2* ***Temperature (℃)*** *25, 37, and 4*	***Success rate:*** ✗ ✗ ***Comments:*** *$NaBH_4$ hydrolysis****

***** **Reductive amination using $NaBH_4$**: The stability of $NaBH_4$ in water is dependent on the pH of the solution and is believed that borohydride activity begins to be lost below pH 9 [78]. Thus, H_3BO_3 activated $NaBH_4$ was not used further for any reaction and care was taken to perform the reaction at around pH 9 (using 1M NaOH). Although the initial reaction was maintained at around pH 9, an interesting increase in pH was observed after 15 min of incubation time, to pH 9.6. The pH increase was caused by the hydrolysis of $NaBH_4$ in water (equation 1), leading to the formation of the strongly basic meta-borate ion in the reaction [132] (see equation 2).*

$$NaBH_4 + 2H_2O \longrightarrow NaBO_2 + 4H_2 \quad \text{...equation 1}$$

$$BH_4^- + 2H_2O \longrightarrow 4H_2 + BO_2^- \quad \text{...equation 2}$$

Further, to prevent $NaBH_4$ hydrolysis, reduction time was reduced to 5 min and alternatively experiments was done in the presence of solvents, in order to favour condensation of an amine with an aldehyde to form an imine [133](section 7.9.4.1), but successful immobilisation conditions could not be found. The use of $NaBH_3CN$ despite of its greater pH stability and selectivity was not used due to the toxicity associated with the $NaBH_3CN$ itself, as well as with the side products(hydrogen cyanide and sodium cyanide) formed during the reaction [134]. Alternatively, STAB was preferred as it is mild, convenient, and more reactive toward protonated imines than aldehydes [130]. Additionally, STAB is more selective of a reducing agent than $NaBH_4$ at neutral or slightly acidic pH (pH 6)[130],[135].

Details	Conditions/Variables	Success/Comments
Alternatively, *reductive amination reaction was done in the presence of* ***sodium triacetoxyborohdyride (STAB)****: STAB was dissolved in isopropanol(section 7.9.4.2)*	***Reaction:*** *O-CPNFs + GOX (2 mg/mL)* *O-CPNFs + β-gal (2.9 mg/mL)* ***Time (h):*** 1 ***Temperature (℃):*** 26	✓ ✓ *Comment:* ***Inefficient cross-linking****

*****Inefficient reductive amination reaction:*** *Other factors contributing towards unsuccessful reductive amination include the presence of water in the reaction system, preventing formation of the intermediate imines or Schiff bases and decomposing the hydride reagent [135]. To compensate for any decomposed hydride, the reaction was done with additional amounts of STAB. In general, polar aprotic solvents, such as DME (dimethoxyethane), ACN, or THF (tetrahydrofuran) are considered suitable for this reaction [130]. The use of these solvents despite of their suitability was avoided in this work due to the fibril stability issues in polar aprotic solvents (as discussed in Chapter Two). Additionally, attempt to develop a practical complete solvent-based reaction system was also hindered by the poor solubility and inactivation of the enzymes. Thus, further work using any other modified reaction condition, was not attempted.*

3.10. References

[1] R.A. Sheldon, Enzyme immobilisation: The quest for optimum performance, *Advanced Synthesis & Catalysis*, 349 (2007) 1289-1307.

[2] R. Wilson, A. Turner, Glucose oxidase: An ideal enzyme, *Biosensors and Bioelectronics*, 7 (1992) 165-185.

[3] R.G. Bodade, C.N. Khobragade, S. Arfeen, Optimisation of culture conditions for glucose oxidase production by a *Penicillium chrysogenum* SRT 19 strain, *Engineering in Life Sciences*, 10 (2010) 35-39.

[4] C.M. Wong, K.H. Wong, X.D. Chen, Glucose oxidase: Natural occurrence, function, properties and industrial applications, *Applied microbiology and biotechnology*, 78 (2008) 927-938.

[5] S.B. Bankar, M.V. Bule, R.S. Singhal, L. Ananthanarayan, Glucose oxidase - an overview, *Biotechnology Advances*, 27 (2009) 489-501.

[6] V. Rosilio, M.-M. Boissonnade, J. Zhang, L. Jiang, A. Baszkin, Penetration of glucose oxidase into organised phospholipid monolayers spread at the solution/air interface, *Langmuir*, 13 (1997) 4669-4675.

[7] B.D. Malhotra, A. Chaubey, Biosensors for clinical diagnostics industry, *Sensors and Actuators B: Chemical*, 91 (2003) 117-127.

[8] J. Vartiainen, M. Rättö, S. Paulussen, Antimicrobial activity of glucose oxidase-immobilised plasma-activated polypropylene films, *Packaging Technology and Science*, 18 (2005) 243-251.

[9] T. Tzanov, S.A. Costa, G.M. Gübitz, A. Cavaco-Paulo, Hydrogen peroxide generation with immobilised glucose oxidase for textile bleaching, *Journal of Biotechnology*, 93 (2002) 87-94.

[10] A. Farooq, S. Ali, N. Abbas, G.A. Fatima, M.A. Ashraf, Comparative performance evaluation of conventional bleaching and enzymatic bleaching with glucose oxidase on knitted cotton fabric, *Journal of Cleaner Production*, 42 (2013) 167-171.

[11] M.D. Gouda, S.A. Singh, A.A. Rao, M.S. Thakur, N.G. Karanth, Thermal inactivation of glucose oxidase mechanism and stabilisation using additives, *Journal of Biological Chemistry*, 278 (2003) 24324-24333.

[12] S. Rauf, A. Ihsan, K. Akhtar, M. Ghauri, M. Rahman, M. Anwar, A. Khalid, Glucose oxidase immobilisation on a novel cellulose acetate–polymethylmethacrylate membrane, *Journal of Biotechnology*, 121 (2006) 351-360.

[13] M. Demura, T. Asakura, Porous membrane of *Bombyx mori* silk fibroin: Structure characterisation, physical properties and application to glucose oxidase immobilisation, *Journal of Membrane Science*, 59 (1991) 39-52.

[14] C. Shan, H. Yang, J. Song, D. Han, A. Ivaska, L. Niu, Direct electrochemistry of glucose oxidase and biosensing for glucose based on graphene, *Analytical Chemistry*, 81 (2009) 2378-2382.

[15] S.M. Pilkington, S.J. Roberts, S.J. Meade, J.A. Gerrard, Amyloid fibrils as a nanoscaffold for enzyme immobilisation, *Biotechnology Progress*, 26 (2010) 93-100.

[16] L. Sasso, S. Suei, L. Domigan, J. Healy, V. Nock, M. Williams, J. Gerrard, Versatile multi-functionalisation of protein nanofibrils for biosensor applications, *Nanoscale*, 6 (2014) 1629-1634.

[17] K. Gulla, M. Gouda, M. Thakur, N. Karanth, Enhancement of stability of immobilised glucose oxidase by modification of free thiols generated by reducing disulfide bonds and using additives, *Biosensors and Bioelectronics*, 19 (2004) 621-625.

[18] B. Appleton, T. Gibson, J. Woodward, High temperature stabilisation of immobilised glucose oxidase: Potential applications in biosensors, *Sensors and Actuators B: Chemical*, 43 (1997) 65-69.

[19] T.P. Shukla, L.E. Wierzbicki, Beta-galactosidase technology: A solution to the lactose problem, *Critical Reviews in Food Science & Nutrition*, 5 (1975) 325-356.

[20] M. Puri, S. Gupta, P. Pahuja, A. Kaur, J. Kanwar, J. Kennedy, Cell disruption optimisation and covalent immobilisation of β-d-galactosidase from *Kluyveromyces marxianus* YW-1 for lactose hydrolysis in milk, *Applied Biochemistry and Biotechnology*, 160 (2010) 98-108.

[21] M. Di Serio, C. Maturo, E. De Alteriis, P. Parascandola, R. Tesser, E. Santacesaria, Lactose hydrolysis by immobilised β-galactosidase: The effect of the supports and the kinetics, *Catalysis Today*, 79 (2003) 333-339.

[22] C. Carpio, P. Gonzalez, J. Ruales, F. Batista-Viera, Bone-bound enzymes for food industry application, *Food Chemistry*, 68 (2000) 403-409.

[23] M. Marrakchi, S.V. Dzyadevych, F. Lagarde, C. Martelet, N. Jaffrezic-Renault, Conductometric biosensor based on glucose oxidase and beta-galactosidase for specific lactose determination in milk, *Materials Science and Engineering: C*, 28 (2008) 872-875.

[24] C. Pan, B. Hu, W. Li, Y. Sun, H. Ye, X. Zeng, Novel and efficient method for immobilisation and stabilisation of β-d-galactosidase by covalent attachment onto magnetic Fe_3O_4–chitosan nanoparticles, *Journal of Molecular Catalysis B: Enzymatic*, 61 (2009) 208-215.

[25] Q. Husain, S.A. Ansari, F. Alam, A. Azam, Immobilisation of *Aspergillus oryzae* β galactosidase on zinc oxide nanoparticles *via* simple adsorption mechanism, *International Journal of Biological Macromolecules*, 49 (2011) 37-43.

[26] Q.Z. Zhou, X. Dong Chen, Immobilisation of β-galactosidase on graphite surface by glutaraldehyde, *Journal of Food Engineering*, 48 (2001) 69-74.

[27] T. Palai, P.K. Bhattacharya, Kinetics of lactose conversion to galacto-oligosaccharides by β-galactosidase immobilised on PVDF membrane, *Journal of Bioscience and Bioengineering*, 115 (2013) 668-673.

[28] L. Betancor, H.R. Luckarift, J.H. Seo, O. Brand, J.C. Spain, Three-dimensional immobilisation of β-galactosidase on a silicon surface, *Biotechnology and Bioengineering*, 99 (2008) 261-267.

[29] V. Scognamiglio, I. Pezzotti, G. Pezzotti, J. Cano, I. Manfredonia, K. Buonasera, G. Rodio, M.T. Giardi, A new embedded biosensor platform based on micro-electrodes array (MEA) technology, *Sensors and Actuators B: Chemical*, 176 (2013) 275-283.

[30] L.S. Jasti, S.R. Dola, N.W. Fadnavis, U. Addepally, S. Daniels, S. Ponrathnam, Co-immobilised glucose oxidase and β-galactosidase on bovine serum albumin coated allyl glycidyl ether (AGE)–ethylene glycol dimethacrylate (EGDM) copolymer as a biosensor for lactose determination in milk, *Enzyme and Microbial Technology*, 64 (2014) 67-73.

[31] S.S. Asraf, P. Gunasekaran, Current trends of β-galactosidase research and application, *Current Research, Technology and Education Topics in Applied Microbiology and Microbial Biotechnology*, (2010) 880-890.

[32] P.P. Campos, M.L. Moraes, D. Volpati, P.B. Miranda, O.N. Oliveira Jr, M. Ferreira, Amperometric detection of lactose using β-galactosidase immobilised in layer-by-layer Films, *ACS Applied Materials & Interfaces*, 6 (2014) 11657-11664.

[33] E. Loğoğlu, S. Sungur, Y. Yildiz, Development of lactose biosensor based on β-galactosidase and glucose oxidase immobilised into gelatin, *Journal of Macromolecular Science Part A: Pure and Applied Chemistry*, 43 (2006) 525-533.

[34] D. Kashyap, P. Vohra, S. Chopra, R. Tewari, Applications of pectinases in the commercial sector: A review, *Bioresource Technology*, 77 (2001) 215-227.

[35] R.S. Jayani, S. Saxena, R. Gupta, Microbial pectinolytic enzymes: A review, *Process Biochemistry*, 40 (2005) 2931-2944.

[36] D.B. Pedrolli, A.C. Monteiro, E. Gomes, E.C. Carmona, Pectin and pectinases: Production, characterisation and industrial application of microbial pectinolytic enzymes, *Open Biotechnology Journal*, 3 (2009) 9-18.

[37] V. Suneetha, K. Prathyusha, Bacterial pectinases and their potent biotechnological application in fruit processing/juice production industry: A review, *Journal of Phytology*, 3 (2011).

[38] K.M. Pasha, P. Anuradha, D. Subbarao, Applications of Pectinases in Industrial Sector, International. *Journal of Pure Applied Sciences and Technology*, 16 (2013) 89-95.

[39] G. Hoondal, R. Tiwari, R. Tewari, N. Dahiya, Q. Beg, Microbial alkaline pectinases and their industrial applications: A review, *Applied Microbiology and Biotechnology*, 59 (2002) 409-418.

[40] T. Li, S. Li, N. Wang, L. Tain, Immobilisation and stabilisation of pectinase by multipoint attachment onto an activated agar-gel support, *Food Chemistry*, 109 (2008) 703-708.

[41] Z. Lei, Q. Jiang, Synthesis and properties of immobilised pectinase onto the macroporous polyacrylamide microspheres, *Journal of Agricultural and Food Chemistry*, 59 (2011) 2592-2599.

[42] Y. Liu, Q. Li, Y.-Y. Feng, G.-S. Ji, T.-C. Li, J. Tu, X.-D. Gu, Immobilisation of acid pectinase on graphene oxide nanosheets, *Chemical Papers*, 68 (2014) 732-738.

[43] T. Li, N. Wang, S. Li, Q. Zhao, M. Guo, C. Zhang, Optimisation of covalent immobilisation of pectinase on sodium alginate support, *Biotechnology Letters*, 29 (2007) 1413-1416.

[44] M.J. Van Der Maarel, B. Van Der Veen, J. Uitdehaag, H. Leemhuis, L. Dijkhuizen, Properties and applications of starch-converting enzymes of the α-amylase family, *Journal of Biotechnology*, 94 (2002) 137-155.

[45] P.V. Aiyer, Amylases and their applications, *African Journal of Biotechnology*, 4 (2005).

[46] A. El-Fallal, M.A. Dobara, A. El-Sayed, N. Omar, Starch and microbial α-Amylases: From concepts to biotechnological applications, *Carbohydrates - Comprehensive Studies in Glycobiology and Glycotechnology* (2012).

[47] R. Gupta, P. Gigras, H. Mohapatra, V.K. Goswami, B. Chauhan, Microbial α-amylases: A biotechnological perspective, *Process Biochemistry*, 38 (2003) 1599-1616.

[48] S. Sivaramakrishnan, D. Gangadharan, K.M. Nampoothiri, C.R. Soccol, A. Pandey, a-Amylases from microbial sources-an overview on recent developments, *Food Technology and Biotechnology*, 44 (2006) 173-184.

[49] J. Bryjak, Glucoamylase, α-amylase and β-amylase immobilisation on acrylic carriers, Biochemical Engineering Journal, 16 (2003) 347-355.

[50] V. Ivanova, E. Dobreva, Catalytic properties of immobilised purified thermostable α-amylase from *Bacillus licheniformis* 44MB82-A, *Process Biochemistry*, 29 (1994) 607-612.

[51] T. Kimura, M. Ogata, H. Kobayashi, M. Yoshida, K. Oishi, T. Nakakuki, Continuous production of maltotetraose using a dual immobilised enzyme system of maltotetraose-forming amylase and pullulanase, *Biotechnology and Bioengineering*, 36 (1990) 790-796.

[52] M.V. Kahraman, G. Bayramoğlu, N. Kayaman-Apohan, A. Güngör, α-Amylase immobilisation on functionalised glass beads by covalent attachment, *Food Chemistry*, 104 (2007) 1385-1392.

[53] E. Abadulla, T. Tzanov, S. Costa, K.-H. Robra, A. Cavaco-Paulo, G.M. Gübitz, Decolourisation and detoxification of textile dyes with a laccase from *Trametes hirsuta*, *Applied and Environmental Microbiology*, 66 (2000) 3357-3362.

[54] S.R. Couto, J.L. Toca-Herrera, Lacasses in the textile industry, *Biotechnology and Molecular Biology Reviews*, 1 (2006) 115-120.

[55] H. Call, I. Mücke, History, overview and applications of mediated lignolytic systems, especially laccase-mediator-systems (Lignozym®-process), *Journal of Biotechnology*, 53 (1997) 163-202.

[56] P. Widsten, A. Kandelbauer, Laccase applications in the forest products industry: A review, *Enzyme and Microbial Technology*, 42 (2008) 293-307.

[57] L. Lloret, G. Eibes, T. Lú-Chau, M. Moreira, G. Feijoo, J. Lema, Laccase-catalysed degradation of anti-inflammatories and estrogens, *Biochemical Engineering Journal*, 51 (2010) 124-131.

[58] R.C. Minussi, G.M. Pastore, N. Duran, Potential applications of laccase in the food industry, *Trends in Food Science & Technology*, 13 (2002) 205-216.

[59] G.S. Dhillon, S. Kaur, S.K. Brar, M. Verma, Flocculation and haze removal from crude beer using in-house produced laccase from *Trametes versicolor* cultured on brewer's spent grain, *Journal of Agricultural and Food Chemistry*, 60 (2012) 7895-7904.

[60] T. Kuuva, R. Lantto, T. Reinikainen, J. Buchert, K. Autio, Rheological properties of laccase-induced sugar beet pectin gels, *Food Hydrocolloids*, 17 (2003) 679-684.

[61] K. Brijwani, A. Rigdon, P.V. Vadlani, Fungal laccases: Production, function, and applications in food processing, *Enzyme Research*, (2010) 1-10.

[62] M. Fernández-Fernández, M. Sanromán, D. Moldes, Recent developments and applications of immobilised laccase, *Biotechnology Advances*, 31 (2013) 1808-1825.

[63] M. Roth, Fluorescence reaction for amino acids, *Analytical Chemistry*, 43 (1971) 880-882.

[64] M. Friedman, Applications of the ninhydrin reaction for analysis of amino acids, peptides, and proteins to agricultural and biomedical sciences, *Journal of Agricultural and Food Chemistry*, 52 (2004) 385-406.

[65] S. Moore, Amino acid analysis: Aqueous dimethyl sulfoxide as solvent for the ninhydrin reaction, *Journal of Biological Chemistry*, 243 (1968) 6281-6283.

[66] M. Freidman, J. Pang, G. Smith, Ninhydrin-reactive lysine in food proteins, *Journal of Food Science*, 49 (1984) 10-13.

[67] H.M. Berman, J. Westbrook, Z. Feng, G. Gilliland, T. Bhat, H. Weissig, I.N. Shindyalov, P.E. Bourne, The protein data bank, *Nucleic Acids Research*, 28 (2000) 235-242.

[68] L.J. Domigan, *New nanomaterials: Amyloid fibrils from waste proteins*, PhD Thesis, University of Canterbury, (2012).

[69] S. Pilkington, *Incorporating glucose oxidase activity into amyloid fibrils*, Master's Thesis, University of Canterbury, (2009).

[70] M. Garvey, S. Gras, S. Meehan, S. Meade, J. Carver, J. Gerrard, Protein nanofibres of defined morphology prepared from mixtures of crude crystallins, *International Journal of Nanotechnology*, 6 (2009) 258-273.

[71] J. Healy, K. Wong, E.B. Sawyer, C. Roux, L. Domigan, S.L. Gras, M. Sunde, N.G. Larsen, J. Gerrard, M. Vasudevamurthy, Polymorphism and higher order structures of protein nanofibres from crude mixtures of fish lens crystallins: Toward useful materials, *Biopolymers*, 97 (2012) 595-606.

[72] A.J. Kiss, A.Y. Mirarefi, S. Ramakrishnan, C.F. Zukoski, A.L. DeVries, C.-H.C. Cheng, Cold-stable eye lens crystallins of the Antarctic nototheniid toothfish *Dissostichus mawsoni*, *Journal of Experimental Biology*, 207 (2004) 4633-4649.

[73] A.Y. Mirarefi, S. Boutet, S. Ramakrishnan, A.J. Kiss, C.-H.C. Cheng, A.L. DeVries, I.K. Robinson, C.F. Zukoski, Small-angle X-ray scattering studies of the intact eye lens: effect of crystallin composition and concentration on microstructure, *Biochimica et Biophysica Acta (BBA)-General Subjects*, 1800 (2010) 556-564.

[74] A.J. Kiss, C.-H.C. Cheng, Molecular diversity and genomic organisation of the α-, β-, and γ eye lens crystallins from the Antarctic toothfish *Dissostichus mawsoni*, *Comparative Biochemistry and Physiology Part D: Genomics and Proteomics*, 3 (2008) 155-171.

[75] A.J. Kiss, A.L. Devries, R.M. Morgan-Kiss, Comparative analysis of crystallins and lipids from the lens of Antarctic toothfish and cow, *Journal of Comparative Physiology B*, 180 (2010) 1019-1032.

[76] T. Greiling, J.I. Clark, Early lens development in the zebrafish: A three-dimensional time-lapse analysis, *Developmental Dynamics*, 238 (2009) 2254-2265.

[77] G.T. Hermanson, *Bioconjugate techniques*, Academic Press, USA (2013).

[78] M. Aslam, A. Dent, *Bioconjugation: Protein coupling techniques for the biomedical sciences*, Macmillan Reference, London (1998).

[79] P.W. Riddles, R.L. Blakeley, B. Zerner, Reassessment of Ellman's reagent, *Methods in Enzymology*, 91 (1983) 49-60.

[80] G.L. Ellman, Tissue sulfhydryl groups, *Archives of Biochemistry and Biophysics*, 82 (1959) 70-77.

[81] T.E. Creighton, Disulphide bonds and protein stability, *BioEssays*, 8 (1988) 57-63.

[82] N.J. Darby, T.E. Creighton, Functional properties of the individual thioredoxin-like domains of protein disulfide isomerase, *Biochemistry*, 34 (1995) 11725-11735.

[83] A. Cooper, S.J. Eyles, S.E. Radford, C.M. Dobson, Thermodynamic consequences of the removal of a disulphide bridge from hen lysozyme, *Journal of Molecular Biology*, 225 (1992) 939-943.

[84] S.F. Betz, Disulfide bonds and the stability of globular proteins, *Protein Science*, 2 (1993) 1551-1558.

[85] J.A. Burns, J.C. Butler, J. Moran, G.M. Whitesides, Selective reduction of disulfides by tris (2-carboxyethyl) phosphine, *The Journal of Organic Chemistry*, 56 (1991) 2648-2650.

[86] J.C. Han, G.Y. Han, A Procedure for quantitative determination of Tris(2-Carboxyethyl)phosphine, an odorless reducing agent more stable and effective than dithiothreitol, *Analytical Biochemistry*, 220 (1994) 5-10.

[87] E.B. Getz, M. Xiao, T. Chakrabarty, R. Cooke, P.R. Selvin, A Comparison between the sulfhydryl reductants Tris(2-carboxyethyl)phosphine and dithiothreitol for use in protein biochemistry, *Analytical Biochemistry*, 273 (1999) 73-80.

[88] H.J. Hoenders, H. Bloemendal, Lens proteins and aging, Journal of Gerontology, 38 (1983) 278-286.

[89] R.E. Perry, M. Swamy, E. Abraham, Progressive changes in lens crystallin glycation and high-molecular-weight aggregate formation leading to cataract development in streptozotocin-diabetic rats, *Experimental Eye Research*, 44 (1987) 269-282.

[90] W. De Jong, J. Mulders, C. Voorter, G. Berbers, W. Hoekman, H. Bloemendal, Post-translational modifications of eye lens crystallins: Crosslinking, phosphorylation and deamidation, *Advances in Post-Translational Modifications of Proteins and Ageing*, (1988) 95-108.

[91] K.K. Sharma, P. Santhoshkumar, Lens aging: Effects of crystallins, *Biochimica et Biophysica Acta (BBA)-General Subjects*, 1790 (2009) 1095-1108.

[92] P.G. Hains, R.J. Truscott, Post-translational modifications in the nuclear region of young, aged, and cataract human lenses, *Journal of Proteome Research*, 6 (2007) 3935-3943.

[93] P.G. Hains, R.J. Truscott, Age-dependent deamidation of lifelong proteins in the human lens, *Investigative Ophthalmology & Visual Science*, 51 (2010) 3107-3114.

[94] T. Takata, J.T. Oxford, B. Demeler, K.J. Lampi, Deamidation destabilises and triggers aggregation of a lens protein, βA3-crystallin, *Protein Science*, 17 (2008) 1565-1575.

[95] V.N. Lapko, D.L. Smith, J.B. Smith, In vivo carbamylation and acetylation of water-soluble human lens αB-crystallin lysine 92, *Protein Science*, 10 (2001) 1130-1136.

[96] J.B. Smith, Y. Sun, D.L. Smith, B. Green, Identification of the posttranslational modifications of bovine lens αB-crystallins by mass spectrometry, *Protein Science*, 1 (1992) 601-608.

[97] S. Meehan, Y. Berry, B. Luisi, C.M. Dobson, J.A. Carver, C.E. MacPhee, Amyloid fibril formation by lens crystallin proteins and its implications for cataract formation, *Journal of Biological Chemistry*, 279 (2004) 3413-3419.

[98] H. Schachter, H.H. Freeze, Glycosylation diseases: Quo vadis?, *Biochimica et Biophysica Acta (BBA)-Molecular Basis of Disease*, 1792 (2009) 925-930.

[99] R.G. Spiro, Glycoproteins, *Advances in Protein Chemistry*, 27 (1973) 349-467.

[100] V.J. Stevens, C.A. Rouzer, V.M. Monnier, A. Cerami, Diabetic cataract formation: Potential role of glycosylation of lens crystallins, *Proceedings of the National Academy of Sciences of the United States of America*, 75 (1978) 2918-2922.

[101] D.A. Armbruster, Fructosamine: Structure, analysis, and clinical usefulness, *Clinical Chemistry*, 33 (1987) 2153-2163.

[102] H.T. Sojar, O.P. Bahl, A chemical method for the deglycosylation of proteins, *Archives of Biochemistry and Biophysics*, 259 (1987) 52-57.

[103] A.W. Stitt, Advanced glycation: an important pathological event in diabetic and age related ocular disease, *British Journal of Ophthalmology*, 85 (2001) 746-753.

[104] P. Ulrich, A. Cerami, Protein glycation, diabetes, and aging, *Recent Progress in Hormone Research*, 56 (2001) 1-22.

[105] N.A. Ansari, R. Ali, Glycated lysine residues: A marker for non-enzymatic protein glycation in age-related diseases, *Disease markers*, 30 (2011) 317-324.

[106] G. Münch, D. Schicktanz, A. Behme, M. Gerlach, P. Riederer, D. Palm, R. Schinzel, Amino acid specificity of glycation and protein–AGE crosslinking reactivities determined with a dipeptide SPOT library, *Nature Biotechnology*, 17 (1999) 1006-1010.

[107] N.R. Thotakura, O.P. Bahl, [28] Enzymatic deglycosylation of glycoproteins, Methods in Enzymology, 138 (1987), 350-359.

[108] T.H. Steinberg, K.P.O. Top, K.N. Berggren, C. Kemper, L. Jones, Z. Diwu, R.P. Haugland, W.F. Patton, Rapid and simple single nanogram detection of glycoproteins in polyacrylamide gels and on electroblots, *Proteomics*, 1 (2001) 841-855.

[109] C. Hart, B. Schulenberg, T.H. Steinberg, W.Y. Leung, W.F. Patton, Detection of glycoproteins in polyacrylamide gels and on electroblots using Pro-Q Emerald 488 dye, a fluorescent periodate Schiff-base stain, *Electrophoresis*, 24 (2003) 588-598.

[110] V. Leskovac, S. Trivić, G. Wohlfahrt, J. Kandrač, D. Peričin, Glucose oxidase from *Aspergillus niger*: The mechanism of action with molecular oxygen, quinones, and one-electron acceptors, *International Journal of Biochemistry & Cell Biology*, 37 (2005) 731-750.

[111] C.M. Binder, D.D. Dixon, E. Almaraz, M.A. Tius, B. Singaram, A simple procedure for C–C bond cleavage of aromatic and aliphatic epoxides with aqueous sodium periodate under ambient conditions, *Tetrahedron Letters*, 49 (2008) 2764-2767.

[112] B. Kozuilić, I. Leuštek, B. Pavlović, P. Mildner, S. Barbarić, Preparation of the stabilised glycoenzymes by cross-linking their carbohydrate chains, *Applied Biochemistry and Biotechnology*, 15 (1987) 265-278.

[113] J.R. Dyer, Use of periodate oxidations in biochemical analysis, *Methods of Biochemical Analysis*, 3, (1956) 111-152.

[114] H. Iwata, Y. Ikada, Intramolecular Crosslinking in gelation. *Bulletin of the Institute for Chemical Research, Kyoto University*, 57 (1979).

[115] V.C. Barry, P. Mitchell, 731. Properties of periodate-oxidised polysaccharides. Part II. The structure of some nitrogen-containing polymers, *Journal of the Chemical Society*, (1953) 3631-3635.

[116] C.D. Hurd, P.J. Baker Jr, R.P. Holysz, W.H. Saunderz Jr, Cyclic modifications of the dialdehyde from periodate oxidation of methyl α-d-glucopyranoside, *Journal of Organic Chemistry*, 18 (1953) 186-191.

[117] R.L. Levine, D. Garland, C.N. Oliver, A. Amici, I. Climent, A.-G. Lenz, B.-W. Ahn, S. Shaltiel, E.R. Stadtman, Determination of carbonyl content in oxidatively modified proteins, *Methods in Enzymology*, (1990) 464-478.

[118] R.L. Levine, J.A. Williams, E.R. Stadtman, E. Shacter, Carbonyl assays for determination of oxidatively modified proteins, *Methods in Enzymology*, (1994) 346-357.

[119] C.S. Mesquita, R. Oliveira, F. Bento, D. Geraldo, J.V. Rodrigues, J.C. Marcos, Simplified 2, 4-dinitrophenylhydrazine spectrophotometric assay for quantification of carbonyls in oxidised proteins, *Analytical Biochemistry*, 458 (2014) 69-71.

[120] J.X. Khym, The reaction of methylamine with periodate-oxidised adenosine 5'-phosphate, *Biochemistry*, 2 (1963) 344-350.

[121] G.E. Means, R.E. Feeney, Reductive alkylation of amino groups in proteins, *Biochemistry*, 7 (1968) 2192-2201.

[122] P.K. Nakane, A. Kawaoi, Peroxidase-labeled antibody a new method of conjugation, *Journal of Histochemistry & Cytochemistry*, 22 (1974) 1084-1091.

[123] H. Ghafuri, M. Hashemi, One-pot reductive amination of aldehydes by the dihydropyridine in water, *Scientia Iranica*, 19 (2012) 1591-1593.

[124] B.T. Cho, S.K. Kang, Direct and indirect reductive amination of aldehydes and ketones with solid acid-activated sodium borohydride under solvent-free conditions, *Tetrahedron*, 61 (2005) 5725-5734.

[125] I. Saxena, R. Borah, J.C. Sarma, Reductive amination of aromatic aldehydes and ketones with nickel boride, *Journal of the Chemical Society, Perkin Transactions 1*, (2000) 503-504.

[126] D. Menche, J. Hassfeld, J. Li, G. Menche, A. Ritter, S. Rudolph, Hydrogen bond catalysed direct reductive amination of ketones, *Organic Letters*, 8 (2006) 741-744.

[127] S. Hoffmann, M. Nicoletti, B. List, Catalytic asymmetric reductive amination of aldehydes *via* dynamic kinetic resolution, *Journal of the American Chemical Society*, 128 (2006) 13074-13075.

[128] M. Saidi, R.S. Brown, A. Ziyaei-Halimjani, Reductive amination of aldehydes with sodium borohydride and lithium aluminum hydride in the presence of lithium perchlorate, *Journal of the Iranian Chemical Society*, 4 (2007) 194-198.

[129] T. Mizuta, S. Sakaguchi, Y. Ishii, Catalytic reductive alkylation of secondary amine with aldehyde and silane by an iridium compound, *Journal of Organic Chemistry*, 70 (2005) 2195-2199.

[130] A.F. Abdel-Magid, K.G. Carson, B.D. Harris, C.A. Maryanoff, R.D. Shah, Reductive amination of aldehydes and ketones with sodium triacetoxyborohydride. Studies on direct and indirect reductive amination procedures1, *Journal of Organic Chemistry*, 61 (1996) 3849-3862.

[131] E.W. Baxter, A.B. Reitz, Reductive aminations of carbonyl compounds with borohydride and borane reducing agents, *Organic Reactions*, (2002).

[132] H. Schlesinger, H.C. Brown, A. Finholt, J.R. Gilbreath, H.R. Hoekstra, E.K. Hyde, Sodium borohydride, its hydrolysis and its use as a reducing agent and in the generation of hydrogen, *Journal of the American Chemical Society*, 75 (1953) 215-219.

[133] D.E. Ward, C.K. Rhee, Chemoselective reductions with sodium borohydride, *Canadian Journal of Chemistry*, 67 (1989) 1206-1211.

[134] A.E. Moormann, Reductive amination of piperidines with aldehydes using borane-pyridine, *Synthetic Communications*, 23 (1993) 789-795.

[135] A.F. Abdel-Magid, S.J. Mehrman, A review on the use of sodium triacetoxyborohydride in the reductive amination of ketones and aldehydes, *Organic Process Research & Development*, 10 (2006) 971-1031.

Chapter Four

Glutaraldehdye-based crosslinking of PNFs

4.1. Introduction

In this chapter learnings from the previous chapter were applied to functionalise crystallin PNFs. GA-based crosslinking of oxidised crystallin PNFs was developed to achieve a reproducible and versatile crosslinking method. To understand the potential of crystallin PNFs to act as a versatile nanoscaffold, a diverse range of industrially relevant enzymes including GOX, β-gal, pectinase, α-amylase, and laccase (section 3.2, Chapter Three) were studied. The extent of functionalisation was evaluated using gel electrophoresis (SDS-PAGE), TEM, enzyme-activity assays, thermostability and reusability studies.

4.2. GA-based crosslinking

GA as shown in **Figure 4.1**. is one of the most commonly used and studied homo-bifunctional crosslinking agents for immobilising enzymes [1]. Glutaraldehyde has had great success as a crosslinker because of its commercial availability, low cost, and high reactivity [2, 3].

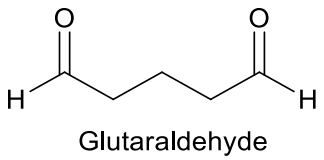

Figure 4.1. *Structure of glutaraldehyde [1].*

Crosslinking by GA is based on the availability of free amino groups on the surface of the enzyme, mainly provided by lysine and arginine amino acids [4]. However, GA is known to react not only with amine groups but with several other functional groups of proteins, including, thiol, phenol, imidazole moieties, and with itself [5]. The mechanism by which GA reacts with proteins is still under debate [1],[6], and several studies have revealed that GA in aqueous solutions can exist in more than one molecular forms such as a monomer, dimer, trimer or polymer, leading to many different possible reaction mechanisms [3]. The possible reaction mechanism could progress either *via* a Schiff base formation (see **Figure 3.18**, Chapter Three) or *via* the formation of a pyridinium crosslink as illustrated in **Figure 4.2**.

As discussed earlier (section 3.6, Chapter Three), both glycosylation and glycation could result in a blocked amine by a sugar derivative [1]. The results from glycoprotein staining and aldehyde group-based assay suggested the presence of carbohydrate groups on the surface of crystallin PNFs (section 3.7, Chapter Three).

Thus, in the first part of this chapter, GA binding to the oxidised crystallin PNFs will be discussed, and results from the amine and aldehyde group-based assays will be presented to ensure GA-activation of PNFs, followed by immobilisation studies.

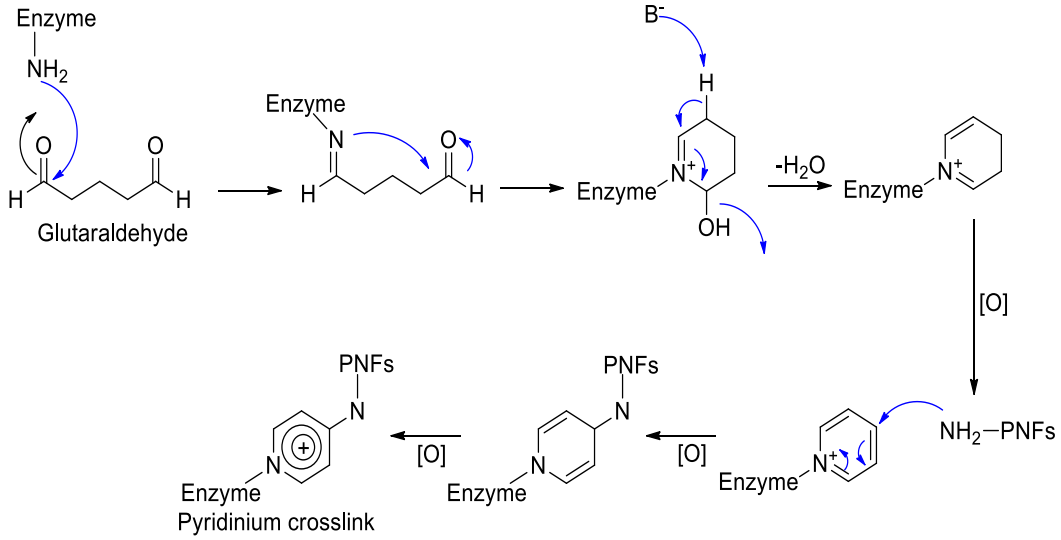

***Figure 4.2**. Proposed mechanism of GA crosslinking via the formation of pyridinium crosslink, Meade et al. (2003) [6].*

As the structure of the glycoprotein shell in crystallin PNFs is unknown, the presence of carbohydrates may influence the binding of GA to surface lysine residues, by limiting access of the crosslinker to free amino groups (section 3.6, Chapter Three). Therefore, an additional treatment based on periodate oxidation using sodium metaperiodate was used (section 7.7.3) to expose lysine (-NH_2) groups on the surface of the PNFs (**Figure 3.14**, Chapter Three), in order to create free amine moieties to react with the GA. The effect of periodate oxidation on the availability of lysine residues for crosslinking was assessed using the amino group-based assays (as discussed earlier in Chapter Three, section 3.3.1, and 3.3.2), OPA assay (section 7.6.1), and the ninhydrin assay (section 7.6.2). The results of these assays are summarised in **Table 4.1.**

***Table 4.1.** Summary of calculated amino group availability of crude crystallin PNFs, using the OPA and ninhydrin assays. Sample concentration is calculated from a standard curve obtained using lysine, therefore values were multiplied by two to obtain the amino group concentration.*

Sample	OPA assay (µM)	Ninhydrin assay (µM)
Crude crystallin protein	324± 20	327±21
Oxidised crude crystallin protein	411± 22	409±18
Crude crystallin protein fibrils	47±29	39±16
Oxidised crude crystallin protein fibrils	104±21	98±13

**All the samples used above were at the concentration of 10 mg/mL.*

As ascertained by each of two assays, an increase was observed in the amino group availability of the oxidised crystallin PNFs indicating that deglycosylation/oxidation was successful. These results are in agreement with the results obtained by the DNPH assay (section 3.7, Chapter Three, and further experiments were conducted to assess GA binding to the oxidised crystallin PNFs.

4.2.1. GA-activation of crystallin PNFs

The conditions chosen for GA-activation of oxidised crystallin PNFs were based on a previously established method of GA-based crosslinking for insulin PNFs [7, 8]. The reaction was done using a starting concentration of ~10 mg/mL oxidised crystallin PNFs, with a starting concentration of 2.5 mM GA in PBS (pH 7.4), at 26 °C for 1 h (section 7.10). Previous work done by Pilkington *et al.* (2010), has shown that GA crosslinking occurs very quickly under the chosen conditions [9]. Thus, 1 h was selected as the reaction time to achieve efficient crosslinking, whilst preventing aggregate formation.

Due to the high reactivity of GA and as the crosslinking targets are the same on both proteins (enzymes and crystallin PNFs-mainly lysine groups), GA crosslinking can lead to the formation of large, often poorly defined protein aggregates if the reaction is not completed in a controlled way [10]. Hence to obtain effective crosslinking and to avoid the formation of aggregates, a two-step GA-activation protocol was used (section 7.10). In two-step protocol the GA is first reacted with one of the proteins, creating an activated protein, followed by the addition of the second protein. This protocol limits the intramolecular crosslinking, and maximises the intermolecular crosslinking [1]. The chemical procedure used for GA-based covalent crosslinking on the modified crystallin PNFs is illustrated in **Figure 4.3,** and is useful for the attachment of any moiety containing free surface amine groups to the nanoscaffold.

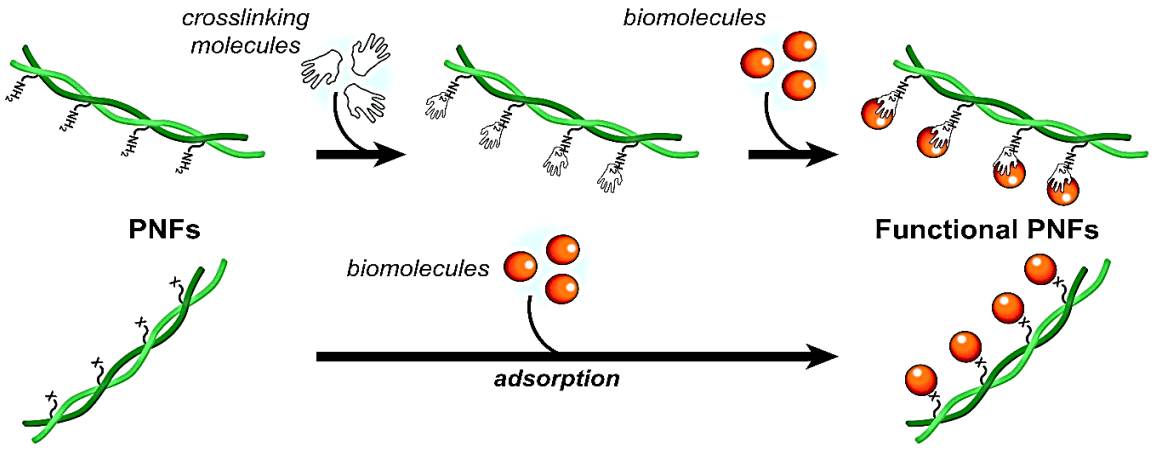

***Figure 4.3**. Schematic representation of functionalised crystallin PNFs showing crosslinking (top) - where crosslinker (GA) is first attached to oxidised crystallin PNFs, followed by the addition of biomolecule/enzyme, and non-covalent association (bottom) - where enzyme/biomolecule is physically adsorbed onto the oxidised crystallin PNFs via side chains of available amino acids (lysine, cysteine, carboxylic acid groups).*

The functionalisation of CPNFs, including surface modification and enzyme immobilisation, was achieved *via* a three-step process. The first step involves the surface modification of the CPNFs *via* periodate oxidation (refer to section 3.7.3, Chapter Three), followed by two-step GA- activation process (illustrated in **Figure 4.3**), leading to the covalent attachment of the enzyme to the newly introduced functional groups. In addition to the covalent crosslinking *via* GA, physical adsorption (non-covalent association) was also investigated for immobilising enzymes onto the oxidised crystallin PNFs. The concentration of GA present can also have a major influence on the crosslinking reaction and procedure needs to be thoroughly investigated to achieve optimised conjugation. Therefore, it was decided to remove any excess or unreacted GA after 1 h incubation, by washing the GA-treated oxidised crystallin PNFs, and recollecting the fibrils by centrifugation. The collected GA-activated fibrils were then resuspended in PBS (pH 7.4) (section 7.10). To demonstrate that GA-activated oxidised crystallin PNFs could be collected by centrifugation, a ThT assay was done, and OPA and DNPH assays were used to determine the extent of GA binding.

4.2.2. ThT assay for characterising GA-activated crystallin PNFs

The ThT assay was done as detailed in section 7.1.2. This assay is pH dependent [11], therefore GA-activated oxidised PNFs and oxidised PNFs were re-dissolved in ThT buffer (pH 8.0), prior to the ThT assay. Upon centrifugation, the fluorescence of the supernatant (sample c) compared to the initial fluorescence of the crystallin amyloid PNFs dropped to about the level of the blank solution (sample d), containing ThT only **(Figure 4.4)**. Upon comparing the ThT fluorescence of the oxidised crystallin PNFs (sample a) with GA-activated oxidised crystallin PNFs (sample b), no significant change in ThT fluorescence can be observed. This confirms that centrifugation can be used to collect PNFs and GA does not have any negative impact on the native β-sheet conformation of the PNFs.

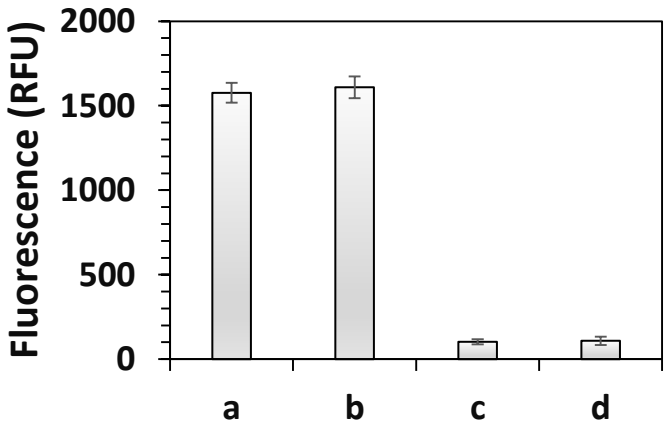

Figure 4.4. *ThT fluorescence of crystallin PNF samples (CPNFs), where a - oxidised CPNFs-initial, b – GA-activated oxidised CPNFs-collected after centrifugation, c - supernatant collected post-centrifugation, and d - blank solution containing ThT dye and buffer only as a control. All measurements were carried out in triplicate and the errors bars represent the standard deviation of the mean of three replicates.*

4.2.3. Amino group characterisation of GA-activated crystallin PNFs

To investigate the extent of GA binding to the oxidised crystallin PNFs, the OPA (section 7.6.1) and ninhydrin assays (section 7.6.2) were used. The result obtained as shown in **Figure 4.5 (i),** suggests that the number of free amino groups has decreased upon addition of GA to the oxidised crystallin PNFs samples (sample c), as compared to the oxidised crystallin PNFs only (control-sample b) consistent with successful conjugation to GA.

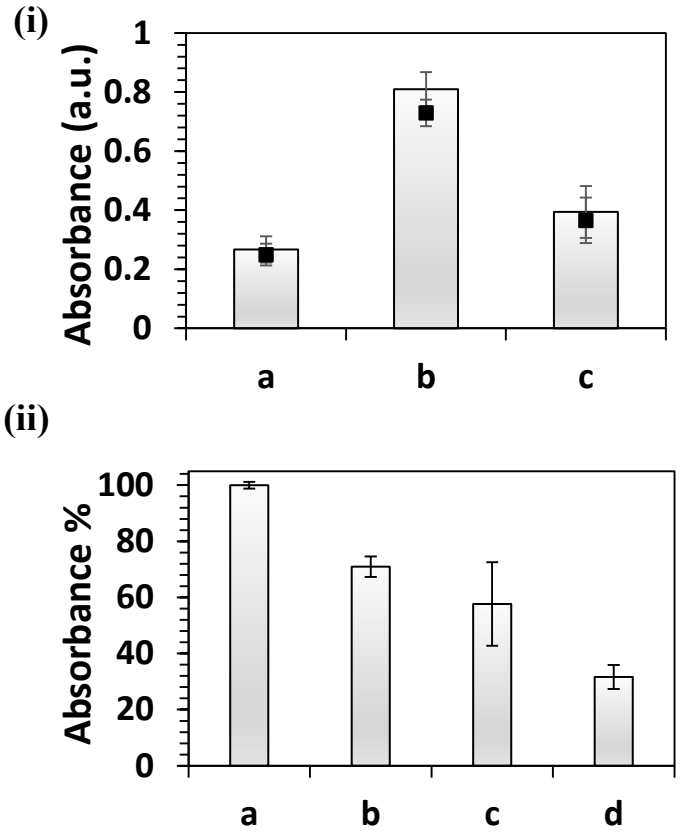

Figure 4.5. (i) *Amino group availability assays for crude crystallin PNFs, where grey bars - OPA assay, absorbance measured at 340 nm and black bars - ninhydrin assay, absorbance measured at 570 nm. Sample a - crystallin PNFs, b - oxidised crystallin PNFs, and c - GA-activated oxidised crystallin PNFs.* ***(ii)*** *Carbonyl group availability of oxidised crystallin amyloid fibrils (O-CPNFs) characterised by DNPH assay, absorbance measured at 450 nm, where a - GA + O-CPNFs (at time, 0), b - GA + O-CPNFs (after an h), c - GA + O-CPNFs (post-centrifugation in pellet), d - unbound GA + buffer (post-centrifugation in supernatant). Error bars represent the standard deviation of the mean of three replicates.*

4.2.4. DNPH assay to evaluate GA binding

The DNPH assay (section 7.8) was done to assess if there was any decrease in aldehyde group availability of GA, during the reaction. After 1 h incubation, the aldehyde group availability upon GA binding to the oxidised crystallin fibrils compared to the initial value of the oxidised crystallin PNFs with GA dropped significantly, as shown in **Figure 4.5 (ii)**, sample c.

The presence of aldehyde groups in the pellet (due to the GA binding) and in the supernatant (due to the excessive unbound GA, being removed) further confirms that GA has been successfully crosslinked. Both the amino group-based assay and the DNPH assay support that oxidised crystallin PNFs can be effectively activated by using GA. However, there are some discrepancies between the GA binding results obtained from the amine-based and aldehyde-based (DNPH) assay. The extent of GA binding as indicated by the OPA assay (section 4.2.3 - decrease in the value after the reaction with GA) is dissimilar to the value evaluated from the DNPH assay. There is a significant amount of decrease in aldehyde group availability of GA after the reaction (supernatant sample (d) – **Figure 4.5 (ii)**), which is less likely to be possible only through lysine-amine linkages, as lysine group availability on the surface of oxidised crystallin PNFs (as characterised by the OPA assay, **Table 4.1**) is not equivalent to the amount required for the observed reduction in aldehyde group availability of GA.

The results implicates that GA binding is not necessarily occurring *via* lysine-amine linkages and is possible that some other binding is also occurring. As explained in section 4.1, it is difficult to state the exact reaction mechanism for the GA binding, and is likely that some aldehyde-aldehyde linkage is also occurring between the aldehyde groups of the oxidised crystallin PNFs and the GA, known as an aldol condensation reaction [4]. **Figure 4.6** shows some fundamental aldol condensates of GA, formed in aqueous solution [12].

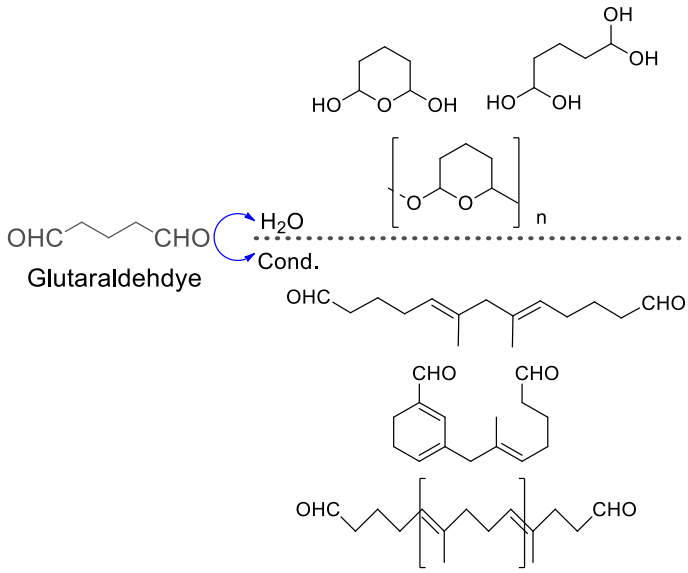

Figure 4.6. *Structures of monomers and polymers forms (cyclic and open chain hemialdals, hydrates, and aldals) (repeating units) of GA in aqueous solution (above dotted line), and some fundamental aldol condensates drawn in their aldehyde group form (below the line), Holmquist and Lewin (1991) [12].*

"The success of GA as a crosslinking agent is based on the large number of different types of molecules present simultaneously in the reagent solution" - Peters et al. (1977) [13].

4.3. Functionalising CPNFs with GOX - a model enzyme system

To investigate enzyme immobilisation onto GA-activated crystallin PNFs, GOX was used as a model enzyme. As mentioned earlier (section 3.2.1), the GOX dimer has 5 lysine residues potentially available for crosslinking.

4.3.1. GOX-GA crosslinking method development

To study the impact of GA on GOX activity, GOX at the starting concentration of ~2.2 mg/mL was incubated with 0.5 mM, 1 mM, and 2 mM GA solution prepared in PBS (pH 7.4) in 1:1 ratio, for 1 h at 26 °C. The SDS-PAGE **(Fig. 4.7)** was done (section 7.1.1), followed by the GOX activity assay *(see Appendix B, Section B1.1)* to investigate the impact of GA binding on the activity of the enzyme (GOX).

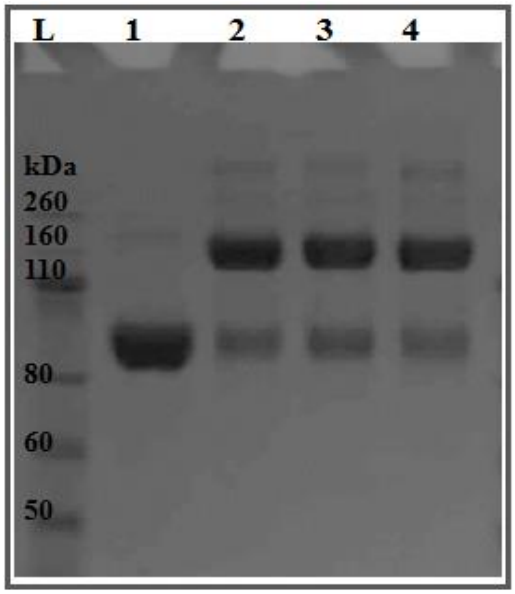

Figure 4.7*. SDS-PAGE of GOX crosslinked intramolecularly, using different concentrations of GA for 1 h at 26°C. L - Ladder, Lane 1 - 0 mM GA, Lane 2 - 0.5 mM GA, Lane 3 - 1 mM GA, and Lane 4 - 2 mM GA.*

GOX runs as a single protein band at ~80 kDa upon SDS-PAGE **(Figure 4.7, Lane 1)**. When GOX is crosslinked to another molecule of GOX with GA (Lane 2) there is a decrease in the protein band at ~80 kDa, and a new larger protein band at ~160 kDa appears, indicating crosslinking and dimer formation. This provides evidence that GOX at ~2.2 mg/mL (starting concentration) has sufficient lysine groups available for crosslinking even when using the lowest final concentration of 0.5 mM GA. To assess the impact of GA binding on the GOX activity, the Amplex Red assay was done (*Appendix B, section B1.1*) on the samples used for SDS-PAGE **(Figure 4.7)**. The GOX activity assay **(Figure 4.8)** shows no significant difference between GOX only (sample a) and GOX with GA samples. This suggests that the addition of GA does not affect or interfere with the readings of the Amplex Red reagent. However, a small negligible increase was observed in absorbance readings on the addition of GA (sample b, c and d compared to sample a).

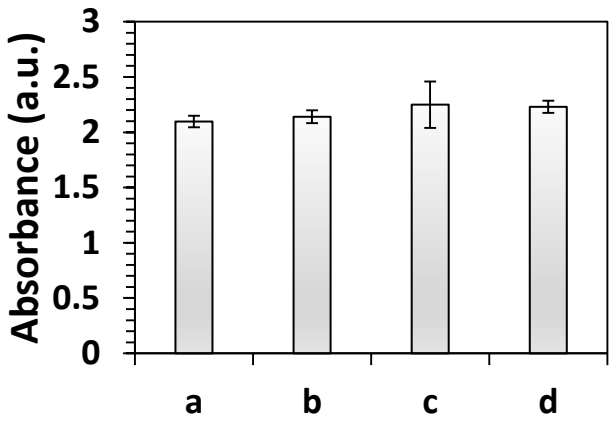

Figure 4.8. *Activity of GOX when crosslinked to another GOX molecule for 1 h at 26 °C with different concentrations of GA, where a - GOX + 0 mM GA, b - GOX + 0.5 mM GA, c - GOX + 1 mM GA, and d - GOX + 2 mM GA.*

This observed increase in the presence of GA is likely to be caused by the production of an auto-fluorescent reaction product of GA on reaction with proteins. GA has been used previously for inducing auto-fluorescence in microscopy studies [14]. The auto-fluorescent product is characterised by a broad emission spectrum from 475-700 nm and therefore can be detected at the wavelength used for the Amplex Red assay (450-485 nm).

4.3.2. Immobilising GOX onto GA-activated crystallin PNFs

GA-activated oxidised crystallin PNFs at a concentration of ~10 mg/mL was incubated with ~2.2 mg/mL of GOX in 1:1 ratio (250 µL each) for 1 h at 26 °C, and the reaction was quenched with an equal part of 100 mM Tris buffer (pH 8.0) (section 7.11.1). The crosslinked samples, and controls were evaluated with SDS PAGE **(Figure 4.9)**. The SDS-PAGE shows that when GOX is immobilised to the GA-activated oxidised crystallin PNFs, the GOX band (Lane 3), as compared to the GOX only control (Lane 1) and GOX with oxidised crystallin amyloid fibrils only (Lane 2), cannot be seen. This is due to amyloid fibrils being large and insoluble are unable to enter the polyacrylamide gel, as shown by the oxidised crystallin PNFs controls (Lanes 4 and 5). Thus, if GOX has been successfully immobilised to the fibrils, the immobilised GOX cannot enter the polyacrylamide gel [8].

The SDS PAGE in **Figure 4.9**, therefore, provides evidence that GOX can be immobilised to GA-activated oxidised crystallin PNFs. To establish how much GOX activity was associated with the crystallin PNFs, the samples from **Figure 4.9** were tested using the Amplex Red activity assay **(Figure 4.10)**. The GOX-functionalised crystallin PNF samples were centrifuged to collect the PNFs, and the supernatant retested for GOX activity *(Appendix B, section B1.1).* To ensure that after subsequent washes no activity is found in the supernatant and rest of the enzyme is crosslinked to the CPNFs, activity assays were also done on the supernatant collected after each of the three washes **(Table 4.2)**.

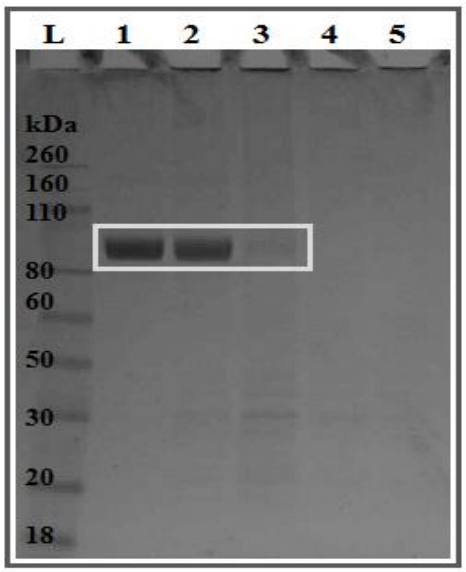

Figure 4.9. *SDS-PAGE of GOX immobilisation onto GA activated oxidised crystallin amyloid fibrils (O-CPNFs). L - Ladder; Lane 1 - GOX only (control), Lane 2 - GOX + O-CPNFs, Lane 3 - GOX + GA activated O-CPNFs, Lane 4 - O-CPNFs only, and Lane 5 - GA activated O-CPNFs. Highlighted section correspond to the molecular weight of GOX.*

As shown in **Figure 4.10**, ~9% of the GOX activity is lost after centrifugation even in the absence of fibrils. When GOX is immobilised to the GA-activated crystallin amyloid fibrils (sample c), ~67% more GOX activity is centrifuged with the GA-activated oxidised crystallin PNFs. Upon comparison of the activity of the supernatant of the samples, GOX with GA activated oxidised crystallin PNFs has significantly less activity in the supernatant, ~21% which demonstrates the effectiveness of the immobilisation. As expected, no GOX activity was detected for crystallin PNFs only (sample d) and for GA activated crystallin PNFs (sample e), implying that the presence of GA is not interfering with the GOX activity assay. This provides evidence that there is active GOX immobilised to the PNFs.

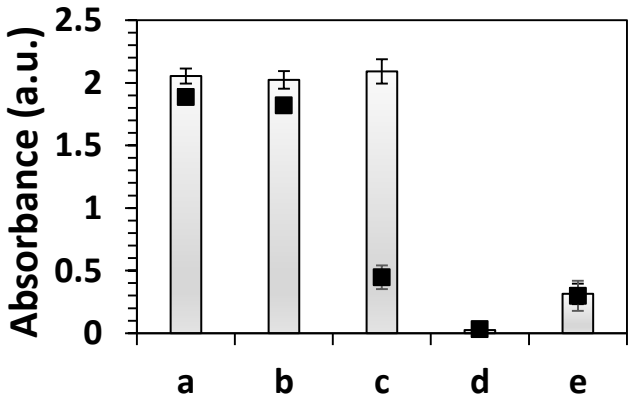

Figure 4.10. *Amplex Red activity assay for GOX-functionalised GA-activated O-CPNFs, where grey bars - initial GOX activity and black bars - GOX activity in the supernatant (after centrifugation), where a - GOX only (control), b - GOX + O-CPNFs, c - GOX + GA activated O-CPNFs, d - O-CPNFs only, and e - GA activated O-CPNFs. Error bars represent the standard deviation of the mean of three replicates.*

The results in **Figure 4.10**, also demonstrate that when GOX is incubated with oxidised crystallin PNFs (with and without GA-sample b and c), the initial activity (grey bars) of the enzyme is almost completely preserved, implying that the presence of crystallin PNFs does not inhibit activity. Both the SDS-PAGE and the activity assay done for characterising immobilised samples, provides evidence that GOX has been successfully covalently immobilised to the PNFs.

***Table 4.2**. The amount of activity retained in the supernatant for GOX immobilised onto the GA activated CPNFs sample, collected after second wash as determined by the Amplex Red assay (Appendix B, section B1.1).*

Sample	GOX activity%
Supernatant 1(After first wash)	21±9
Supernatant 2 (after PNFs washed twice)	8±4

Note: All measurements were carried out in triplicate and the errors bars represent the standard deviation of the mean. No activity was observed in the supernatant after the third wash.

4.3.3. TEM as a tool to investigate GOX-functionalised crystallin PNFs

Once GOX had been immobilised to the GA-activated crystallin PNFs, TEM was used to assess any change in the morphology of the amyloid fibrils (section 7.1.3). The representative images of the structure and morphologies of GOX-functionalised amyloid fibrils and controls as viewed under TEM are shown in **Figure 4.11**.

TEM images of GOX alone show a cloudy pattern as grid assembly and staining may cause the GOX dimer to be in a denatured anhydrous state **(Figure 4.11- c)**. The addition of GA causes the formation of denser cloud structures **(Figure 4.11- d)**. When GOX is added to oxidised crystallin PNFs, there is some association **(Figure 4.11- e and f)**. The sample with GOX covalently crosslinked to GA activated oxidised crystallin amyloid fibrils shows an increased association, as expected **(Figure 4.11- g and h)**. It is important to consider that not all GOX is immobilised to the fibrils, as cloudy structures **(Figure 4.11- g)** similar to those observed in the GOX only sample are visible. The results obtained are in agreement to similar study done on GOX functionalised insulin PNFs by Pilkington *et al.* (2010) [9], who reported that GOX appeared as small round structures on the fibrils (as can be seen in **Figure 4.11- g and h**) and overall fibril morphology remained unchanged upon the addition of GOX and GA.

4.4. Crystallin PNFs as a versatile biomolecule nanoscaffold

After successfully immobilising GOX, the reproducibility and versatility of this method was further investigated by immobilising other commercially important enzymes: β-gal, pectinase, α-amylase and laccase. The concentrations of other enzymes were chosen so that they offered a comparable amount of amine groups as accessible by GOX at ~2.2 mg/mL for the crosslinking reaction (see section 7.11.2).

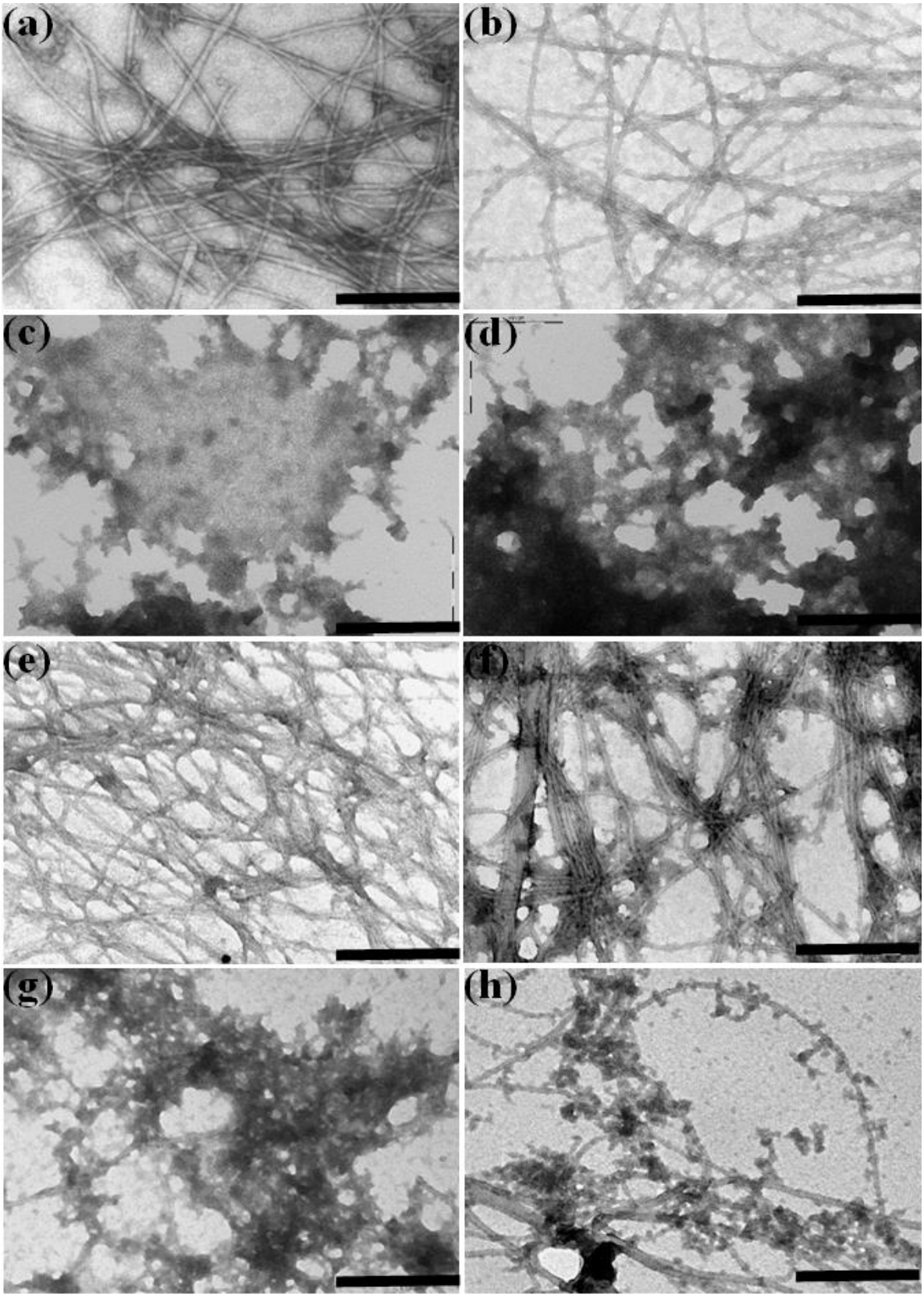

***Figure 4.11**. Representative TEM images of GOX crosslinked samples and controls, where a - O-CPNFs, b - GA activated O-CPNFs, c - GOX only, d - GOX + GA, e and f - GOX + O-CPNFs, and g and h - GOX + GA activated O-CPNFs. Scale bar is 200 nm.*

4.4.1. Method development for functionalising CPNFs with other important industrial enzymes.

As described in (section 3.2), the surface of all the enzymes used in this work, do have lysine residues theoretically available for crosslinking with GA. Enzyme concentration was determined by using Bradford assays (section 7.1.5) and the amino group availability *via* the OPA assay (section 7.6.2) for all the enzymes. For the crosslinking reaction, the GA-activated CPNFs (10 mg/mL) were mixed with enzymes in 1:1 ratio, and incubated for 1 h at 26 °C (section 7.11.2).

4.4.2. Characterisation of functionalised crystallin PNFs

(a) Gel electrophoresis: After the crosslinking reaction had taken place, crosslinked samples and associated controls were analysed by SDS-PAGE (section 7.1.1) to confirm that enzymes had been successfully immobilised to the crystallin PNFs. As stated earlier, if enzymes have been successfully immobilised to the PNFs, they cannot enter the polyacrylamide gel. The results of the SDS-PAGE for each of the enzymes used for the crosslinking experiments are shown in **Figure 4.12.** The SDS-PAGE results for (a) β-gal, (b) pectinase, (c) α-amylase, and (d) laccase immobilised samples as shown in **Figure 4.12**, illustrates that when enzyme is added to the crystallin PNFs (non-covalent association, Lane 2), the protein bands appear to be similar to the enzyme only protein bands (Lane 1). However, when the enzyme is covalently crosslinked to the GA-activated CPNFs, there is a significant decrease in the protein band intensities as compared to the controls (Lane 1 and 2). The SDS-PAGE results suggest that the enzymes have been covalently crosslinked to the GA-activated CPNFs. The SDS-PAGE results **(Figure 4.12 (a) for β-gal, and 4.12 (b) for pectinase)**, show several other protein bands in addition to the bands corresponding to the molecular weight of the native enzyme, implicating impurities associated with the enzymes.

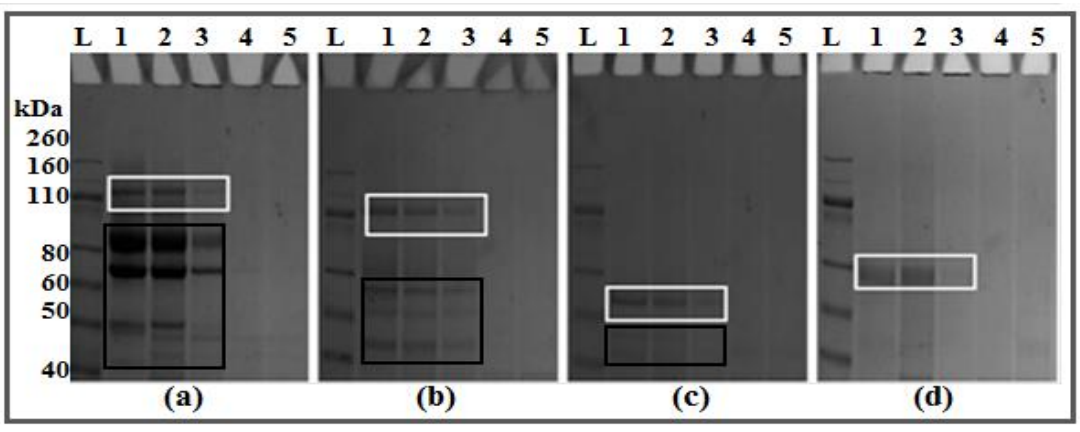

Figure 4.12. *SDS-PAGE of (a) β-Gal, (b) Pectinase, (c) α-Amylase, and (d) Laccase immobilisation onto GA-activated oxidised crystallin PNFs (O-CPNFs). L - Ladder; Lane 1- Enzyme only (control), 2 - Enzyme + O-CPNFs, 3 - Enzyme + GA-activated O-CPNFs, 4 - O-CPNFs only, and 5 – GA-activated O-CPNFs. Highlighted sections (white) corresponds to the molecular weight (kDa) of the enzymes, and black indicates the presence of other protein bands due to impure enzyme preparations.*

The enzyme preparations used in this study were obtained commercially and very little information is available on either the purity of the enzyme or on the method of purification. An attempt was made to purify pectinase, which resulted in 65% loss of pectinase activity. It is not an unexpected result as previous studies have shown that commercial enzymes are not purified further in order to retain maximum activity [15]. Hence, the commercial enzymes were used as such, without any further purification, as purification often results in poor yield of the enzyme, frequently below 10% of the activity of the original material [15] and also to ensure that the process was relevant and scalable in a commercial setting, in which a purification step may prove prohibitively expensive.

(b) ***Activity assay based characterisation:*** To establish how much enzymatic-activity was associated with the functionalised crystallin PNFs, the samples from **Figure 4.12** were assayed for activity (*Appendix B, section B1.1 - B1.5*). Firstly, the activity of all samples was tested in solution, and then in order to test the extent of crosslinking, the samples were centrifuged to collect the amyloid fibrils, and the supernatant retested for activity using enzyme-specific activity assays. For β-gal activity, the *o*-nitrophenyl-β-D-galactoside (ONPG) assay was used (section B1.2). The activity of pectinase was determined by the 3, 5-dinitrosalicyclic acid method (DNS assay) [16] using pectin as a substrate (section B1.3). For determining the activity of free and immobilised amylase (section B1.4), DNS assay was used for measuring the amount of reducing sugar produced using starch as a substrate, in addition to the potassium iodide (KI) assay *(results shown in Appendix E, Figure E1)*. The activity of crosslinked laccase samples were assayed by monitoring the absorbance increase from oxidation of syringaldazine at 530 nm (section B1.5) [17].

The Bradford assay (section 7.1.5) was used for determining the initial protein concentration and protein concentration in the supernatant (post-centrifugation), to assess the amount of enzyme being immobilised. An initial activity reading was taken for each of the samples and this was used as the 100% value. The results obtained from the enzyme-specific activity assays presented as a relative percentage of the initial reading, and the protein concentration (mg/mL) as determined by the Bradford assay for each of the crosslinked enzyme samples are shown in **Figure 4.13.**

Upon centrifuging, only enzymes crosslinked to the fibrils were collected and any free enzymes remained in the supernatant. The decrease in both the activity and protein concentration from the initial value to the supernatant samples upon immobilisation **(Figure 4.13 (i-iv), sample c)** demonstrates the extent of the crosslinking. When enzymes are covalently crosslinked to the GA-activated crystallin PNFs, the samples (sample c) show a significant drop in enzymatic activity and protein concentration, in agreement with the electrophoretic studies when comparing to the enzyme only samples **(Figure 4.13 (i-iv), sample a)**. This confirms that when enzyme is added to the GA-activated crystallin PNFs, covalent crosslinking does indeed occur. A slight drop was also observed when the enzymes were added to the crystallin PNFs in the absence of GA **(Figure 4.13 (i-iv), sample b)**, which can be attributed to non-covalent association or physical adsorption of the enzyme on to the PNFs.

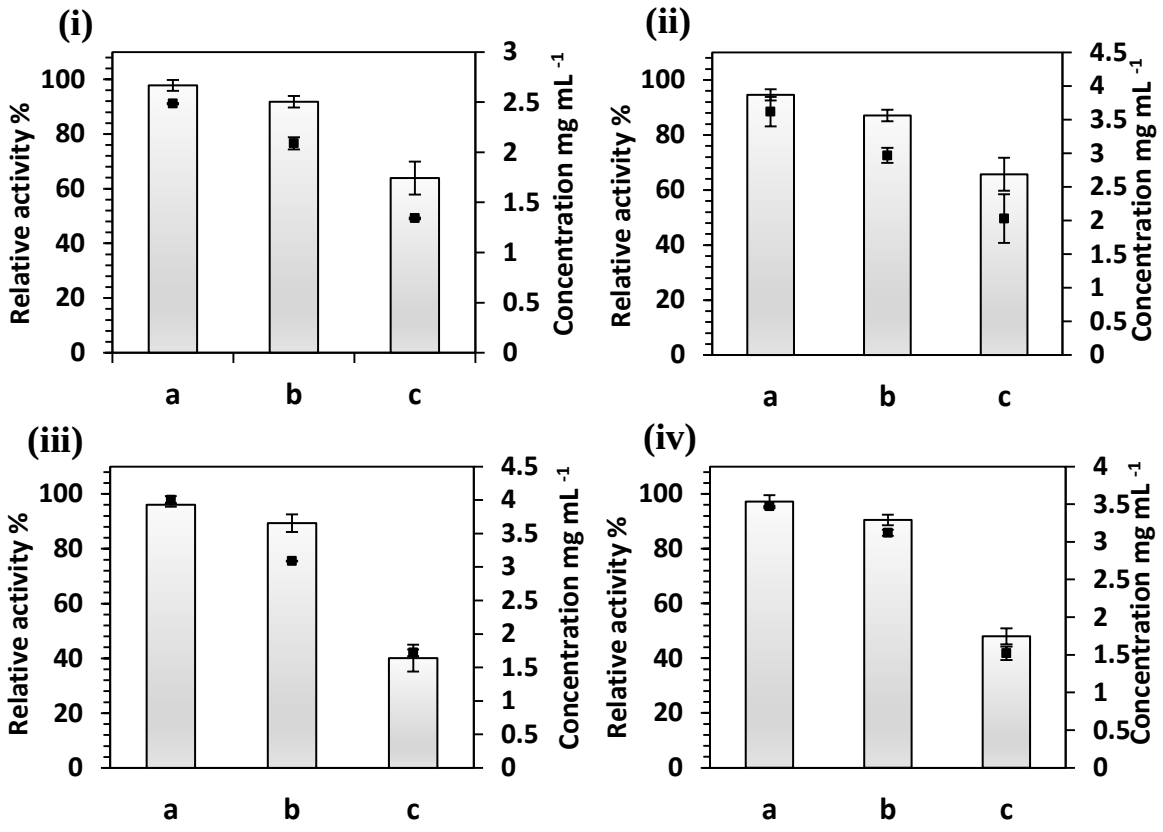

Figure 4.13*. Bradford (black bars) and activity (grey bars) assay studies of functionalised CPNFs and control samples, where a - enzyme only, b - enzyme + CPNFs (non-covalent association), and c - enzyme + GA-activated CPNFs (covalent crosslinking). (i) β-Gal, (ii) Pectinase, (iii) α-Amylase, and (iv) Laccase samples.*

The amount of enzyme being immobilised onto crystallin PNFs and activity retained by the immobilised enzyme for all the enzymes used for crosslinking experiments, as determined from **Figure 4.13**, is shown in **Table 4.3**. The immobilisation efficiency and retained activity results **(Table 4.3)** indicate a very good correlation between the protein concentration and activity-based assays.

Table 4.3. *The amount of the enzyme immobilised onto crystallin PNFs - CPNFs (non-covalent association), and GA activated crystallin PNFs- GA-CPNFs (covalent crosslinking).*

Enzyme	Crosslinked samples	Immobilisation efficiency%	Retained activity%
β-Gal	CPNFs	15 ± 2	8.0 ± 6
	GA-CPNFs	**46 ± 8**	**36 ± 8**
Pectinase	CPNFs	17 ± 2	12 ± 3
	GA-CPNFs	**43 ± 9**	**34 ± 7**
α-Amylase	CPNFs	10 ± 2	10 ± 4
	GA-CPNFs	**56 ± 4**	**59 ± 4**
Laccase	CPNFs	16 ± 9	9.5 ± 7
	GA-CPNFs	**59 ± 3**	**51 ± 4**

The amount of immobilised enzyme was calculated using the following equation: $E_{Immobilised} = (E_{Loaded} - E_{Supernatant})$ and is represented as $IE = [(E_{Immobilised})/(E_{Loaded})] \times 100$, where IE (%) is the immobilisation efficiency, and $E_{Immobilised}$ (mg/mL) is the amount of enzyme immobilised onto crystallin PNFs. E_{Loaded} is the initial concentration of enzyme, and $E_{Supernatant}$ (mg/mL) is the concentration of enzyme in the supernatant as determined by using the Bradford method (section 7.1.5). The amount of activity retained by the immobilised enzyme was calculated as: Retained activity = Activity (*Initial* - *Supernatant*), where initial activity of all enzymes was given an activity of 100%, and activity in supernatant is the sum of enzymatic activity retained in the supernatant after wash 1 and wash 2 respectively, as determined by enzyme-specific activity assays (*Appendix B*) and represented as a relative percentage values.

For all the enzymes used in this work, covalent crosslinking using GA-activated CPNFs yielded better immobilisation efficiency rates as compared to the non-covalent association **(Table 4.3)**. Additionally, the activity assay results suggest that the covalent crosslinking of enzymes onto GA-activated crystallin PNFs does not have any adverse impact on the activity of the immobilised enzymes. GOX, α-amylase and laccase crosslinking resulted in better immobilisation efficiencies as compared to the β-gal and pectinase, with GOX (section 4.3.2) showing the maximum retained activity ~67%. The poor immobilisation efficiency and activity retention values of β-gal and pectinase as compared to the other enzymes is likely due to the impure enzyme preparation (see SDS-PAGE image, **Figure 4.12**). Studies have shown that the purity of the enzyme has a significant impact on the activity and effectivity of immobilisation [18, 19].

(c) ***TEM investigation of functionalised crystallin PNFs:*** TEM was used (section 7.1.3) to investigate the morphology of the functionalised crystallin PNFs **(Figure 4.14)**.

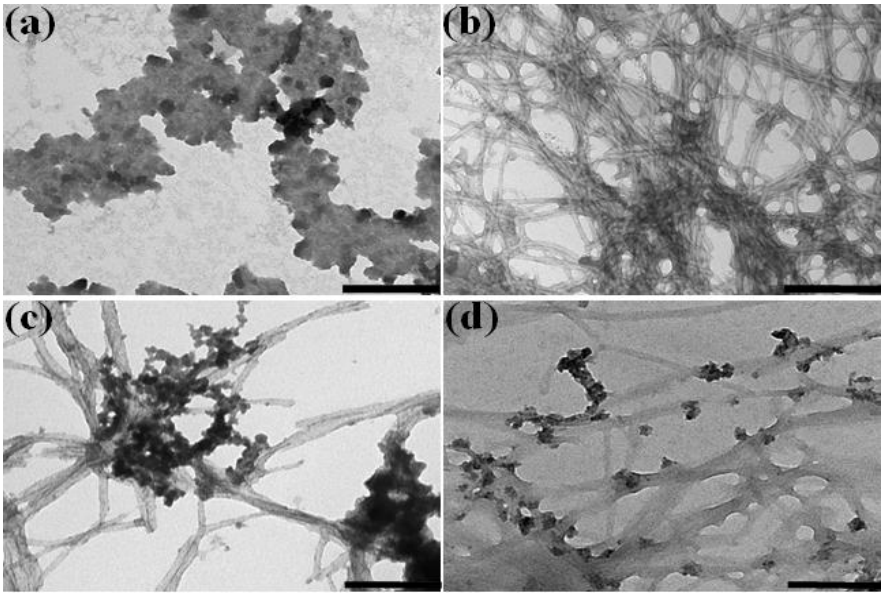

Figure 4.14*. Representative TEM images of β-gal-functionalised GA activated oxidised crystallin amyloid fibrils (O-CPNFs). Sample a - β-gal-only, b – GA-activated O-CPNFs, and c and d - β-gal + GA-activated O-CPNFs. Scale bar is 200 nm.*

Upon immobilisation of β-gal to the amyloid fibrils, the presence of rounded structures was seen, suggesting successful functionalisation of crystallin PNFs (sample c and d) as compared to GA-activated crystallin PNFs only (sample b). Similar results were also seen for pectinase, α-amylase, and laccase functionalised CPNFs **(Figure 4.15)**. The TEM results provide corroborating evidence of successful functionalisation of activated CPNFs, without having any adverse impact on the morphology of the fibrils.

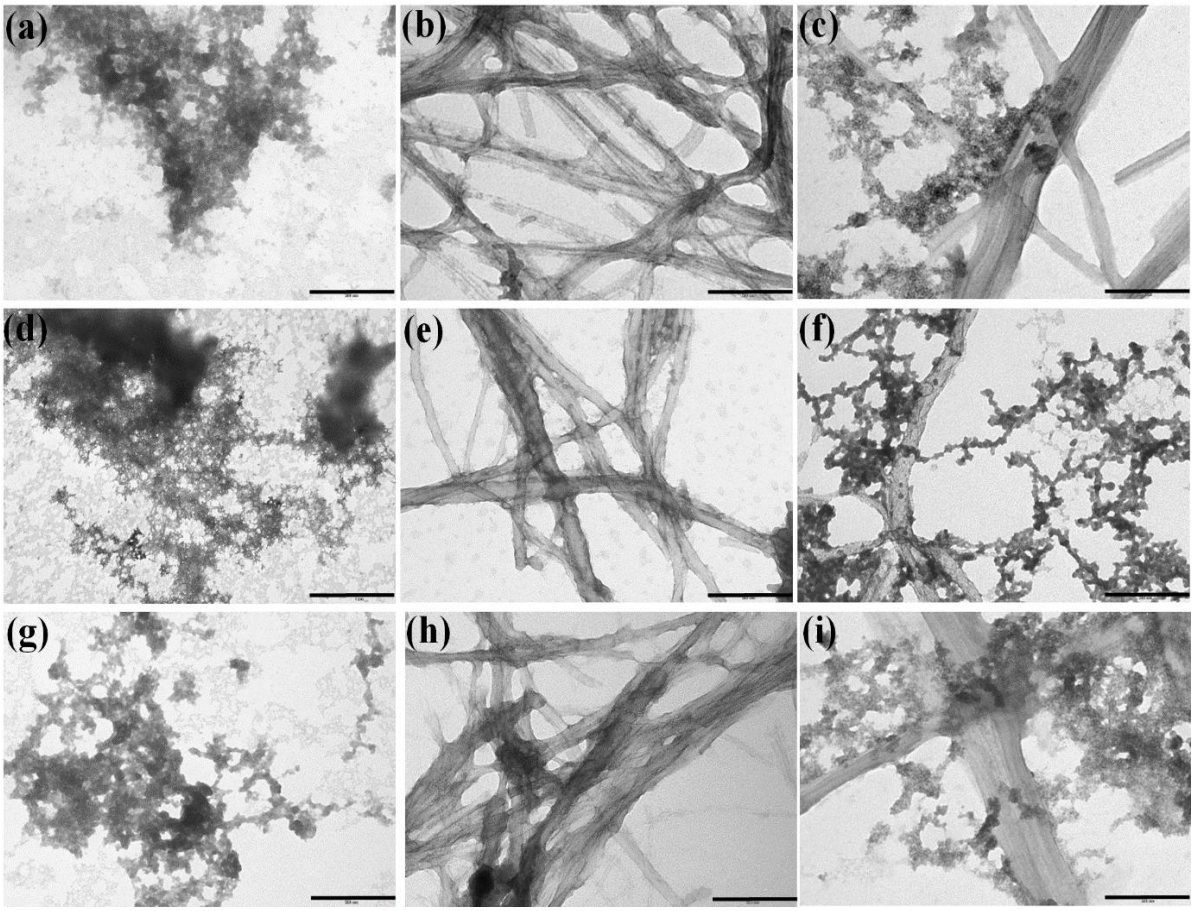

***Figure 4.15**. Representative TEM images of functionalised crystallin PNFs, and controls viewed at 89,000 × magnification. From top, **Row 1** - Pectinase, **Row 2** - α-Amylase, and **Row 3** - Laccase, where sample a, d and g - native enzyme; sample b, e and h – GA-activated CPNFs; and sample c, f and i - enzyme + GA-activated CPNFs (covalent crosslinking). Scale bar is 200 nm.*

4.5. Impact of functionalisation

The thermal inactivation of native enzymes is one of the important limitations for their application in industrial settings. The possible effect of using crystallin PNFs as nanoscaffolds for immobilising enzymes on the preservation of enzymatic activity upon heating was investigated using α-amylase-functionalised crystallin PNFs. α-Amylase samples were considered instead of pectinase samples as α-amylase had better immobilisation yield and also because α-amylase was relatively pure enzyme preparation as compared to the pectinase.

4.5.1. α-Amylase-functionalised crystallin PNFs VS free α-amylase

For the thermostability experiments, samples were pre-heated at 40, 55, and 75 °C over 24 h, followed by cooling at room temperature immediately, prior to the activity measurements (section 7.12). The activity of all individual samples at time zero were given an activity of 100%, and subsequent measurements were compared relative to this measurement **(Figure 4.16)**.

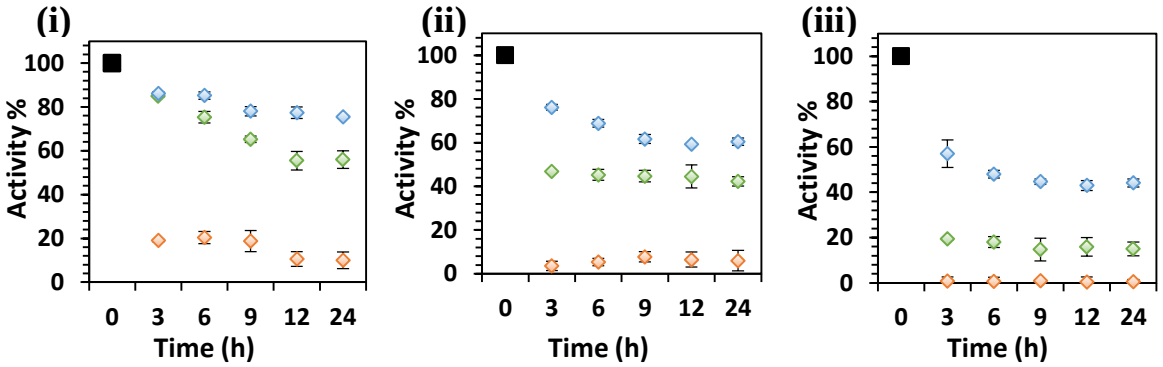

Figure 4.16. *Thermostability studies of α-amylase-functionalised crystallin PNFs at (a) 40 °C, (b) 55 °C, and (c) 75 °C, over the time period of 24 h, where black bars – 100% activity at t = 0, blue bars - covalent crosslinking, green bars - free enzyme, and red bars - non-covalent association.*

The results **(Figure 4.16)** show that as the temperature increases, the stability of the free enzyme reduces rapidly as compared to the immobilised form. At 40 and 55 °C **(Figure 4.16 (i) and (ii))**, the covalently immobilised α-amylase retains ~65-75% of its activity after the time period of 24 h, whilst the free enzyme (α-amylase), retains ~40-45% activity. At 75 °C **(Figure 4.15 (iii))**, the covalently immobilised α-amylase retains ~55% of its relative activity, compared to ~15-20% for the free enzyme. When α-amylase is associated to CPNFs without any crosslinker (non-covalent association), only ~3% activity is retained at 40 and 55 °C and complete loss of activity is observed at 75 °C. This decrease or complete loss of activity suggests the inactivation of enzyme caused by the denaturation and the leakage of enzymes from crystallin PNFs due to heating and diffusional effects (common limitations of adsorption method, as discussed earlier in section 1.4, Chapter One). In contrast, at all the selected temperatures, 40 °C, **Figure 4.16 (i)**, 55 °C, **Figure 4.16 (ii)**, and 75 °C, **Figure 4.16 (iii)**, the sample which retains the greatest relative activity is the sample where α-amylase is covalently immobilised to the crystallin PNFs using GA. These results suggest that covalent crosslinking using GA is an effective method for functionalising crystallin PNFs without any major loss of enzymatic activity upon heating.

4.5.2. Effect of GA on thermostability of crystallin PNFs functionalised with α-amylase

To investigate the impact of GA alone on the thermal stability of crosslinked samples, activity assays using the same conditions were also done on the GA crosslinked α-amylase samples (α-amylase and GA only, without crystallin PNFs) (section 7.12) **(Figure 4.17)**.

The samples containing GA crosslinked α-amylase retained about the same amount of activity as the free α-amylase control, implying that the presence of GA is not providing the increase in thermostability and therefore, it is most likely that this improved thermostability is due to the PNFs. Increased thermal stability has been reported for a number of immobilised enzymes, and the support material is thought to preserve the tertiary structure of the enzyme providing conformational benefits, which protects the enzyme against heat denaturation [20]. Previous work by Raynes *et al.* (2011) reported a significant increase in the relative thermostability of organophosphate hydrolase (OPH) activity when it was crosslinked to the insulin PNFs, both in the presence and absence of GA [8]. However, in contrast to these results no increase in temperature stability was observed when organophosphate hydrolase was crosslinked to the crystallin PNFs using GA [8].

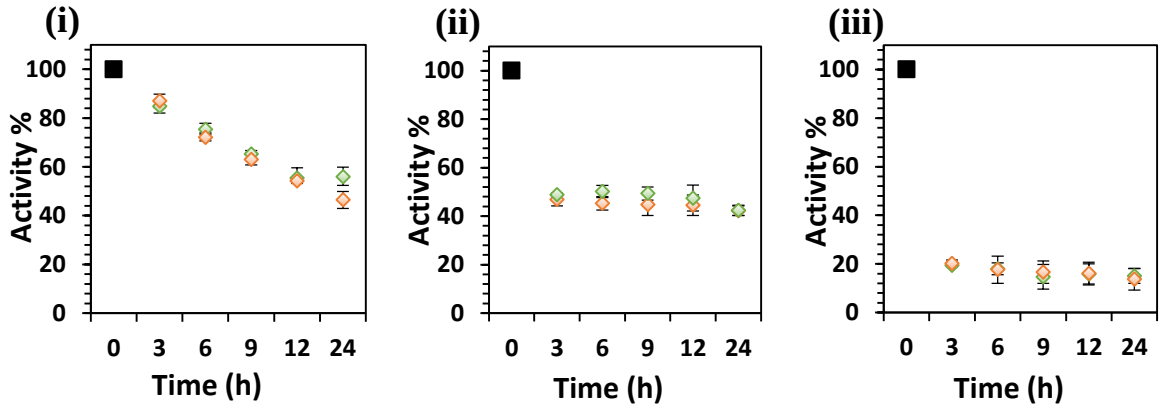

***Figure 4.17**. Thermostability studies of free α-amylase (green bars), and α-amylase in the presence of GA (red bars) at (a) 40 °C, (b) 55 °C, and (c) 75 °C, over the time period of 24 h. The activity of all individual samples at time zero were given an activity of 100% (black bars). The loss in relative activity was characterised by using starch-iodine assay, absorbance measured at 620 nm. Error bars represent the standard deviation of the mean of three replicates.*

This is not an unexpected result as multipoint interaction between the protein molecule and the matrix during immobilisation often involve some structural readjustment on the part of the protein molecule. Enzymes immobilised on the same support by the same method can behave differently. In a previous study by Sardar *et al.* (1997), successful immobilisation of a variety of enzymes to polymeric support resulted in varied thermostability results [21]. Therefore, it is likely that the increased stability of α-amylase is because of the way it is orientated upon immobilisation onto the crystallin PNFs scaffold.

Additionally, glycosylated crystallin PNFs were used for the crosslinking studies by Raynes *et al.* (2011) in contrast to the de-glycosylated/oxidised crystallin PNFs used in this work. De-glycosylated crystallin PNFs have more functional groups available for the effective crosslinking, therefore, leading to the better covalent crosslinking as observed by this method.

4.6. Storage stability and reusability of crystallin PNFs functionalised with α-amylase

The operational stability of immobilised enzymes is one of the most important factors affecting the utilisation of an immobilised enzyme system. In order to investigate the enzyme-nanoscaffold, the α-amylase-functionalised crystallin PNFs were examined by using the same conditions repeatedly 4 times over the time period of 30 days, with samples being washed, and stored at 4 °C in between each use (section 7.13). The measured activities are shown in **Figure 4.18**. The relative activity of immobilised enzymes **(Figure 4.18)** shows an initial drop over the first two days, with an activity loss ranging from approximately 10-15%. It was observed that the covalently bound enzyme demonstrated overall activity loss of approximately ~18% after 4 runs over the time period of 30 days.

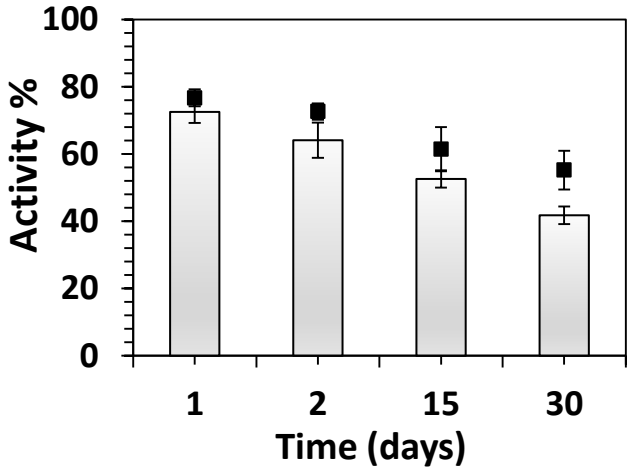

***Figure 4.18**. Timecourse of % activity of α-amylase-functionalised CPNFs, stored at 4 °C, over the time period of 30 days, where grey bars - amount of starch hydrolysed, as characterised by starch-iodine assay, and black bars - amount of reducing sugars produced as detected by the DNS assay.*

In general, enzymes in solution are not stable and their activity decreases gradually. The activity measurements were also carried out for the free enzyme stored at 4 °C for a period of 16 days using the same conditions. The free enzyme lost all its activity within 16 days **(Figure 4.19)**. Kahraman *et al.* (2007) has previously reported a complete loss of free α-amylase activity at 4 °C within 15 days [20]. These results indicate that the catalytic activity of the immobilised α-amylase is preserved over consecutive uses and immobilised α-amylase retains ~80% of its activity for at least 30 days without any inconsistency in results. Sohrabi *et al.* (2014) reported that α-amylase immobilised on modified magnetite nanoparticles retained ~80% of activity after 12 days [22].

Retained activities of α-amylase immobilised on various other supports, such as beads or microspheres, and hybrid materials were previously stated as 75-90% after 25 days of storage [20], [23-25]. The result suggests that the covalent crosslinking method developed here has improved the stability of α-amylase and helps to maintain the activity longer.

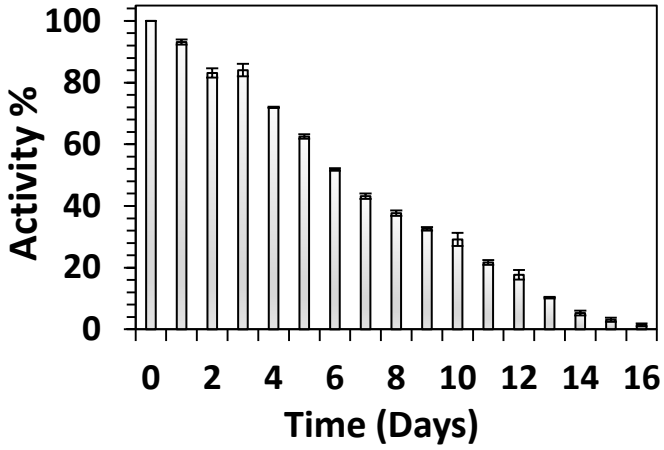

Figure 4.19. *Storage stability of free α-amylase. The loss in activity was characterised by using starch-iodine assay, absorbance measured at 620 nm. Error bars represent the standard deviation of three replicates.*

4.7. Conclusion

Crystallin PNFs show potential as a versatile nanoscaffold for active biocatalysts. For all the enzymes used in this work, regardless of the size, tertiary or quaternary structure, catalytic activity, and substrate recognition, the covalent attachment of the enzyme *via* GA was found to be more effective than the non-covalent association. The degree of immobilisation and retained catalytic activity post-immobilisation differed between biomolecules; however, no significant loss in the activity of immobilised enzymes was noticed.

A thermostability study resulted in the immobilised α-amylase displaying better thermostability than the free enzyme. The covalent attachment of the enzymes onto crystallin PNFs also resulted in improved stability and reusability. The GOX- and β-gal-functionalised crystallin PNFs were further investigated for use in a model biosensing application, such as the creation of a glucose and a lactose based electrochemical sensing platform (see Chapter Five, Part A). The future goals of this research should include extending this functionalisation method to other functional moieties, growth factors and biomolecules, as well as using the functional crystallin PNF nanoscaffolds in industrially relevant systems.

4.8. References

[1] G.T. Hermanson, *Bioconjugate techniques*, Academic Press, US (2013).

[2] M. Beier, J.D. Hoheisel, Versatile derivatisation of solid support media for covalent bonding on DNA-microchips, *Nucleic Acids Research*, 27 (1999) 1970-1977.

[3] I. Migneault, C. Dartiguenave, M.J. Bertrand, K.C. Waldron, Glutaraldehyde: Behavior in aqueous solution, reaction with proteins, and application to enzyme crosslinking, *Biotechniques*, 37 (2004) 790-806.

[4] Y. Wine, N. Cohen-Hadar, A. Freeman, F. Frolow, Elucidation of the mechanism and end products of glutaraldehyde crosslinking reaction by X-ray structure analysis, *Biotechnology and Bioengineering*, 98 (2007) 711-718.

[5] A. Habeeb, R. Hiramoto, Reaction of proteins with glutaraldehyde, *Archives of Biochemistry and Biophysics*, 126 (1968) 16-26.

[6] S.J. Meade, A.G. Miller, J.A. Gerrard, The role of dicarbonyl compounds in non-enzymatic crosslinking: A structure-activity study, *Bioorganic & Medicinal Chemistry*, 11 (2003) 853-862.

[7] S. Pilkington, *Incorporating glucose oxidase activity into amyloid fibrils*, Master's Thesis, University of Canterbury (2009).

[8] J.K. Raynes, F.G. Pearce, S.J. Meade, J.A. Gerrard, Immobilisation of organophosphate hydrolase on an amyloid fibril nanoscaffold: Towards bioremediation and chemical detoxification, *Biotechnology Progress*, 27 (2011) 360-367.

[9] S.M. Pilkington, S.J. Roberts, S.J. Meade, J.A. Gerrard, Amyloid fibrils as a nanoscaffold for enzyme immobilisation, *Biotechnology Progress*, 26 (2010) 93-100.

[10] S. Avrameas, T. Ternynck, The cross-linking of proteins with glutaraldehyde and its use for the preparation of immunoadsorbernts, *Immunochemistry*, 6 (1969) 53-66.

[11] H. Levine, Thioflavin T interaction with synthetic Alzheimer's disease β-amyloid peptides: Detection of amyloid aggregation in solution, *Protein Science*, 2 (1993) 404-410.

[12] L. Holmquist, M. Lewin, Separation of glutaraldehyde and some of its aldol condensation products by hydroxyl-aldehyde group affinity chromatography, *Journal of Biochemical and Biophysical Methods*, 22 (1991) 321-329.

[13] K. Peters, F.M. Richards, Chemical crosslinking: Reagents and problems in studies of membrane structure, *Annual Review of Biochemistry*, 46 (1977) 523-551.

[14] T. Fester, R. Berg, C. Taylor, An easy method using glutaraldehyde-introduced fluorescence for the microscopic analysis of plant biotrophic interactions, *Journal of Microscopy*, 231 (2008) 342-348.

[15] M.F. Chaplin, C. Bucke, *Enzyme technology*, CUP Archive, (1990).

[16] G.L. Miller, Use of dinitrosalicylic acid reagent for determination of reducing sugar, *Analytical Chemistry*, 31 (1959) 426-428.

[17] A. Manole, D. Herea, H. Chiriac, V. Melnig, Laccase immobilised on hydrotalcites as a 3rd generation biosensor type, *Biomaterials in Biophysics Medical Physics and Ecology*, (2008)11.

[18] R. Messing, *Immobilised enzymes for industrial reactors*, Elsevier (1975).

[19] L. Cao, *Carrier-bound immobilised enzymes: Principles, application and design*, Wiley-VCH: Germany, (2005) 1-52.

[20] M.V. Kahraman, G. Bayramoğlu, N. Kayaman-Apohan, A. Güngör, α-Amylase immobilisation on functionalised glass beads by covalent attachment, *Food Chemistry*, 104 (2007) 1385-1392.

[21] M. Sardar, R. Agarwal, A. Kumar, M. Gupta, Noncovalent immobilisation of enzymes on an enteric polymer Eudragit S-100, *Enzyme and Microbial Technology*, 20 (1997) 361-367.

[22] N. Sohrabi, N. Rasouli, M. Torkzadeh, Enhanced stability and catalytic activity of immobilised α-amylase on modified Fe_3O_4 nanoparticles, *Chemical Engineering Journal*, 240 (2014) 426-433.

[23] O. Türünç, M.V. Kahraman, Z.S. Akdemir, N. Kayaman-Apohan, A. Güngör, Immobilisation of α-amylase onto cyclic carbonate bearing hybrid material, *Food Chemistry*, 112 (2009) 992-997.

[24] M.V. Kahraman, N. Kayaman-Apohan, A.e. Ogan, A. Güngör, Soybean oil based resin: A new tool for improved immobilisation of α-amylase, *Journal of Applied Polymer Science*, 100 (2006) 4757-4761.

[25] H. Tümtürk, S. Aksoy, N. Hasırcı, Covalent immobilisation of α-amylase onto poly (2-hydroxyethyl methacrylate) and poly (styrene-2-hydroxyethyl methacrylate) microspheres and the effect of Ca^{2+} ions on the enzyme activity, *Food Chemistry*, 68 (2000) 259-266.

Chapter Five

An investigation into the use of amyloid PNFs

5.1. Introduction

This chapter combines the experimental approaches of the previous two chapters to investigate the creation of materials with surface-assembled amyloid PNFs. Modifying surfaces (metal, glass or cellulose) by attaching amyloid PNFs can provide an easy way for the handling and recovery of the nanoscaffold, while retaining the benefits of an increase in surface area [1], and can also lead to the development of novel amyloid fibril-based functional materials. The self-assembling nature of amyloid PNFs, and availability of intrinsic side chain chemistry from their amino acid composition, could also potentially allow for a bottom-up approach to functional bionanomaterial design [2, 3]. Amyloid fibrils obtained from crystallin and whey protein (as detailed in section 7.2) and functionalised PNFs (prepared *via* crosslinking as detailed in Chapter Three and Four) were used to investigate the creation of materials with surface-assembled PNFs.

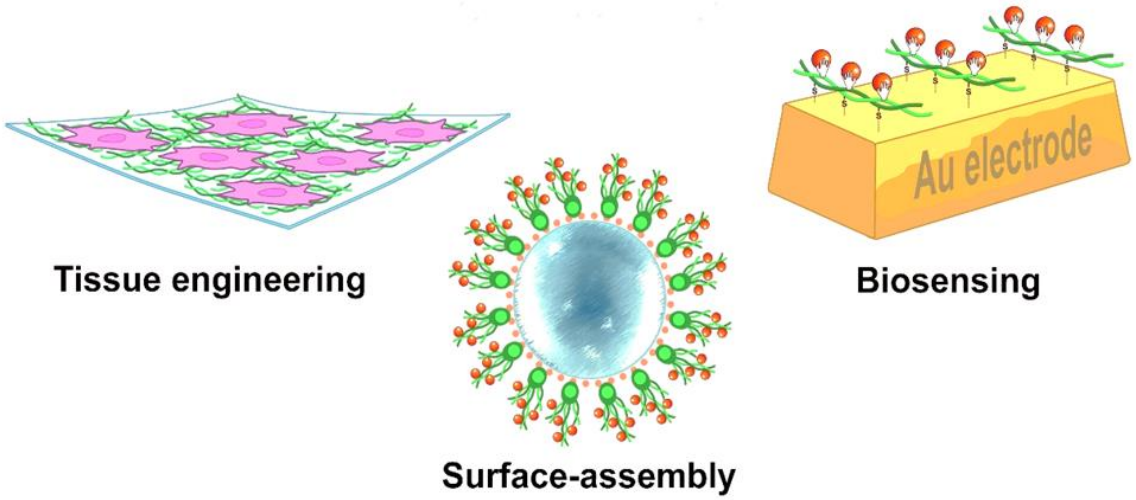

The first part of this chapter, focuses on the development of a PNF-based biosensing element. Both GOX- and β-gal-functionalised PNFs were used to modify Au electrodes, and cyclic voltammetry (CV) was done for glucose and lactose analysis. In the next section, to create materials with surface-assembled PNFs, PNFs were assembled on glass surface and characterised by a range of methods, to establish whether the simple methodology developed by Raynes (2012) [4] for creating surfaces with self-assembled insulin PNFs is applicable to PNFs obtained from other protein sources. The surface-assembled amyloid fibril nanoscaffold was then functionalised with a biotechnologically important enzyme, such as β-gal leading to the making of active bionanomaterial. The last part of this chapter explores PNFs for designing biomaterials with potential applications in tissue engineering. In addition to the PNFs, native proteins (crystallin, and whey) were also used to prepare silk-protein composite films, followed by characterisation and cell growth studies.

Part A- Construction of a biosensing element for glucose and lactose detection

5.2. Biosensors

One of the main analytical applications of immobilised enzymes is to develop enzyme-based biosensors [5]. The most widely accepted definition of a biosensor is: "a self-contained analytical device that incorporates a biologically active material in intimate contact with an appropriate transduction element for the purpose of detecting (reversibly and selectively) the concentration or activity of chemical species in any type of sample"[6]. Biosensing is the detection and quantification of biological and chemical species, and is crucial for many areas of healthcare, clinical medicine, food safety, and environmental monitoring [7]. The use of high surface area nanomaterials in the sensing technology has allowed fabrication of biosensors with improved sensitivity, and faster response times [8, 9]. A range of nanostructures such as NPs, nanowires, NTs, nanoribbons, nanorods, nanobelts and nanosheets have been explored extensively in the construction of biosensors with set applications of biosensors nanotechnology for biological and chemical analysis [10].

There have been some previous investigations into the use of nanomaterials as immobilisation scaffolds for the creation of enzyme electrode sensors, specifically using PNTs/PNFs such as nanotubes from the FF peptide [11, 12], the ionic complementary peptide EFK16-11 [13], fluorescent antibody nanotubes [14], cysteine-containing peptide nanofibrils [15], and more recently from the whey PNFs [16]. One of the advantages of using PNFs is that they can interact with a gold surface (electrode) *via* thiol groups, without any surface modification [11]. On the surface of the gold electrode, the amyloid fibrils interact with the gold surface *via* sulfhydryl groups, and an enzyme (GOX, and β-gal in this study) is in turn covalently bound to the amyloid fibrils, *via* the crosslinker, as illustrated in **Figure 5.1.**

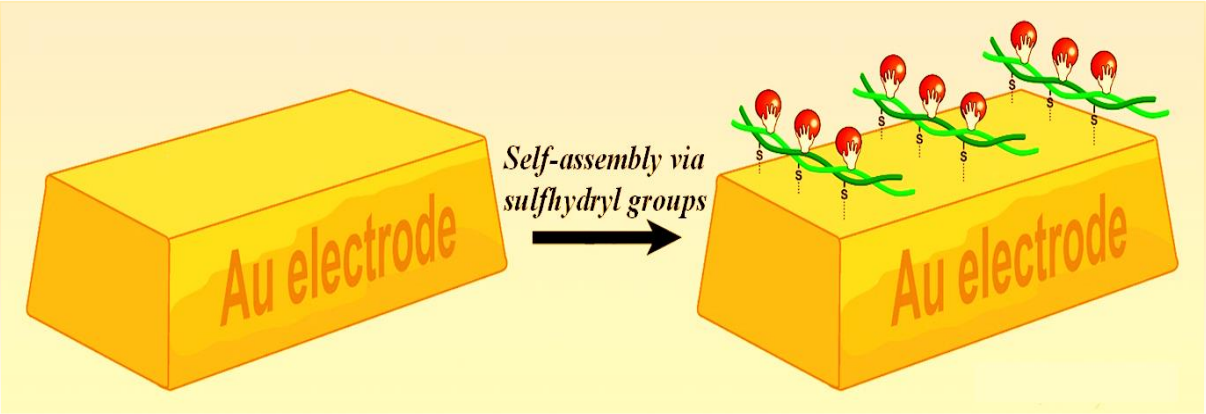

Figure 5.1. *A schematic representation of Au electrode modified with PNFs. Functionalised PNFs can self-assemble onto metal electrode, such as Au via available sulfhydryl groups.*

In this work, crystalllin PNFs – the industrially relevant amyloid forming protein was used to develop a biosensing platform for glucose and lactose detection, and the potential of dual-functionalised whey PNFs was also investigated for developing a lactose-based sensor.

5.3. Surface-assembly of functionalised PNFs - Towards biosensing

As a proof of concept, and to verify the immobilisation of GOX and β-gal onto crystallin PNFs, electrochemistry studies were done on GOX- and β-gal-functionalised CPNFs. The electrochemical behaviour of the functionalised crystallin PNFs was examined using CV (section 7.14) in the presence of the mediator ferrocenemethanol (FcOH) (1.5 mM in PBS, pH 7.4). Under normal circumstances, direct electron transfer between the active site of reduced GOX and a metal electrode takes place slowly or not at all because the gap between the active site and the electrode surfaces is too large for electron transfer [17]. Thus, an electron transfer mediator is used to overcome this problem. Ferrocene is usually used as an electron acceptor mediator, and derivatives of ferrocene being soluble in water are the largest class of one electron oxidants due to their water solubility properties [17]. In this work, FcOH (a ferrocene derivative) was used as a mediator because it can penetrate the active site of GOX [18]. Also, FcOH can be used in solution, unlike ferrocene which is water insoluble and thus, can diffuse freely between the enzyme and electrode [17].

For electrochemistry experiments, commercial screen-printed electrodes with an appropriate connector from DropSens (Oveido, Spain) were used. The functionalised crystallin PNFs were deposited onto the gold electrode, and the excess solvent evaporated (section 7.14). Modified electrodes were prepared fresh before each experiment for consistency.

The catalytic activity of the modified electrodes with GOX-functionalised crystallin PNFs was quantified in the presence of excess glucose (500 mM), using FcOH as a mediator in solution (section 7.14.1). In the presence of GOX, glucose is oxidised to gluconolactone in the solution being examined. Electron transfer from the reduced enzyme to the gold electrode then occurs *via* the mediator molecule present, in this case FcOH solution. In the electron transfer reaction, ferrocenes are one electron oxidising systems, however, glucose/gluconolactone is two electron and two proton system. Thus, two equivalents of ferrocene and ferrocenium are involved in the reaction.

The catalytic activity of the modified electrode can be expressed as the current amplification (CA), defined by:

$$CA = (iFcOH + iFcOH + Glu)/ iFcOH$$

Where, *iFcOH* is the anodic peak current recorded at the electrode in the absence of glucose (for the mediator alone), and *iFcOH + Glu* is the anodic peak current recorded in the presence of glucose (mediator + Glucose) [19]. A typical cyclic voltammogram of the electrode response to glucose (500 mM) in a FCOH mediator is shown in **Figure 5.2.**

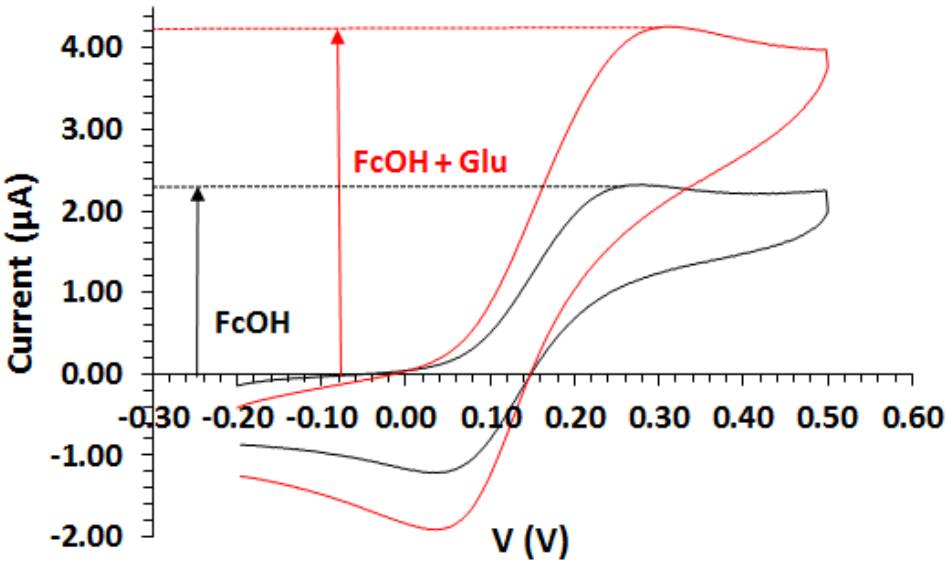

Figure 5.2. *A typical cyclic voltammogram of the electrode response to glucose (500 mM) in a FCOH mediator (1.5 mM) (red-FcOH + Glu) and to the mediator (black-FcOH) alone.*

5.4. Response of single enzyme-based electrodes modified with

(a) GOX-functionalised crystallin PNFs - GOX immobilised via adsorption onto reduced, and non-reduced crystallin PNFs

The influence of the presence of the PNFs on current amplification was examined by comparing the average current amplification in the presence of excess (500 mM) glucose for the GOX-only modified gold electrodes (Au/GOX), and the GOX-functionalised amyloid fibril modified gold electrodes (Au/GOX-CPNFs for non-reduced crystallin amyloid fibrils, and Au/GOX-CPNFs-SH for reduced crystallin PNFs, obtained *via* TCEP treatment – refer **Table 3.5**, Chapter Three). The GOX-only control was created by the same methods as detailed in section 7.14.1, with the exception that only GOX was deposited, and any anchorage of the enzyme to the electrode surface was due to nonspecific adsorption.

The GOX sample used was diluted in PBS to obtain the same activity as of the functionalised PNFs used for modifying electrodes. The average CA in the presence of 500 mM glucose for each of these three samples is shown in **Figure 5.3.** An increase in CA value was observed when using GOX-functionalised crystallin fibrils as compared to adsorbed GOX-only, suggesting an increase in enzyme immobilisation due to the large surface-to-volume ratio of the amyloid fibril nanoscaffold. Similarly, an increase in the CA response was also observed for Au/GOX-CPNFs-SH electrode, where the electrode was modified using GOX-functionalised reduced crystallin PNFs.

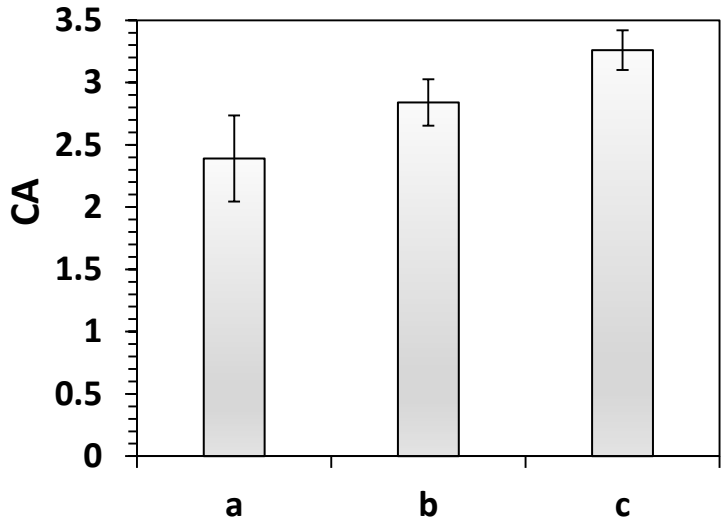

Figure 5.3. *Average current amplification (CA) for GOX modified gold electrode (Au/GOX), and gold electrode modified with functionalised PNFs, where* ***(a)*** *– Au/GOX,* ***(b)*** *- Au/GOX-CPNFs (gold electrode modified with non-reduced crystallin PNFs), and* ***(c)*** *- Au/GOX-CPNFs-SH (gold electrode modified with reduced crystallin PNFs). Each value represents the average of three replicates, with error bars representing the standard deviation of the mean of three replicates.*

This increase was in agreement with the activity assay results that suggested better immobilisation efficiency for crystallin fibrils reduced *via* treatment with TCEP **(Table 3.5, b)**. The other potential reason for this increase in current response could be due to the better attachment of reduced PNFs to the gold surface because of sulfhydryl-metal interactions as compared to physical adsorption only. This increase in the anchorage of the thiolated whey PNFs to the gold electrode has also been reported previously [16].

It should be noted that there was quite high error for the GOX-only modified electrodes as compared to the electrodes modified using PNFs. This is due to the GOX getting washed away and repeated use of GOX-only modified electrode resulting in lower responses. In contrast, washing and repeated use of the modified electrode resulted in little reduction in the observed response, indicating that the fibrils are well adhered to the gold electrode and the electrode is reusable.

(b) Functionalised crystallin PNFs obtained via GA-based immobilisation

The single enzyme based electrochemistry reaction was also done with functionalised CPNFs obtained *via* GA-based crosslinking (as discussed in Chapter Four). Two separate electrodes were prepared using GOX (section 7.14.1) and β-gal-functionalised CPNFs (section 7.14.2) for glucose and lactose analysis respectively, followed by CV (section 7.14).

The ferrocene mediated electrochemical reaction for each of the enzyme system is illustrated in **Figure 5.4.** The electrochemical response for both glucose and lactose analysis is based on hydrogen peroxide (H_2O_2) sensing as shown in **Figure 5.4** *(equation 5.1 and 5.2).*

For glucose sensing, immobilised GOX catalysis the oxidation of glucose using oxygen as an electron acceptor, leading to the production of H_2O_2 (equation 5.1). The H_2O_2 produced is then electrochemically detected at the electrode surface [20]. For lactose analysis, immobilised β-gal cleaves lactose producing glucose and galactose, and the released glucose is cleaved further by the dissolved GOX (see equation 5.2).The current produced due to GOX catalysis reaction is then measured by using CV.

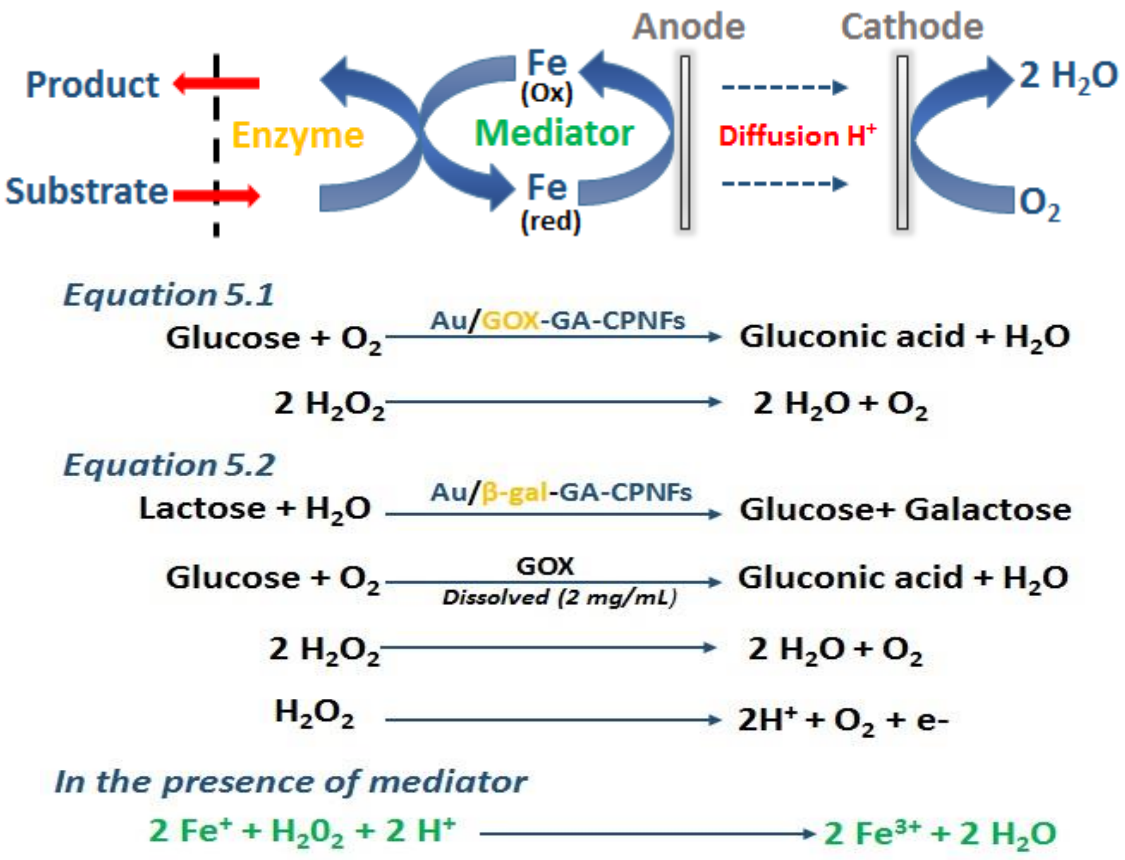

Figure 5.4. *A schematic representation of ferrocene mediated electrochemical reaction, where equation 5.1 and 5.2 represents electrochemical reactions specific to glucose and lactose respectively.*

In the presence of analytes (glucose and lactose, red line) **(Figure 5.5)**, the anodic current was amplified due to the catalytic oxidation of glucose by GOX modified electrode (Au/GOX-GA-CPNFs) **(Figure 5.5 (i))**, and lactose by β-gal modified electrode (Au/β-gal-GA-CPNFs) **(Figure 5.5 (ii))**, mediated by FcOH. In the absence of analyte, no change in response due to the presence of functionalised crystallin PNFs in the ferrocene mediator solution was detected for Au electrodes modified with functionalised PNFs. These results, in agreement with the gel electrophoresis and solution activity assays (Chapter Four), confirm that GOX and β-gal were successfully crosslinked to the GA activated CPNFs. The electrochemistry results indicate that the functionalised crystallin PNFs retain activity when deposited on Au surface and are able to electrochemically react with the respective analyte i.e. glucose for GOX-, and lactose for β-gal-functionalised PNFs.

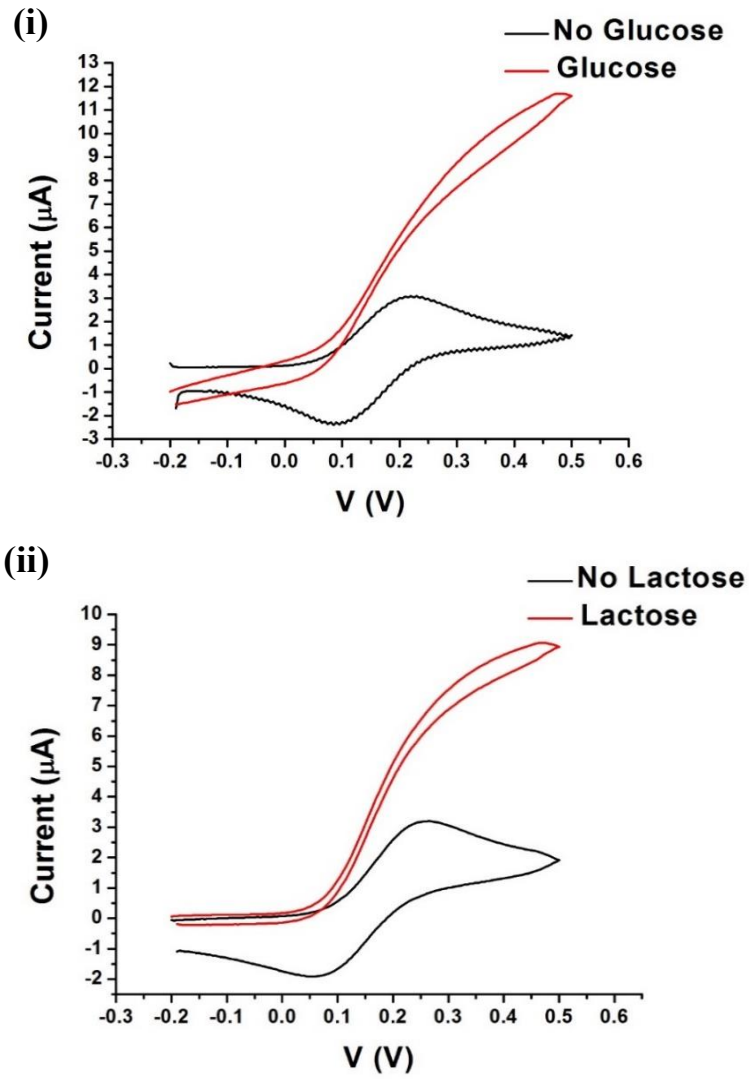

Figure 5.5. *Cyclic voltammogram of the functionalised crystallin PNFs (CPNFs) modified electrodes:* ***(i)*** *GOX-functionalised CPNFs* ***(ii)*** *β-gal-functionalised CPNFs in the absence (black line) and presence (red line) of excess glucose and lactose respectively (500 mM), using 1.5 mM FcOH.*

(c) A comparative analysis - Free enzyme vs functionalised crystallin PNFs

Previous studies have shown that the use of nanoscaffolds as a biosensing element can increase the overall sensitivity and stability of enzymatic biosensors [21, 22]. Thus, electrochemistry experiments were done to study the influence of functionalised crystallin PNFs on current amplification by comparing the electrode response in the presence of excess analyte for the enzyme-only modified Au electrodes, and the enzyme-functionalised crystallin PNFs modified electrodes **(Figure 5.6)**. An increase in current response was observed **(Figure 5.6 (i))** when using GOX-functionalised crystallin PNFs as compared to adsorbed GOX-only, proposing better enzyme attachment to the electrodes and an increase in immobilised enzyme due to the large surface-to-volume ratio of the crystallin PNF nanoscaffold.

The results obtained are in agreement to a similar study done on whey PNFs, where several different variations of a glucose biosensing platform using PNFs obtained from WPI were investigated [16]. However, for the electrode modified with β-gal-functionalised crystallin PNFs, no significant difference was observed in current response in the presence of crystallin PNFs as compared to adsorbed β-gal-only **(Figure 5.6 (ii))**.

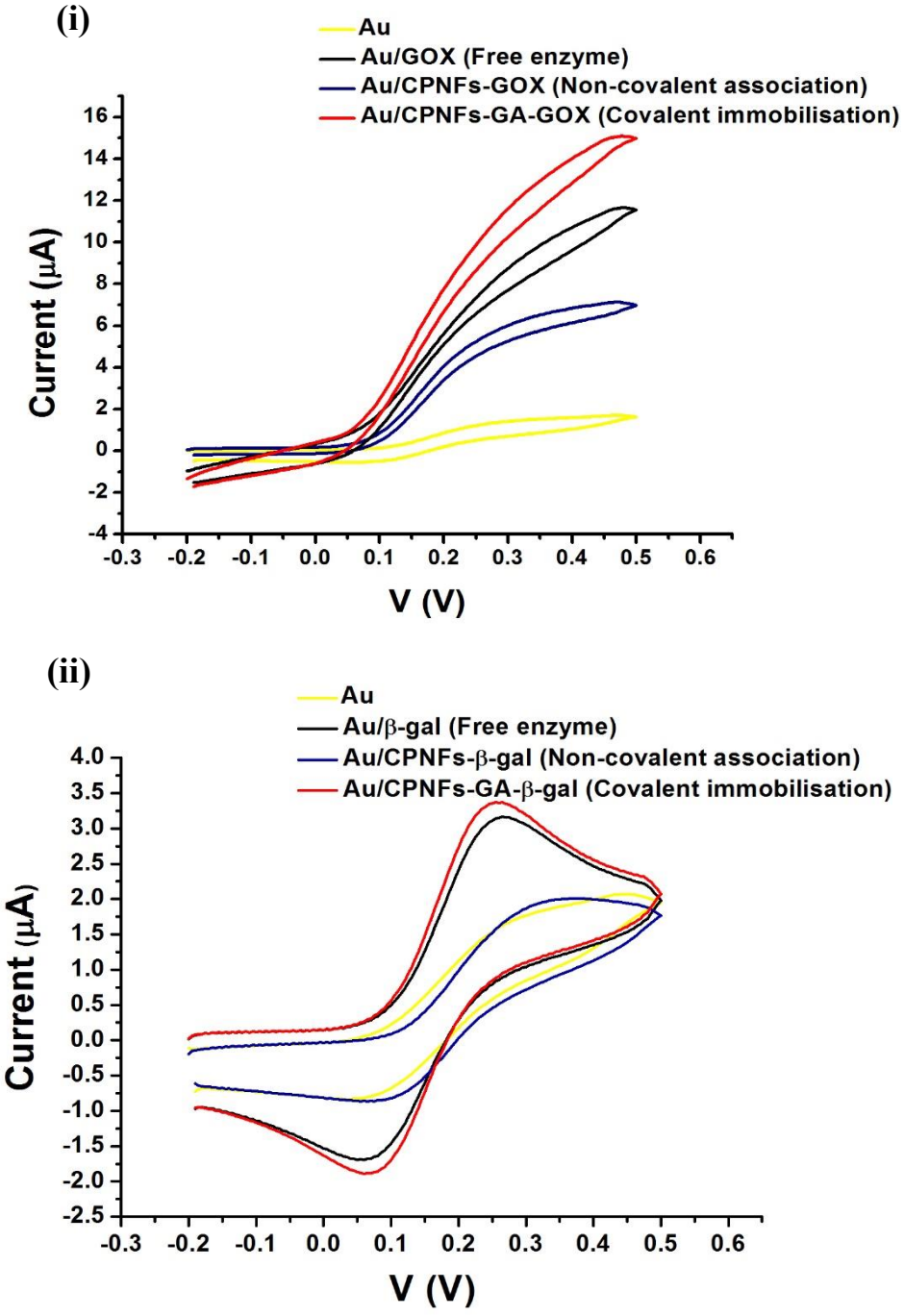

Figure 5.6*. Comparison of electrodes modified with* ***(i)*** *GOX-, and* ***(ii)*** *β-gal-functionalised crystallin PNFs. with free enzyme, enzyme attached via non-covalent association, and enzyme covalently crosslinked onto the modified crystallin PNFs using GA. Potential sweep rates are 100 mV* s^{-1}*, using an Au counter and Ag pseudo-reference electrode.*

This difference in electrochemical behaviour of GOX-, and β-gal-functionalised crystallin PNFs could be due to the lower enzyme immobilisation efficiency for β-gal as compared to the GOX sample used (refer to Chapter Four, **Table 4.3**). Additionally, in contrast to the glucose analysis where GOX was immobilised onto the electrode, for lactose analysis GOX (equation 5.2) was dissolved within the lactose solution, and could be responsible for the observed difference in current response as GOX was not present in close vicinity.

5.5. Dual-functionalised amyloid fibrils

To explore if the two enzymes could be bound to the same PNFs scaffold and function in a co-operative manner, dual-functionalisation of PNFs was also investigated. The utilisation of dual-functionalisation has several applications and advantages e.g. using a dual enzyme system enables a high local concentration of substrates in the microenvironment of an enzyme system, leading to kinetic advantages [23]. Reduced diffusion time of the substrate and significant enhancement in the sensitivity for co-immobilised enzyme based biosensing platform have been demonstrated previously, such as co-immobilisation of histamine dehydrogenase and putrescine oxidase enzymes onto screen printed electrode allowed selective, and sensitive determination of histamine, and putrescine (biogenic amines produced by microbial decarboxylation)[24].

Further, GOX and β-gal were co-immobilised onto whey PNFs to obtain a dual-functionalised PNFs. Dual-functionalised PNFs were then used to evaluate if the presence of both enzymes on the same nanoscaffold (whey PNFs) improves electrode sensitivity for lactose analysis. Lactose is a disaccharide consisting of glucose and galactose units bonded through a β-1→4 glycosidic linkage, and is most notably found in milk. Lactose analysis is often used to evaluate the quality of milk [25], and a precise control of lactose levels is also important because of the lactose intolerant population [26]. Therefore, lactose quantification is vital for both food industry and public health.

To obtain dual-functionalised PNFs, both one step (simultaneous), and sequential immobilisation of GOX and β-gal was studied, *via* GA-based crosslinking. After the crosslinking reaction, SDS-PAGE and activity assays were used to determine the extent of crosslinking.

5.5.1. Dual immobilisation crosslinking reaction

Based on the results of amino group availability assays (section 3.4.1) suggesting the presence of lysine groups on the surface of whey PNFs, it was decided to use GA as a crosslinking agent for the co-immobilisation of GOX and β-gal onto whey PNFs. Different reaction orders, and conditions were initially investigated to optimise the crosslinking reaction. After the crosslinking method development, the immobilisation conditions chosen were: a starting concentration of 10 mg/mL whey amyloid fibrils (100 µL); with a starting concentration of 7.5 mM GA (100 µL); and a starting concentration of 2 mg/mL GOX (50 µL), and 4.2 mg/mL β-gal (50 µL); incubated for 1 h at 37 °C and quenched with 100 µL of 100 mM Tris buffer (pH 8.0) (section 7.11.3). SDS-PAGE **(Figure 5.7)** was done for the immobilised enzyme samples to assess the extent of crosslinking.

SDS-PAGE shows that when enzymes (GOX+β-gal) are co-immobilised to the whey PNFs using GA (Fig. 5.7 - Lane 4 to Lane 8, different reaction orders as detailed in **Table 5.1**) the intensity of enzyme bands, when compared to the positive control (Lane 3 - enzyme + GA in the absence of whey PNFs), decreased, suggesting that the enzymes has been immobilised and therefore, were not able to enter the gel due to size restrictions.

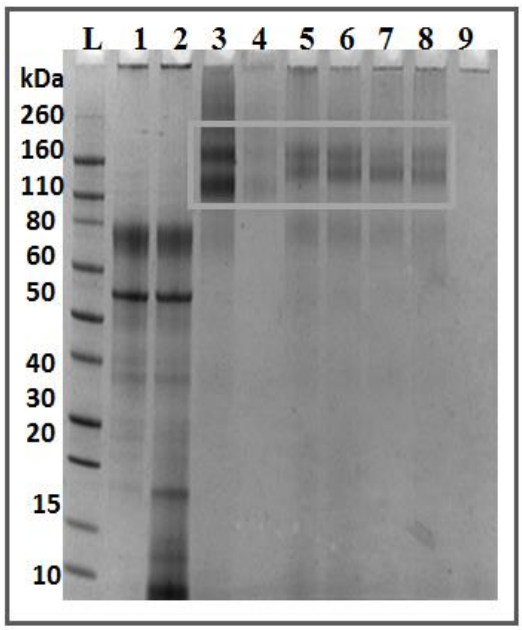

Figure 5.7. *SDS-PAGE for the co-immobilisation reaction for whey PNFs via GA. L-Ladder; Lane 1 - Enzyme-only sample (GOX+β-gal); Lane 2 - Enzyme + WPNFs; Lane 3 - Enzyme + GA; Lane 4 to Lane 8 - Enzyme + GA + WPNFs, different reaction orders studied as detailed below in* ***Table 5.1****; Lane 9 - WPNFs + GA sample. Highlighted section correspond to the molecular weight of the enzymes in the presence of GA, and GA + WPNFs.*

Table 5.1. *Summary of GOX-, and β-gal-functionalised PNFs activities, as determined by the enzyme-specific activity assays, where arrow indicates 15 min incubation time, at 37 °C. GOX activity was determined by using Amplex Red assay (Appendix B, section B1.1), and ONPG assay (Appendix B, section B1.2) was done for β-gal activity, for all the samples used for dual-immobilisation reaction.*

Sample	Reaction details	Activity of GOX %	Activity of β-gal%
1	ENZ+PBS+PBS	100	100
2	ENZ+PBS+WPNFs	92±3	94±1.8
3	ENZ+GA+PBS	91±2	93±3
4	**WPNFs+GA→Enz**	**48±14**	**52±9**
5	ENZ+WPNFs+GA	32±11	31±8
6	GOX+WPNFs →GA+β-gal	34±13	38±4
7	β-gal+WPNFs→GA+GOX	36±9	34±14
8	GOX+WPNFs →GA→β-gal	32±3	38±5.9
9	WPNFs+GA+PBS	-	-

**The values given are the approximate values calculated from the activity assays and represented as % of initial activity remained after washing the fibrils (3X), with error represented as standard deviation of the mean of three replicates. Total reaction time was 1h, with samples kept at 37 °C.*

5.5.2. Activity of dual-functionalised WPNFs

To quantify the amount of enzyme that was being immobilised to whey PNFs in the presence of GA, activity assays were done on the immobilised enzyme samples pre- and post-centrifugation, yielding the relative activity/amount of both the enzymes immobilised to the whey amyloid fibrils. **Table 5.1**, details different reaction orders used for the co-immobilisation reaction, and also the relative activity of the enzyme immobilised (*via* each reaction) onto the whey PNFs. As can be seen, the sample which had the most activity (48% of GOX and 52% of β-gal activity) associated with the whey PNFs was sample 4, where enzymes and whey PNFs were incubated first with GA for 15 min, followed by the addition of enzymes (GOX+β-gal). The activity assay results confirm that GA can be used to covalently immobilise both GOX and β-gal to whey PNFs in one step reaction.

5.5.3. Lactose analysis using dual-functionalised WPNFs

Dual-functionalised whey PNFs were used to prepare PNF-based electrodes as detailed in section 7.14, and investigated to analyse lactose. The catalytic activity of the modified electrodes was quantified in the presence of excess lactose (500 mM), using FcOH as a mediator in solution (section 7.14.3). The dual-functionalised whey PNFs sample chosen for electrochemistry studies was that prepared by one step reaction i.e. sample 4, **Table 5.1**, due to better immobilisation yield. The approach for determining lactose concentration was based on the electrochemical reaction as shown in *equation 5.2* **(Figure 5.4)**, and is illustrated in **Figure 5.8**.

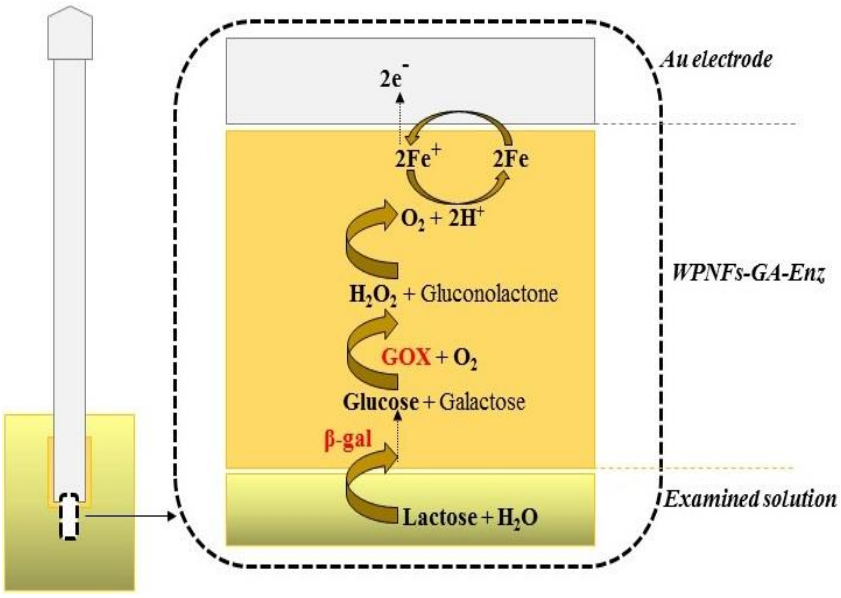

Figure 5.8. *Mechanism of action of the Au electrode with dual-functionalised whey amyloid PNFs in the presence of lactose. Immobilised β-gal cleaves the disaccharide lactose, producing glucose and galactose. The glucose reacts with the immobilised GOX to produce H_2O_2. The sensor functional principle is based on FcOH oxidation by H_2O_2 at the Au electrode, as electron transfer from the reduced enzyme to the Au electrode occurs via ferrocene mediator and current response measured by using CV.*

(a) Response of Au electrodes modified with dual-functionalised PNFs

The enzyme-only control sample was created by the same method used for single enzyme electrochemistry studies, with the exception that a mixture of both the enzymes (GOX+β-gal) was physically adsorbed onto the electrode surface (see 7.14.3).

(i)

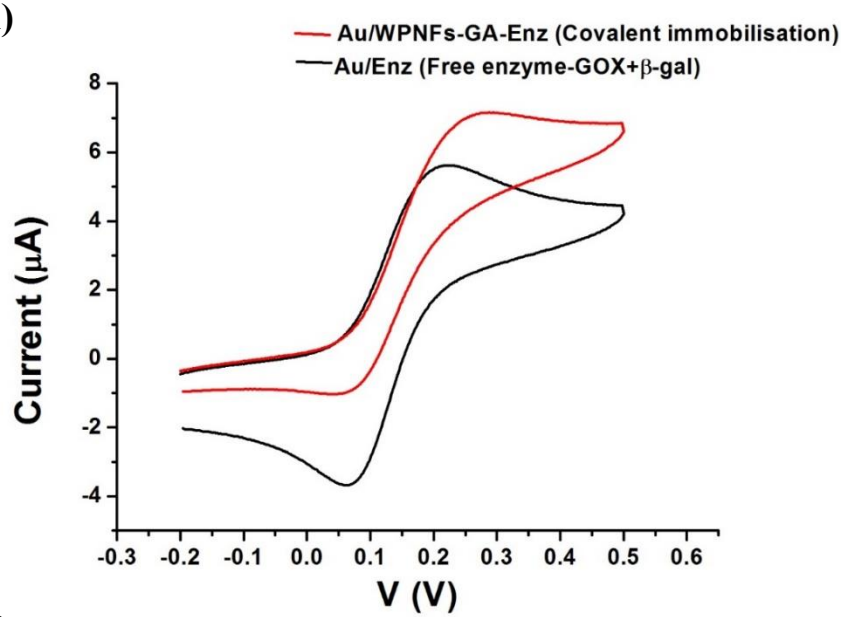

(ii)

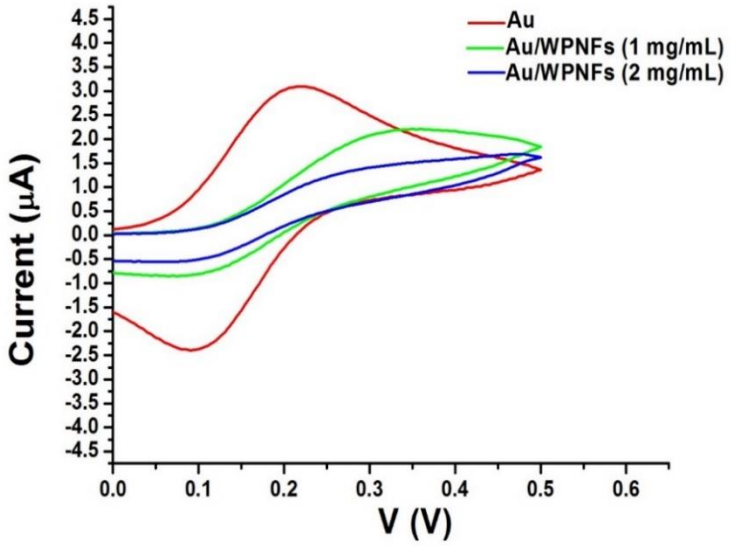

Figure 5.9. *Cyclic voltammogram of the dual-functionalised whey PNFs (WPNFs) modified electrodes:* ***(i)*** *Comparison of lactose responses for dual-functionalised whey PNFs (red line) where enzymes (GOX+β-gal) are covalently crosslinked onto whey PNFs using GA, with free enzyme attached onto the electrode via adsorption (black line).* ***(ii)*** *Comparison of lactose responses for bare electrode (Au) in the absence (red line), and in the presence of whey PNFs (green line - 1 mg/mL; and blue line - 2 mg/mL), where the signal is solely caused by the ferrocene mediator (1.5 mM FcOH). Potential sweep rates are 100 mV* s^{-1}*, using an Au counter and Ag pseudo-reference electrode.*

The enzyme sample used was diluted in PBS (pH 7.4) to have the same activity in solution, as determined by the activity assays for the WPNFs-GA-Enz (GOX+β-gal) sample used. Dual-functionalised whey PNFs were also adsorbed onto the Au electrodes to obtain PNF-based electrode (section 7.14 and 7.14.3). Similar to the results obtained with the single enzyme-based electrodes, an increase in current response was observed **(Figure 5.9 (i))** for the electrode with dual-functionalised whey PNFs (red line) as compared to the adsorbed enzyme mixture-only (black line), ascertaining the advantages of using PNFs in biosensing applications. A control voltammogram for Au (bare electrode), and Au electrode with whey PNFs at different concentrations, in the presence of lactose, are also shown in **Figure 5.9 (ii).**

(b) Electrochemical response as a function of lactose concentration

Further, the electrochemical response studies of Au/WPNFs-GA-Enz electrode (electrode modified with dual-functionalised PNFs) was done as a function of lactose with different concentrations from 0–100 mM at scan rate of 100 mV/s, using a single electrode for all the concentrations, and electrochemical response detected *via* CV technique (section 7.14). The corresponding calibration curve **(inset (a), Fig. 5.10)** shows the magnitude of peak current increased with increasing lactose concentration. These current values were used to form the calibration plot (concentration vs current – **Figure 5.10**). A linear working range of the Au/WPNFs-GA-Enz electrode shows linear response to lactose from 0.3 to 2.5 mM as shown in **Figure 5.10**, with linear regression coefficient of 0.976.

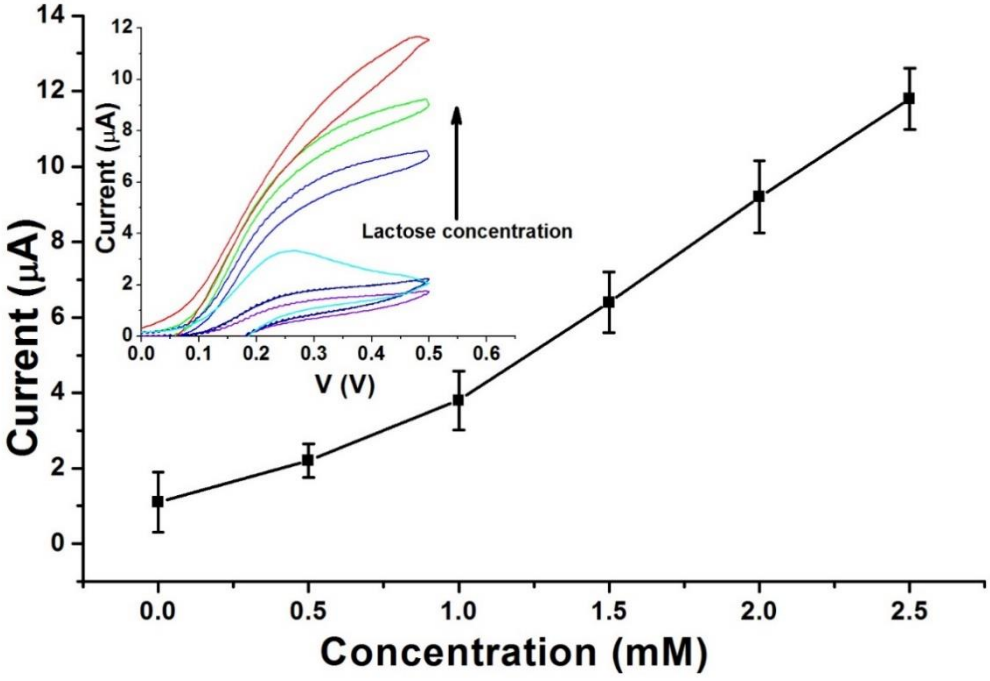

Figure 5.10. *A linear graph between lactose concentration and value of current obtained from CV with different concentration of lactose (0-100 mM). Inset (a) the electrochemical response of Au/WPNFs-GA-Enz electrode as a function of lactose concentration showing variation from 0.0-2.5 mM. Detection limit (LOD) of the fabricated Au/WPNFs-GA-Enz electrode for lactose analysis was calculated from slope of the curve (using 3 sigma method) and was found to be 0.53 mM.*

5.6. Conclusion

The electrochemistry work done on both functionalised crystallin, and whey PNFs has shown that functionalised PNFs can be self-assembled onto Au electrodes leading to the creation of an amyloid fibril-based biosensing element. The voltammograms with GOX-functionalised crystallin PNFs, and dual-functionalised whey PNFs exhibited an increase in anodic peak current response in the presence of PNFs, compared to free enzyme attached to the electrodes *via* adsorption suggesting an increase in enzyme loading due to the improved surface-to-volume ratio in the presence of PNFs. These results look promising for the development of PNF-based biosensing platform with improved sensitivity and also provide a useful step towards understanding the potential applications of functionalised PNFs, and other protein nanostructures with similar surface chemistries, in the biosensor field. Future work is needed for improving sensitivity and selectivity of dual-functionalised PNFs based electrode, and to use dual-functionalised PNFs for simultaneous detection of both the analytes (glucose and lactose).

5.7. References

[1] C. Ha, C.B. Park, Template-directed self-assembly and growth of insulin amyloid fibrils, *Biotechnology and Bioengineering*, 90 (2005) 848-855.

[2] S. Scanlon, A. Aggeli, Self-assembling peptide nanotubes, *Nano Today*, 3 (2008) 22-30.

[3] R.J. Williams, R.J. Mart, R.V. Ulijn, Exploiting biocatalysis in peptide self-assembly, *Peptide Science*, 94 (2010) 107-117.

[4] J.K. Raynes, *Immobilising biomolecules on amyloid fibrils for biotechnology applications*, PhD Thesis, University of Canterbury (2012).

[5] A.A. Homaei, R. Sariri, F. Vianello, R. Stevanato, Enzyme immobilisation: An update, *Journal of Chemical Biology*, 6 (2013) 185-205.

[6] M.A. Arnold, M.E. Meyerhoff, Recent advances in the development and analytical applications of biosensing probes, *Critical Reviews in Analytical Chemistry*, 20 (1988) 149-196.

[7] E.B. Bahadır, M.K. Sezgintürk, Applications of commercial biosensors in clinical, food, environmental, and biothreat/biowarfare analyses, *Analytical Biochemistry*, 478 (2015) 107-120.

[8] C. Jianrong, M. Yuqing, H. Nongyue, W. Xiaohua, L. Sijiao, Nanotechnology and Biosensors, *Biotechnology Advances*, 22 (2004) 505-518.

[9] S.K. Vashist, A. Venkatesh, K. Mitsakakis, G. Czilwik, G. Roth, F. von Stetten, R. Zengerle, Nanotechnology-based biosensors and diagnostics: Technology push versus industrial/healthcare requirements, *Bionanoscience*, 2 (2012) 115-126.

[10] A. Tiwari, A.P. Turner, *Biosensors nanotechnology*, John Wiley & Sons, (2014).

[11] M. Yemini, M. Reches, E. Gazit, J. Rishpon, Peptide nanotube-modified electrodes for enzyme-biosensor applications, *Analytical Chemistry*, 77 (2005) 5155-5159.

[12] M. Yemini, M. Reches, J. Rishpon, E. Gazit, Novel electrochemical biosensing platform using self-assembled peptide nanotubes, *Nano Letters*, 5 (2005) 183-186.

[13] H. Yang, S.Y. Fung, W. Sun, S. Mikkelsen, M. Pritzker, P. Chen, Ionic-complementary peptide-modified highly ordered pyrolytic graphite electrode for biosensor application, *Biotechnology Progress*, 24 (2008) 964-971.

[14] R.I. MacCuspie, I.A. Banerjee, C. Pejoux, S. Gummalla, H.S. Mostowski, P.R. Krause, H. Matsui, Virus assay using antibody-functionalised peptide nanotubes, *Soft Matter*, 4 (2008) 833-839.

[15] B. Viguier, K. Zór, E. Kasotakis, A. Mitraki, C.H. Clausen, W.E. Svendsen, J. Castillo-León, Development of an electrochemical metal-ion biosensor using self-assembled peptide nanofibrils, *ACS Applied Materials & Interfaces*, 3 (2011) 1594-1600.

[16] L. Sasso, S. Suei, L. Domigan, J. Healy, V. Nock, M. Williams, J. Gerrard, Versatile multi-functionalisation of protein nanofibrils for biosensor applications, *Nanoscale*, 6 (2014) 1629-1634.

[17] V. Leskovac, S. Trivić, G. Wohlfahrt, J. Kandrač, D. Peričin, Glucose oxidase from *Aspergillus niger*: The mechanism of action with molecular oxygen, quinones, and one-electron acceptors, *The International Journal of Biochemistry & Cell Biology*, 37 (2005) 731-750.

[18] M. Alvarez-Icaza, H. Kalisz, H. Hecht, K.-D. Aumann, D. Schomburg, R. Schmid, The design of enzyme sensors based on the enzyme structure, *Biosensors and Bioelectronics*, 10 (1995) 735-742.

[19] J. Lehr, B.E. Williamson, F. Barrière, A.J. Downard, Dependence of catalytic activity and long-term stability of enzyme hydrogel films on curing time, *Bioelectrochemistry*, 79 (2010) 142-146.

[20] A. Merkoçi, *Biosensing using nanomaterials*, John Wiley & Sons, Mew York (2009).

[21] R.S. Dey, R.K. Bera, C. Raj, Nanomaterial-based functional scaffolds for amperometric sensing of bioanalytes, *Analytical and Bioanalytical Chemistry*, 405 (2013) 3431-3448.

[22] J. Lei, H. Ju, Signal amplification using functional nanomaterials for biosensing, *Chemical Society Reviews*, 41 (2012) 2122-2134.

[23] S. D'souza, Immobilised enzymes in bioprocess, *Current Science*, 77 (1999) 69-79.

[24] W. Henao-Escobar, L. Del Torno-de Román, O. Domínguez-Renedo, M. Alonso-Lomillo, M. Arcos-Martínez, Dual enzymatic biosensor for simultaneous amperometric determination of histamine and putrescine, *Food Chemistry*, 190 (2016) 818-823.

[25] M. Ammam, J. Fransaer, Two-enzyme lactose biosensor based on β-galactosidase and glucose oxidase deposited by AC-electrophoresis: Characteristics and performance for lactose determination in milk, *Sensors and Actuators B: Chemical*, 148 (2010) 583-589.

[26] D.L. Swagerty Jr, A.D. Walling, R.M. Klein, Lactose intolerance, *American Family Physician*, 65 (2002) 1845-1850.

Chapter Five

Part B- Surface-assembled PNFs and industrial applications

5.8. Surface-assembly of PNFs

Two methods by which immobilisation of amyloid PNFs to different surfaces can be achieved are – adsorption (as demonstrated in Part A) and covalent bonding. The fibrils self-assembly process relies on a nucleated growth mechanism (section 1.6.2) [1]. Considering that, the surface-assembly process developed in this project was based around covalent immobilisation of amyloid seeds to the surface, from which mature amyloid PNFs can then assemble. An overview of the template-directed protein nanofibril surface-assembly process is shown in **Figure 5.11**. First, the material surface (glass beads) is derivatised to allow binding of the amyloid template, followed by self-assembly of the PNFs, which can leads to formation of the mature amyloid PNFs from the bound seeds. The surface assembled PNFs can then be functionalised with biomolecules to create novel nanomaterials.

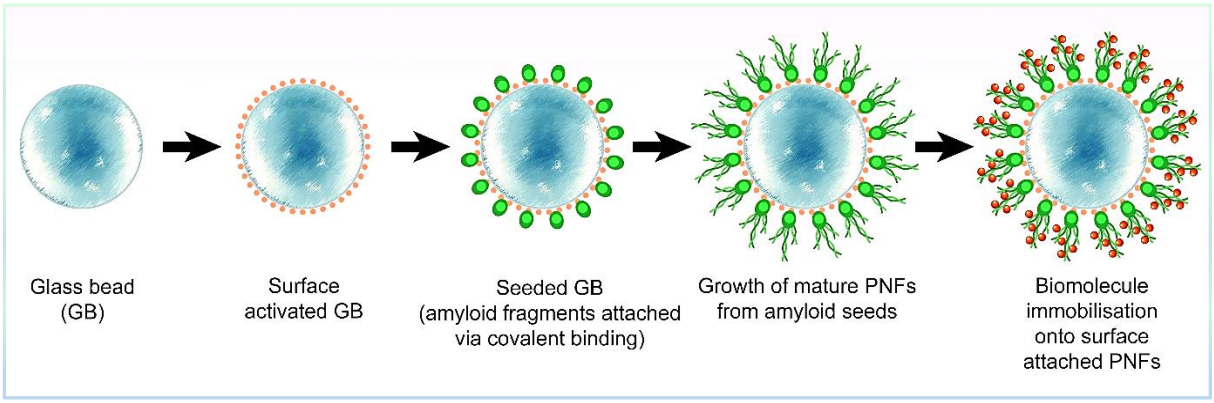

Figure 5.11. *Overview of template-directed amyloid fibril surface-assembly process. First the surface (glass beads) is chemically derivatised, followed by covalent binding of the seeds, which can leads to assembly of the mature PNFs from the bound seeds. The surface assembled amyloid fibrils can then be decorated with biomolecules (enzymes in this case) by either physical adsorption or covalent coupling.*

5.8.1. Derivatisation of glass surface

Glass (SiO_2) was chosen as a model surface as glass chemistry is well understood [2], and derivatisation methods can be directly applied to other organic materials used as a support for covalent enzyme immobilisation, including cellulose because of the similar surface chemistry in the form of the hydroxyl groups [3]. Additionally, bovine insulin PNFs have previously been self-assembled on a glass surface [4], and the transparency of glass allows for spectrophotometric assays to be used.

Most of the surfaces used need to be chemically modified to create active surfaces which can be then readily functionalised. Surface activation or modification depends upon the immobilisation/functionalisation method to be employed. For example, the surface of gold is activated with aminoethanethiol for the covalent immobilisation of the enzymes [5] or alternatively can be modified by alkanethiols for facilitating enzyme adsorption [6]. In this work, to chemically activate glass surface before assembling PNFs, amine functionalisation of the glass surface was achieved by a chemical treatment with 3-aminopropyl triethoxysilane (APTS). APTS is an organo-functional silane that has a non-hydrolysable amino group, and three ethoxy groups which can react with the surfaces containing hydroxyl groups, followed by a condensation reaction to create an aminated surface coating **(Figure 5.12)** [7]. In the case of APTS modified glass, the reaction is self-catalysed by the amine groups of APTS. The APTS reaction is often a preferred choice for modifying glass surfaces as it offers a chemical link between the silane and the glass surface, and not a physical coating of molecules on the surfaces as in other surface immobilisation approaches [8].

Firstly, to remove all contaminants and to generate surface hydroxyl groups, glass beads were treated with freshly prepared Piranha solution (70% H_2SO_4, 30% H_2O_2) overnight at room temperature. The glass beads were then cleaned with copious amounts of distilled water and dried (section 7.15.1). Glass beads treated in this way were enriched with surface hydroxyl groups and were therefore suitable for functional silanisation [9]. Glass beads with the OH-enriched surface were then immersed in APTS solution and incubated at room temperature for silanisation (section 17.5.2). The procedure is illustrated schematically in **Figure 5.12**.

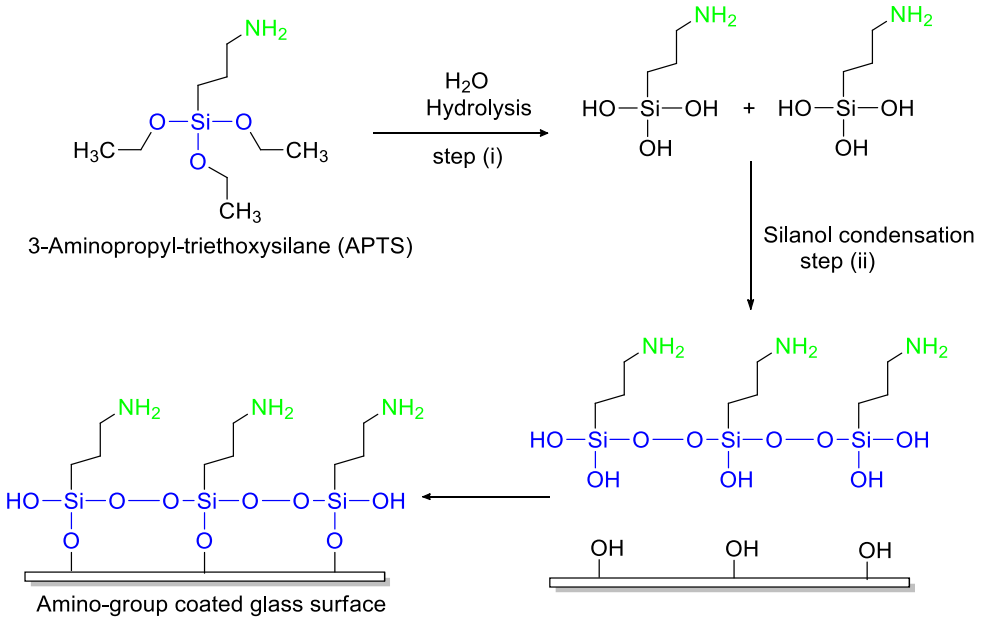

Figure 5.12. *Reaction scheme of APTS hydrolysis (step i), followed by condensation to a surface containing hydroxyl groups such as glass or cellulose (step ii) [10].*

The reaction between APTS and a glass surface firstly involves a hydrolysis step of the APTS **(step (i) Figure 5.12)**, followed by condensation reaction **(step (ii), Figure 5.12)**.

In this process, the silanol groups of the hydrolysis product interact with the exposed hydroxyl groups of the silicon substrate on the silica surface/glass beads through a covalent interaction to form the –Si–O–Si–R–NH_2 structure, leaving the amine functionality on the surface. These reactive primary amines on the surface then serve as a functional platform for derivatisation chemistry to serve a variety of technological applications [10].

5.8.2. Characterisation of the chemically derivatised surfaces

The amino group activation of the glass surface was investigated using a qualitative ninhydrin assay for the presence or absence of free amino groups, using the methods adapted from Sarin and Kent (1981) [11]. The underlying principle is the reaction of ninhydrin with a primary amine to form Ruheman's purple, which is highly conjugated with a strong absorption around 570 nm (section 7.6.2). The measurements were done by measuring the absorbance of Ruheman's purple complex at the wavelength of 570 nm (as explained earlier in section 3.3.1.2).

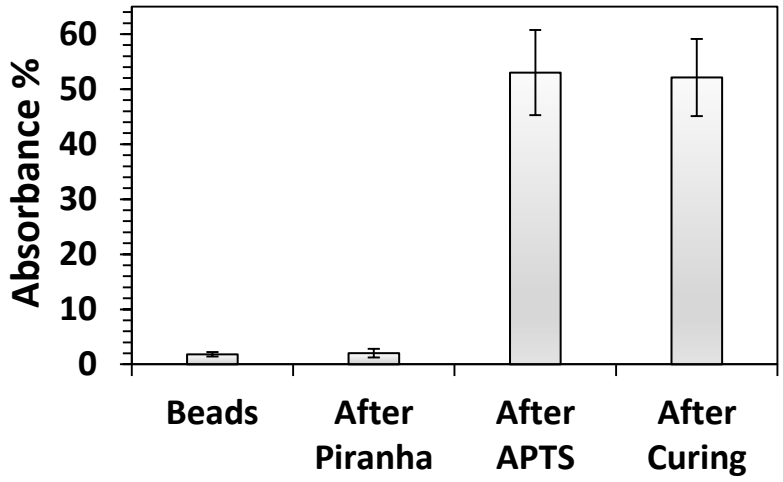

Figure 5.13. *Amino group availability of APTS treated bead samples as detected by the ninhydrin assay. The obtained readings are represented as relative absorbance to the 3 % APTS solution, taken as the 100 % value, corresponding to the amount of NH_3 groups initially present in the solution. Error bars represent the standard deviation of the mean of three replicates.*

The results of ninhydrin assay for beads with and without APTS treatment, and also post-heating (after curing) APTS treated beads at 110 °C are shown in **Figure 5.13**. The high readings obtained for APTS treated and cured samples are indicative of successful reactions of ninhydrin with primary amines present on the surface, due to the surface bound APTS on the glass surface. These primary amine groups sticking off the surface are readily available for conjugation and can then be directly coupled with biomolecules containing carboxyl or aldehyde groups. Alternatively, the APTS derivatised surface can be modified further with crosslinkers or spacer arms to create required functional groups for coupling biomolecules [10].

In this work, the APTS activated surface was then further activated with N, N' – disuccinimidyl carbonate (DSC) (section 7.15.4) to yield a N-hydroxysuccinimide ester (NHS) reactive surface **(Figure 5.14)**, that is able to spontaneously react with proteins or PNFs through their ε-amino group of lysine residues and the N-terminal α-amino group [10, 12, 13]. This surface chemistry is a straight forward procedure allowing the covalent immobilisation of proteins through amide coupling chemistry [14] and is readily applicable to other types of materials such as polyesters, polyamides and polycarbonates, where silanes have been used as coatings for many different applications [7, 13].

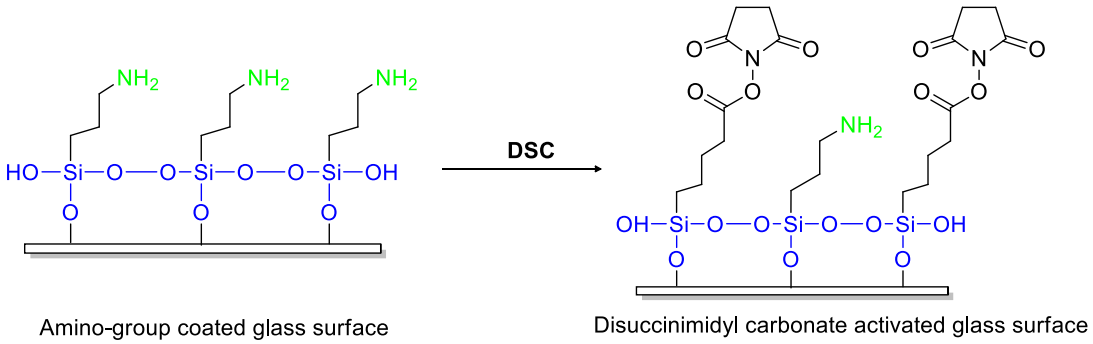

Figure 5.14. . *Reaction scheme of DSC activation of APTS treated glass surface to form terminal NHS-carbonate groups, which then could be coupled to amine groups [10].*

5.9. Template-directed growth of PNFs

Amyloid fibril formation proceeds *via* a nucleated growth mechanism which allows the assembly of mature amyloid fibrils from the covalently bound amyloid oligomeric species (seeds or fragments), when the seeded surface is placed in a solution of native protein, and heated at low pH. Therefore, the first step in template-directed growth is the covalent immobilisation of the amyloid template (seeds or fragments) to the glass bead surface.

Previous work by Ha and Park (2005) [15] used insulin seeds as their template for the surface-assembly of insulin PNFs. The protein seeds were created by incubating a fresh solution of insulin and heating it until the end of the lag phase or just before the exponential growth phase (see section 1.6.2). The protein species formed just before the exponential growth phase are classified as seeds if they are able to eliminate the lag phase in a fresh solution of the same amyloid forming protein [16]. Alternatively, fragmented fibrils obtained by mechanical means or by overnight freezing [17] can also be used for template-directed growth of mature PNFs, as demonstrated by Raynes (2012), where insulin amyloid fibril fragments were produced by exposing mature insulin PNFs to -20 °C overnight freezing, followed by thawing [4].

In this work, both seeds (obtained by heating the protein solution (10 mg/mL) for 5 h at the conditions used for making PNFs, section 7.2), and fragmented amyloid fibrils (obtained by sonicated mature amyloid fibrils, section 7.16) were initially studied for template-directed growth of crystallin, and whey PNFs onto the surface of glass-beads.

However, the incubation time required for producing seeds varied between repetitions thus, amyloid fragments were chosen over amyloid seeds for reproducible template-directed amyloid fibril formation.

5.9.1. Method development for template-directed assembly of whey PNFs

A sonication method similar to the one used for fragmenting crystallin PNFs (as explained earlier in Chapter Two, section 2.5) was used for the fragmentation of whey PNFs (section 7.16). Mature whey PNFs were subjected to a range of sonication times (0-40 sec). The resulting solutions were assessed for fragmentation by TEM, and it was found that a sonication time of 15 sec was needed to fragment the whey PNFs. TEM images for whey PNFs, before and after sonication are shown in **Figure 5.15.**

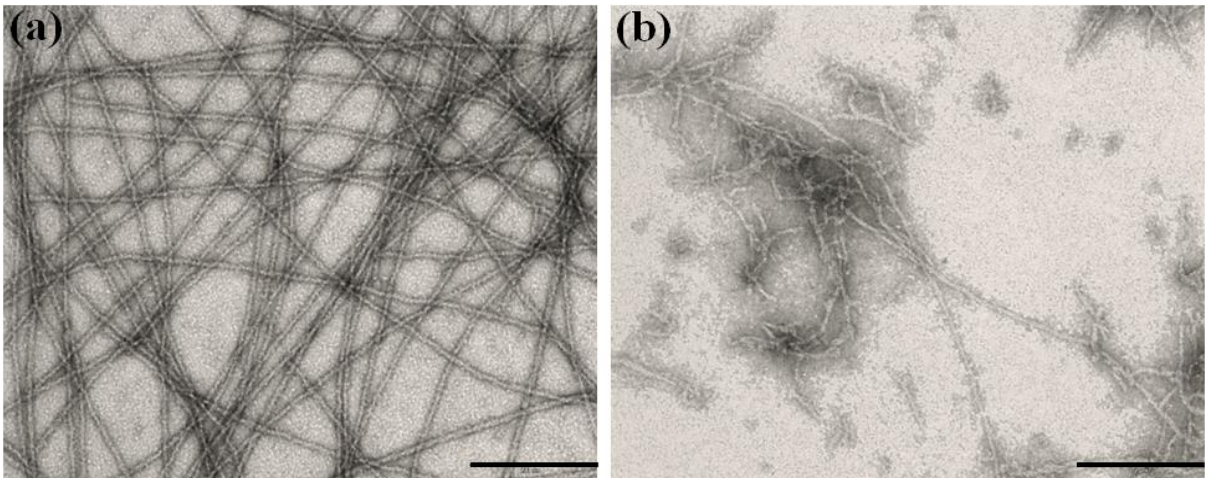

Figure 5.15. *Representative TEM images of whey PNFs, where (a) - mature fibrils and (b) - fragmented PNFs obtained after sonication (15 sec). Scale bar is 200 nm.*

To study the impact of the addition of fragments onto the amyloid fibril growth (in solution) for both crystallin and whey PNFs, fragmented amyloid fibrils (section 7.16) were added at 20% v/v concentration of the crystallin, and whey protein solution kept at 80 °C for fibrillation, respectively (section 7.2). As shown in **Figure 5.16**, the addition of fragments induced amyloid fibril formation faster, with a reduced lag phase of 30 min, compared to 2-3 h in the absence of fragments, starting from 2-3 h. The results are in agreement with literature suggesting that the addition of a preformed nucleus (or 'seed') to a supersaturated protein solution accelerates fibrillation relative to the spontaneous self-assembly of fibrils [18].

The optimum pH required for effective amide coupling between the fragmented PNFs and activated glass surface reaction is pH 9.0, thereby, the fragments were buffer exchanged into 50 mM HEPES (pH 9.0), and then added to the whey protein solution kept at 80 °C, at pH 2.0, and at pH 3.7 for crystallin PNFs. The exchanging of buffer does not have any negative impact on the ability of fragments to seed the formation of PNFs, as demonstrated in **Figure 5.16** – both pH 2.0 or pH 3.7 (dotted lines) for whey and crystallin PNFs respectively, and pH 9.0 (dashed lines) show a similar trend, suggesting accelerated amyloid fibril growth in the presence of fragmented PNFs.

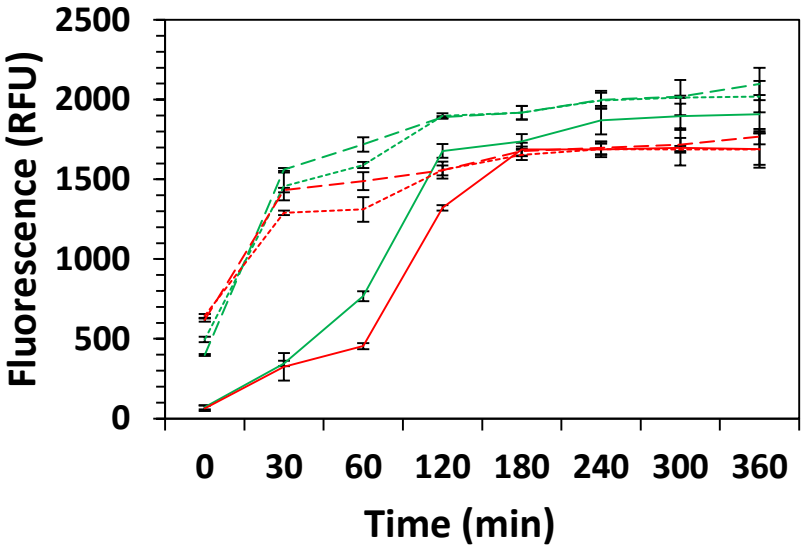

Figure 5.16. *Time course profile of (a) crystallin (green), and (b) whey amyloid PNFs (red) formation at 80 °C, where solid line - in the absence of fragmented PNFs, dotted line - in the presence of 20% (v/v) fragments at pH 2.0 for whey (red), and pH 3.7 for crystallin (green), and dashed line - in the presence of 20% (v/v) fragments at pH 9.0, as monitored by ThT fluorescence. For seeded and fragmented measurements, readings were normalised to the initial ThT reading of the seeded or fragmented solution. Measurements are the average of 3 replicates of each sample and the error is the standard deviation of the mean of three replicates.*

5.9.2. ThT assay for glass beads

The self-assembly process of PNFs from the surface bound fragments was studied using the ThT fluorescence assay, in a 96 well plate reader (section 7.15.5). To eliminate the auto-fluorescent effect of the glass beads from the study, a solution of mature PNFs was prepared, and the fluorescence was measured with and without a glass bead in the wells of the 96 well plate. ThT fluorescence for mature PNF samples in the presence and absence of glass beads is shown in **Table 5.2**. Glass beads placed in amyloid fibril/ThT solution decreases the ThT fluorescence by ~10% **(Table 5.2)**. This confirmed that the glass beads only hinder ThT fluorescence slightly, and thus ThT fluorescence measurements in the 96 well plates was used further for the verification of surface-assembled PNFs.

Table 5.2. *ThT fluorescence of samples with and without glass beads. Measurements are the average of three replicates of each sample and the error is the standard deviation of the mean.*

Sample	ThT fluorescence (RFU)	Error
Bead	198	± 3
No bead	189	± 2
Bead + whey PNFs	818	± 53
Whey PNFs	898	± 72
Bead + crystallin PNFs	698	± 58
Crystallin PNFs	718	± 87

5.9.3. Template-directed self-assembly of whey PNFs

The glass beads were placed in a solution of fragmented whey amyloid solution (pH 9.0) to covalently bind them to the glass surface *via* amide coupling chemistry for 2 h. The beads with the covalently bound whey amyloid fragments were then rinsed with water to remove any unbound amyloid fragment from the bead surface. After washing, the beads with surface attached fragmented whey PNFs only were placed into a solution containing dissolved whey protein (10 mg/mL) at pH 2.0, and incubated for 22 h (section 7.15.6). The self-assembly of whey PNFs from the surface bound fragments was studied using ThT fluorescence assay, in the 96 well plate reader (section 7.15.5). Glass beads were taken from the protein solution at a given time intervals and washed thoroughly in water to remove any unbound PNF, followed by the ThT assay.

As can be seen in **Fig 5.17**, the glass beads which had been seeded with the fragments (red bars), followed by amyloid fibril assembly, exhibited a significant increase in ThT fluorescence indicating the presence of mature whey amyloid fibrils. This implies that by seeding the surface of the glass beads with the fragments, template-directed amyloid fibril assembly can occur. The high ThT readings obtained for the beads which were not immersed in the fragmented solution (non-seeded), but directly placed into the whey protein solution suggests that amyloid fibrils can also be directly-assembled onto the surfaces and seeding is not essentially required for the amyloid fibril assembly process **(Fig. 5.17, green bars)**. However, the glass beads which had been seeded with the fragments, then amyloid fibrils assembled, had the shortest lag phase for amyloid fibril formation.

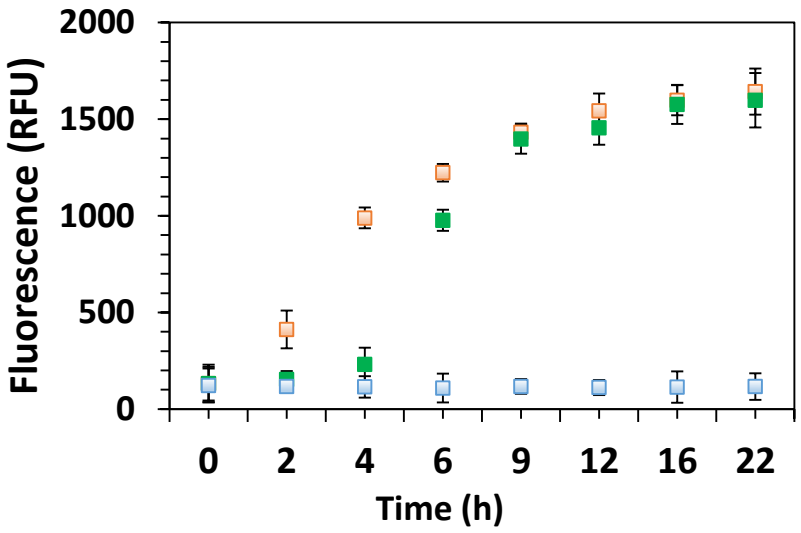

Figure 5.17. *Time course profile of template-directed assembly of whey amyloid fibrils at 80 °C, as monitored by ThT fluorescence, where blue bars- seeded, not immersed in solution, green bars - not seeded, immersed in solution, and red bars - seeded, immersed in solution. Measurements are the average of 3 replicates of each sample and the error is the standard deviation of the mean.*

To ensure that the obtained ThT readings were for the fibrils assembled on the surface of the beads, ThT assay was done on the (a) *Washed bead samples*: The bead samples were washed thoroughly in water to remove any unbound PNFs, and (b) *Stored and washed bead samples*: The washed bead samples were stored at 4° C for the time period of 7 days, followed by the ThT assay. The obtained ThT readings are shown in **Table 5.3**. Both seeded (beads seeded with fragments) and non-seeded bead samples with mature amyloid fibrils assembled retain significant fluorescence compared to the control bead samples, even after storage and subsequent washing step. This implies that the obtained ThT readings were for the fibrils covalently attached onto the surface and not because of the fibrils present free in solution.

Table 5.3. *ThT fluorescence of whey PNF samples assembled on glass beads after* ***(a)*** *washing to remove amyloid fibrils from the solution phase, and* ***(b)*** *after storage at 4° C and subsequent washing after 7 days. Measurements are the average of 3 replicates of each sample and the error is the standard deviation of the mean.*

Sample	ThT Fluorescence (RFU)		Error	
	(a)	(b)	(a)	(b)
Bead (control)	208	205	±8	±4
Bead + fragmented WPNFs	229	214	±15	±14
Seeded, immersed in solution	934	901	±121	±98
Non-seeded, immersed in solution	844	867	±119	±143

5.9.4. Template-directed self-assembly of crystallin PNFs

The same protocol used for the derivatisation of the glass beads with the whey template-directed amyloid self-assembly was used for the crystallin template-directed PNFs self-assembly (section 7.15.7). To study the crystallin protein self-assembly process, three different approaches were used:

i. ***Seeded beads:*** Similar to the whey PNFs assembly, glass beads were placed into the fragmented crystallin PNFs solution and incubated for 2 h. The beads were then washed with dH_2O, and left to dry, followed by ThT assay to ensure the attachment of the fragments onto the glass beads (shown in **Table 5.4**). Glass beads with covalently bound crystallin were placed in a solution of crystallin protein extracted from fish eye lenses and heated for 24 h at 80 °C. The beads were then left in the crystallin solution at room temperature for at least 3 days.

ii. ***While heating:*** Surface activated non-seeded glass beads were placed into crystallin protein solution, and heated for 24 h at 80 °C. The beads were then left in the crystallin solution at room temperature for at least 3 days.

iii. ***After heating:*** Crystallin protein solution was heated for 24 h at 80 °C, and surface activated non-seeded glass beads were added to the heated crystallin protein solution before leaving the crystallin protein solution at room temperature for 3 days.

Glass beads were taken from the protein solution after 3 days of incubation at room temperature and washed thoroughly in water to remove any unbound PNFs, followed by ThT assay.

To ensure that the obtained ThT reading was due to the mature amyloid PNFs assembled onto the glass beads, bead samples after initial washing step were further placed into dH_2O (200 µL), and incubated for 10 min at room temperature (3X) and left to dry, followed by ThT assay.

Table 5.4. *ThT fluorescence of bead samples before and after glass beads were placed into the fragmented crystallin PNFs solution. Measurements are the average of three replicates of each sample and the error is the standard deviation of the mean.*

Sample	ThT Fluorescence (RFU)	Error
Bead	199	±4
Bead + fragmented CPNFs	398	±16

As shown in **Figure 5.18**, there is negligible difference in the ThT readings obtained for each of the samples before and after washing step and samples retain fluorescence. High ThT reading was obtained for not only the seeded beads but for all the methods studied suggesting the presence of mature crystallin PNFs. This implies that crystallin PNFs can be self-assembled onto the surfaces *via* both template-directed and direct-assembly process.

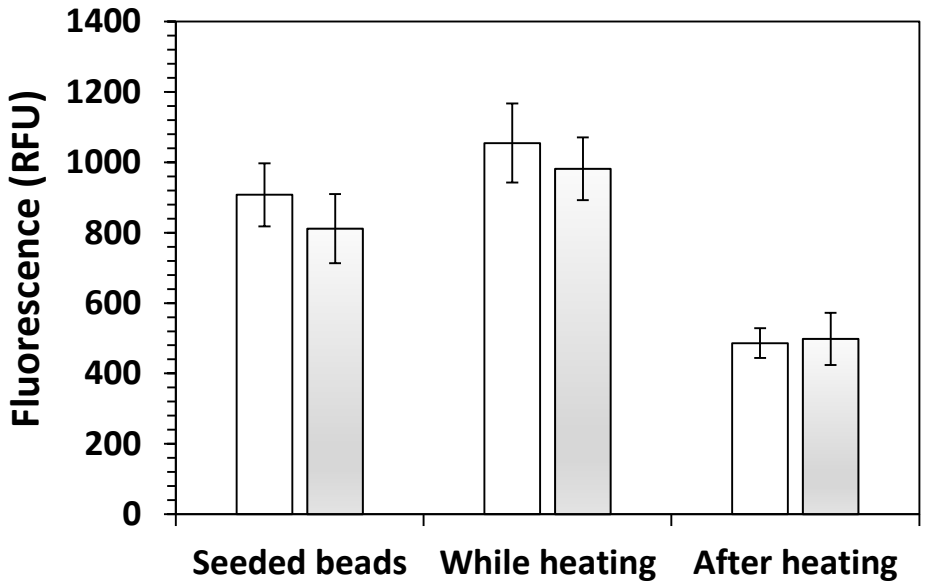

Figure 5.18. *ThT fluorescence of glass bead samples with surface assembled crystallin PNFs, where blank - initial, and filled bar - after washing. Measurements are the average of 3 replicates of each sample and the error is the standard deviation of the mean.*

5.10. Impact of chemical derivatisation

Experimentation was carried out to ensure full surface derivatisation was necessary for maximum surface-assembly of the PNFs. This was achieved by performing ThT assay on a variety of control bead samples. All three conditions as discussed earlier in section 5.9.4, such as seeded beads, while heating, and after heating were studied for the glass beads obtained after each step of the surface derivatisation process.

As shown in **Figure 5.19**, for both whey and crystallin PNFs, the non-seeded bead samples, which had the full surface derivatisation (sample e, red bars), placed into the protein solution while heating have the highest ThT fluorescence indicating presence of surface-assembled PNFs.

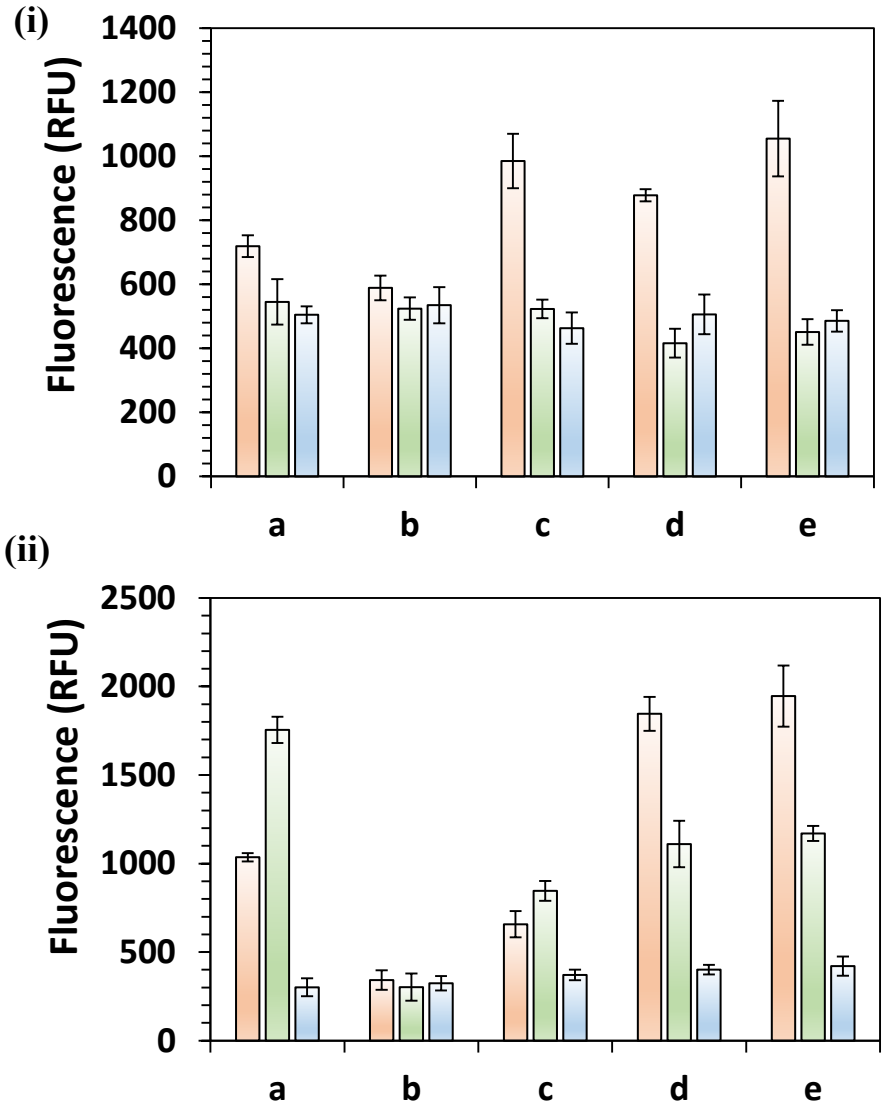

Figure 5.19. *ThT fluorescence of glass bead controls,* ***(i)*** *crystallin bead samples, and* ***(ii)*** *whey bead samples. Measurements are the average of 3 replicates of each sample and the error is the standard deviation of the mean, where a - no treatment, b - Piranha treated, c - APTS treated, d - after curing, and e - DSC treatment. Red bars - while heating (non-seeded beads were added to the protein solution kept at 80 °C), green bars - seeded beads (seeded beads were added to the protein solution kept at 80 °C, and blue bars - after heating (non-seeded beads were added to the heated protein solution before leaving the protein solution at room temperature for 3 days*

High ThT readings were also obtained for the seeded beads, followed by the beads added to the protein solution kept at room temperature after heating (blue bars).

Interestingly, bead samples without any surface derivatisation (sample a) also show a relatively high ThT fluorescence implying that there is a relatively strong intrinsic association between the glass beads, the amyloid fragments and PNFs. The obtained result show that PNFs can also be surface-assembled onto the glass beads without any surface activation. This is understandable, as crystallin PNFs do not have sufficient lysine groups available for crosslinking (discussed in Chapter Three, section 3.4.2), and template-directed assembly relies on the availability of lysine groups to react with the DSC surface activated surface, and is likely possible that mature amyloid PNFs are assembling *via* both adsorption (direct-surface assembly), and crosslinking (through APTS, or DSC activated functional groups). However, the glass beads which had been activated and then amyloid PNFs assembled, had the highest ThT fluorescence confirming that full surface derivatisation is required for maximum surface-assembly of the PNFs.

5.11. Confocal microscopy

Confocal microscopy has been used previously by Kerb *et al.* (2005) to study the binding of ThT to amyloid fibrils, and thus in addition to the ThT assay, confocal microscopy was also used as an alternative method to investigate the presence of PNFs on the surface of the glass beads. For the confocal microscopy study, in addition to 5 mm beads, 425-600 μm glass beads were also used. The use of small beads for attaching PNFs was considered to aid with confocal imaging. The use of microbeads will also provide the large surface area for enzyme immobilisation, leading to better packaging efficiency for industrial applications.

The PNF assembled bead samples and associated controls were kept in clear wall glass bottom dishes, followed by the addition of ThT stain and incubation in dark for 6 min, and viewed using confocal microscopy as described in section 7.17. Unbound ThT gives a fluorescence spectrum with an excitation/emission maximum of 385/435 nm, whereas bound ThT undergoes a spectral shift with an excitation/emission maxima at 450/482 nm.[19] Therefore, to avoid background fluorescence from the unbound ThT, excitation of 425 nm and an emission detection of 485-495 nm was used.

The micrographs of the surface of the template-directed amyloid fibril glass bead samples is shown in **Figure 5.20**. As can be seen, the blank glass bead (sample a and b) surface does not have any fluorescence whereas the bead sample with PNFs assembled *via* template-directed growth showed significant fluorescence on the surface (sample c-f), confirming the presence of PNFs onto the glass bead surface. The coverage of the amyloid fibrils on the glass surface is regular, and the micrograph results provide evidence that both whey and crystallin PNFs can be surface-assembled on glass beads *via* template-directed growth.

5.12. Surface assembled PNFs for biomolecule immobilisation

β-Gal immobilisation was investigated on glass surface assembled whey PNFs as a potential manufacturing route to create enzymatically functional PNF-based nanomaterials.

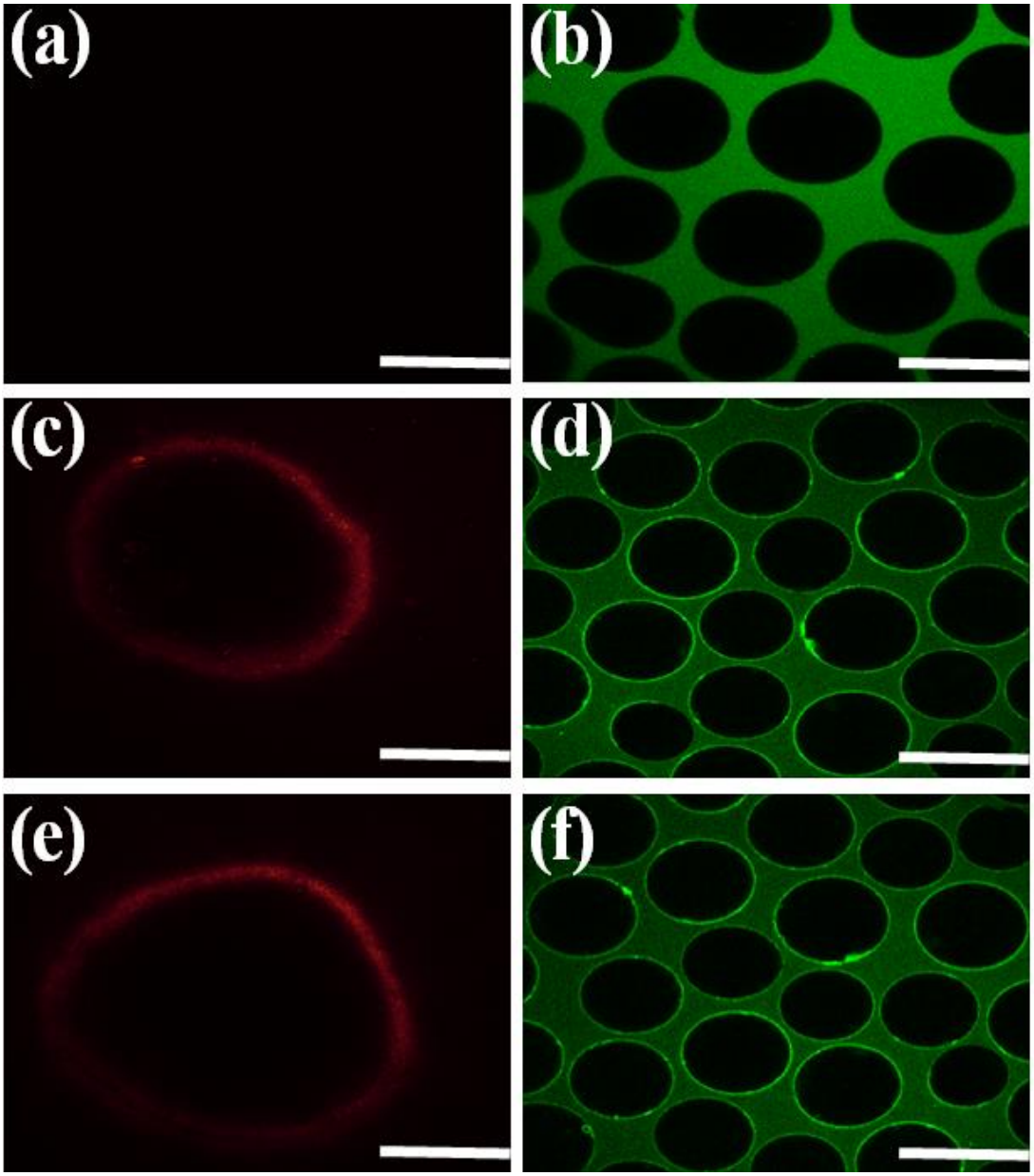

Figure 5.20. *Representative confocal micrographs of the surface of 5 mm (scale bar – 2 mm), and 425-600 µm glass beads (scale bar – 1mm), where left side - 5 mm bead samples, and right side- micro bead samples.* ***Row 1*** *- control bead samples,* ***Row 2*** *- seeded, plus whey PNFs, and* ***Row 3*** *- seeded, plus crystallin PNFs. The beads were stained with ThT dye, an excitation of 425 nm and an emission detection of 485-595 nm were used.*

5.12.1 β-Gal functionalisation and characterisation of surface-assembled whey amyloid fibrils

β-Gal surface immobilisation was based on the method developed for dual-immobilisation of GOX, and β-gal onto the whey amyloid PNFs using GA (Chapter Five, Part A, section 5.4). Briefly, all of the bead samples were first immersed in a solution containing 5 mM GA for 1 h, then washed thoroughly and placed in a 2.9 mg/mL solution of β-gal for 2 h at 37 °C, before being thoroughly washed again (section 7.18.1).

The resulting immobilised β-gal samples were investigated for activity in a plate reader using the ONPG assay (section 7.18.2), and the presence of amyloid fibrils determined using ThT assay (section 7.15.5). The results as obtained from both assays are summarised in **Table 5.5.** The sample that showed the most β-gal activity and highest ThT fluorescence is sample 8, where β-gal was immobilised onto GA-treated surface-activated beads, with PNFs assembled *via* template-directed growth. Both ThT readings and β-gal activity of sample 5 was also relatively high, implying that there were mature whey amyloid fibrils attached to the surface of the glass beads, even without seeds present. The relative higher activity readings for sample 6, again suggests that seeding is not essential for the growth of mature PNFs onto the surfaces. On comparing bead samples with PNFs in the presence (sample 5 and 8) and absence (sample 4 and 7) of GA, sample 5 and 8 showed higher activity, reflecting on the importance of the use of GA for immobilising β-gal onto the amyloid fibril functionalised beads.

The samples 2, 3, and 6 also exhibited β-gal activity indicating a strong interaction between β-gal and the activated glass surface, because the ThT fluorescence of these samples is low, implying the lack of PNFs present on the surface that are aiding in immobilisation. However, the beads which were seeded, the amyloid fibrils assembled, and β-gal immobilised (sample 8), had the highest β-gal fluorescence detected in the plate reader, proposing that surface-assembly of whey PNFs on glass beads, and subsequent immobilisation with β-gal, enabled more β-gal to be immobilised to the glass surface.

Table.5.5. *ThT fluorescence (ThT) and β-gal activity (ONPG assay) of whey PNF samples immobilised to glass beads. Surface activation - APTS and DSC derivatised beads, Seed - beads seeded with whey PNFs, PNFs - whey amyloid fibrils assembled, GA - GA activation. Each sample had six replicates, three for the ONPG assay (absorbance measured at 420 nm), and three for the ThT assay (RFU). The errors represent the standard deviation of the mean.*

Sample	Surface activation	Seed	PNFs	GA	ONPG	O. Error*	ThT	T. Error**
1.	-	-	-	-	0.1506	±0.012	202	±6
2.	+	-	-	-	0.4356	±0.034	228	±12
3.	+	-	-	+	0.4496	±0.025	221	±19
4.	+	-	+	-	0.5023	±0.056	954	±67
5.	+	-	+	+	0.6986	±0.080	953	±59
6.	+	+	-	-	0.2891	±0.021	283	±16
7.	+	+	+	-	0.4967	±0.007	976	±102
8.	+	+	+	+	**0.8983**	±0.058	995	±95

**O.Error – standard deviation of the mean of three replicates for ONPG assay*
***T.Error – standard deviation of the mean of three replicates for ThT assay*

The high β-gal activity readings obtained for sample 2, 3, and 6 revealing β-gal absorption to the control glass beads was not an unexpected result as the surface chemistry on the glass can react with the amine groups of β-gal, leading to the covalent linking of the enzyme. To get rid of this background reading an extensive washing step was undertaken. The glass bead samples were placed in a small beaker with β-gal buffer (100 mM PBS, pH 7.4), and changed to the fresh buffer every 6 h for ~24 h. Washing the beads for a long period of time will wash the loosely bound β-gal, leaving only the strongly bound β-gal.

The bead samples were then analysed for β-gal activity by the ONPG assay, and the ThT assay to ensure the washing step did not remove any of the surface assembled PNFs, see **Table 5.6**.

Table 5.6. *ThT fluorescence (ThT) and β-gal activity (ONPG assay) of whey PNF samples immobilised to glass beads. Surface activation - APTS and DSC derivatised beads, Seed - beads seeded with whey PNFs, PNFs - whey amyloid fibrils assembled, and GA - GA activation. Each sample had six replicates, three for the ONPG assay (absorbance measured at 420 nm), and three for the ThT assay (RFU). The errors represent the standard deviation of the mean.*

Sample	Surface activation	Seed	PNFs	GA	ONPG	O. Error	ThT	T. Error
1.	+	-	-	-	0.3981	±0.015	219	±8
2.	+	-	-	+	0.3687	±0.011	196	±26
3.	+	+	-	-	0.4393	±0.046	235	±43

As can be seen in **Table 5.6**, the extensive washing step produced very similar results to samples in **Table 5.5**, suggesting that the β-gal in the bead samples without PNFs is covalently crosslinked onto the surface activated beads *via* amine groups. Following the successful immobilisation of β-gal to the surface assembled PNFs, it was decided to try and create a reusable β-gal nanomaterial bead system with potential commercial applications. The β-gal-functionalised surface-assembled PNFs were then tested for their ability to be reused sequentially.

5.12.2. Reusable surface-assembled PNF-based bead system

Studies have shown that glucose and galactose, two monosaccharides obtained by hydrolysis of lactose have several advantages in comparison to lactose, such as they are four times sweeter than lactose, are more soluble and digestible [4], and can be consumed by people with a lactose intolerance [1, 5]. Thus, lactose hydrolysis has significant importance and immobilised β-gal offers the possibility of continuous flow processing, so that easy regeneration of the immobilised enzyme and low cost operation can be achieved in industrial processing. By immobilising β-gal to the surface-assembled whey amyloid PNFs, it was anticipated that the β-gal PNF glass beads would be easily recovered and reused after each reaction. Therefore, a reusable system can be created that saves on production cost, allow a higher enzyme loading and better catalytic efficiency. The hydrolysis reaction was set up for the bead samples listed in **Table 5.7.**

Table 5.7. List of bead samples used for hydrolysis reaction.

Bead samples	Surface activation	Seed	PNFs	GA
1. *Surface activated bead*	+	-	-	-
2. *Surface activated and GA*	+	-	-	+
3. *Surface activated with PNFs*	+	-	+	-
4. *Surface activated, with PNFs and GA*	+	-	+	+
5. *Surface activated, seeded*	+	+	-	-
6. *Surface activated, seeded with PNFs*	+	+	+	-
7. *Surface activated, seeded with PNFs and GA*	+	+	+	+

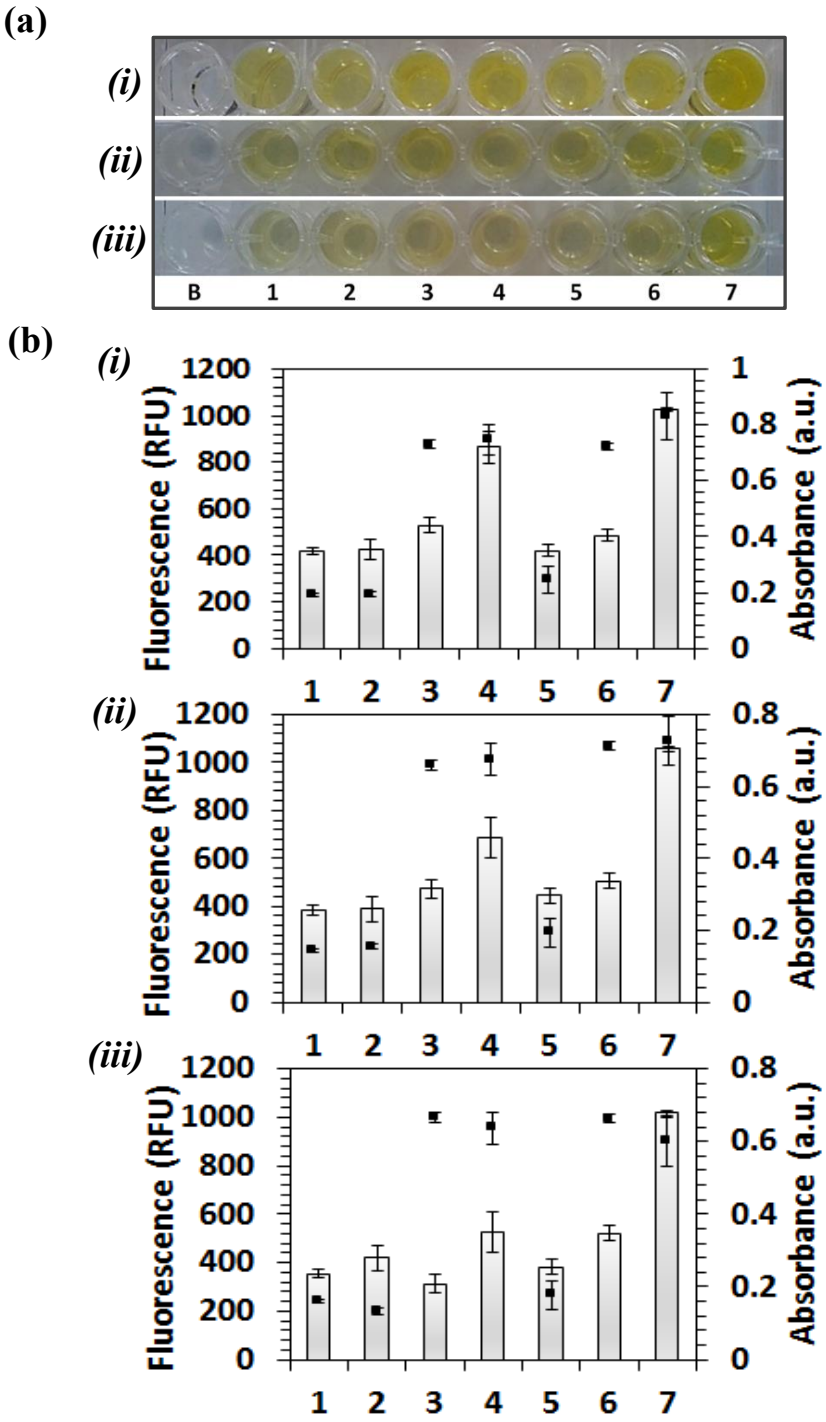

Figure 5.21. (a) *Image of the bead samples used for the hydrolysis reaction, showing the presence of yellow coloured cleaved product - o-nitophenol, after ONPG assay.* ***(b)*** *ThT fluorescence (grey bars) and β-gal activity (black bars) of glass beads with β-gal-functionalised surface-assembled whey PNFs. (i) after first hydrolysis reaction, (ii) after second hydrolysis reaction, and (iii) after third hydrolysis reaction. Bead samples: b - Not treated, 1 - surface activated, 3 – surface activated with GA, 4 -surface activated with PNFs, 5- surface activated seeded, 6 – surface activated, seeded, with PNFs, and 7 – surface activated, seeded, with PNFs, and GA. Each sample had six replicates, three for the ONPG assay (absorbance measured at 420 nm), and three for the ThT assay (RFU). The errors represent the standard deviation of the mean.*

To determine the activity of β-gal immobilised onto the whey PNF glass beads, it was decided to use ONPG (a lactose analog) instead of lactose, as ONPG assay has been used previously in this work for analysing β-gal activity *(Appendix B, section B1.2)*, where β-gal activity is measured directly by the amount of ONPG cleaved, leading to the production of galactose and o-nitrophenol, which can be easily quantified using a spectrophotometer. For hydrolysis reaction, all the bead samples were incubated with ONPG solution, and kept in dark at 37 °C for 30 min (section 7.18.2). The beads were thoroughly washed in dH_2O before being used for the next hydrolysis reaction. This procedure was repeated until immobilised β-gal activity had ceased for controls samples. The hydrolysed solution of each of the samples was carefully removed after 30 min without touching the glass beads, and analysed for β-gal activity. The results as obtained by the ONPG assay, for each of the hydrolysis reaction are shown in **Figure 5.21.** The image of all the bead samples showing the presence of o-nitrophenol (a hydrolysed or cleaved form of ONPG) solution after each of the hydrolysis reaction, for all the bead samples is shown in **Figure 5.21 (a)**.

In first hydrolysis reaction, all of the bead samples showed β-gal activity, with the ONPG assay readings showing very similar results **(Figure 5. 21 (i))**. The second hydrolysis reaction as shown in **Figure 5.21 (ii)**, had a very similar trend, but this time the amount of ONPG hydrolysed by the bead sample which had all the treatments, was much more prominent compared to the other bead samples (sample 7). By the third next reaction **(Figure 5.21 (iii))**, the bead sample that retained maximum β-gal activity was that with amyloid fibrils assembled, sample 4, and 7 (with and without seeding, respectively), and GA used for β-gal immobilisation. The reason that reduced β-gal activity was observed for the other bead samples could be due to leaching of the immobilised enzyme over time, under the studied conditions.

This provides evidence that the presence of the surface-assembled amyloid fibrils provides better stability to the immobilised β-gal. Functionalisation of the surface-assembled whey amyloid PNFs with β-gal showed that the glass beads which were seeded and amyloid PNFs assembled, displayed the maximum activity. The catalytic activity of the immobilised β-gal was preserved over three uses. Considering the immobilised β-gal beads as a proof-of-concept system, the results are promising as the studied hydrolysis reaction was based on single bead sample-only.

5.13. Conclusion

This chapter demonstrated the commercial potential of amyloid PNFs as a nanoscaffold. Novel amyloid fibril based biomaterials can be created by functionalising surface attached PNFs with enzymes or active components. Previous work by Raynes (2012) has shown that bovine insulin amyloid fibrils can be surface-assembled *via* template-directed growth. In this work, both crystallin and whey PNFs were surface-assembled *via* both template- and direct-surface-assembly methods, with and without surface-derivatisation. The results shown in this chapter demonstrates that the presence of PNFs on the surfaces allows for a greater amount of enzyme immobilisation or a better environment leading to the improved stability and activity of the enzyme.

Also, these findings propose that surface-assembly could be applicable to any amyloid forming protein, and any other surface with similar surface chemistry. PNFs were also successfully surface-assembled onto the microbeads, however due to difficulty in handling, and performing enzyme-specific activity assays, functionalisation or enzyme immobilisation studies were conducted using only 5mm glass bead samples. Further optimisation of the enzyme immobilisation conditions could increase the enzymatic activity, reusability and storage life of the immobilised enzyme bead system, and optimisation of this technology towards smaller micro glass beads could also potentially increase the specific-enzyme activity.

5.14. References

[1] J.D. Schmit, K. Ghosh, K. Dill, What drives amyloid molecules to assemble into oligomers and fibrils?, *Biophysical Journal*, 100 (2011) 450-458.

[2] F. Janowski, G. Fischer, W. Urbaniak, Z. Foltynowicz, B. Marciniec, Aminopropylsilane treatment for the surface of porous glasses suitable for enzyme immobilisation, *Journal of Chemical Technology and Biotechnology*, 51 (1991) 263-272.

[3] P. Zucca, E. Sanjust, Inorganic materials as supports for covalent enzyme immobilisation: Methods and mechanisms, *Molecules*, 19 (2014) 14139-14194.

[4] J.K. Raynes, *Immobilising biomolecules on amyloid fibrils for biotechnology applications*, PhD Thesis, University of Canterbury (2012).

[5] K.J. Stine, K. Jefferson, O.V. Shulga, Nanoporous gold for enzyme immobilisation, *Enzyme Stabilisation and Immobilisation: Methods and Protocols*, (2011) 67-83.

[6] F. Arduini, S. Guidone, A. Amine, G. Palleschi, D. Moscone, Acetylcholinesterase biosensor based on self-assembled monolayer-modified gold-screen printed electrodes for organophosphorus insecticide detection, *Sensors and Actuators B: Chemical*, 179 (2013) 201-208.

[7] J.A. Howarter, J.P. Youngblood, Optimisation of silica silanisation by 3-aminopropyltriethoxysilane, *Langmuir*, 22 (2006) 11142-11147.

[8] A. Simon, T. Cohen-Bouhacina, M. Porté, J. Aimé, C. Baquey, Study of two grafting methods for obtaining a 3-aminopropyltriethoxysilane monolayer on silica surface, *Journal of Colloid and Interface Science*, 251 (2002) 278-283.

[9] F. Zhang, M. Srinivasan, Self-assembled molecular films of aminosilanes and their immobilisation capacities, *Langmuir*, 20 (2004) 2309-2314.

[10] G.T. Hermanson, *Bioconjugate techniques*, Academic Press, USA (2013).

[11] V.K. Sarin, S.B.H. Kent, J.P. Tam, R.B. Merrifield, Quantitative monitoring of solid-phase peptide synthesis by the ninhydrin reaction, *Analytical Biochemistry*, 117 (1981) 147-157.

[12] M. Beier, J.D. Hoheisel, Versatile derivatisation of solid support media for covalent bonding on DNA-microchips, *Nucleic Acids Research*, 27 (1999) 1970-1977.

[13] J.V. Edwards, N.T. Prevost, B. Condon, A. French, Covalent attachment of lysozyme to cotton/cellulose materials: Protein verses solid support activation, *Cellulose*, 18 (2011) 1239-1249.

[14] N. Nakajima, Y. Ikada, Mechanism of amide formation by carbodiimide for bioconjugation in aqueous media, *Bioconjugate Chemistry*, 6 (1995) 123-130.

[15] C. Ha, C.B. Park, Template-directed self-assembly and growth of insulin amyloid fibrils, *Biotechnology and Bioengineering*, 90 (2005) 848-855.

[16] J.D. Harper, C.M. Lieber, P.T. Lansbury Jr, Atomic force microscopic imaging of seeded fibril formation and fibril branching by the Alzheimer's disease amyloid-β protein, *Chemistry & Biology*, 4 (1997) 951-959.

[17] W.-F. Xue, A.L. Hellewell, E.W. Hewitt, S.E. Radford, Fibril fragmentation in amyloid assembly and cytotoxicity: When size matters, *Prion*, 4 (2010) 20-25.

[18] J.-C. Rochet, P.T. Lansbury Jr, Amyloid fibrillogenesis: Themes and variations, *Current Opinion in Structural Biology*, 10 (2000) 60-68.

[19] H. Levine, Thioflavine T interaction with synthetic Alzheimer's disease β-amyloid peptides: Detection of amyloid aggregation in solution, *Protein Science*, 2 (1993) 404-410.

Chapter Five

Part C - PNFs in biomedical applications

5.15. Protein and PNF-based scaffolds for tissue regeneration

More recently amyloid fibrils have been investigated for their suitability as self-assembling biomaterials or hybrid materials for biomedical applications [1-4]. A number of amyloid forming proteins and peptides have been shown to form hydrogels with potential applications in tissue engineering or drug delivery [5-7]. For example, Kyle *et al.* (2011), showed that a peptide derived from hen lysozyme forms pH dependent gels, which may be used in scenarios where a responsive material is desirable [8]. Responsive materials such as these have potential biomedical applications, where biocompatibility and/or biodegradability is sought after [9]. A number of published studies have demonstrated that amyloid fibril coated surfaces promote cell growth and adhesion [1, 10]. Recently, Jacob *et al.* (2015), developed amyloid-based nontoxic hydrogels, capable of forming a 3D meshwork, and demonstrated the use of these hydrogels for 2D/3D cell culture and stem cell differentiation [5]. Based on reported literature, in this work, PNFs obtained from crude proteins were studied to create PNF-based biomaterials with potential applications in tissue engineering.

5.16. Tissue engineering and composite materials

Tissue engineering is defined as the application of principles and methods of engineering and life sciences for the development of biological substitutes, to restore, maintain or improve tissue function [11]. The field of tissue engineering is highly multi-disciplinarily and relies extensively on the use of scaffolds/biomaterials to act as a template for tissue formation [12]. These cell scaffolds are typically seeded with cells and/or growth factors, and are either cultured *in vitro* to synthesise tissues, followed by the implantation into an injured site, or are implanted directly into the injured site for *in vivo* regeneration of tissues or organs, using the body's own systems [12].

The state of the art in the biomaterial design has continuously evolved over past few decades. Various biomaterials as broadly categorised into three individual groups: ceramic, natural and synthetic polymers have been studied and used in different manners for tissue engineering applications [12-15]. Each of these individual biomaterial group has their own advantages and disadvantages, and in order to obtain amalgamated properties of the two or more materials, polymer/biomaterial blending is becoming increasingly common. Synthetic materials such as poly-lactic-glycolic acid (PLGA), polylactic acid (PLA), polyglycolic acid (PGA) have reduced bioactivity but high mechanical strength. In contrast to the synthetic polymers, biological/natural materials such as collagen, elastin, chitosan, have high biologically activity and typically promote excellent cell adhesion and growth, but generally have poor mechanical strength [12].

Hence, a composite material obtained by mixing synthetic polymer with a natural material will help in omitting the disadvantage associated with each of the individual group. For example, the (PLGA)-collagen (synthetic-natural blend) composite materials with better biocompatibility and mechanical properties have been used to prefabricate a tissue engineering trachea [16]. Irrespective of the choice of biomaterial from which the scaffold is fabricated, a number of key features that needs to be considered while designing a biomaterial with potential applications in tissue engineering include: biocompatibility, rate of degradation/biodegradability, mechanical strength and stability, scaffold architecture including porosity, microstructure, shape, and size, and cost effective manufacturing technology [12].

5.17. Silk as a biomaterial for tissue engineering

Silk proteins, especially the fibroin produced by *Bombyx mori*, due to their tuneable mechanical properties, biocompatibility, morphological flexibility, controlled proteolytic degradation, ambient processing conditions, and ability to immobilise growth factors *via* amino acid modifications [17], have been extensively investigated as a scaffolding material for tissue engineering applications [18-27]. Silks are unique group of fibrous proteins with remarkable mechanical properties produced in fibre form by silkworms and spiders [17]. The most extensively characterised silks are from the domesticated silkworm, *Bombyx mori*, and from spiders (*Nephila clavipes* and *Araneus diadematus*). The Bombyx mori silkworm cocoon is generally comprised of three main proteins: sericin, a glue like glycoprotein, and light and heavy fibroin chains, 25 and 325kDa, respectively [18]. Silk fibrous proteins, are characterised by a highly repetitive primary sequence (dominance of hydrophobic domains with short side chain amino acids in the primary sequence) that leads to significant homogeneity in secondary structure (β-sheets in the case of many of the silks) [17]. The highly organised β-sheet crystal regions and semi-crystalline regions within the fibroin proteins imparts high mechanical strength to the silk fibres [17], and also contributes to silk's elasticity compared to fibres of similar tensile integrity [18].

Silk fibroin offers a number of advantages to current tissue regeneration materials. Silk processing is a simple, highly-scalable, and robust process unlike other biopolymer materials, such as collagen and fibrin which require more intense purifying and processing steps [28]. In addition, silk has been found to be highly biocompatible upon implantation, and induces lower inflammatory responses than collagen and PLA films [29]. Silk also offers slow biodegradation rates and increased native tissue re-modeling time, and enhanced mechanical stability of the re-modelled native tissue [17]. Other materials such as synthetic PGA or natural collagen degrade much more rapidly and do not offer extended native tissue re-modeling time [30, 31]. Despite the various advantages, due to their brittle nature [32], shortage of cell specific-binding sites, and limited growth factor-adsorbing capacity [33], the blending of silk fibroin materials with other polymers has been investigated to improve the functional shortcomings while taking advantage of the structural benefits from using silk fibroin [34-37].

5.18. Silk-PNF composite materials for tissue engineering

Both amyloids and silk fibroin exhibit remarkable structural and physical properties as discussed in section 1.9, Chapter One and section 5.12 (above), respectively. Although these two classes of β-sheet-rich, natural proteinaceous fibrous materials are among the most intensively investigated types of protein assemblies, however, they have not yet been combined as a biomaterial to support cell growth. To the best of my knowledge there has been only one reported study in which both of these materials have integrated together into artificial materials, and investigated for structural and material properties by controlling the molecular design of each of the component (i.e. amyloid fibrils obtained from lysozyme and silk fibroin [38]. In the present work, the focus was to develop a PNF-based scaffold for tissue engineering, hence silk-PNF composite films were cast and initial characterisation of the resulting composite materials was carried out.

5.18.1. Silk-blend films

Bombyx mori silk fibroin solution was prepared as described in Rockwood *et al.* (2011) [39]. Briefly, degummed fibres (achieved by boiling fibres for 20 min in 0.02 M sodium carbonate (Na_2CO_3) solution) were dissolved in 9.3 M lithium bromide (LiBr) solution in 1:4 (w/v) ratio at room temperature, and kept at 60 °C for 4 h. The extracted solution was then dialysed (MWCO 3500) in water for 48 h. The final concentration of aqueous silk solution was determined by weighing the remaining solid after drying (section 7.19.1). Protein solutions were prepared by dissolving 40 mg/mL of dry whey protein isolate powder and freeze dried crystallin proteins in dH_2O (section 7.19.2). Mature amyloid PNFs prepared as described in section 7.2, were centrifuged and concentrated to 4% solution (section 7.19.3). The concentration of all the constituents i.e. silk protein solution, PNFs (both whey and crystallin), and proteins (WPI and crystallin protein powder) was kept at 40 mg/mL (section 7.19). Silk-blend films were prepared on flat polydimethylsiloxane (PDMS) substrate of 0.5-1.0 mm thickness as detailed in section 7.20, and allowed to dry overnight.

5.18.2. SEM analysis of silk-blend films

Scanning electron microscopy (SEM) was used to observe physical changes in film topography **(Figure 5.22)**. Dried film samples were peeled off from the PDMS substrate and placed on top of conductive tape mounted on a SEM sample stub, followed by platinum coating (section 7.21). Under SEM, silk only sample showed a highly smooth surface **(Figure 5.22 a-b)**, which does not change significantly after the addition of proteins **(Figure 5.22 c-f)**. The SEM images obtained for silk-crystallin and silk-whey protein blends showed that both proteins have similar impact on the surface morphology of the films, as expected due to similar molecular weight range of both protein (16-18.5 kDa). The morphology of blend films was drastically influenced as anticipated by the addition of PNFs. The surface of silk-PNFs blend films showed a high degree of surface roughness relative to the silk-only and silk-protein blend films **(Figure 5.22 g and i)**. The presence of PNFs within the silk films was clearly observed at higher magnification **(Figure 5.22 h and j)**.

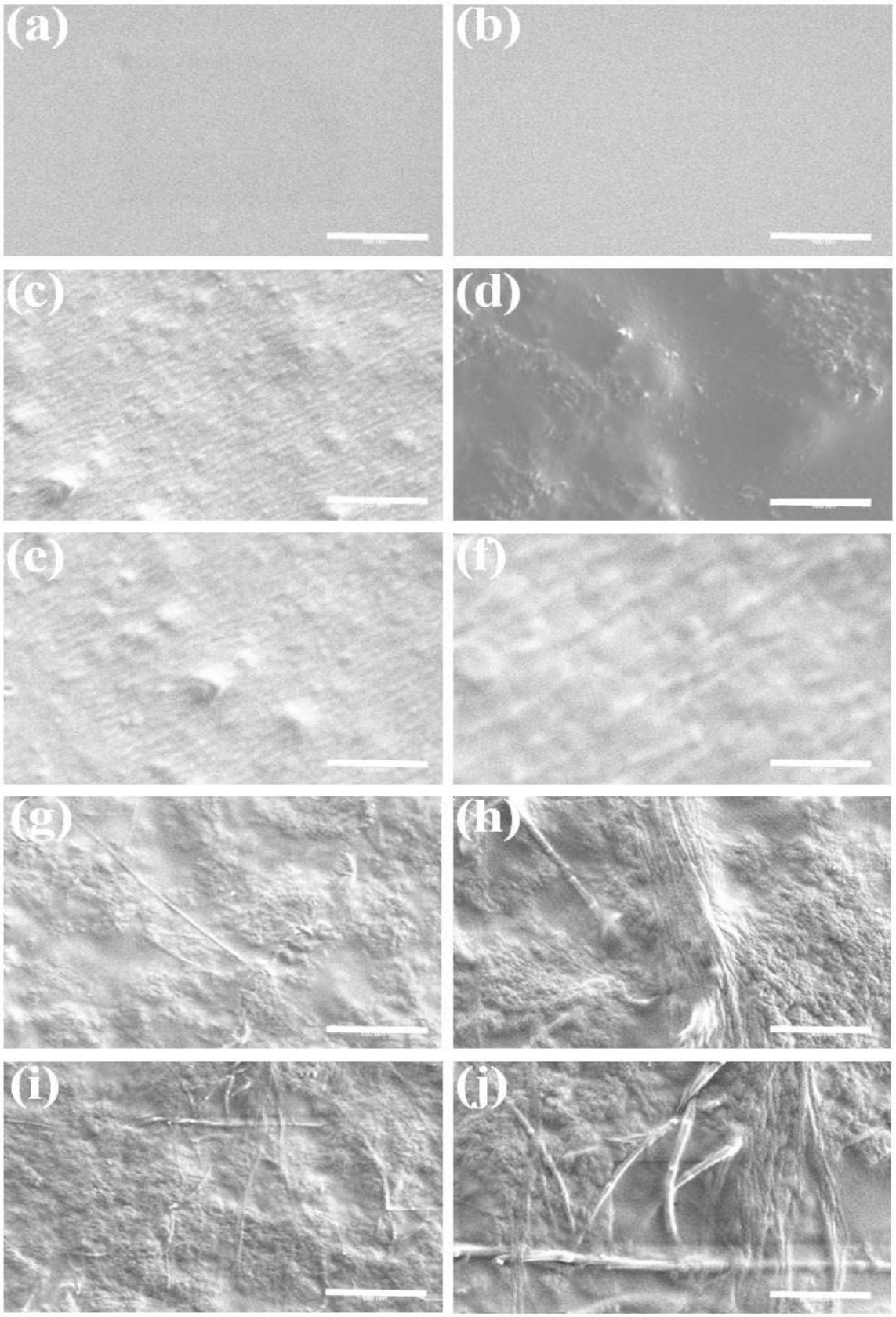

Figure 5.22. *SEM images of film topography, where (a-b) - silk only, (c-d) - silk:crystallin protein, (e-f) - silk:whey protein, (g-h) - silk:crystallin PNFs, and (i-j) - silk:whey PNFs in 1:1 ratio. Left panel - 5000x, and right panel - 15,000x magnification. Scale bar – 1 μm.*

5.19. Proteolytic degradation

In tissue engineering, biodegradability of the biomaterials is of great importance as a scaffold should allow the formation of cells to produce their own extracellular matrix, over time, to eventually replace the implanted scaffold [40]. An ideal scaffold should, therefore, degrade at a similar rate as the growth of new tissue [22]. The by-products of this degradation should be non-toxic, and easily metabolised and cleared from the body without interference with other organs [12]. Understanding the factors that control the rate of degradation is, thus, critical in designing functional tissue scaffold materials.

Silk fibroins have been investigated for diverse range of applications in the biomedical field, and are classified as enzymatically degradable biomaterials [17, 40]. Several biodegradation studies on silk fibroins have demonstrated that proteases play a significant role in the enzymatic degradation of silk fibroins [41-44]. Considering this, *in vitro* proteolytic degradation of silk-only, and silk-blend samples was done using proteases, including α-chymotrypsin, protease type XIV, and collagenase. Weight loss to determine the degradation rate, and SDS–PAGE was used to analyse the degradation products.

To assess if there is any loss in enzymatic activity of proteases used over the time period of 7 days at 37 °C, enzymatic solutions (1mg/mL in PBS, pH 7.4) were prepared (section 7.22.1) and incubated at 37 °C. A 50 µL aliquot was taken for each of the enzyme solution every 24 h, and added to the BSA solution (5 mg/mL in PBS, pH 7.4), followed by 1 h incubation at 37 °C (section 7.22.1). Decay of the enzymatic activity was determined using SDS-PAGE (section 7.1.1). The results, suggested that at least 60-75% of the initial enzyme activity was lost after 3 days of incubation (results not shown). Thus, enzyme solutions were replaced every 24 h, over the time period of 7 days to account for protease activity loss due to 37 °C incubation.

For enzymatic degradation of the silk-only and silk-blend films, pre-casted films (S1-S9) (section 7.20, **Table 7.14**), were immersed in 75% ethanol for 4-6 h to induce crystallinity (section 7.20.1), followed by 1 h drying. Previous studies have shown that the immersion in alcohal, such as methanol or ethanol can induce crystallinity in silk films, making films more stable [45], and is possible to control the degradation rate of the silk fibroin scaffolds by controlling the β-sheet structure content for a specific tissue engineering application [46]. After ethanol annealing, annealed films were removed from the PDMS discs and immersed in 250 µL of enzyme solution (or PBS for control) prepared as detailed in section (7.22.1), and incubated at 37 °C. After every 24 h, samples were centrifuged (section 7.22.3) to accumulate blend film residues, and supernatant removed (section 7.22.2) to run SDS-PAGE immediately. The blend film residues were then dried overnight and the mass determined using an analytical balance (section 7.22.3). After drying, samples were weighed and the percent weight loss was calculated by comparing each group to the control samples (films incubated in PBS at 37 °C, without enzymes). Nine samples from each group were taken at each time point to get statistically significant data. Fresh enzyme solution was added to each tube, followed by incubation at 37°C.

The samples were analysed every day for weight loss and SDS–PAGE to determine when the degradation of materials by different enzymes became significantly different.

5.19.1. SDS-PAGE analysis

Background controls for each group were enzyme solutions without silk materials incubated at 37 °C for 24 h, and controls for silk-blend films were incubated in PBS (pH 7.4). As detailed in section 5.12, silk fibroin is composed of a high molecular weight chain (H-chain) of 350 kDa and two lower molecular mass protein components: the light chain and P25 glycoprotein [47]. For all the samples (films incubated in PBS, and with proteases) no distinct bands were observed for silk fibroin light chain (L-chain) of 26 kDa [48], and glycoprotein P25, 30 kDa [49] (**Figure 5.23 (a)**, ~25-30 kDa). Both light chain and P25 glycoprotein combined account for approximately 5% of the amino acids present in silk fibroin [47], and is possible that the concentration of these proteins in the supernatant was too low to be detected by SDS-PAGE, as also reported by Brown *et al.* 2015 [44]. Additionally, silk proteins are obtained from hydrolysed fibroins, and thus will have a random assortment of peptides, instead of any intact proteins. In **Figure 5.23 (a)**, a faint protein band of soluble protein fragments was observed for silk only sample at ~20 kDa.

It is not possible to see distinct bands for PNFs on SDS-PAGE due to their size restrictions (as mentioned previously in Chapter Four); however, low molecular crude non-fibrillated protein bands as can be seen in **Figure 5.23 (a)**, (Lane 4-9) would be observed on gel image if, PNFs were leaching or silk:PNF films were degraded.

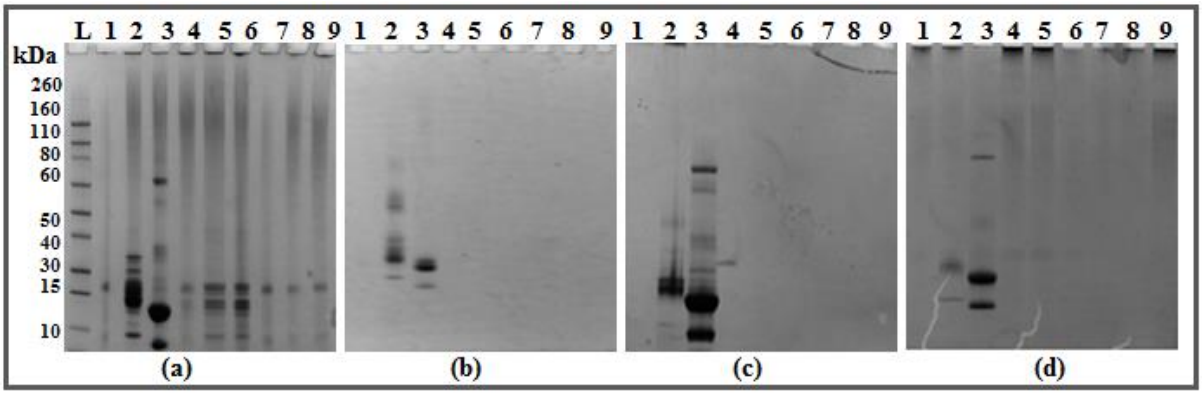

Figure 5.23. *SDS-PAGE of silk-only, and silk-blend samples. L - Ladder, 1 - silk-only, 2 - silk-CP (50:50), 3 - silk-WP (50:50), 4 - silk-CPNFs (75:25), 5 - silk-CPNFs (50:50), 6 - silk-CPNFs (25:75), 7 - silk-WPNFs (75:25), 8 - silk-WPNFs (50:50), 9 - silk-WPNFs (25:75), where a - solutions diluted at 2 mg/mL, b - supernatant taken from the film samples incubated in PBS (pH 7.4) - after 1 day, c - after 3 days, and d - after 5 days.*

For the film samples incubated in PBS, no distinct bands were seen for silk-only, and silk-PNF blends films, suggesting that the silk-only, and silk:PNF blend films are stable in PBS **(Figure 5.23 b-d, Lane 1, and 4-9)** up to 5 days. In contrast to the silk-PNF blend films, silk-protein blend films were not as stable and proteins bands for crystallins and whey proteins were detected after 24 h incubation **(Figure 5.23 b, Lane 2-3)**.

For silk-protein films a slow release of proteins was observed as protein bands were present throughout the incubation period (5 days) **(Figure 5.23 (b-d), Lane 2-3)**. The proteases (protease type XIV, α-chymotrypsin) used in this work are serine proteases, and cleave amide bonds adjacent to aliphatic, aromatic or hydrophobic residues. Chymotrypsin cleaves peptide bonds that are next to aromatic amino acid residues (phenylalanine, tyrosine or tryptophan) [50], whereas collagenase cleaves amino acid sequences found in collagen i.e. Gly–Ile, Gly–Leu, Gly–Val, Gly–Phe, Gly–Asn, Gly–Ser [44]. **Table. 5.8** shows cleavage sites for protease type XIV, α-chymotrypsin, and collagenase.

Initially films samples were incubated in proteases at the concentration of 1 mg/mL at 37°C for 24 h, but film samples with proteins formed irregular debris that could not be washed and weighed. Previous work by Lu *et al.* (2010) on silk film degradation has demonstrated that reducing protease concentration (5.6 to 2.3 U/mL) inhibits debris formation [51]. Therefore, a lower concentration (0.5 mg/mL) was used further to slow down the degradation rate (section 7.18.3.3).

Table 5.8. *Summary of protease cleavage sites. Taken from Brown et al. (2015) [44].*

Protease	Source	Cleavage sites	Reference
Protease type XIV	*Streptomyces griseus*	Adjacent to His, Tyr, Trp, Phe, Lys, Arg	**[52]**
α-Chymotrypsin	Bovine Pancreas	Adjacent to Trp, Tyr, Phe, Ile, Val, Leu	**[41, 52]**
Collagenase	*Clostridium histolyticum*	X-Gly-Pro, where X= any amino acid	**[44]**

For the films incubated with protease type XIV **(Figure 5.24, top panel)**, at 24 h of enzyme exposure, no distinct bands were observed for any of the sample, but the intensity of lower molecular weight bands increased for silk-protein blend film samples **(Figure 5.24, top panel-a, Lane 2-9)** relative to the silk-, and enzyme-only lanes (Lane 1 and Lane 10, respectively). After 3 days, the intensity of low molecular weight bands increased significantly for silk:protein blend films **(Figure 5.24, top panel-b, Lane 2-3)**, indicating the degradation of crystallin and whey proteins into small peptides with a molecular weight ranging from 15-25 kDa. Protease type XIV is a mixture of serine proteases and a reported molecular mass range from 16-26 kDa. Thus, it is likely possible that degradation bands overlapped with the protease bands, as can be seen the intensity of lower molecule weight bands for silk-protein blend films **(Figure 5.24, top panel-b, Lane 2 and 3)** is more, relative to the enzyme only **(Figure 5.24, top panel-b, Lane-10)** sample. The appearance of a smear of lower molecular weight bands after 5 days **(Figure 5.24, top panel, Lane 2-9)** was observed for all the samples except silk- and enzyme-only **(Figure 5.24, top panel, Lane 1 and 10, respectively)**, proposing that films degraded rapidly after 3 days. Supernatant from silk films incubated with protease XIV did not contain detectable silk bands or smear of bands at any day, suggesting better stability than the blend films.

For the samples incubated with chymotrypsin (**Figure 5.24, middle panel**), distinct bands at 50 and 30-40 Kda were seen for all the samples, along with a smear of lower molecular weight bands after 24 h incubation **(Figure 5.24 (a), middle panel, Lane 1-9 relative to the enzyme-only, Lane 10)**.

Similar to the 24 h incubation, a smear of low molecular weight bands was also observed after 3 days **(Figure 5.24 (b), middle panel),** with degradation bands (between 10-20 kDa) appearing for silk blend films (more distinct for silk:protein blend films, Lane 2-3, relative to silk:PNF blend films, Lane 4-9). After 5 days **(Figure 5.24 (c), middle panel)**, lower molecule weight degradation bands were more prominent for silk-PNF (Lane 4-9), and silk-only (Lane 1) samples relative to the silk-protein samples (Lane 2-3). This observed difference is likely due to the different degradation rates of silk:protein, and silk:PNF or silk-only films.

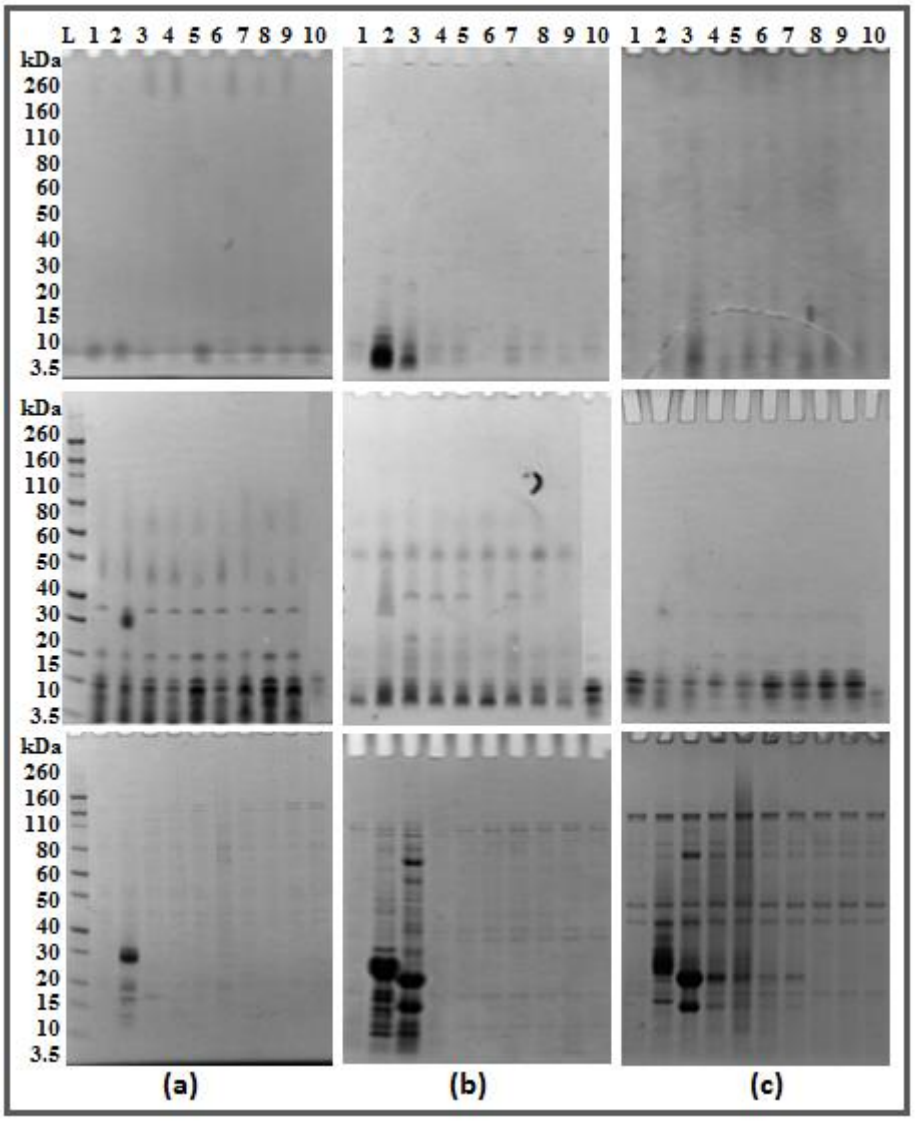

Figure 5.24. *SDS-PAGE of degradation products released from silk-only, and silk-blend films, in the presence of protease type XIV (top panel), α-chymotrypsin (middle panel), and collagenase (bottom panel), where a - after 1 day, b - after 3 days, and c - after 5 days. L-Ladder, 1 - silk-only, 2 - silk-CP (50:50), 3 - silk-WP (50:50), 4 - silk-CPNFs (75:25), 5 - silk-CPNFs (50:50), 6 - silk-CPNFs (25:75), 7 - silk-WPNFs (75:25), 8 - silk-WPNFs (50:50), 9 - silk-WPNFs (25:75), and 10 - enzyme-only sample. Supernatant was taken from film samples incubated with enzymes (PBS, pH 7.4).*

This decreased intensity of lower molecular weight bands for silk:protein films after 5 days **(Figure 5.24 (c), middle panel, Lane 2-3)** compared to the 3 days image **(Figure 5.24 (b), middle panel, Lane 2-3)** suggests that silk:protein blend films were degraded rapidly and the concentration of proteins remained in the supernatant after 3 days was lower than initially present, thus, after 5 days no significant protein or degradation bands can be detected. On the contrary, strong degradation bands were observed for silk-only, and silk-PNF blend films after 5 days, suggesting to slow degradation of these films. Lack of any distinct protein band for silk-protein blend films, and appearance of degradation bands for all the samples after 24 h incubation suggests that chymotrypsin degradation is relatively faster than protease type XIV, and degradation peptides released from films degraded by α-chymotrypsin are of molecular mass less than 15 kDa. The appearance of lower molecular weight bands with size smaller than 2.5 kDa has also been reported previously by Brown *et al.* (2015) for silk film degradation by chymotrypsin [44].

For collagenase **(Figure 5.24, bottom panel)**, supernatant from silk-blend films had no distinct protein bands for any of the samples except silk-crystallin protein (Lane 2) due to leaching of the proteins after 24 h of incubation **(Fig 5.24 (a), bottom panel, Lane 2)**. After 3 days **(Fig. 5.24 (b), bottom panel)**, multiple mid- and low-molecular weight protein degradation bands ranging from 92 kDa to 3.5 kDa were observed for silk-protein blend films only (Lane 2-3). After 5 days **(Fig. 5.24 (c), bottom panel)**, the degradation bands as observed after 3 days for silk-protein films were still present suggesting continuous slow degradation of the proteins. Additionally, a distinct band between 25-30 kDa was observed for silk-protein (Lane 2-3) and silk-CPNFs (Lane 4-6) blend films. The absence of any distinct degradation bands for other samples, suggests that crystallin proteins and crystallin PNFs were least stable to collagenase relative to the other film samples. For both proteins (crystallins, and whey), there are not many collagenase cleavage sites *(Appendix F, Table F1)*, and degradation of proteins was not expected. However, previous work by Li *et al.* (2003) showed that despite the scarcity of collagenase cleavage sites, collagenase can degrade porous silk sheets more than α-chymotrypsin [42], and it is likely that longer incubation time would result in degradation of all the film samples despite of the scarcity for collagenase cleavage sites.

5.19.2. Mass loss

In agreement with the SDS-PAGE results for protease type XIV degradation, silk-protein blend films showed no significant change in weight for 72 h in the presence of protease type XIV, with films retaining 85% of their weight similar to the weight loss observed for films in PBS **(Figure 5.25 i)**. A significant drop (52%) was observed in the weight of the films after 5 days, for films with proteins relative to the films with PNFs (40%), and silk only (31%) sample.

For the samples incubated with chymotrypsin **(Figure 5.25 ii)**, a gradual loss in weight was observed with blend films showing 10% decrease in mass after 24 h incubation relative to the films dissolved in PBS. A further 10% decrease was observed after 3 days, followed by a further drop of 5% in 5 days. The silk-only sample retained 75% of mass after 5 days.

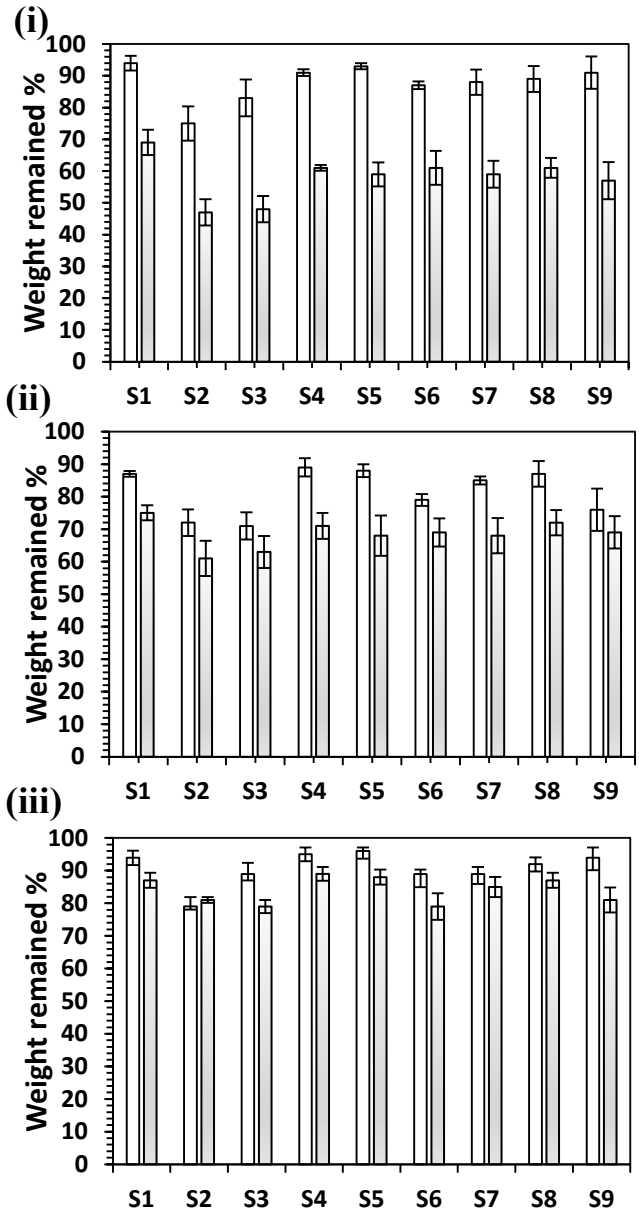

Figure 5.25. *Weight loss from enzymatic degradation of silk-blend films, where blank bars - after 3 days, and filled bars - after 5 days. S1 - silk-only, S2 - silk-CP (50:50), S3 - silk-WP ((50:50), S4 - silk-CPNFs (75:25), S5 - silk-CPNFs (50:50), S6 - silk-CPNFs (25:75), S7 - silk-WPNFs (75:25), S8 - Silk-WPNFs (50:50), S9 - silk-WPNFs (25:75), and* ***(i)*** *protease type XIV,* ***(ii)*** *α-chymotrypsin, and* ***(iii)*** *collagenase. The remaining mass of degraded silk-blend films was measured after each time point and compared against the samples incubated in the presence of PBS (pH 7.4). Values are mean standard deviation of n=9.*

For the samples incubated with collagenase **(Figure 5.25 iii)**, no significant drop in the mass was observed relative to the films incubated in the PBS, with all film samples exhibiting 15-20% loss in mass after 5 days as anticipated from the SDS-PAGE results. Amongst all the enzymes studied, minimum weight loss was observed for the samples incubated in collagenase, followed by chymotrypsin, and protease type XIV.

A similar trend for chymotrypsin and protease type XIV have been reported previously for silk film degradation and it was stated that the observed difference could also be due to the inability of chymotrypsin to cleave β-sheet structure [44]. This could also be held true for this work, as in this case silk, both proteins (whey and crystallins), and PNFs have native β-sheet structure. Silk-protein blend films showed high degree of weight loss in comparison to the silk only sample, due to the proteins dissolving/diffusing out of the carrier film, as demonstrated by the distinct protein bands observed on the SDS-PAGE in the presence of PBS only **(Figure 5.23)**. Silk-PNF blend samples showed slower degradation (absence of any distinct bands for 72 h and least drop in weight) relative to silk-protein blend films in the presence of enzymes, and therefore, were more stable than the silk-protein blends, corroborating with the PNF stability results (section 2.2, Chapter Two). However, longer incubation for silk-PNF samples is required to understand the proteolytic degradation of silk-PNF, with PNFs only sample as a control.

Both weight analysis and SDS-PAGE results suggested that the silk-blend films can be degraded by serine proteases, and different proteases exhibit different degradation rate. The number of cleavage sites for protease type XIV, and chymotrypsin are similar, and thus both enzymes should degrade films at the same rate. In this case, the α-chymotrypsin degradation was relatively faster than the protease type XIV degradation but mass loss was relatively higher for protease type XIV, suggesting more degradation at a slow rate. Previous studies have reported such difference in the behavior of these two enzymes, and demonstrated that protease type XIV has the potential to cleave silk at multiple locations along the length of the protein [53]. Although SDS-PAGE results corroborated with the mass loss studies, a further study using SEM is required to understand the surface topography of degraded films, and to conclude on the observed degradation results. However, these results suggest that degradation rate of the silk-blend films is dependent on the film composition, and could be matched to the potential application by tuning the film composition.

5.20. Optical transmittance

Optical transparency of blend films was investigated as for some applications, such as corneal regeneration, transparent material is needed. The human cornea is a transparent tissue and is mainly responsible for the refractive property of the eye. Thus, it is very important for corneal replacement materials to fulfil specific optical standards. Based on the spectrophotometric quantification, Ventura *et al*. (2005) established that a minimum threshold of 60% transparency is required for materials for corneal tissue engineering [54]. In a recent study, Andrades *et al.* (2015) evaluated optical transparency of tissues and materials used for corneal tissue engineering such as amniotic membrane and collagen scaffolds *via* a photographic-based assay and suggested a new threshold value of 72% [55]. All the films were prepared directly through drying the silk and blend solutions into a 24 well plate without lids, at room temperature (section 7.23). In ethanol annealing process, the films obtained after drying were immersed in 75% ethanol solution for about 6 h to increase β-sheet content (section 7.20.1). Transparency of the solutions **(Figure 5.26)**, and films were investigated with UV-visible spectrophotometry **(Figure 5.27)**.

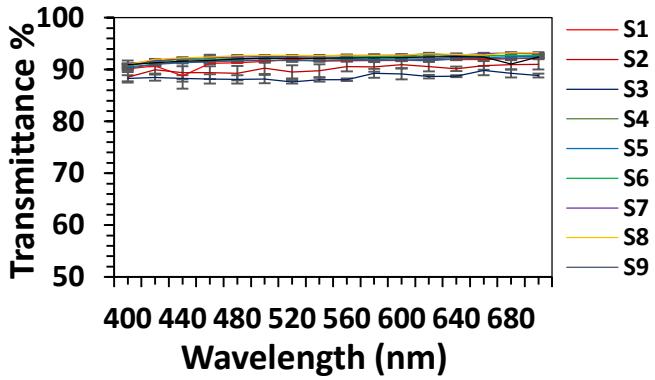

Figure 5.26. *Percentage transparency of silk-only, and silk-blend solutions, where S1- silk-only, S2 - silk-CP (50:50), S3 - silk-WP ((50:50), S4 - silk-CPNFs (75:25), S5 - silk-CPNFs (50:50), S6 - silk-CPNFs (25:75), S7 - silk-WPNFs (75:25), S8 - silk-WPNFs (50:50), S9 - silk-WPNFs (25:75), and blank- 150 µL of dH_2O. Error bars represent the standard deviation of the mean of three replicates.*

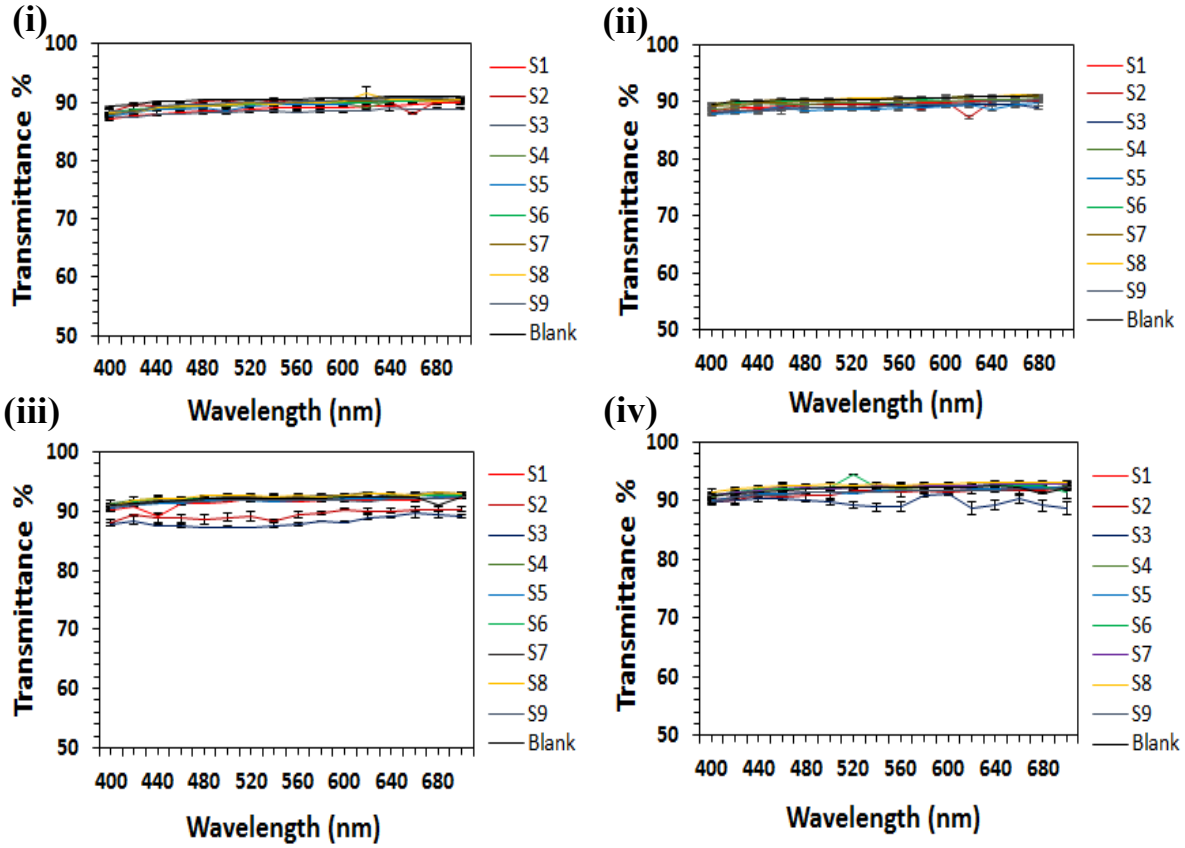

Figure 5.27. *Percentage transparency of silk-blend films with different ratios, where **(i)** control silk films, **(ii)** annealed silk films, **(iii)** control silk films in the presence of PBS (pH 7.4), and **(iv)** annealed silk films in the presence of PBS (pH 7.4). S1- silk-only, S2 - silk-CP (50:50), S3 - silk-WP (50:50), S4 - silk-CPNFs (75:25), S5 - silk-CPNFs (50:50), S6 - silk-CPNFs (25:75), S7 - silk-WPNFs (75:25), S8 - silk-WPNFs (50:50), S9 - silk-WPNFs (25:75), and blank- 24-well plate with no films in (i and ii), and 150 µL of PBS (pH 7.4) in (iii and iv). Error bars represent the standard deviation of the mean of three replicates.*

.

Spectral evaluation showed high transmission (transmittance between 85 and 90%) across most of the visible spectrum, which established the samples to be transparent. There was no major difference in the light transmission spectra obtained for solutions **(Figure 5.26)** and films **(Figure 5.27 – dried films (i) and annealed films (ii))**.

In the visible spectrum (between 400 and 700 nm) each film sample transmitted between 85% and 92% of incident light, and in the middle of the spectrum (at 500 nm) 92 ± 0.1% of light was transmitted **(Figure 5.27)**. No distinct change in the transparency of the silk film (S1) was observed on the addition of either proteins (sample S2 and S3), or PNFs at selected concentrations (sample S4-S9). Further, to evaluate the impact of PBS or solution on the transparency of the films, pre-cast films were hydrated in PBS before (1 h) and during the measurement. Transmission spectra of both control and ethanol annealed pre-casted films in the presence of PBS showed high transmittance (85-92%) **(Figure 5.27, iii and iv)**. Spectral evaluation of both pre-casted dried and hydrated films showed that each of the blend film sample (S1-S9) exhibits good level of optical transparency (85-92%) and meet the requirements of minimum threshold (60-72%) required for materials for corneal tissue engineering.

5.21. Hydrophobicity

Considering that surface wettability of biomaterials plays an important role in cell biocompatibility, static contact angle measurements were carried out on the films obtained from silk-only, silk-proteins, and silk-PNF blends to assess differences in surface wettability, as a function of material composition. It is generally believed that hydrophillic surfaces promote greater cell attachment and proliferation relative to hydrophobic surfaces [56, 57]. However, Menzies *et al.* (2010) reviewed various biomaterials used for different tissue engineering applications, and substantiated that depending upon the potential application of the concerned biomaterial, enhanced wettability (low contact angle/hydrophilic) may not necessarily be an advantageous property [58]. The wettability of the films as determined using static contact angle measurements (section 7.24) for both as-cast (control or not annealed) and ethanol annealed films as shown in **Figure 5.28**, is summarised in **Figure 5.29.**.

The contact angle measurements of silk blend films (~38°±4 for both silk-crystallin-S2, and silk-whey protein blends – S3) were significantly lower than the silk-only film sample that had a contact angle of ~53°. An increase in contact angle was anticipated for the films with PNFs as SEM analysis of silk:PNF blend films showed rough surfaces for the films with PNFs. However, no drastic difference was observed in the contact angle measurements of silk:PNF blend films relative to silk-only sample **(refer Table in Figure 5.29)**. Blend films with 25% and 50% PNFs (75:25 (S4 and S7), 50:50 (S5 and S8)) exhibited lower contact angle values, and 75% PNF-blend films (S6 and S9) showed a slight increase relative to silk-only films, for both whey and crystallin PNFs.

Upon annealing, a drop in contact angle values for the silk-protein (S2 and S3), 25:75 (S4 and S7), and 50:50 (S5 and S8) silk:PNFs blended films was observed, whereas, samples with the high amount of silk i.e. silk-only (S1), 75:25 (S4 and S7) silk:PNFs blend films displayed an increase.

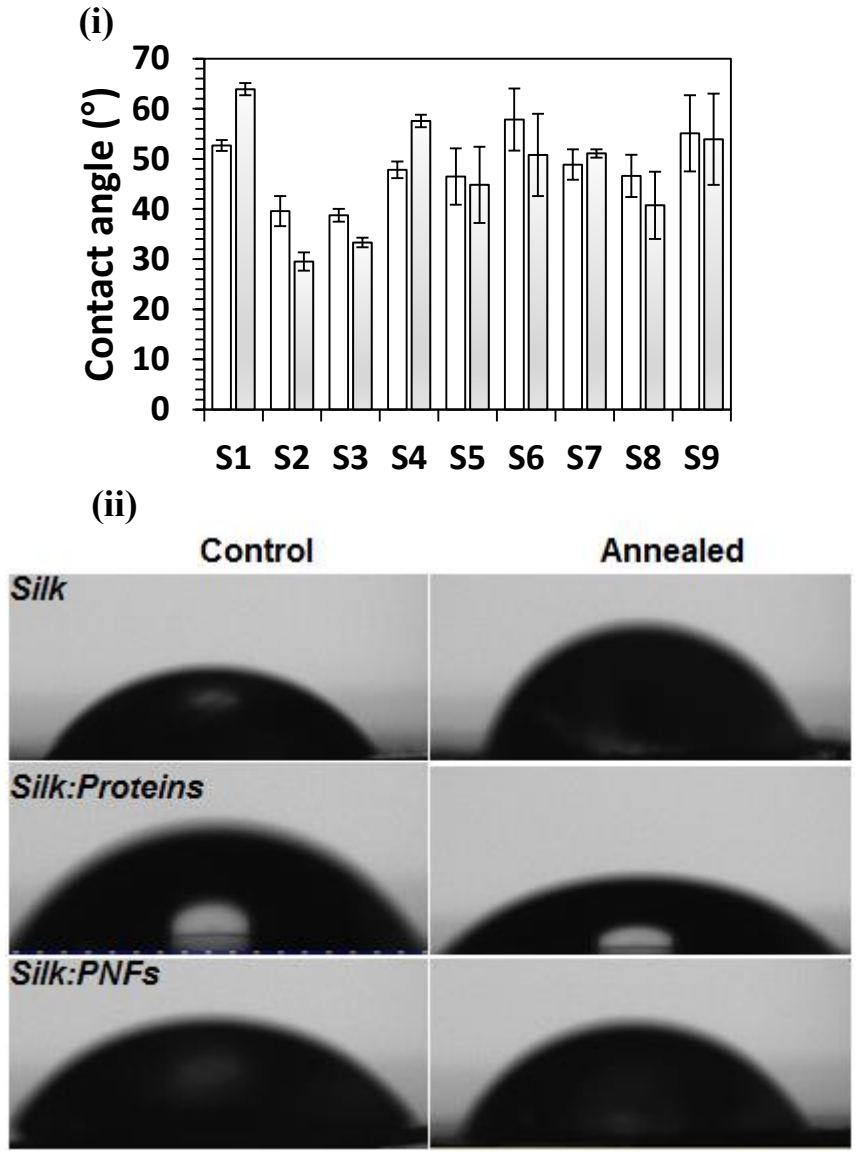

***Figure 5.28**. **(i)** Wet contact angle measurements of the silk-blend films, blank bars – not annealed films, and filled bars - after ethanol annealing, where S1-silk-only, S2 - silk-CP (50:50), S3 - silk-WP (50:50), S4 - silk-CPNFs (75:25), S5 - silk-CPNFs (50:50), S6 - silk-CPNFs (25:75), S7 - silk-WPNFs (75:25), S8 - silk-WPNFs (50:50), and S9 - silk-WPNFs (25:75). Error bars represent the standard deviation of the mean of three replicates. **(ii)** Images of the water droplets on the silk, silk:whey protein, and silk:crystallin PNF (50:50) blend films.*

It should be noted that there was quite a high error for the films with PNFs due to the heterogeneity of the fibrils in films, as also evident from SEM images. **Figure 5.29**, shows contact angle measurement of 75% crystallin PNF film (25:75 silk:PNF blend) at two different points, for the same film.

As scan be seen, two different contact angle values (56±6.4), and (84±7.8) were obtained for the same film at two different points, confirming that within the same film, PNFs are not spread homogeneously. The contact angle value obtained for the silk-only sample (S1) co-related well with the published literature, which also showed decreased wettability (higher contact angle/hydrophobicity) for silk films after water, or methanol annealing [59, 60]. These results demonstrate that composition and annealing effect the surface roughness and contact angle of silk-blend films.

Sample	Details	Contact angle (°)	
		Control	Annealed
S1	Silk (100)	52±1.1	63±1.2
S2	Silk:CP (50)	39±2.2	29±1.8
S3	Silk:WP (50)	38±1.2	33±0.9
S4	Silk:CPNFs (75:25)	47±1.6	57±1.2
S5	Silk:CPNFs (50:50)	46±5.6	42±3.2
S6	Silk:CPNFs (25:75)	57±6.2	51±8.2
S7	Silk:WPNFs (75:25)	49±3.3	49±1.5
S8	Silk:WPNFs (50:50)	47±4.2	53±6.7
S9	Silk:WPNFs (25:75)	55±7.6	53±9.1

Figure 5.29. *Summary of contact angle measurements for all the samples, as illustrated in Figure 5.28. (i). Bottom - images of contact angle measurements for silk:crystallin PNFs (25:75) showing different contact angle measurements* ***(i)*** *56±6.4 and* ***(ii)*** *84±7.8, for the same film sample, at different points.*

5.22. Biocompatibility of silk-PNF blend films

To evaluate the potential of using the blend films in tissue engineering application and to investigate the biocompatibility of blend films, *in vitro* cell culture experiments were performed. Mouse embryonic fibroblast cells were cultured on the blend films for 72 h, and cell attachment and spreading study was done (section 7.25). Initially, cell culture experiments were also conducted on silk-protein blend films, but silk-protein blend films were not stable, in the presence of Dulbecco's Modified Eagle's Medium (DMEM) media at 37 °C.

Thus, further cell viability studies were done using silk-only, and silk-PNF blend films. All experiments were repeated multiple times (3×3 images were recorded for 3 separate experiments done on different days) to ensure reproducibility of silk-blend films. An attempt was made to evaluate the proliferation rate of fibroblast cells on the blend films using 3-(4, 5-dimethylthiazol-2-yl)-2, 5-diphenyltetrazolium bromide (MTT) assay; however, due to the proteinaceous nature of the films there was increased background absorbance values and assay artifacts were observed *(see Appendix F, Figure F1)*. Instead, cell quantification **(Figure 5.30)** and cell morphology (spreading) **(Figure 5.31)** were analysed from the light microscopy images taken at each time-point, for each of the sample, using ImageJ methods adapted from Li *et al.* (2014) [61], as detailed in section 7.25.2.

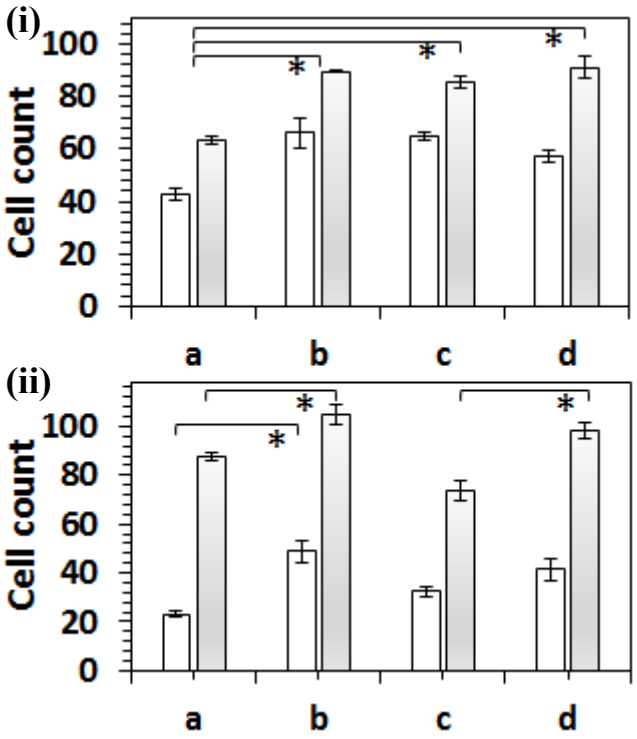

Figure 5.30. (i) *Average of number of cells per 5x image on different surfaces, where a - silk-only, b - silk:CPNFs (50:50), c - silk:WPNFs (50:50), and d - TCP surface.* ***(ii)*** *Average of number of cells per 5x image in the presence of increasing concentration of PNFs, where a - silk:CPNF (75:25), b - silk:CPNFs (25:75), c - silk:WPNF(75:25), and d - silk:WPNFs (25:75). Blank bars - 24 h and filled bars - 72 h. Error bars represent the standard deviation of the mean of three replicates. * represents significance values: $p \leq .05$, where solid-line – silk-only (sample a)to silk-PNF(b and c) and TCP samples (sample d) in (i), and lower concentration of PNFs (25%, sample a and c) to higher concentration of PNFs (75%, sample b and d) in (ii).*

For all the samples, up to 72 h of cultivation, the number of fibroblast cells cultured on the silk-PNF blend films increased with the increasing culture period. As can be seen in **Figure 5.30 (i)**, silk-PNF blend films (sample - b and c), and TCP (sample d) had similar cell number and rate of proliferation over 3 days. Amongst silk-only (sample a) and silk-PNF blend films (b and c), silk-PNF blend films showed better proliferation and cell viability, with significant differences ($p \leq .05$).

On comparing, the number of viable cells on the silk:PNF blend films with increased concentration of PNFs, an increase in the number of cells, after 72 h, was observed for films with higher percentage of PNFs **(Figure 5.30 (ii) filled bars, sample b and d)** relative to the film samples with lower percentage of PNFs **(Figure 5.30 (ii) filled bars, sample a and c)**. Cell images for 25% and 75% PNF content films at 24 h, and 72 h time-point, for both whey and crystallin fibrils are *shown in Appendix F, Figure F2.*

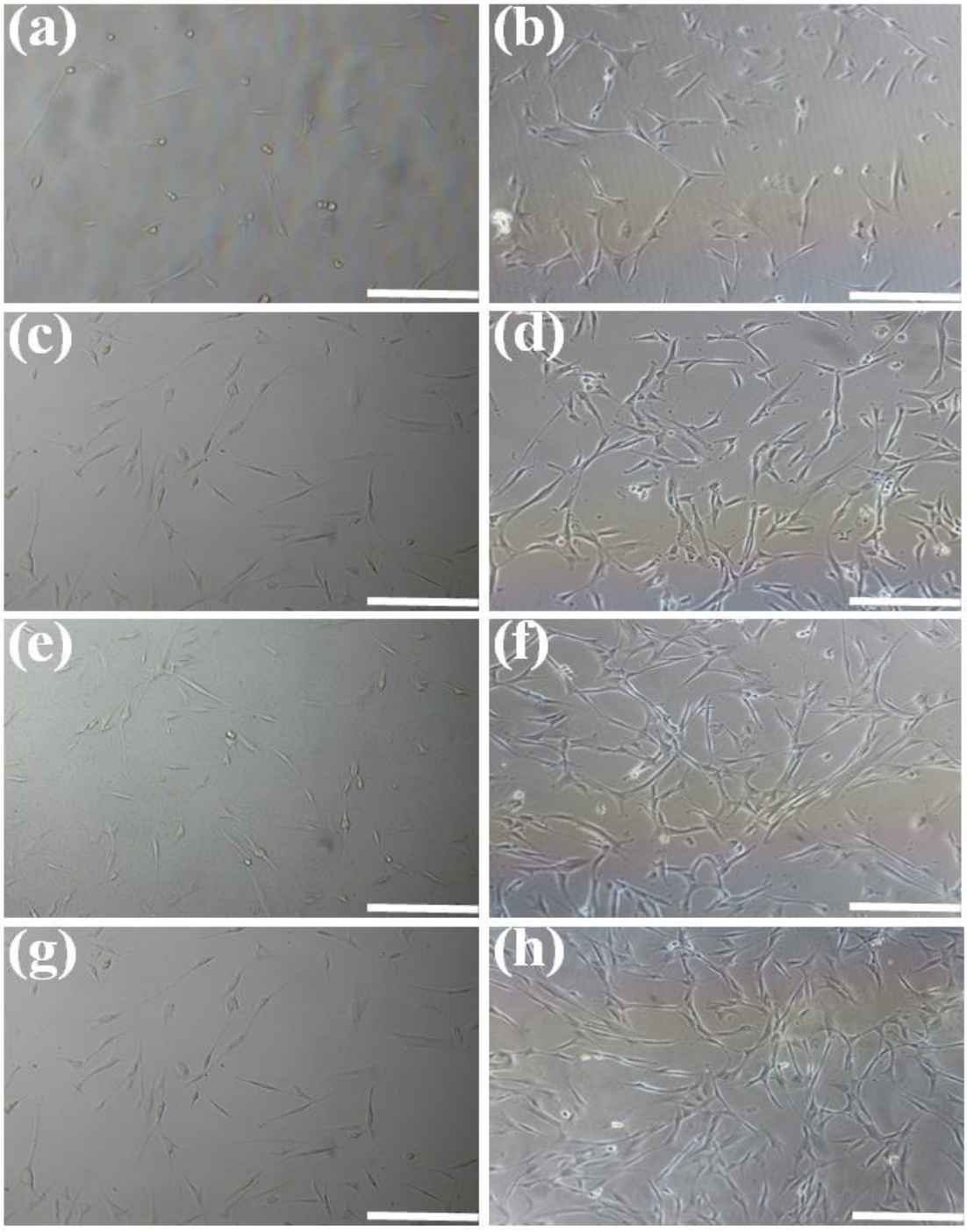

Figure 5.31. *Images of mouse fibroblast cells cultured cultured on - silk only (a and b), silk:CPNF (50:50) (c and d), silk:WPNFs (50:50) (e and f), and TCP (g and h), where (left panel) is 24 h, and (right panel) is 72 h. Scale bar-100 µm.*

For investigated cell morphology, adhesion and spreading, surface area of the cells was measured for each 24, 42, and 72 h time-point as spreading is quantified by a significant flattening of the cells and an increase in overall surface area [62]**.** An unspreaded fibroblast cells appear as a rounded structures, whereas with time cells adhere to the surface and achieve normal spreading, and typical elongated spindle-like morphology, resulting in increased surface area, as can be seen in **Figure 5.31 (right panel)**. Under the light microscope, the extension of cells was observed within 18 h of incubation (results not shown). At the 24 h time-point, it was observed that a few cells had adhered on to the scaffold **(Figure 5.31, left panel)** with the majority of the cells randomly distributed on the surface of the blend films. At the 42 h time-point, the typical spindle-like morphology and adhesion of fibroblast cells on the blend films was observed (results not shown). After 72 h incubation, the cell number appeared to have significantly increased compared with that at the 42 h, and the cells displayed the appropriate, extended spindle shape morphology **(Figure 5.31. right panel)**.

Cell attachment and morphology, results showed that cells on the silk-only surface had slower proliferation rate relative to the silk-CPNF and silk-WPNF blend films up to 72 h. On comparing the cell proliferation rate of silk-PNF films to the TCP surface, significant difference for both silk:CPNF, and silk:WPNF blend films was noticed, with cells showing better proliferation rate on silk-PNF blend films at all the given time-points ($p \leq .05$), except t = 24 h for silk:CPNF blend films (0.231, $p \geq .05$) **(Figure 5.32)**. The higher surface area values observed for silk-blend films compared to the silk-only, and TCP surface suggested that blend films could support fibroblast cells viability and proliferation. The improved cell adhesion, spreading, and proliferation of fibroblasts in the presence of PNFs could be due to increased roughness of the surface or due to the presence of cell adhesion sites; however, further studies are required to confirm the advantageous properties of PNFs to act as a cellular scaffold.

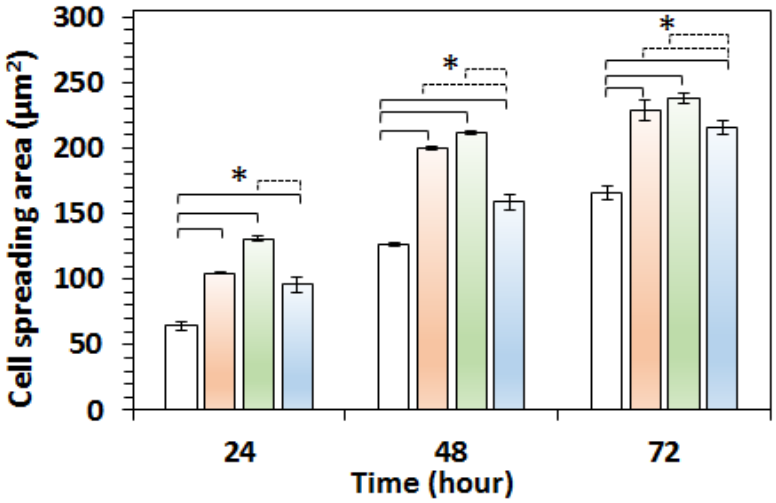

Figure 5.32*. Analysis of fibroblast cell spread area on silk blend, and TCP surfaces after 24, 48 and 72 h incubation, where blank bars - silk-only, red bars - silk:CPNF (50:50), green bars - silk:WPNF (50:50), and blue bars - TCP (control samples). Error bars represent the standard deviation of the mean of three replicates. * represents significance values: $p \leq .05$, where, solid-line – silk-only to silk-PNF samples, and dotted line – TCP to silk-PNF samples.*

5.23. Conclusion

This section has investigated the use of PNFs as a cellular growth scaffolds. PNFs were blended with other biocompatible fibrous protein, namely silk, and the obtained composite films were studied for their suitability as a biomaterial with applications in tissue engineering. The transmission of visible light through the blend films was found to be greater than 80%, which makes them highly suitable for ophthalmic applications. *In vitro* proteolytic degradation of the blend films in the presence of serine proteases, and collagenase over 5 days, demonstrated that the blend films are biodegradable, and silk-PNF blend films are more stable than silk-protein blend films. Silk-protein blend films were not stable for cell growth and proliferation studies; however, the rapid degradation of these films, releasing proteins in the environment, suggests the possibility of using silk-protein blend films in applications where rapid degradation is sought after, such as drug delivery.

In vitro cell proliferation studies revealed that silk:PNF blend films support cell proliferation, and had better cellular adhesion and proliferation rate relative to the silk-only films. Thus, PNFs demonstrate their potential to be used as substrates for the attachment and proliferation of cells, and can be interesting materials for tissue regeneration or scaffold preparation that temporarily supports the formation of new tissue and organs. Further characterisation in terms of mechanical integrity, long term *in vitro* stability, and proliferation of other cell lines/cells is required to demonstrate the potential of these blend films for tissue engineering applications.

5.24. References

[1] S.L. Gras, A.K. Tickler, A.M. Squires, G.L. Devlin, M.A. Horton, C.M. Dobson, C.E. MacPhee, Functionalised amyloid fibrils for roles in cell adhesion, *Biomaterials*, 29 (2008) 1553-1562.

[2] N.P. Reynolds, M. Charnley, R. Mezzenga, P.G. Hartley, Engineered lysozyme amyloid fibril networks support cellular growth and spreading, *Biomacromolecules*, 15 (2014) 599-608.

[3] C. Li, A.K. Born, T. Schweizer, M. Zenobi-Wong, M. Cerruti, R. Mezzenga, Amyloid-hydroxyapatite bone biomimetic composites, *Advanced Materials*, 26 (2014) 3207-3212.

[4] N.P. Reynolds, K.E. Styan, C.D. Easton, Y. Li, L. Waddington, C. Lara, J.S. Forsythe, R. Mezzenga, P.G. Hartley, B.W. Muir, Nanotopographic surfaces with defined surface chemistries from amyloid fibril networks can control cell attachment, *Biomacromolecules*, 14 (2013) 2305-2316.

[5] R.S. Jacob, D. Ghosh, P.K. Singh, S.K. Basu, N.N. Jha, S. Das, P.K. Sukul, S. Patil, S. Sathaye, A. Kumar, Self healing hydrogels composed of amyloid nano fibrils for cell culture and stem cell differentiation, *Biomaterials*, 54 (2015) 97-105.

[6] D.M. Ryan, B.L. Nilsson, Self-assembled amino acids and dipeptides as noncovalent hydrogels for tissue engineering, *Polymer Chemistry*, 3 (2012) 18-33.

[7] G. Bhak, S. Lee, J.W. Park, S. Cho, S.R. Paik, Amyloid hydrogel derived from curly protein fibrils of α-synuclein, *Biomaterials*, 31 (2010) 5986-5995.

[8] S. Kyle, A. Aggeli, E. Ingham, M.J. McPherson, Production of self-assembling biomaterials for tissue engineering, *Trends in Biotechnology*, 27 (2009) 423-433.

[9] S.H. Waterhouse, J.A. Gerrard, Amyloid fibrils in bionanotechnology, *Australian Journal of Chemistry*, 57 (2004) 519-523.

[10] M.N. Bongiovanni, D.B. Scanlon, S.L. Gras, Functional fibrils derived from the peptide TTR1-cycloRGDfK that target cell adhesion and spreading, *Biomaterials*, 32 (2011) 6099-6110.

[11] R. Langer, J. Vacanti, Tissue engineering, *Science*, 260 (1993) 920-926.

[12] F.J. O'brien, Biomaterials & scaffolds for tissue engineering, *Materials Today*, 14 (2011) 88-95.

[13] B. Dhandayuthapani, Y. Yoshida, T. Maekawa, D.S. Kumar, Polymeric scaffolds in tissue engineering application: A review, *International Journal of Polymer Science*, 2011 (2011).

[14] B. Guo, P.X. Ma, Synthetic biodegradable functional polymers for tissue engineering: A brief review, *Science China Chemistry*, 57 (2014) 490-500.

[15] T.G. Kim, H. Shin, D.W. Lim, Biomimetic scaffolds for tissue engineering, *Advanced Functional Materials*, 22 (2012) 2446-2468.

[16] W. Wu, X. Feng, T. Mao, X. Feng, H.-W. Ouyang, G. Zhao, F. Chen, Engineering of human tracheal tissue with collagen-enforced poly-lactic-glycolic acid non-woven mesh: A preliminary study in nude mice, *British Journal of Oral and Maxillofacial Surgery*, 45 (2007) 272-278.

[17] C. Vepari, D.L. Kaplan, Silk as a biomaterial, *Progress in Polymer Science*, 32 (2007) 991-1007.

[18] G.H. Altman, F. Diaz, C. Jakuba, T. Calabro, R.L. Horan, J. Chen, H. Lu, J. Richmond, D.L. Kaplan, Silk-based biomaterials, *Biomaterials*, 24 (2003) 401-416.

[19] Y. Wang, H.-J. Kim, G. Vunjak-Novakovic, D.L. Kaplan, Stem cell-based tissue engineering with silk biomaterials, *Biomaterials*, 27 (2006) 6064-6082.

[20] B.D. Lawrence, M. Cronin-Golomb, I. Georgakoudi, D.L. Kaplan, F.G. Omenetto, Bioactive silk protein biomaterial systems for optical devices, *Biomacromolecules*, 9 (2008) 1214-1220.

[21] A.R. Murphy, D.L. Kaplan, Biomedical applications of chemically-modified silk fibroin, *Journal of Materials Chemistry*, 19 (2009) 6443-6450.

[22] V. Kearns, A. MacIntosh, A. Crawford, P. Hatton, Silk-based biomaterials for tissue engineering, *Topics in Tissue Engineering*, 4 (2008) 1-19.

[23] J.G. Hardy, T.R. Scheibel, Composite materials based on silk proteins, *Progress in Polymer Science*, 35 (2010) 1093-1115.

[24] D.G. Harkin, K.A. George, P.W. Madden, I.R. Schwab, D.W. Hutmacher, T.V. Chirila, Silk fibroin in ocular tissue reconstruction, *Biomaterials*, 32 (2011) 2445-2458.

[25] E.M. Pritchard, D.L. Kaplan, Silk fibroin biomaterials for controlled release drug delivery, *Expert Opinion on Drug Delivery*, 8 (2011) 797-811.

[26] E.S. Gil, B. Panilaitis, E. Bellas, D.L. Kaplan, Functionalised silk biomaterials for wound healing, *Advanced Healthcare Materials*, 2 (2013) 206-217.

[27] E.Y. Kim, N. Tripathy, J.Y. Park, S.E. Lee, C.-K. Joo, G. Khang, Silk fibroin film as an efficient carrier for corneal endothelial cells regeneration. *Macromolecular Research*, 2 (2015)189-195

[28] J.Y. Wong, J.D. Bronzino, D.R. Peterson, *Biomaterials: Principles and practices*, CRC Press, (2012).

[29] L. Meinel, S. Hofmann, V. Karageorgiou, C. Kirker-Head, J. McCool, G. Gronowicz, L. Zichner, R. Langer, G. Vunjak-Novakovic, D.L. Kaplan, The inflammatory responses to silk films *in vitro* and *in vivo*, *Biomaterials*, 26 (2005) 147-155.

[30] X. Hu, W. Lui, L. Cui, M. Wang, Y. Cao, Tissue engineering of nearly transparent corneal stroma, *Tissue engineering*, 11 (2005) 1710-1717.

[31] B.D. Lawrence, J.K. Marchant, M.A. Pindrus, F.G. Omenetto, D.L. Kaplan, Silk film biomaterials for cornea tissue engineering, *Biomaterials*, 30 (2009) 1299-1308.

[32] N. Bhardwaj, S.C. Kundu, Silk fibroin protein and chitosan polyelectrolyte complex porous scaffolds for tissue engineering applications, *Carbohydrate Polymers*, 85 (2011) 325-333.

[33] S. Yan, Q. Zhang, J. Wang, Y. Liu, S. Lu, M. Li, D.L. Kaplan, Silk fibroin/chondroitin sulfate/hyaluronic acid ternary scaffolds for dermal tissue reconstruction, *Acta biomaterialia*, 9 (2013) 6771-6782.

[34] W. Luangbudnark, J. Viyoch, W. Laupattarakasem, P. Surakunprapha, P. Laupattarakasem, Properties and biocompatibility of chitosan and silk fibroin blend films for application in skin tissue engineering, *Scientific World Journal*, 2012 (2012).

[35] K. Hu, Q. Lv, F. Cui, Q. Feng, X. Kong, H. Wang, L. Huang, T. Li, Biocompatible fibroin blended films with recombinant human-like collagen for hepatic tissue engineering, *Journal of Bioactive and Compatible Polymers*, 21 (2006) 23-37.

[36] A.W. Morgan, K.E. Roskov, S. Lin-Gibson, D.L. Kaplan, M.L. Becker, C.G. Simon, Characterisation and optimisation of RGD-containing silk blends to support osteoblastic differentiation, *Biomaterials*, 29 (2008) 2556-2563.

[37] C. Foss, E. Merzari, C. Migliaresi, A. Motta, Silk fibroin/hyaluronic acid 3D matrices for cartilage tissue engineering, *Biomacromolecules*, 14 (2012) 38-47.

[38] S. Ling, C. Li, J. Adamcik, Z. Shao, X. Chen, R. Mezzenga, Modulating materials by orthogonally oriented β-Strands: Composites of amyloid and silk fibroin fibrils, *Advanced Materials*, 26 (2014) 4569-4574.

[39] D.N. Rockwood, R.C. Preda, T. Yücel, X. Wang, M.L. Lovett, D.L. Kaplan, Materials fabrication from *Bombyx mori* silk fibroin, *Nature Protocols*, 6 (2011) 1612-1631.

[40] Y. Cao, B. Wang, Biodegradation of silk biomaterials, *International Journal of Molecular Sciences*, 10 (2009) 1514-1524.

[41] T. Arai, G. Freddi, R. Innocenti, M. Tsukada, Biodegradation of *Bombyx mori* silk fibroin fibres and films, *Journal of Applied Polymer Science*, 91 (2004) 2383-2390.

[42] M. Li, M. Ogiso, N. Minoura, Enzymatic degradation behavior of porous silk fibroin sheets, *Biomaterials*, 24 (2003) 357-365.

[43] K. Numata, P. Cebe, D.L. Kaplan, Mechanism of enzymatic degradation of beta-sheet crystals, *Biomaterials*, 31 (2010) 2926-2933.

[44] J. Brown, C.-L. Lu, J. Coburn, D.L. Kaplan, Impact of silk biomaterial structure on proteolysis, *Acta Biomaterialia*, 11 (2015) 212-221.

[45] R. Rajkhowa, B. Levin, S.L. Redmond, L.H. Li, L. Wang, J.R. Kanwar, M.D. Atlas, X. Wang, Structure and properties of biomedical films prepared from aqueous and acidic silk fibroin solutions, *Journal of Biomedical Materials Research Part A*, 97 (2011) 37-45.

[46] Y. Hu, Q. Zhang, R. You, L. Wang, M. Li, The relationship between secondary structure and biodegradation behavior of silk fibroin scaffolds, *Advances in Materials Science and Engineering*, 2012 (2012).

[47] S. Inoue, K. Tanaka, F. Arisaka, S. Kimura, K. Ohtomo, S. Mizuno, Silk fibroin of *Bombyx mori* is secreted, assembling a high molecular mass elementary unit consisting of H-chain, L-chain, and P25, with a 6: 6: 1 molar ratio, *Journal of Biological Chemistry*, 275 (2000) 40517-40528.

[48] K. Yamaguchi, Y. Kikuchi, T. Takagi, A. Kikuchi, F. Oyama, K. Shimura, S. Mizuno, Primary structure of the silk fibroin light chain determined by cDNA sequencing and peptide analysis, *Journal of Molecular Biology*, 210 (1989) 127-139.

[49] K. Tanaka, S. Inoue, S. Mizuno, Hydrophobic interaction of P25, containing Asn-linked oligosaccharide chains, with the HL complex of silk fibroin produced by *Bombyx mori*, *Insect Biochemistry and Molecular Biology*, 29 (1999) 269-276.

[50] L.B. Evnin, J.R. Vásquez, C.S. Craik, Substrate specificity of trypsin investigated by using a genetic selection, *Proceedings of the National Academy of Sciences of the United States of America*, 87 (1990) 6659-6663.

[51] Q. Lu, X. Hu, X. Wang, J.A. Kluge, S. Lu, P. Cebe, D.L. Kaplan, Water-insoluble silk films with silk I structure, *Acta Biomaterialia*, 6 (2010) 1380-1387.

[52] C.A. Bauer, Active centers of Streptomyces griseus protease 1, Streptomyces griseus protease 3, and α-chymotrypsin: Enzyme-substrate interactions, *Biochemistry*, 17 (1978) 375-380.

[53] R.L. Horan, K. Antle, A.L. Collette, Y. Wang, J. Huang, J.E. Moreau, V. Volloch, D.L. Kaplan, G.H. Altman, *In vitro* degradation of silk fibroin, *Biomaterials*, 26 (2005) 3385-3393.

[54] L. Ventura, G.T. de Jesus, G.C. de Oliveira, S.J. Sousa, Portable light transmission measuring system for preserved corneas, *Biomedical Engineering Online*, 4 (2005) 70.

[55] M. Gonzalez-Andrades, J. de la Cruz Cardona, A.M. Ionescu, C.A. Mosse, R.A. Brown, Photographic-based optical evaluation of tissues and biomaterials used for corneal surface repair: A new easy-applied method, *PloS One*, 10 (2015) e0142099.

[56] K. Webb, V. Hlady, P.A. Tresco, Relative importance of surface wettability and charged functional groups on NIH 3T3 fibroblast attachment, spreading, and cytoskeletal organisation, *Journal of Biomedical Materials Research*, 41 (1998) 422.

[57] T. Ruardy, J. Schakenraad, H. Van der Mei, H. Busscher, Adhesion and spreading of human skin fibroblasts on physicochemically characterised gradient surfaces, *Journal of Biomedical Materials Research*, 29 (1995) 1415-1423.

[58] K.L. Menzies, L. Jones, The impact of contact angle on the biocompatibility of biomaterials, *Optometry & Vision Science*, 87 (2010) 387-399.

[59] H.J. Jin, J. Park, V. Karageorgiou, U.J. Kim, R. Valluzzi, P. Cebe, D.L. Kaplan, Water-stable silk films with reduced β-sheet content, *Advanced Functional Materials*, 15 (2005) 1241-1247.

[60] S. Hofmann, C.W.P. Foo, F. Rossetti, M. Textor, G. Vunjak-Novakovic, D. Kaplan, H. Merkle, L. Meinel, Silk fibroin as an organic polymer for controlled drug delivery, *Journal of Controlled Release*, 111 (2006) 219-227.

[61] X. Li, H. Yang, H. Huang, T. Zhu, Cellcounter: Novel open-source software for counting cell migration and invasion *in vitro*, *BioMed Research International*, 2014 (2014).

[62] M. Brugmans, J.J. Cassiman, L. Vanderheydt, A.J. Oosterlinck, R. Vlietinck, H. Van Den Berghe, Quantification of the degree of cell spreading of human fibroblasts by semi-automated analysis of the cell perimeter, *Cytometry*, 3 (1983) 262-268

Chapter Six

Summary and Future work

6.1. Overview

Amyloid fibrils provide several advantages as a protein nanomaterial and have the potential to contribute significantly in future technologies. Previous work has identified crystallin proteins extracted from bovine [1], and fish eye lenses [2] as a cheap and readily available source for the self-assembly of amyloid PNFs; however little work has been done to realise their potential in bionanotechnology. Thus, the main focus of this research was to characterise crystallin PNFs obtained from hoki fish eye lenses in terms of their applicability to bionanotechnological applications, and to create a functional PNF-based nanoscaffold by incorporating enzymatically active components. The work was broadened to include whey amyloid PNFs and also to investigate the utilisation of PNFs for developing cell scaffolds.

Enzymes were chosen in this work for creating functionalised or active PNFs as many industrial enzymes are quite expensive and suffer from the serious drawback of poor stability and reusability. Additionally, for the successful application of enzymes, these catalysts need to be fully functional under, often harsh, processing conditions. To address some of these issues, PNFs are ideally suited as a readily functionalised nanoscaffold for enzyme immobilisation because of their innate strength, stability, and proteinaceous nature, and successful immobilisation of industrially important enzymes onto amyloid fibrils leads to the creation of cheap and readily available protein-based highly efficient matrices.

Stability and cytotoxicity studies were done to investigate the suitability of crystallin PNFs as a scaffold for industrial applications, followed by immobilisation of industrially relevant enzymes and subsequent characterisation. To investigate the potential applications of PNFs obtained from crude proteins, PNFs were either assembled onto surfaces (metal, and glass), or blended with other proteins to create novel PNF-based bionanomaterials. GOX- and β-gal-functionalised PNFs were adsorbed onto Au electrodes to develop PNF-based biosensing elements, and cyclic voltammetry was done. Active glass beads were created by immobilising β-gal to the surface-assembled whey PNFs to create nanosupports with increased surface area for biomolecule adsorption or immobilisation. Silk:PNF blend films were studied in order to obtain PNF-based scaffolds for cell growth and tissue engineering applications.

This was the first time that crystallin PNFs were characterised for their stability and bio-compatibility, followed by successful functionalisation and utilisation for developing PNF-based bionanotechnologies, such as crystallin PNF-based electrodes for glucose, and lactose analysis.

Previous work has used PNFs obtained from other proteins or peptides for developing GOX-based biosensing elements; however, co-immobilisation and utilisation of the dual-functionalised whey PNFs for developing PNF-based electrodes for lactose analysis is reported for the first time. The preliminary results for PNF-based scaffolds with applications in tissue regeneration look promising, although further work is necessary to optimise the use of amyloid PNFs in this way.

6.2. Characterisation and functionalisation of PNFs

To assess the biophysical aspects of PNFs before exploring them for potential applications, bovine insulin, crystallin, and whey amyloid fibrils were formed in solution, and studied for their stability under various industrial conditions, such as at a wide range of pHs, a variety of temperatures, in the presence of industrially related solvents, on exposure to proteolytic enzymes, and over long periods of storage (Chapter Two). ThT assays and TEM imaging were used to analyse amyloid fibrils under given conditions.

Under all the studied conditions, crystallin PNFs offered similar and often improved stability properties relative to amyloid fibrils obtained from whey, and bovine insulin proteins. Further to investigate the biosafety of crystallin PNFs, a cytotoxicity study using the Hec-1a cell line was done. Cell viability as measured by the CVS assay, showed no evidence of cytotoxicity. For long term stability studies of crystallin PNFs, the results obtained from IRM studies suggested that crystallin amyloid fibrils maintains their structural integrity over the time period of 36 months. This study provided evidence that crystallin PNFs can potentially be used as nanomaterials, particularly in applications such as biosensing and enzyme immobilisation, which require prolonged solvent contact and stability over a wide range of pHs and temperatures. Following stability studies, crystallin amyloid fibrils were further characterised for available surface residues and investigated as a novel nanosupport for immobilising enzymes (Chapter Three).

Initially, a GA-based crosslinking method as described by Pilkington *et al*. (2010) was studied for crosslinking GOX to crystallin PNFs [3], but as the established method did not result in successful immobilisation, a number of alternative methods were investigated including: using different lysine group-based crosslinkers, TCEP-based reduction, and sodium periodate-based oxidation of crystallin PNFs (Chapter Three, **Table 3.5**). Different assays were used for characterising available amino groups such as, the OPA, and the ninhydrin assay for amino group determination, Ellman's assay for detecting the presence of sulfhydryl groups, and the DNPH assay for carbonyl group estimation. After successfully characterising CPNFs for available amino residues, different immobilisation methods were studied to immobilise enzymes onto the crystallin PNFs, such as physical adsorption and covalent crosslinking. Different crosslinkers (GA, FA, MG, Sulfo-SMCC), reaction orders, and conditions were investigated to obtain active or functionalised crystallin PNFs. GOX-functionalised crystallin PNFs were successfully obtained *via* both physical adsorption and amine-thiol covalent linking (*via* Sulfo-SMCC reaction, **Table 3.5**).

The oxidised CPNFs were also successfully functionalised with GOX, and β-gal *via* indirect reductive amination, in the presence of reducing agent (STAB) **(Table 3.5)**. However, due to reproducibility issues, GA-based crosslinking was investigated further to obtain active crystallin PNFs with improved enzymatic stability and reusability (Chapter Four).

6.3. Functionalisation of PNFs

Building on the observations made (Chapter Three) attention was focussed on developing a reliable crosslinking method to obtain functionalised crystallin PNFs. This was achieved by using simple, versatile GA-based activation of oxidised crystallin PNFs, followed by incubation with biomolecules (Chapter Four). To understand the potential of crystallin PNFs to act as a versatile nanoscaffold, a diverse range of industrially relevant enzymes including GOX, β-gal, pectinase, α-amylase, and laccase were studied. Gel electrophoresis (SDS-PAGE) was done to confirm the immobilisation of enzymes, followed by the enzyme-specific activity assay (*Appendix B*) to determine the extent of immobilisation. TEM analysis of the functionalised PNFs was also done to visually confirm the presence of immobilised enzymes, and to ensure that the crosslinking reaction had no adverse impact on the morphology of PNFs.

For all the enzymes investigated in this work, covalent crosslinking of enzymes onto GA-activated oxidised crystallin PNFs resulted in better immobilisation efficiencies relative to the non-covalent immobilisation (physical adsorption). Further to study the impact of immobilisation on the stability of the enzyme, thermostability study using α-amylase functionalised crystallin PNFs was done at 40, 55, and 75 °C. Free α-amylase prepared by dissolving the enzyme in PBS (pH 7.4) to have the same activity as the α-amylase-functionalised PNFs was used as a control sample. The results showed that α-amylase immobilised to crystallin PNFs *via* covalent crosslinking had better stability relative to the free enzyme at all the selected temperatures. The results from the re-usability studies showed that α-amylase-functionalised crystallin PNFs retained ~80% of its activity when stored at 4 °C for at least 30 days without any inconsistency in results. In contrast, the free enzyme had complete activity loss within 16 days.

The immobilisation method developed in this research suggests that crystallin PNFs can act as a versatile scaffold for immobilising biomolecules. All the enzymes studied in this work were successfully immobilised onto crystallin PNFs and no significant loss in the activity of immobilised enzymes was observed. However, immobilisation efficiency, and retained activity differed between the different enzymes used, suggesting that for individual biomolecules, optimisation of the method is required to ensure effective immobilisation.

6.4. Potential applications and proof of concepts

The second main objective of this work was to develop PNF-based bionanotechnologies. Thus, PNFs were further investigated to develop PNF-based nanomaterials, as assembling amyloid fibrils on surfaces could potentially allow for a bottom-up approach to functional bionanomaterial design [4, 5].

6.4.1. Biosensing

GOX- and β-gal-functionalised PNFs were adsorbed onto the gold electrodes to create PNF-based biosensing elements (Chapter Five, Part A). The electrochemical behaviour of the modified electrodes was then quantified in the presence of analytes (500 mM of glucose and lactose), using FcOH as a mediator in solution. For both GOX and β-gal modified electrodes, the anodic current was seen to be amplified in the presence of analytes (glucose and lactose for GOX and β-gal modified electrodes respectively). These results corroborated the SDS-PAGE and enzyme-specific activity assays, confirming that both GOX and β-gal can be successfully immobilised onto the PNFs.

To study the influence of functionalised crystallin PNFs on current amplification the electrode response was measured for both the enzyme only modified Au electrodes, and the enzyme functionalised crystallin PNFs modified electrodes in the presence of excess analyte. For GOX-functionalised crystallin PNFs modified electrode an increase in current response was observed relative to the adsorbed GOX only electrode, suggesting improved sensitivity of the electrodes in the presence of PNFs. However, no significant increase in electrochemical response was detected for the electrode modified with β-gal-functionalised crystallin PNF relative to the β-gal (enzyme-only) modified electrode. This could be due to the lower immobilisation efficiency of β-gal-functionalised PNFs as compared to the GOX-functionalised amyloid PNFs. Additionally, in contrast to the GOX electrochemical reaction, the β-gal electrochemical reaction was not directly dependent on the immobilised β-gal activity, but also on the dissolved GOX activity, and observed difference in current amplification could be due to the diffusional limitations.

To further improve the sensitivity of the β-gal active PNF-based electrode, co-immobilisation of GOX and β-gal was considered. Co-immobilisation improves electron transfer between the redox center of the enzyme and electrode due to the localised high concentrations of the intermediates, thereby resulting in faster response times and often higher sensitivity [6]. To explore if the two enzymes could be bound to the same PNFs scaffold and function in a co-operative manner, GOX and β-gal were co-immobilised onto the whey PNFs *via* the GA-based crosslinking reaction. The results obtained from amino group-based assays (section 3.4.1, Chapter Three), suggested the presence of available lysine groups onto the surface of whey PNFs, which can be potentially used for crosslinking. Thus, to confirm if simple methodology developed for crystallin PNFs can be applied to other PNFs or similar structures with available amino residues for crosslinking, whey PNFs were studied for dual-functioanalisation work. Dual-functionalised PNFs were then used to evaluate if the presence of both enzymes on the same nanoscaffold improved electrode sensitivity for lactose analysis.

Current amplification achieved with dual-functionalised whey PNFs modified electrodes was compared to enzyme (GOX+β-gal) only modified electrode, where the enzyme sample used was diluted in PBS (pH 7.4), to have the same activity in solution as the dual-functionalised whey PNF sample used. The dual-functionalised PNFs modified electrode showed improved current amplification as compared to the enzyme only modified electrodes.

Successful development of PNF-based electrodes provides evidence that functionalised PNFs retain their activity even after being adsorbed onto the electrodes (Au surface), and also have a positive impact on the sensitivity of biosensing elements. Although an increase in current amplification was observed for all the samples studied in the presence of PNFs, the concentration of PNFs used for modifying electrodes was low (1.5 mg/mL to 2 mg/mL) due to the blocking behaviour of PNFs. This blocking behaviour has also been reported previously for similar bionanostructures, such as FF peptide nanowires [7].

Thus, work needs to be done to improve the sensitivity of the PNF-based electrodes to realise the full potential of the available surface area for enzyme immobilisation. Previous work in our lab has demonstrated that whey PNFs can be modified with conducting polymers [8]. To improve the sensitivity of the lactose electrode (dual-functionalised PNF-based electrode) and to overcome the blocking behaviour of PNFs, modifying whey PNFs with conducting polymers could be considered.

6.4.2. Surface-assembly

Previous work by Raynes (2012) has shown that insulin PNFs can be attached onto a glass surface *via* template-directed growth. To investigate if surface-assembly is a generic property of PNFs, and to establish that a simple methodology developed by Raynes (2012) [9] for creating surfaces with self-assembled insulin PNFs is applicable to the PNFs obtained from other protein sources, a surface-assembly study was done for both crystallin and whey PNFs. Different methods were investigated for surface-assembly studies, such as with and without chemical derivatisation, addition of glass beads at different stages of the fibrillation process, and template-directed or direct surface-assembly, followed by ThT assay and confocal microscopy.

Whey and crystallin amyloid fibrils were successfully assembled on the surface of 5 mm and micro-glass beads. This is the first time that direct-surface assembly of amyloid fibrils was investigated. High ThT readings were obtained for the bead samples incubated with protein solutions during the fibrillation process (while heating) suggesting that crystallin and whey amyloid fibrils can be surface-assembled *via* both template and direct surface-assembly methods. The images obtained by microscopy (confocal microscopy) showed a reasonably complete surface coverage of the surface-assembled PNFs **(Figure 5.20)**. To investigate the impact of surface-assembled whey amyloid fibrils on the immobilisation efficiency and enzyme activity, β-gal was immobilised to the surface-assembled whey amyloid fibrils *via* GA crosslinking (Chapter Five, Part B), to create a PNF-based active bionanomaterial. A gain in immobilised β-gal was observed in the presence of PNFs relative to the enzyme immobilised to the glass surface samples. The surface immobilised β-gal samples were further analysed for activity over repetitive uses in order to investigate the effect of the PNFs on the surface of the glass beads.

β-Gal activity as determined by the ONPG assay showed that the glass beads with the surface-assembled whey PNFs retained significantly more activity after three consecutive uses relative to the control bead samples. Glass beads or other materials with similar surface chemistry, such

as cellulose-based materials are widely used in industry, and have been used in applications in which a range of enzymes have been immobilised to them [10, 11].

Reusability studies of the surface-assembled active PNFs suggest that surface-assembled PNFs could provide more surface area and a more stable environment, leading to better immobilisation and improved activity of the immobilised enzymes.

6.4.3. Tissue engineering

There have been a limited number of previous studies on the use of amyloid fibrils obtained from peptides and other proteins, as a scaffold to promote cell adhesion and proliferation studies [12, 13]. Silk fibroin offers a number of advantages to current tissue regeneration materials and has been extensively investigated as a scaffolding material for tissue engineering applications. In this work, PNFs were blended with silk fibroin to create a novel composite biomaterial with potential applications in tissue engineering. Despite the various advantages, the blending of silk fibroin materials with PNFs was investigated to improve the functional shortcomings, such as shortage of cell specific-binding sites, and limited growth factor-adsorbing capacity, while taking advantage of the structural benefits from using silk fibroin. Silk-protein blend films with crystallin and whey proteins were also studied as a control.

In this work, an initial study was carried out to investigate the suitability of PNF-silk films for tissue engineering applications. Composite films were characterised using SEM, followed by proteolytic degradation, wettability, and optical transparency studies. The results from degradation studies suggest that PNF-blend films are biodegradable, and that the degradation rate of the silk-blend films is dependent on the film composition, and could be matched to the potential application by tuning the film composition. Blend films had 85-92% transmittance over the visible range, and can be used for tissue engineering applications, in which transparency is sought after, such as corneal regeneration. Cell growth and proliferation studies were also done using fibroblast cell line. The preliminary results showed that PNFs obtained from crude protein sources are biocompatible, and cells showed better adhesion and proliferation in the presence of PNFs, relative to the silk-only or silk-protein blend films.

6.5. Future work

This work has shown that amyloid fibrils obtained from crude protein sources can act as a versatile nanoscaffold by increasing the surface area for biomolecule immobilisation. The intrinsic surface chemistry of the amyloid fibrils enabled functionalisation of PNFs with enzymes *via* covalent crosslinking and physical adsorption methods. The results from cell viability studies alleviates some concerns about the potential toxicity of amyloid fibrils obtained from non-amyloidogenic crude proteins. The results from biosensing, surface-assembly, and cell growth studies provide evidence that PNFs can be utilised for the creation of functional bionanomaterials. Future work should implement industrial applications of the functionalised PNFs to develop reusable nanomaterials.

Initial research into the creation of PNF-assembled bead system using micro-sized beads was commenced, but analysis and handling of the microbeads proved more difficult than the 5 mm glass beads, therefore future work is needed to transfer the technology to the micro system, which could further improve enzyme packaging, and catalytic efficiency of the reaction. For tissue engineering applications, future cell viability (live-dead assays), and proliferation studies using different cell lines are needed to confirm the observed results.

To understand the end product formation of films with PNFs, proteolytic degradation of PNFs needs to be studied for longer durations, using SDS-PAGE and SEM for visually confirming the degradation products and structural topography of degraded films with PNFs, respectively. The finding that PNFs improve fibroblast adhesion was interesting, and further studies will be carried out to investigate whether this was due to increased surface roughness or the presence of cell binding sites on PNFs. Building on the protein immobilisation platform developed in this thesis, there is also the opportunity to modify PNFs with growth factors. These studies, along with mechanical analysis of the materials formed, would increase the potential for PNFs obtained from crude protein sources to be utilised in biomedical engineering.

6.6. References

[1] M. Garvey, S. Gras, S. Meehan, S. Meade, J. Carver, J. Gerrard, Protein nanofibres of defined morphology prepared from mixtures of crude crystallins, *International Journal of Nanotechnology*, 6 (2009) 258-273.

[2] J. Healy, K. Wong, E.B. Sawyer, C. Roux, L. Domigan, S.L. Gras, M. Sunde, N.G. Larsen, J. Gerrard, M. Vasudevamurthy, Polymorphism and higher order structures of protein nanofibres from crude mixtures of fish lens crystallins: Toward useful materials, *Biopolymers*, 97 (2012) 595-606.

[3] S.M. Pilkington, S.J. Roberts, S.J. Meade, J.A. Gerrard, Amyloid fibrils as a nanoscaffold for enzyme immobilisation, *Biotechnology Progress*, 26 (2010) 93-100.

[4] S. Scanlon, A. Aggeli, Self-assembling peptide nanotubes, *Nano Today*, 3 (2008) 22-30.

[5] R.J. Williams, R.J. Mart, R.V. Ulijn, Exploiting biocatalysis in peptide self-assembly, *Peptide Science*, 94 (2010) 107-117.

[6] L. Betancor, H.R. Luckarift, Co-immobilised coupled enzyme systems in biotechnology, *Biotechnology and Genetic Engineering Reviews*, 27 (2010) 95-114.

[7] L.Sasso, I. Vedarethinam, J. Emneus, W.E Svendsen, J. Castillo-Leoon, Self-assembled diphenylalanine nanowires for cellular studies and sensor applications, *Journal of Nanoscience and Nanotechnology*, 12 (2012) 3077-3083.

[8] L. Sasso, S. Suei, L. Domigan, J. Healy, V. Nock, M. Williams, J. Gerrard, Versatile multi-functionalisation of protein nanofibrils for biosensor applications, *Nanoscale*, 6 (2014) 1629-1634.

[9] J.K. Raynes, *Immobilising biomolecules on amyloid fibrils for biotechnology applications*, PhD Thesis, University of Canterbury (2012).

[10] J. Gomez, A. Bodalo, E. Gomez, J. Bastida, A. Hidalgo, M. Gómez, Immobilisation of peroxidases on glass beads: An improved alternative for phenol removal, *Enzyme and Microbial technology*, 39 (2006) 1016-1022.

[11] M. Hartmann, X. Kostrov, Immobilisation of enzymes on porous silicas-benefits and challenges, *Chemical Society Reviews*, 42 (2013) 6277-6289.

[12] S.L. Gras, A.K. Tickler, A.M. Squires, G.L. Devlin, M.A. Horton, C.M. Dobson, C.E. MacPhee, Functionalised amyloid fibrils for roles in cell adhesion, *Biomaterials*, 29 (2008) 1553-1562.

[13] N.P. Reynolds, M. Charnley, R. Mezzenga, P.G. Hartley, Engineered lysozyme amyloid fibril networks support cellular growth and spreading, *Biomacromolecules*, 15 (2014) 599-608.

Chapter Seven

Experimental

7.1. General methods and materials

Unless otherwise stated, chemicals, reagents, and solvents were purchased from Sigma-Aldrich or Thermo Fischer Scientific, and were of analytical grade. Whey protein isolate 895 (WPI) was generously supplied by Fonterra, New Zealand. *Macruronus novaezelandiae* (Hoki), fish eye lenses were obtained from the local fish suppliers, Christchurch, New Zealand.

Unless otherwise stated, enzymes were manipulated on ice or at 4 °C, and for enzymatic assays BioRad SmartSpec Plus Spectrophotometer or a Labtech FLUOstar OPTIMA plate reader was used. Centrifugation was done using an Eppendorf 5810R on a small scale (< 2 mL) using an F-45-30-11. For medium and large scale centrifugation a Thermo Scientific Sorvall RC6 plus centrifuge was used with either a SS-34 or FiberLite F10-6x500y rotor, respectively. pH measurements were made using an UltraBasic 10 benchtop pH meter, fitted with a high performance glass body pH/Tris electrode, obtained from Denver Instrument Co. Polyacrylamide gel electrophoresis (SDS-PAGE), was routinely run using a NuPAGE gel run system from Thermo Fischer Scientific. All buffers and solutions were prepared in filtered water using a Vacuubrand 2C (John Morris Scientific, Chatswood, NSW, Australia).

7.1.1. Sodium dodecyl sulfate polyacrylamide gel electrophoresis (SDS-PAGE)

SDS-PAGE was run to confirm the purity of proteins/enzymes, and also to assess the extent of crosslinking and proteolytic degradation of PNFs/proteins. SDS is an anionic detergent, meaning that when dissolved its molecules have a net negative charge, and binds non-covalently to protein. The negative charge contributes to the linearisation of the polypeptide chain by electrostatic repulsion and consecutively allows for electrophoretic separation of SDS coupled proteins in an electric field.

Regular analysis of protein samples used precast Invitrogen Bolt® 4-12% Bis-Tris gels with 10 or 15 wells. Samples were mixed with sample buffer and reducing agent (DTT to reduce disulphide bonds in the sample) to give a total of ~5 ng/μL of protein. Samples were then incubated at 90 °C for 3-5 min and then briefly centrifuged before being loaded into the gel. An Invitrogen Novex Sharp pre-stained protein standard was also loaded into the gel. Electrophoresis was carried out at room temperature at a constant voltage of 165 V for ~35 min. The gel was then immersed in stain and microwaved for ~30 sec before placing on a Bio-Rad Ultra Rocker for 15-30 min. The gel was then immersed in destain and placed on the Bio-Rad Ultra Rocker until appropriately destained. The gel was viewed and photographed using a SYNGENE GelDoc. All the solutions used for SDS-PAGE are summarised in **Table 7.1.**

Table 7.1. *Details of SDS-PAGE gel solutions:*

Reagent	Details
MES-SDS running buffer, [pH 7.4]	50 mM MES 50 mM Tris base 0.1% SDS 1 mM EDTA
Coomassie R-250	2.5 ng/L Coomassie R-250 10% (v/v) glacial acetic acid 45% (v/v) methanol 45% (v/v) dH_2O
Destaining solution	40% (v/v) ethanol 10% (v/v) acetic acid 60% (v/v) dH_2O

7.1.2. Thioflavin T (ThT) assay

ThT dye is an amyloid protein specific dye [1]. The increase of ThT fluorescence was used to monitor fibrillation of proteins, using methods adopted from Raynes (2012) [2]. ThT working stain was made up in ThT buffer as detailed in **Table 7.2.** This was filtered and stored in the dark for up to a maximum of two days. 180 µL of ThT working stain was added to the 96-well flat, transparent glass plate containing 20 µL of sample. After 6 min of incubation at room temperature, ThT fluorescence was measured using a BMG Labtech FLUOstar Optima plate reader with excitation/emission filters of 450 and 485 nm, respectively (LeVine III 1999) [3]. Three replicates of each sample were measured.

Table 7.2. *Details of ThT assay:*

Reagent	Details
ThT buffer	50 mM Tris base 100 mM NaCl [pH 7.5],
ThT dye	2.5 mM in ThT buffer Filter through 0.2 µm
ThT working stain	176 µl of ThT buffer 4 µl of ThT dye

7.1.3. Transmission electron microscopy (TEM)

Formvar-coated copper grids (200 mesh) (ProSciTech) were coated with protein samples and negatively stained with a 2% uranyl acetate solution. TEM micrographs (14,000 x and 89,000 x magnification) were obtained on a Morgagni 268D TEM (FEI Company, Oregon, USA) operating at 80 kV, fitted with a 40 µm objective aperture. Micrographs were representative of 3 images chosen as being an overall representation of the entire sample. Many thanks to Jackie Healy (University of Canterbury) for her efforts to obtain TEM micrographs.

7.1.4. NanoDrop protein determination

Two µL of protein solution was pipetted onto a Thermo Fisher Scientific NanoDrop 1000 after being blanked against the appropriate buffer. Absorbance measurements were carried out at in triplicate at 280 nm. Proteins absorb light at 280 nm due to aromatic amino acids, such as tryptophan and tyrosine. The number of aromatic residues in a protein's sequence gives rise to the extinction coefficient of a protein, which was predicted using the web-based program "ExPASy" [4]. For protein mixtures/crude proteins an absorbance coefficient of 1.0 M-1 cm-1 was used. After calibration of the machine with water and blanking with respective buffer, the absorbance of 2 µL of protein solution was measured. Measurements were undertaken at 280 nm in triplicate. Through application of Beer's law the concentration of protein was calculated automatically by the NanoDrop software.

7.1.5. Bradford assay for determining protein concentration

Bradford assay was done using the Bio-Rad protein assay reagent and method based on the Bradford dye-binding procedure [5]. Bio-Rad reagent was diluted with nanopure water in 1:4 ratio for obtaining working solution. 10 µL of appropriately diluted protein solution was added to 200 µL of Bio-Rad protein working solution, mixed thoroughly and incubated at room temperature for 5 min exactly. The absorbance of the solutions was measured at 595 nm against a blank, consisting of 10 µL buffer/dH_2O and 200 µL of Bio-Rad protein assay reagent. A standard curve was generated using BSA in a concentration range from 0 to 0.2 mg/mL.

7.2. Amyloid fibrillation

Bovine insulin, WPI, and crude crystallin proteins were used for the formation of amyloid fibrils in this work.

7.2.1. Insulin PNFs

Insulin amyloid fibrils were formed using in-house methods modified from Nielsen *et al*. (2001) [6]. Bovine insulin powder was dissolved at a concentration of 5.8 mg/mL (1 mM) in insulin fibril incubation buffer as detailed in **Table 7.3**. The insulin solution was then incubated at 60 ºC for at least 24 h. The samples were then analysed for amyloid fibrils using ThT (section 7.1.2), and TEM (section 7.1.3).

Table 7.3. *Details of insulin fibril buffer:*

Buffer	Contents
Insulin fibril buffer	25 mM HCl 100 mM NaCl Sterile filter [pH 1.6]

7.2.2. Whey PNFs

A 10 mg/mL solution of WPIs in Milli-Q water was adjusted to pH 1.6 using 1M HCl. The solution was stirred at 4 °C overnight and then incubated at 80 °C for 22 h [7].

After heat incubation, the samples were cooled down on an ice bath for 10 min and finally stored at room temperature for 7 days to allow for fibril formation. The samples were then analysed for amyloid fibrils using ThT (section 7.1.2), and TEM (section 7.1.3).

7.2.3. Crystallin PNFs

For crystallin PNFs, crystallin proteins were extracted from fish eye lenses in extraction buffer **(Table 7.4)**, using an IKA® Ultra Turrax® Tube disperser with Tube ST-20. After homogenisation was complete, the sample was centrifuged for 30 min at 10,000 rpm, the supernatant collected and protein concentration estimated using the NanoDrop (section 7.1.4) with an extinction coefficient of 1. For detailed information on crystallin fibrillation process see *Appendix G*. Briefly, the crude crystallin stock solution was diluted to 10 mg/mL into pre-heated 25% n-propanol to 80 °C, pH 3.8. The sample was incubated for 1 h at 80 °C in a heating block and then centrifuged at 12,000 rpm for 2 min and the supernatant collected and heated overnight at 80 ºC. The sample was then left at room temperature for at least three days for the amyloid fibrils to assemble, and analysed for amyloid fibrils using ThT (section 7.1.2), and TEM (section 7.1.3).

Table 7.4. *Details of crystallin extraction buffer:*

Buffer	Contents
Crystallin extraction buffer	50 mM Tris base 1 mM DTT 5 mM EDTA Sterile filter [pH 7.5]

7.3. Stability studies

To study the stability of PNFs, pre-formed fibrils (section 7.2) were subjected to the selected conditions by resuspending in an appropriate buffer/solvent. ThT assay was used to indicate the presence of fibrils, and TEM was then used to visually confirm the presence of fibrils.

7.3.1. Effect of solvents

To study the influence of solvents onto the pre-formed PNFs, PNFs prepared as detailed in section 7.2 were collected by centrifugation at 12,500 rpm for 10 min, and resuspended in the test solvent **(Table 7.5)**. PNFs were incubated in the test solvent for time period of 3 h. Presence of fibrils was assessed by the ThT assay (section 7.1.2) at time = 0, and after 3 h of incubation at room temperature, followed by TEM analysis (section 7.1.3).

7.3.2. Effect of pH

To study the impact of pH, PNFs prepared as detailed in section 7.2 were collected by centrifugation at 12,500 rpm for 10 min, and resuspended in appropriate buffers at required pH **(Table 7.5)**. Presence of fibrils was assessed by the ThT assay (section 7.1.2) immediately and also after 24 h of incubation at room temperature followed by TEM analysis (section 7.1.3).

Table 7.5. *Details of various buffers and solvents used for stability studies:*

Solutions	Details
Acetate buffer	100 mM sodium acetate, [pH 2.0-4.0]
Phosphate buffer	100 mM sodium phosphate, [pH 6-7.2]
HEPES(4-(2-hydroxyethyl)-1-piperazineethanesulfonic acid) buffer	100 mM HEPES, [pH 8.0-9.0]
Borate buffer	100 mM sodium borate, [pH 11.0]
Methanol (MeOH)	100% MeoH
Ethanol (EtOH)	100% EtOH
Iso-propanol (iPrOH)	100% iPrOH
Dimethyl sulfoxide (DMSO)	100% DMSO
Acetonitrile (ACN)	100% ACN

7.3.3. Effect of temperature

For temperature stability, pre-formed fibrils (section 7.2) were incubated at selected temperatures (-20 °C, 4 °C, 22 °C, 37 °C and 80 °C) for the time period of 24 h and aliquots were taken after 3 h, 6 h, 12 h and 24 h. The presence and morphologies of amyloid PNFs were confirmed using the ThT assay (section 7.1.2) and TEM imaging (section 7.1.3).

7.3.4. Proteolytic degradation of amyloid PNFs

PNFs prepared as detailed in section 7.2 were collected by centrifugation at 12,500 rpm for 10 min, and resuspended in required buffers. For trypsin and Proteinase K hydrolysis, the pH of the fibril solutions was adjusted to 7.5. For pepsin it was kept at pH 1.6. The total volume was adjusted with distilled water to yield a final protein concentration of ~10 mg/mL. Enzymes were added in an enzyme:fibril ratio of 1:20 (w/w). The fibril samples were incubated with the enzymes for 3 h, taking 200 µL aliquots at various time intervals (0, 20, 60, 180 min).

Proteinase K and trypsin hydrolysis were terminated by adjustment to pH 1-2 with 1 M HCl, and pepsin digestion through adjustment to pH 7 with 100 mM $NaHCO_3$. The presence and morphologies of amyloid PNFs were confirmed using the ThT assay (section 7.1.2) and TEM imaging (section 7.1.3). Enzyme stock solutions were prepared (10 mg/mL) by dissolving 20 mg/mL enzyme in appropriate buffer **(see Table 7.6)**. Diluted 1:1 with 100% glycerol, aliquoted into 200 µL, snap frozen and stored at -20 °C.

Table 7.6. *Fibril proteolysis buffers:*

Solutions	Contents
Trypsin	50 mM Tris base 100 mM NaCl Sterile filter [pH 7.5]
Pepsin	10 mM HCl 100 mM NaCl Sterile filter [pH 3-4]
Proteinase K (PK)	50 mM Tris base 100 mM NaCl Sterile filter [pH 7.5]

7.4. Cytotoxicity studies

Due to the association of amyloid PNFs with neurodegenrative diseases, the potential toxicity of crystallin PNFs was investigated using Hec-1a cells.

7.4.1. Hec-1a cell line-Subculturing

Hec-1a cells (passage 10) were cultured in Minimum Essential Medium (MEM) (GIBCO®, Carlsbad, CA, USA) with GlutaMAX™ (1x), penicillin (100 U/mL), streptomycin (100 mg/mL), and 5% fetal bovine serum (FBS). Cells were washed with sterile PBS and harvested in trypsin EDTA (1x) for 10-15 min. The cells were diluted 1:1 in PBS (pH 7.4) and centrifuged at 1,500 rpm for 5 min. The supernatant was replaced and the pellet taken up in 10 mL of medium. Viable cell density was determined using a hemocytometer. The Hec-1 cells were diluted to 4 x 108 cells/mL in media and used to seed 12-well plates (500 µL/well) for 48 h at 37 °C (80% confluence).

7.4.2. Treatment

Medium was removed from the seeded Hec-1a cells prior to treatment. Each treatment consisted of 500 µL of sample protein at ~10 mg/mL in PBS (final concentration ~5 mg/mL) mixed with 500 µL of medium (MEM) respectively. Cells were incubated at 37 °C for 24 h. At least three replicates for each condition were measured. The control used was cells + medium + buffer (PBS). Further, to assess if cells use protein as a nutrient source, cells were pre-incubated in the absence of FBS overnight to starve them prior to the addition of treatments.

7.4.3. Crystal violet assay

The medium of the treated cells was discarded and 300 µL of crystal violet stain was added to each of the 12 wells. After staining for 15 min the excess stain was thoroughly washed off with distilled water until completely removed. The plates were dried before re-solubilising the stained cells in 1 mL of 2% SDS solution per well. After solubilising the dye-containing cells, the absorbance of the solutions was measured at 570 nm on a Labtech FLUOstar OPTIMA plate reader (BMG Labtech GmbH, Offenburg, Germany).

7.5. Infrared (IR) microscopy studies

After storage in the original solvent for long periods of time (up to 37 months), the fibril samples were washed in water 3 times by centrifugation (10,000 rpm for 10 min each wash) and concentrated to a final concentration > 100 mg/mL. Infrared microspectroscopy was carried out by Ljiljana Puskar, Mark J. Tobin, and Celine Valery at the Australian Synchrotron, using the IRM beamline which combines a Bruker V80v Fourier transform infrared (FTIR) spectrometer and a Hyperion 2000 IR microscope with a liquid nitrogen cooled narrow-band mercury cadmium telluride (MCT) detector.

A small amount of washed fibril sample was placed between two diamond windows of a ThermoFisher (Waltham, MA, USA) micro compression cell and the data collected in transmission mode with a microscope aperture defining a measurement area of 5 μm x 5 μm on the sample. The supernatant from the last wash was used as the background. Each spectrum was collected in the mid-infrared spectral range (4000–700 cm^{-1}) with 64 co-added scans and spectral resolution of 4 cm^{-1}. Bruker OPUS 6.5 software was used for data collection and Bruker OPUS 7.2 for the spectral analysis and for the calculation of the second derivative using a 9 to 15 point Savitzky-Golay filter. Many thanks to Celine Valery and Luigi Sasso for the help with analysing the data.

7.6. Characterisation of PNFs and assays

7.6.1. *o*-Phthaldialdehyde (OPA) assay

The OPA assay was carried out using in-house methods, based on those of Roth (1971) [8]. The OPA solution was prepared as detailed in **Table 7.7**. OPA solution (200 μL) was added to 20 μL of the sample of interest, in a 96 microwell plate and kept for five min in dark conditions. The absorbance of the sample was then read at a wavelength of 340 nm using a BioRad SmartSpec Plus Spectrophotometer.

Table 7.7. *Details of OPA assay reagent:*

Reagent	Details
OPA Buffer	25 mL of 100 mM sodium borate
OPA solution	40 mg OPA reagent in 1mL of methanol 100 μL of mercaptoethanol Final volume adjusted to 50 mL with dH_2O

7.6.1.1. OPA standard curve

A standard curve for the OPA assay was created using lysine, dissolved in nanopure H_2O at concentrations from 0-200 μM, using the protocol described in section 7.6.1. All samples were assayed in triplicate.

7.6.1.2. OPA assay of samples

The OPA assay was carried out on samples containing either native protein or amyloid fibrils using the protocol described in section 7.6.1. A control sample containing the fibril formation buffer was also assayed. All samples were assayed in triplicate.

7.6.2. Ninhydrin assay

The ninhydrin assay was carried out using in-house methods [9]. Ninhydrin buffer was prepared by a 1:3 mixture of lithium acetate buffer and ninhydrin solution (**Table 7.8**), and stored, covered with foil, at 4 °C. The ninhydrin buffer was added to diluted protein samples in a 1:1 ratio, along with a blank sample containing PBS. The samples were heated at 90 °C for ten min, vortexed after 5 min and then placed back to heat.

The samples were then cooled on ice. 300 µL of 95% (v/v) ethanol was then added to 300 µL of each sample and vortexed, followed by the absorbance measurement of the sample at a wavelength of 570 nm. 250 µL of the sample was added to the 96 microwell plate, and read at 570 nm, using a BioRad SmartSpec Plus Spectrophotometer.

Table 7.8. *Details of ninhydrin assay reagent:*

Reagent	Details
Ninhydrin buffer	4 M Lithium acetate buffer [pH 5.2, adjusted with acetic acid]
Ninhydrin solution	0.01 M ninhydrin 0.01 hydridantin 75% (v/v) DMSO

7.6.2.1. Ninhydrin standard curve

A standard curve for the ninhydrin assay was created using lysine, dissolved in dH_2O at concentrations from 0 – 200 µM, using the protocol described in section 7.6.2. All samples were assayed in triplicate.

7.6.2.2. Ninhydrin assay of samples

The ninhydrin assay was carried out on samples containing either native protein or amyloid PNFs using the protocol described in section 7.6.2. Samples were diluted with 95% ethanol when needed to obtain an absorbance below 1.0. A control sample containing the fibril formation buffer was also assayed. All samples were assayed in triplicate.

7.6.3. Ellman's assay

Ellman's was carried out using in-house methods, based on those of Riddles *et al*. (1983) [10]. Ellman's solution was prepared as detailed in **Table 7.9**. Ellman's solution (250µL) was added to 50 µL of the sample of interest, in a 96 microwell plate and kept for 15 min in THE dark conditions. The absorbance of the sample was then read at a wavelength of 412 nm using a BioRad SmartSpec Plus Spectrophotometer.

Table 7.9. *Details of Ellman's assay reagent:*

Reagent	Details
Ellman's buffer	100 mM sodium phosphate, [pH 8.0]
Ellman's solution	4 mg/mL of Ellman's reagent in Ellman's buffer

7.6.3.1. Ellman's standard curve

A standard curve for Ellman's assay was created using cysteine, dissolved in dH_2O at concentrations from 0 – 200 µM, using the protocol described section 7.6.3. All samples were assayed in triplicate.

7.6.3.2. Ellman's assay of samples

Ellman's assay was carried out on samples containing either native protein or amyloid fibrils using the protocol described in section 7.6.3. A control sample containing the fibril formation buffer was also assayed. All samples were assayed in triplicate.

7.6.4. TCEP reduction of the crystallin PNFs

Crystallin amyloid PNFs at the final concentration of ~10 mg/mL in PBS (pH 7.4), were treated with 20 mM TCEP bond breaker solution, purchased from Thermo scientific, for 30 min. TCEP treated fibrils were then collected by centrifuging the fibrils for 10 min at 12,500 rpm in an Eppendorf® Minispin® Plus benchtop centrifuge, with the fibrils then resuspended in 100 mM PBS (pH 7.4). This washing step was repeated thrice to ensure the removal of any residual TCEP.

7.6.5. Traut's reagent

Traut's solution was prepared by dissolving 2 mg/mL in PBS (pH 7.4), resulting in 14 mM stock solution. Amyloid fibrils (~10 mg/mL) were then treated using a 10 fold molar excess of Traut's solution added - 46 µL of the 14 mM stock solution to each mL of amyloid fibril solution and incubated for 1 h at room temperature. To separate thiolated amyloid PNFs from excess Traut's reagent, treated fibrils were then collected by centrifuging the fibrils for 10 min at 12,500 rpm in an Eppendorf® Minispin® Plus benchtop centrifuge (3X), and resuspended in 100 mM, PBS (pH 7.4). Sulfhydryl groups were then characterised using Ellman's assay (section 7.6.3).

7.7. Glycosylation of crystallins

7.7.1. Glycoprotein staining

Glycoprotein gels were run using the Molecular Probes Pro-Q Emerald 300 Glycoprotein Gel and Blot Stain Kit (Invitrogen). Details of all the solutions used for glycoprotein staining are detailed below **(Table 7.10)**. Proteins were first separated by standard SDS-PAGE (section 7.1.1). The gel was then fixed by immersing the gel in approximately 100 mL of fix solution, and incubating at room temperature with gentle agitation for 45 min. This step was repeated to ensure the SDS was fully washed out of the gel. The gel was incubated in approximately 100 mL of wash solution, with gentle agitation for 10-20 min. This step was also repeated. The carbohydrates were oxidised by incubating the gel in 25 mL of oxidising solution, with gentle agitation for 30 min. The gel was washed in approximately 100 mL of wash solution with gentle agitation for 10-20 min, and this step was carried out three times.

The gel was stained by incubating in the dark in 25 mL of Pro-Q Emerald 300 staining solution, while gently agitating for 90-120 min. The gel was washed by incubation for 15-20 min in 100

mL wash solution with gentle incubation. The stained gel was visualised using a 300 nm UV transilluminator, and gel images captured using a BioImaging System (Syngene).

Table 7.10. *Details of glycoprotein gel solutions:*

Reagents	Details
Pro-Q Emerald 300 Stock Solution	Pro-Q Emerald 300 reagent dissolved in 6 mL of N,N-Dimethylformamide (DMF)
Fix solution	50% methanol, 5% glacial acetic acid, and dH_2O
Wash solution	3% glacial acetic acid
Oxidising solution	2.5 g periodic acid, 250 mL 3% glacial acetic acid
Pro-Q Emerald 300 Staining Solution	Pro-Q Emerald 300 Stock Solution diluted 50-fold into Pro-Q Emerald 300 Staining Buffer,prepared fresh before each use.

7.7.2. Periodate oxidation of crude crystallin proteins

Periodate oxidation of crude crystallin proteins was done using sodium metaperiodate (Thermo Scientific), prepared in an oxidation buffer **(Table 7.11).** Different concentrations of sodium metaperiodate were investigated: 10 mM, 20 mM, 30 mM, 40 mM, and 50 mM. Reaction sample were incubated for 1 h at room temperature, in dark conditions. The extent of sodium metaperiodate oxidation was then assessed by running a glycoprotein staining gel (section 7.7.1).

Table 7.11. *Details of periodate oxidation reaction:*

Solutions	Details
Oxidation buffer	100 mM sodium acetate Sterile filter [pH 4.5]
Reaction solution	60 mM sodium meta-periodate dissolved in oxidation buffer, and diluted to obtain required concentration ~20 mg/mL crystallin protein in extraction buffer Both in 1:1 ration [pH 4.5]

7.7.3. Periodate oxidation of crystallin PNFs

Crystallin PNFs at the final concentration of ~10 mg/mL was incubated with 30 mM final concentration of sodium metaperiodate in oxidation buffer (**Table 7.11**), and pH re-adjusted to 4.5, for 2 h at room temperature, in dark conditions. Aliquots (500 µL) were taken every 30 min, for 3 h, followed by centrifugation. To remove any excess periodate, treated fibrils were washed, and then collected by centrifuging the PNFs for 10 min at 12,500 rpm in an Eppendorf® Minispin® Plus benchtop centrifuge, and resuspended in 100 mM PBS (pH 7.4).

This washing step was repeated thrice to ensure the removal of any residual periodate. The presence of carbonyl groups were then characterised using DNPH assay (section 7.8)

7.8. DNPH assay

Carbonyl group quantification of oxidised crystallin PNFs was done by using the methods of Mesquita *et al.* (2014) [11]. DNPH solution was prepared at the concentration of 10 mM in 50 mM phosphorous acid (H_3PO_3) buffer and vortexed until it is completely dissolved. For the assay, 400 µL of DNPH solution was added to 400 µL of oxidised crystallin amyloid fibrils and control samples, and incubated for 10 min at room temperature. To this, 200 µl of 6 M NaOH was added and samples incubated for another 10 min at room temperature. The absorbance of the sample was then read at 450 nm against a blank solution containing 100 mM PBS (pH 7.4) as a substitute for the crystallin amyloid PNFs. As hydrazone products formed by the reaction of DNPH with carbonyl groups are highly unstable in alkaline conditions, so incubation time after adding NaOH, was carefully monitored and readings were taken strictly after 10 min for each of the samples.

7.9. Crosslinking experiments

7.9.1. Physical adsorption

GOX was incubated with PNFs in the absence of any crosslinking reagent. Both reduced (TCEP treated, section 7.6.4), and non-reduced crystallin PNFs were studied for physical adsorption experiments.

7.9.1.1. Non-reduced crystallin PNFs

The crosslinking reaction involved ~10 mg/mL crystallin PNFs, and GOX in 100 mM PBS (pH 7.4), at a ratio of 1:1 (250 µL each). Different concentrations of GOX used for crosslinking reaction were: 0.5, 1, and 2 mg/mL. The samples were incubated either at 4 °C for 24 h, or 2 h at 26 °C, after which the samples were run on an SDS-PAGE to ensure that crosslinking had occurred (section 7.1.1).

7.9.1.2. Reduced crystallin PNFs

The reduced CPNFs obtained *via* TCEP reduction (section 7.6.4) were incubated with different concentrations of GOX for the crosslinking reaction as detailed in section 7.9.1.1.

7.9.2. Procedure for sulfydryl group-based crosslinking using Sulfo-SMCC

For Sulfo-SMCC based crosslinking, Sulfo-SMCC was purchased from Thermo Scientific, product number 22360. Method used for the crosslinking of GOX to crystallin amyloid PNFs were based on the protocol provided with the Sulfo-SMCC. Briefly, for GOX coupling to Sulfo-SMCC, ~2.5 mg/mL GOX dissolved in 100 mM PBS (pH 7.4), was treated with 10 molar excess of Sulfo-SMCC for 30 min at room temperature. To separate conjugated GOX-SMCC from unreacted Sulfo-SMCC in the solution, desalting column was used (section 7.9.2.1.). The

crystallin PNFs (~10 mg/mL) were then mixed by inversion with desalted GOX-SMCC in 1:1 ratio (100 µL each) and incubated for 24 h at 4 ºC. To investigate crosslinking, SDS-PAGE was done (section 7.1.1).

Functionalised amyloid PNFs were then collected by centrifuging the sample for 10 min at 12,500 rpm in a Eppendorf® Minispin® Plus benchtop centrifuge (3X), with the fibrils then resuspended in 100 mM PBS (pH 7.4), and stored at 4 °C for activity assay *(Appendix B, section B1.1)* and TEM analysis (7.1.3).

7.9.2.1. Desalting of crosslinked GOX-SMCC

When using the desalting column, the column was first equilibrated with 3 column volumes of the PBS (pH 7.4) before loading the sample. The GOX-SMCC sample was then eluted and fractions collected. For protein quantification, nanoDrop measurements were taken (section 7.1.4) and fractions containing the protein were then pooled.

7.9.3. Direct coupling reaction for functionalising oxidised crystallin PNFs

The crosslinking reaction involved ~10 mg/mL oxidised crystallin PNFs, and GOX in 100 mM PBS (pH 7.4), at a ratio of 1:1 (250 µL each). The sample was incubated for 1 h at 26 °C, after which the samples were run on SDS-PAGE to confirm that crosslinking had occurred (section 7.1.1). Attempts were made by varying the reaction conditions, including using other enzymes, such as β-gal. Details of the different reaction conditions used are summarised in **Table 7.12.**

Table 7.12. *Details of different conditions attempted for functionalising oxidised crystallin PNFs, where GOX - glucose oxidase, β-gal - β-galactosidase, O-CPNFs - oxidised crystallin fibrils:*

Methods	Conditions
Total reaction time	30 - 120 min, 6 h, 12 h, and 24 h reaction
Reaction temperature (°C)	26, 37, and 4
Total reaction time	2-6 h, overnight, or 24 h
O-CPNFs concentration (mg/mL)	10, 15, and 20
Enzyme concentration (mg/mL)	1, 2, 2.5 and 4; alternatively β-gal at ~2.9 was also used
pH of the reaction	100 mM sodium acetate, [pH 5.5] 100 mM sodium phosphate, [pH 7.2] 50 mM HEPES, [pH 8.0]

7.9.4. Reductive amination reaction

7.9.4.1. Using sodium borohdyride ($NaBH_4$) and Boric acid (H_3BO_3)

The method used for functionalising oxidised crystallin amyloid fibrils with GOX *via* reductive amination reaction using $NaBH_4$ and $H3BO_3$, was based on the methods of Cho and Kang (2005) [12]. The crosslinking reaction involved ~10 mg/mL oxidised-crystallin amyloid PNFs, 10 mM $NaBH_4$ and 0.6 mg/mL GOX in 100 mM PBS (pH 7.4), at a ratio of 1:1:1 (100 µL

each). Where H_3BO_3 activated $NaBH_4$ was used, 10 mM H_3BO_3 was mixed with 10 mM $NaBH_4$ (1 mL of each), in dH_2O, and left on bench for 15-20 min for activation.

The amyloid PNFs were first mixed by inversion with GOX, and pre-incubated for 15 min, after which the $NaBH_4$ and H_3BO_3 activated $NaBH_4$ was added and the sample mixed by inversion again. The sample was incubated for 1 h at 26 °C. The degree of crosslinking was then assessed by SDS-PAGE (Section 7.1.1). Alternatively, attempts were made by varying the reaction conditions **(Table 7.13).** Functionalised amyloid fibrils were then collected by centrifuging the sample for 10 min at 12,500 rpm in an Eppendorf® Minispin® Plus benchtop centrifuge (3X), with the fibrils then resuspended in 100 mM PBS (pH 7.4), and stored at 4 °C.

Table 7.13. *Details of different reaction conditions used for crosslinking via reductive amination:*

Conditions	Details
pH of the reaction	100 mM sodium phosphate, [pH 7.4] 100 mM HEPES, [pH 9.0]
Reaction temperature, and time	26, 37, and 4 °C Reaction time- 5 to 15 min Total reaction time- 30 min to 2 h
Concentration of PNFs, and $NaBH_4$ solution	5-20 mg/mL of PNFs; 5 mM-1mM of $NaBH_4$
Solvents	50% MeoH 50% EtOH 50% Tetrahydrofuran (THF)

7.9.4.2. Reductive amination reaction using sodium triacetoxyborohdyride (STAB)

Enzyme immobilisation using STAB was based on the methods of Abdel-Magid (1996) [13]. 1 M STAB was prepared in isopropanol. A starting concentration of ~10 mg/mL oxidised crystallin amyloid PNFs; with a starting concentration of ~2.2 mg/mL GOX. The oxidised crystallin amyloid PNFs were first mixed by inversion with enzyme (~2.2 mg/mL GOX, and ~2.9 mg/mL of β-gal), and pre-incubated for 10 min, after which the STAB was added, and mixed by inversion again. Total reaction volume was 300 µL, including 100 µL of each - crystallin PNFs, enzyme, and STAB. The reaction samples were incubated at 26 °C for 1 h, and a SDS-PAGE gel was done to confirm the crosslinking reaction (Section 7.1.1). Functionalised amyloid fibrils were then collected by centrifuging the sample for 10 min at 12,500 rpm in an Eppendorf® Minispin® Plus benchtop centrifuge (3X), with the fibrils then resuspended in 100 mM PBS (pH 7.4), and stored at 4 °C.

7.10. GA-activation of oxidised crystallin PNFs

Methods used for GA-activation of oxidised crystallin amyloids were based on the protocol established by Pilkington *et al.* (2010) [14]. The reaction involved ~10 mg/mL crystallin PNFs, 2.5 mM GA, in 100 mM PBS (pH 7.4), at a ratio of 1:1. The sample was incubated for 1 h at 26 °C. GA-activated PNFs were then collected by centrifuging the sample for 10 min at 12,500

rpm (3X), with the fibrils then resuspended in 100 mM PBS (pH 7.4), and used for crosslinking experiments.

7.11. Functionalising GA-activated oxidised crystallin amyloid PNFs

GOX was the first enzyme to be immobilised to the GA-activated oxidised crystallin PNFs. The immobilisation methods developed for GOX formed the basis of the immobilisation methods for all subsequent enzyme immobilisation. A two-step immobilisation protocol was implemented, where the amyloid fibrils were first mixed with the GA, followed by the addition of the enzyme [15]. In all of the immobilisation reactions, the components of the immobilisation reaction were added in equal parts. A typical immobilisation reaction contained 250 μL of each component.

7.11.1. GOX immobilisation to the GA-activated oxidised crystallin amyloid fibrils

GA-activated amyloid fibrils (~10 mg/mL) (section 7.10) were mixed with GOX (~2.2 mg/mL) and the reaction incubated at 26 °C for 1 h. To quench the reaction 100 mM Tris buffer (pH 8.0) was added to the immobilisation mixture. Samples were then run on a SDS-PAGE (Section 7.1.1), and analysed for activity using Amplex Red assay *(Appendix B, section B1.1).*

7.11.2. Method development for functionalising crystallin PNFs with other important industrial enzymes

To determine an appropriate concentration for crosslinking enzymes to the GA-activated CPNFs, OPA assay (section 7.6.1) was done on each of the enzyme sample, to ensure that the enzyme sample offers similar number of amine groups as offered by the GOX enzyme sample at the ~2.2 mg/mL concentration. Bradford assay was used (section 7.1.5) to determine the concentration of each enzyme. Enzyme at the selected concentration was added to the GA activated CPNFs (~10 mg/mL), and incubated for 30 min at room temperature. The extent of crosslinking was then assessed by using SDS-PAGE (7.1.1), and checked for their activity to assess the optimal concentration of enzyme for the crosslinking reaction without any significant loss in their activity as assessed by the activity assays *(see Appendix B, section B1.2 – B1.5)*.

For the crosslinking reaction, the GA-activated CPNFs (~10 mg/mL) and enzymes were mixed in 1:1 ratio, at the given concentration as determined by the Bradford assay: 2.5 mg/mL β-gal; 3.5 mg/mL pectinase; 4 mg/mL α-amylase; and 3.5 mg/mL laccase. The reaction samples were mixed by inversion, and incubated for 1 h at 26 °C. To quench the reaction 100 mM Tris buffer (pH 8.0) was added to the immobilisation mixture, followed by SDS-PAGE analysis, to assess the extent of crosslinking. Functionalised amyloid fibrils were then collected by centrifuging the sample for 10 min at 12,500 rpm in an Eppendorf® Minispin® Plus benchtop centrifuge (3X), with the fibrils then resuspended in 100 mM PBS (pH 7.4), and stored at 4 °C.

7.11.3. Co-immobilisation of GOX and β-gal

For co-immobilisation experiment, whey PNFs obtained as detailed in section 7.2.2 were centrifuged (for 10-15 min at 12,500 rpm in an Eppendorf® Minispin® Plus benchtop centrifuge (3X), collected, and resuspended in PBS (pH 7.4).

A starting concentration of ~10 mg/mL whey PNFs (100 µL), with a starting concentration of 7.5 mM GA (100 µL), and a starting concentration of ~2.2 mg/mL GOX (50 µL) and 4.2 mg/mL β-gal (50 µL) were mixed by inversion, and incubated for 1 h at 37 °C. The reaction was quenched with 100 µL of 100 mM Tris buffer (pH 8.0), followed by SDS-PAGE (section 7.1.1), and activity assay analysis (*Appendix B,* using Amplex Red assay (*section B1.1*) for GOX, and ONPG assay *(section B1.2)* for β-gal, respectively).

7.12. Thermostability experiment

Free α-amylase, crosslinked α-amylase, α-amylase with GA and control samples were incubated in temperature controlled dry bath heater (Labnet International Inc., Woodridge, NJ, USA). The temperatures used were 40 °C, 55 °C and 75 °C, and readings were taken at time 0, 3, 6, 9, 12 and 24 h. Samples were allowed to cool by keeping them on ice (5-10 min) before performing starch hydrolysis reaction [16]. The activity of free and immobilised α-amylase samples was determined using starch-iodine test *(Appendix B, section B1.4)* using initial reading for starch (un-hydrolysed starch) as the 100% value. Subsequent activity readings were measured as a % decrease in the initial starch reading, which corresponds to the amount of starch being hydrolysed by the α-amylase samples.

7.13. Reusability experiment

The storage stability of free and immobilised α-amylase at 4 °C was measured by calculating the residual activity over the time period of 30 days. Reusability of immobilised enzyme was also investigated by measuring its activity after repeated cycles of use. After each hydrolysis reaction, the functionalised fibrils were thoroughly washed in 100 mM sodium acetate buffer, pH 4.5 and stored at 4 °C, before being used for the next hydrolysis reaction. The relative activity (compared to initial amount of starch present) of both free and immobilised sample and the amount of reducing sugar produced was determined by using both the starch-iodine and the DNS assay *(Appendix B, section B1.3 and 1.4).*

7.14. Electrochemistry Studies

Electrochemistry studies were done on functional amyloid PNFs, including GOX-, β-gal-, and dual-functionalised amyloid PNFs. Electrochemical characterisation of functionalised PNFs was carried out on commercial screen-printed electrodes (C223AT) from DropSens (Oveido, Spain). 2 µL of functionalised amyloid fibril solution were deposited onto the electrode, and excess solvent removed by evaporation for one h at 37 °C or overnight at room temperature.

Cyclic Voltammetry (CV) was carried out in the presence of 1.5 mM FcOH in 100 mM PBS (pH 7.4) using a potentiostat from eDAQ Pty Ltd (Denistone East, Australia) with a Dropsens connector DRP-CAC to connect the screen-printed electrode to the potentiostat.

7.14.1. Electrochemical characterisation of GOX-functionalised crystallin amyloid PNFs

The catalytic activity of the electrode modified with GOX-functionalised crystallin PNFs (2 mg/mL) was quantified *via* cyclic voltammograms in the absence and presence of excess glucose (500 mM), using 1.5 mM FcOH in 100 mM PBS (pH 7.4) as a mediator in solution. Potential sweep rates were 100 mV/s, using an Au counter and Ag reference electrode. Control experiments were carried out on electrodes modified with GOX-only, which had been diluted in 100 mM PBS (pH 7.4) to have the same activity in solution as the GOX-functionalised crystallin PNFs used for the electrochemistry experiments.

7.14.2. Electrochemical characterisation of β-gal-functionalised crystallin amyloid PNFs

The catalytic activity of the electrode modified with β-gal-functionalised crystallin PNFs (2 mg/mL) was quantified *via* CV, in the absence and presence of excess lactose (500 mM), using 1.5 mM FcOH in 100 mM PBS (pH 7.4) and GOX (2 mg/mL) as a mediator, in solution. Potential sweep rates were 100 mV/s, using an Au counter and Ag reference electrode. Control experiments were carried out on electrodes modified with β-gal only, which had been diluted in 100 mM PBS (pH 7.4) to have the same activity in solution as the β-gal functionalised crystallin PNFs used for the electrochemistry experiments.

7.14.3. Electrochemical characterisation of dual-functionalised PNFs

The catalytic activity of the electrode modified with dual-functionalised whey PNFs (1 mg/mL) was quantified *via* cyclic voltammograms in the absence and presence of excess lactose (500 mM), using 1.5 mM FcOH in 100 mM PBS (pH 7.4) as a mediator in solution. Potential sweep rates were 100 mV/s, using an Au counter and Ag reference electrode. Controls experiments were carried out on electrodes modified with GOX+β-gal enzyme mixture, which had been diluted in 100 mM PBS (pH 7.4) to have the same activity in solution as the dual functionalised whey PNFs used for electrochemistry experiments. For lactose dependent study, different lactose concentrations were prepared by dissolving 20, 40, 60, 80, and 100 mM lactose in PBS (pH 7.4). Stock 20 mM lactose solution was diluted further in PBS (pH 7.4) to obtain 0 - 2.5 mM lactose solution.

7.15. Surface-assembly

5 mm diameter and micro beads (425-600 µm) borosilicate glass beads purchased from Sigma-Aldrich were used as a model surface for the surface-assembly of PNFs. The methods used were adapted from Raynes (2012). [2]

7.15.1. Glass bead surface activation

Glass beads were cleaned overnight in a Piranha solution of 70% H_2SO_4, 30% H_2O_2 followed by rinsing in dH_2O. For rinsing, glass beads were first immersed in dH_2O (500 mL) for 2-3 min, and dH_2O replaced with fresh dH_2O. This step was repeated up to 4-6 times.

7.15.2. APTS activation of glass beads

The beads after Piranha activation (section 7.15.1) were then treated with a 3% APTS solution in ethanol/water (95:5 v/v) for 1 h, immersed in 99.9% ethanol and cured at 110 °C for 1 h. The beads were allowed to cool followed by washing in 95% ethanol and left to dry.

7.15.3. Ninhdyrin assay for glass beads

The ninhydrin assay was carried out on bead samples after surface activation with APTS solution, using the protocol described in section 7.6.2. A control sample containing the 3 % APTS solution was also assayed and used for calibrating the readings. All samples were assayed in triplicate.

7.15.4. N, N'- disuccinimidyl carbonate (DSC) activation of glass beads

The APTS-activated beads (section 7.15.2) were allowed to cool and washed in 95% ethanol followed by treatment with 20 mM DSC in a 50 mM sodium bicarbonate ($NaHCO_3$) (pH 8.5) for 3 h. The beads were then rinsed with dH_2O and left to dry prior to use.

7.15.5. ThT assay on glass beads

Each bead was placed into a well of a 96 well plate and immersed with 200 μL of ThT working stain (section 7.1.2, **Table 7.2**). ThT fluorescence was measured using a BMG Labtech FLUOstar Optima plate reader with excitation/emission filters of 450 and 485 nm, respectively All samples had three replicates.

7.15.6. Glass bead template-directed whey amyloid fibril assembly

Surface-activated glass beads were immersed in whey fragment solution (pH 9.0) (10 mg/mL, 10-15 mL) at room temperature for 2 h. The beads were then rinsed twice with dH_2O before being immersed in incubation buffer (Milli-Q at pH 2.0) containing 10 mg/mL whey protein solution for 22 h at 80 °C (section 7.2.2). The beads were then rinsed thrice in dH_2O.

7.15.7. Glass bead template-directed crystallin amyloid fibril assembly

Surface-activated glass beads were immersed in crystallin fragment solution (pH 9.0) (10 mg/mL, 10-15 mL) at room temperature for 2 h. The beads were then rinsed twice with dH_2O before being immersed in incubation buffer containing ~10 mg/mL crystallin proteins for 24 h at 80 °C (section 7.2.3). The beads were then left at room temperature for at least 3 days before rinsing thrice in dH_2O.

7.15.8. Surface-assembly of PNFs with and without chemical derivatisation

To ensure full surface derivatisation was necessary for maximum surface-assembly of the PNFs, glass beads with and without surface activation/derivatisation were incubated with protein solutions, at different stages. Control beads samples used included:

1. *No treatment (beads without surface activation)* - Beads as purchased from Sigma-Aldrich.
2. *Piranha treated* - Bead samples obtained as detailed in section 7.15.1.
3. *APTS activated/treated* - Bead samples were incubated with a 3% APTS solution in ethanol/water (95:5 v/v) for 1 h, followed by washing with 95% ethanol. Bead samples were left at room temperature to dry.
4. *After curing* - Bead samples were immersed in 99.9% ethanol and cured at 110 °C for 1 h, followed by cooling and washing in 95% ethanol, and left to dry.
5. *DSC treatment* - Bead samples obtained as detailed in section 7.15.4.

All the bead samples (as discussed above) were either incubated with fragmented amyloid PNFs for template-directed growth (section 7.15.6 and 7.15.7) or were incubated with protein solutions – *while heating* (bead samples (10-15 beads) were added to ~10 mg/mL protein solution (30 mL) kept at 80 °C for fibrillation (see section 7.2.2 and 7.2.3 for whey and crystallin fibrillation respectively) or alternatively, bead samples were added to the protein solution *after heating* – when protein solutions were removed and kept at room temperature for 3-7 days.

7.16. Amyloid fibril fragmentation

7.16.1. Crystallin fibril fragmentation

Formed crystallin amyloid fibrils (section 7.2.3) were first centrifuged (12,500 rpm, 10 min) and then buffer exchanged into 50 mM HEPES (pH 9.0) buffer before being subjected to sonication for a 0-60 sec pulse, amplitude 20%, using a microtip. The fragments were verified using TEM (section 7.1.3).

7.16.2. Whey fibril fragmentation

Formed whey amyloid fibrils (section 7.2.2) were first centrifuged (12,500 rpm, 10 min) and then buffer exchanged into 50 mM HEPES (pH 9.0) for surface-assembly work, and in PBS (pH 7.4) for cytotoxicity studies before being subjected to sonication for a 0-40 sec pulse, amplitude 20%, using a microtip. The fragments were verified using TEM (section 7.1.3).

7.17. Confocal microscopy for glass beads

Beads were kept in clear wall glass bottom dishes (one bead sample for 5mm beads, and for microbeads, a tiny amount using spatula was removed and kept in the dish), and stained with (200 µL) of ThT working stain **(Table 7.2)**, and viewed using a Leica Microsystems TCS SP5 confocal microscope with a Leica HCX PL 10x lens. An excitation of 425 nm and emission detection of 485-495 nm was used. The gain was adjusted to suit the most fluorescent sample and kept the same for all subsequent samples. The obtained images were processed using the Leica LAS AF Lite 2.4.1 software. Micrographs were representative of 3 beads (5mm), 3 images were chosen as being an overall representation of the entire sample.

7.18. β-gal functionalisation of surface-assembled whey PNFs

7.18.1. Immobilising β-gal on surface-assembled whey PNFs

Glass beads with surface-assembled whey amyloid PNFs (section 7.12.2) were first immersed in a solution of 5 mM GA to activate the lysine residues and N-terminal residues of the amyloid fibrils before the addition of ~2.9 mg/mL β-gal for 2 h, at 37 °C. The beads were then rinsed 3 times in dH_2O and stored at 4 °C. The beads were assessed for β-gal activity using ONPG assay in the BMG Labtech FLUOstar Optima plate reader with absorbance measured at 412 nm *(Appendix B, section B1.2).*

7.18.2. Reusability studies of β-gal functionalised surface-assembled whey PNFs

Glass beads with surface-assembled whey amyloid PNFs and immobilised β-gal (section 7.18.1) were covered with 250 μL of ONPG solution (*Appendix B, section B1.2)*. The cleavage reaction was carried out for 30 min at 37 °C to allow cleavage of the ONPG. The supernatant (150 μL) was carefully removed and assessed for β-gal activity by measuring the absorbance of cleaved product at 412 nm. The beads where then washed 3-5 times in dH_2O, and re-used for the next hydrolysis reaction.

7.19. Silk blend films

7.19.1. Preparation of silk solution

Bombyx mori degummed silk fibres were kindly provided by David Kaplan, Department of Biomedical Engineering, Tufts University. Silk-fibroin solution was obtained by dissolving degummed silk fibroins in 9.3 M lithium bormide (LiBr) solution in 1:4 w/v ratio, at 60 °C for 4 h, using previously published procedures [17, 18]. The extracted solution as dialysed against distilled water using Slide-a-Lyser dialysis cassettes (Pierce MWCO 3,500) for 72 h to remove salt. The obtained solution was then centrifuged to remove the small amount of silk aggregates or un-dissolved fibroin (3000 rpm, 15 min) (2X), to obtain optically clear solution. The final concentration of the solution was then determined by pipetting 1 mL of the obtained solution onto the weighing boat, followed by drying, and weighing the remaining solid after drying. The final concentration of aqueous silk solution was usually ~7.5 wt%, and was then diluted to 4% with dH_2O, when required.

7.19.2. Preparation of protein solutions

For crystallin protein solution, crystallin proteins extract obtained as detailed in section 7.2.3 was freeze dried, and dissolved in dH_2O at ~40 mg/mL concentration, whenever required. For whey protein solution, WPI were dissolved at 40 mg/mL concentration in dH_2O. Solutions were either kept on ice or stored at 4 °C, and used with-in 3-4 h.

7.19.3. Preparation of PNF solutions

Both crystallin and whey PNFs obtained at 10 mg/mL concentration, as described in section 7.2 were centrifuged (12,500 rpm, 10 min), concentrated, and re-suspended in dH_2O to obtain ~40 mg/mL concentration.

7.19.4. Preparation of silk-protein and silk-PNF blend solutions

Silk, protein, and PNF solutions at 4% (wt/v) concentration was obtained as detailed above, and were mixed in different ratios as detailed in **Table 7.14**, to obtain silk blend solutions. After preparing silk blend solution, solution were mixed by inverting tubes, and kept for at least 1 h at 4 °C or on ice with frequent mixing by inversion, before casting films.

7.20. Film formation

To prepare silk-only, and silk blend films, a 75 µL of silk-only, silk-protein, and silk-PNF blend solutions, prepared in different ratios as detailed in **Table 7.14**, was cast onto 14 mm diameter PDMS disc and allowed to sit at room temperature overnight. For film formation in 24-well TCP, 150 µL of each of the sample was added, and allowed to dry overnight at room temperature.

Table 7.14. *Lists different film samples, and ratios of blend films studied.*

Blends	Ratio
S1. *Silk*	Silk only
S2. *Silk:crystallin proteins*	50:50
S3. *Silk:whey proteins*	50:50
S4. *Silk:CPNFs*	25:75
S5*. Silk:CPNFs*	50:50
S6*. Silk:CPNFs*	75:25
S7*. Silk:WPNFs*	25:75
S8*. Silk:WPNFs*	50:50
S9*. Silk:WPNFs*	75:25

7.20.1. Ethanol annealing of films

The films with PDMS were then transferred into 24 well plate, and immersed in 75% ethanol for 6-12 h for ethanol annealing. It has been shown previously that ethanol annealing increases the β-sheet content of the silk films, and thus makes them water insoluble. For films formed in 24-well plate, 150 µL of 75% ethanol was added to the wells, and left for 6-12 h. Films were removed from the ethanol or ethanol allowed to evaporate and allowed to air dry on bench for 12 h.

7.21. Scanning electron microscopy (SEM)

Surface morphology was examined with FEI (Philips) XL30 scanning electron microscope at 5 KV acceleration voltage, after sputter-coated with platinum.

7.22. Proteolytic degradation of films

7.22.1. Preparation of enzymes

Protease Type XIV from *Streptomyces greiseus***,** collagenase from *Clostridium histolyticum*, and *α*-chymotrypsin from bovine pancreas were all purchased from Sigma-Aldrich. Enzymatic solutions of protease type XIV, chymotrypsin, and collagenase were freshly prepared by dissolving the enzyme powder in PBS (pH 7.4). For each enzyme, 2 mg/mL stock solution was prepared in 100 mM PBS (pH 7.4), and diluted to 0.5 mg/mL final concentration, whenever required using PBS (pH 7.4).

To check if there is any loss in the enzymatic activity of enzymes, at 37 °C, over the time period of 7 days, enzyme solutions prepared as above (1 mg/mL in PBS, pH 7.4) were kept at 37 °C. Samples (50 µL) were taken once every day for 7 days, and incubated with BSA solution, prepared at 5 mg/mL concentration in PBS (1:5) (v/v), pH 7.4 for 1 h, at 37 °C. After incubation, samples were rapidly frozen using liquid nitrogen, and kept at -20 °C, until the reaction was complete (7 days), followed by SDS-PAGE analysis (section 7.1.1).

7.22.2. Degradation of silk blend films

Silk-only and silk-blend films were removed from PDMS discs and immersed in 250 µL PBS (pH 7.4), or enzyme solution (section 7.22.1) and incubated at 37 °C. Once every 24 h for up to 5 days, samples were centrifuged and supernatant removed and replaced with fresh enzyme solution. After removal, supernatant was either directly run on SDS-PAGE (section 7.1.1) or heated to 100 °C for 10 min to denature the enzyme and stored at -80 °C for further analysis.

7.22.3. Mass loss

At each time point one set of films were removed and centrifuged (12,500 rpm, 10 min) to collect the supernatant. Blend films after removal of the supernatant were then dried at 37 °C overnight. Samples were weighed and percentage weight loss was calculated by comparing each blend film to the control (weight of the films incubated with PBS).

7.23. Optical transmittance

In-line transmittance spectra of the silk and blend solutions, films, and as aqueous dispersions in the visible region (400–800 nm) were obtained with a Perkin-Elmer Lambda 19 UV-Vis-NIR spectrophotometer using 24-well glass plates. For solution, 150 µL of solution of each of the samples was added to 24-well plate. For films, 150 µL of solution was added to 24-well plate and allowed to dry overnight, to obtain films.

For annealing, 150 µL of 75% ethanol was added to dried films and incubated for 6-12 h, followed by 1 h drying and spectral analysis (section 7.20.1). For the aqueous dispersion, 150 µL of 100 mM PBS (pH 7.4) was added to each of the sample and incubated for 1 h, followed by spectra measurements in the presence of PBS.

7.24. Contact angle measurements

Static contact angle measurements were done on dry films (n = 3) that were either treated with 75% ethanol, annealed or untreated (control films) at ambient temperature using a contact angle meter (CAM-100). Ultrapure water droplets were used with a drop volume of approximately 20 µL.

7.25. Biocompatibility of silk blend films

For cell culture studies, 150 µL of silk-only, and silk-blend solutions were added into the 24-well TCP, and allowed to dry overnight to obtain films. After drying, 150 µL of 75% ethanol was added to each well to anneal the obtained films and also to surface sterilise the films. Films were left immersed in ethanol for 1 h, followed by 1 h drying within the fume hood.

7.25.1. Cell culture

Mouse fibroblasts (NIH/3T3 ATCC) was cultured in media (DMEM), supplemented with 10% FBS, and 1% Anti-Anti (Antimyocin-Antibiotic, GIBCO) solution, at 37 °C with 5% CO_2/air atmosphere to 80% confluence. Cells were harvested by trypsinisation (5 mL Tryple Express, Invitrogen) and then washed by a twice repeated cycle of dilution in 15 mL media followed by centrifugation (300g for 5-10 min). Processed cells were counted using cell counter, and re-suspended in media, and then added to samples (200 µL, 25,000 cells/cm^2 of well area) and incubated at 37 °C with 5% CO_2/air atmosphere.

7.25.2. Cell imaging and data analysis

At each time point, cells were imaged using optical or light microscope (Nikon EclipseTE2000-U) 10x, and images were analysed using the particle analysis function in the software ImageJ. Before the particle analysis, the images were converted to 8 bit black and white images, and threshold adjusted. The results obtained by the software were compared to images counted by hand and were within 7% accuracy. To account for variations of cell attachment within each experiment, 3 individual samples were prepared.

To account for batch to batch variations, the experiment was repeated 3 times on different days. Cell area was quantified from the same images used for cell number using the line, and wand (tracing) tool and measure function in ImageJ. For statistical analysis, GraphPad tool was used to perform one-tailed, un-paired T-test analysis using mean, SEM, and N data entry format, where mean is average value taken from 5 samples, SEM represents standard error of the mean, and N = 5.

7.26. References

[1] M. Biancalana, S. Koide, Molecular mechanism of Thioflavin-T binding to amyloid fibrils, *Biochimica et Biophysica Acta (BBA)-Proteins and Proteomics*, 1804 (2010) 1405-1412.

[2] J.K. Raynes, *Immobilising biomolecules on amyloid fibrils for biotechnology applications*, PhD Thesis, University of Canterbury, (2012).

[3] H. LeVine 3rd, Thioflavin T interaction with synthetic Alzheimer's disease beta-amyloid peptides: Detection of amyloid aggregation in solution, *Protein science: A publication of the Protein Society*, 2 (1993) 404.

[4] E. Gasteiger, A. Gattiker, C. Hoogland, I. Ivanyi, R.D. Appel, A. Bairoch, ExPASy: The proteomics server for in-depth protein knowledge and analysis, *Nucleic Acids Research*, 31 (2003) 3784-3788.

[5] M.M. Bradford, A rapid and sensitive method for the quantitation of microgram quantities of protein utilising the principle of protein-dye binding, *Analytical Biochemistry*, 72 (1976) 248-254.

[6] L. Nielsen, R. Khurana, A. Coats, S. Frokjaer, J. Brange, S. Vyas, V.N. Uversky, A.L. Fink, Effect of environmental factors on the kinetics of insulin fibril formation: Elucidation of the molecular mechanism, *Biochemistry*, 40 (2001) 6036-6046.

[7] S.M. Loveday, J. Su, M.A. Rao, S.G. Anema, H. Singh, Whey protein nanofibrils: The environment–morphology–functionality relationship in lyophilisation, rehydration, and seeding, *Journal of Agricultural and Food Chemistry*, 60 (2012) 5229-5236.

[8] M. Roth, Fluorescence reaction for amino acids, *Analytical Chemistry*, 43 (1971) 880-882.

[9] M. Freidman, J. Pang, G. Smith, Ninhydrin-reactive lysine in food proteins, *Journal of Food Science*, 49 (1984) 10-13.

[10] P.W. Riddles, R.L. Blakeley, B. Zerner, Reassessment of Ellman's reagent, *Methods in Enzymology*, 91 (1983) 49-60.

[11] C.S. Mesquita, R. Oliveira, F. Bento, D. Geraldo, J.V. Rodrigues, J.C. Marcos, Simplified 2, 4-dinitrophenylhydrazine spectrophotometric assay for quantification of carbonyls in oxidised proteins, *Analytical Biochemistry*, 458 (2014) 69-71.

[12] B.T. Cho, S.K. Kang, Direct and indirect reductive amination of aldehydes and ketones with solid acid-activated sodium borohydride under solvent-free conditions, *Tetrahedron*, 61 (2005) 5725-5734.

[13] A.F. Abdel-Magid, K.G. Carson, B.D. Harris, C.A. Maryanoff, R.D. Shah, Reductive amination of aldehydes and ketones with sodium triacetoxyborohydride. Studies on direct and indirect reductive amination procedures, *The Journal of Organic Chemistry*, 61 (1996) 3849-3862.

[14] S.M. Pilkington, S.J. Roberts, S.J. Meade, J.A. Gerrard, Amyloid fibrils as a nanoscaffold for enzyme immobilisation, *Biotechnology Progress*, 26 (2010) 93-100.

[15] G.T. Hermanson, *Bioconjugate techniques*, Academic press (2013).

[16] Z. Xiao, R. Storms, A. Tsang, A quantitative starch–iodine method for measuring alpha-amylase and glucoamylase activities, *Analytical Biochemistry*, 351 (2006) 146-148.

[17] D.N. Rockwood, R.C. Preda, T. Yücel, X. Wang, M.L. Lovett, D.L. Kaplan, Materials fabrication from *Bombyx mori* silk fibroin, *Nature Protocols*, 6 (2011) 1612-1631.

[18] U.-J. Kim, J. Park, H.J. Kim, M. Wada, D.L. Kaplan, Three-dimensional aqueous-derived biomaterial scaffolds from silk fibroin, *Biomaterials*, 26 (2005) 2775-2785.

Appendix A

IR absorbance spectrum of crystallin PNFs

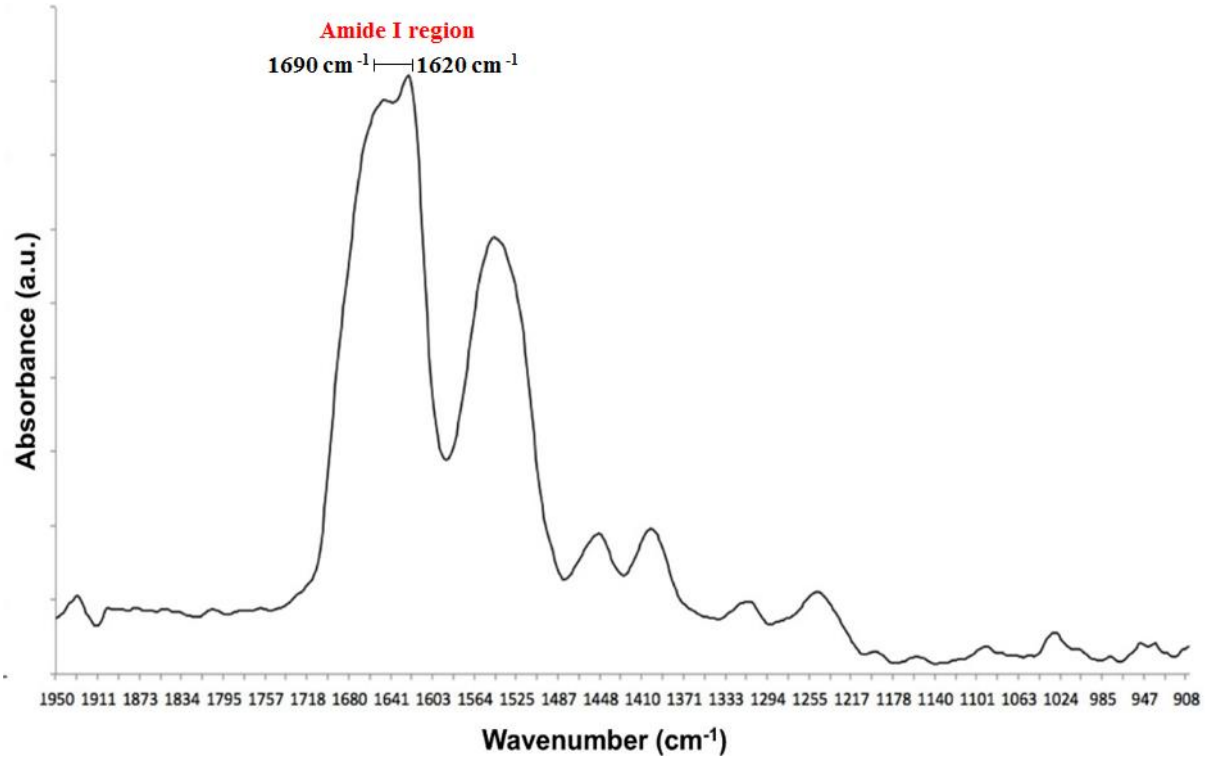

Figure A1. *Typical IR absorbance spectrum of amyloid crystallin nanofibrils, across the whole amide fingerprint region, showing the baseline.*

Appendix B

Enzyme-specific activity assays

To determine enzymatic activity of functionalised PNFs, crosslinked samples were assayed for activity using the spectrophotometric assays, with a BioRad SmartSpec Plus Spectrophotometer. Three replicates of each sample were measured, each data point is representative of averages from triplicate samples, with subtracted blank values for each of the assay. Samples were assayed for initial activity, centrifuged, and the supernatant was retested for activity to assess the amount of activity retained by the enzyme that had been crosslinked to the PNFs. Functionalised amyloid fibrils obtained after crosslinking reactions were collected by centrifuging the sample for 10 min at 12,500 rpm in an Eppendorf® Minispin® Plus benchtop centrifuge, with the fibrils then resuspended in 100 mM phosphate buffer (pH 7.4), and stored at 4 °C.

B1.1 Amplex Red assay

For GOX activity determination, Amplex Red assay (Thermo Fisher Scientific) was used to detect hydrogen peroxide produced by GOX, in the presence of glucose, by using the methods adapted from Raynes (2012) [1]. Samples containing GOX were incubated with Amplex Red assay reagent **(Table B1.1)** for 30 min in dark conditions, and absorbance of the sample was then measured spectrophotometrically at a wavelength of 590 nm. Background fluorescence, as determined for a control sample with no GOX present, was subtracted from each value.

Table B1.1. *Amplex Red assay reagent*

Reagent	Components
Amplex Red assay solution	50 mM Amplex Red reagent
Amplex Red assay buffer	0.1 U/mL horseradish peroxidise 50 M glucose 0.1 M sodium phosphate buffer [pH 7.4]

B1.2. *o*-Nitrophenyl-β-D-galactopyranoside (ONPG) assay for β-gal activity

For β-gal activity determination, ONPG assay (Sigma-Aldrich, MO, catalog no. KI455-01) was used. β-gal catalyse the hydrolysis of β-galactosides (ONPG) to the ONP anion producing a bright yellow colour with a peak absorbance at 420 nm that can be quantified using a spectrophotometer [2]. Samples containing β-gal (50 µl) were incubated with ONPG assay reagent **(Table B1.2)** for 30 min in dark conditions, at 37 °C. The reaction was then quenched by adding stop buffer **(Table B1.2)**, followed by absorbance measurement at a wavelength of 420 nm. Background fluorescence, as determined for a control sample (no β-gal present), was subtracted from each value.

Table B1.2. *ONPG assay reagent*

Reagent	Components
ONPG assay solution	17 µl ONPG reagent 1 µl β-mercaptoethanol
Stop buffer	125 µl stop buffer Final volume 192 µl

B1.3. 2, 4-Dinitrosalicyclic acid (DNS) assay

To determine the activity of pectinase functionalised PNFs, 500 uL of pectin solution prepared in sodium acetate buffer (pH 4.5) was added to 250 uL of pectinase control and pectinase functionalised PNFs, followed by 30 min incubation at 50 °C [3]. To measure the amount of reducing sugars produced by the pectinase or functionalised pectinase PNFs, DNS solution **(Table B1.3)** was added in 1:1 ratio to the sample (300 µL each) and heated at 100°C for 5 min, followed by cooling at room temperature. The absorbance of the cooled sample was then read spectrophotometrically at a wavelength of 575 nm. Background fluorescence, as determined for a control sample without pectinase, was subtracted from each value.

Table B1.3. *DNS assay reagent*

Reagent	Components
Pectin solution	1 mg/mL in 100 mM sodium acetate buffer [pH 4.5]
DNS solution	1 g DNS 0.05 g sodium sulphite 1 g sodium borohydride Dissolved in 100 mL of Milli-Q, stored in dark at 4 °C.

B1.4. Amylase activity assay

For α-amylase activity, DNS assay as detailed in section B1.3 was used to measure the amount of reducing sugars produced, using starch as a substrate. Additionally, the extent of starch hydrolysis was measured by starch-iodine (KI) assay using the methods adapted from Xiao *et al.* (2006)[4]. Assay reaction was initiated by incubating 100 uL of starch solution with 100 uL of amylase control and amylase functionalised PNFs sample, incubated at 50 °C for 30 min. To stop the reaction 20 uL of 1 M HCl was added, followed by the addition of 100 uL of KI solution **(Table B1.4)**. Following colour development, 200 uL of the reaction sample was transferred to 96 well plate and absorbance of the sample was then read spectrophotometrically at a wavelength of 580 nm.

Table B1.4. *KI assay reagent*

Reagent	Components
Starch solution	1 g/L starch dissolved in boiling water, stirred until dissolved completely. Stored at 4 °C (2-3 days)
KI solution	5 mM I_2, 5 mM KI reagent in dH_2O, stored in glass bottle at room temperature.

B1.5. Laccase activity assay

The activity of laccase functionalised PNFs was assayed spectrophotometrically by monitoring the absorbance increase at 530 nm due to the oxidation of syringaldazine (Sigma) in the presence of laccase [5]. The assay mixture consisted of 30 µl of syringaldazine (0.216 mM in absolute methanol), 50 µL mL of laccase enzyme or laccase functionalised crystallin PNFs sample (PNFs were centrifuged and resuspended in PBS (pH 6.5), using 1M KOH), and 100 µL of 100 mM PBS (pH 6.5). Both buffer (PBS) and laccase sample were added first and readings were equilibrated at 37 °C, followed by initiation of the reaction by adding syringaldazine solution. The increase in absorbance at 530 nm was measured spectrophotometrically for each sample for 15 min.

B1.6. References

[1] J.K. Raynes, *Immobilising biomolecules on amyloid fibrils for biotechnology applications*, PhD Thesis, University of Canterbury, (2012).

[2] S.T. Smale, *β-Galactosidase Assay*, Cold Spring Harbor Protocols, (2010) pdb. prot5423.

[3] A.V. Gusakov, E.G. Kondratyeva, A.P. Sinitsyn, Comparison of two methods for assaying reducing sugars in the determination of carbohydrase activities, *International Journal of Analytical Chemistry*, (2011).

[4] Z. Xiao, R. Storms, A. Tsang, A quantitative starch-iodine method for measuring alpha-amylase and glucoamylase activities, *Analytical Biochemistry*, 351 (2006) 146-148.

[5] J. Ride, The effect of induced lignification on the resistance of wheat cell walls to fungal degradation, *Physiological Plant Pathology*, 16 (1980) 187-196.

Appendix C

GA-based crosslinking of GOX to crystallin PNFs

The method for GOX immobilisation to crystallin fibrils was based on the methods of (Pilkington *et al.* 2010), who showed that GOX can be covalently immobilised to insulin amyloid fibrils using GA [1]. The GOX (2 mg/mL) immobilised samples were crosslinked using a final concentration of 50 mM GA, with a final concentration of 3.3 mg/mL crystallin amyloid fibrils for 1 h at 25 °C .The extent of crosslinking was then assessed by SDS-PAGE. Native GOX runs as a monomeric protein band at 80 kDa in a SDS-PAGE gel, due to the dimer being denatured by SDS.

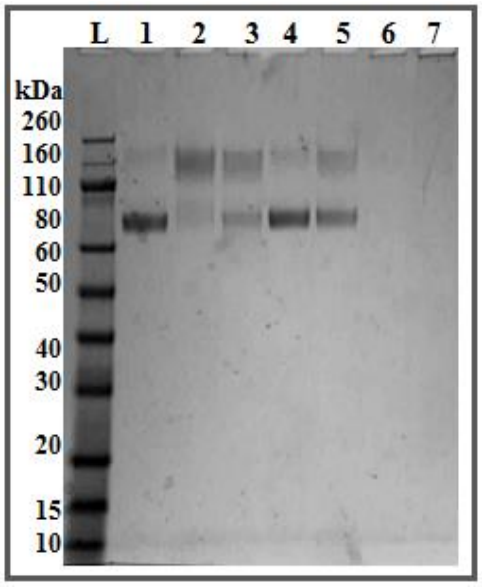

Figure C1. *SDS-PAGE of GA-based crosslinking of GOX onto the crystallin PNFs. L- ladder, Lane 1- GOX only, Lane 2- GOX+GA, Lane 3-5 GOX+GA+CPNFs, different reaction orders, Lane 6- CPNFs only, and Lane 7- CPNFs+GA.*

In **Figure C1,** the monomeric GOX band at approximately 80 kDa is seen in Lane 1. There is also a slight band at approximately 160 kDa, corresponding to the molecular weight of dimer GOX, indicating that the dimer was not completely denatured. Crosslinking GOX alone using GA produces a weak band at 80 kDa, and a strong band at 160 kDa, which corresponds to the stabilisation of the dimer by crosslinking (Lane 2). When GOX was immobilised to crystallin fibrils using GA (Lane 3-GA, CPNFs, and GOX were all added simultaneously) there is no decrease in the intensity of the GOX band on the gel, which indicates that no GOX was immobilised to the crystallin fibrils. When GOX is incubated with GA-activated crystallin fibrils (GA-activated CPNFs were collected by centrifugation, after 1 h incubation with GA) the same bands appear as for GOX only (Lane 4). Similar to Lane 3, no GOX was immobilised to the crystallin fibrils in lane 5, where GOX and GA were incubated first (5 min), and then fibrils were added in order to maintaining the maximum possible surface area for immobilisation of GOX by minimising fibril-fibril crosslinking.

Crude crystallin fibrils show no band, as they remain in the well (Lane 6-with GA and Lane 7-without GA). This gel confirms that no crosslinking of GOX to the crystallin amyloid fibrils was occurring. As the established method did not result in successful immobilisation of GOX to crystallin fibrils, thus, research to achieve immobilisation *via* amino groups to crystallin amyloid fibrils was discontinued, and different methods were employed for immobilising biomolecules to the crystallin amyloid fibrils.

References

[1] S.M. Pilkington, S.J. Roberts, S.J. Meade, J.A. Gerrard, Amyloid fibrils as a nanoscaffold for enzyme immobilisation, *Biotechnology Progress*, 26 (2010) 93-100.

Appendix D

Standard graphs for assays

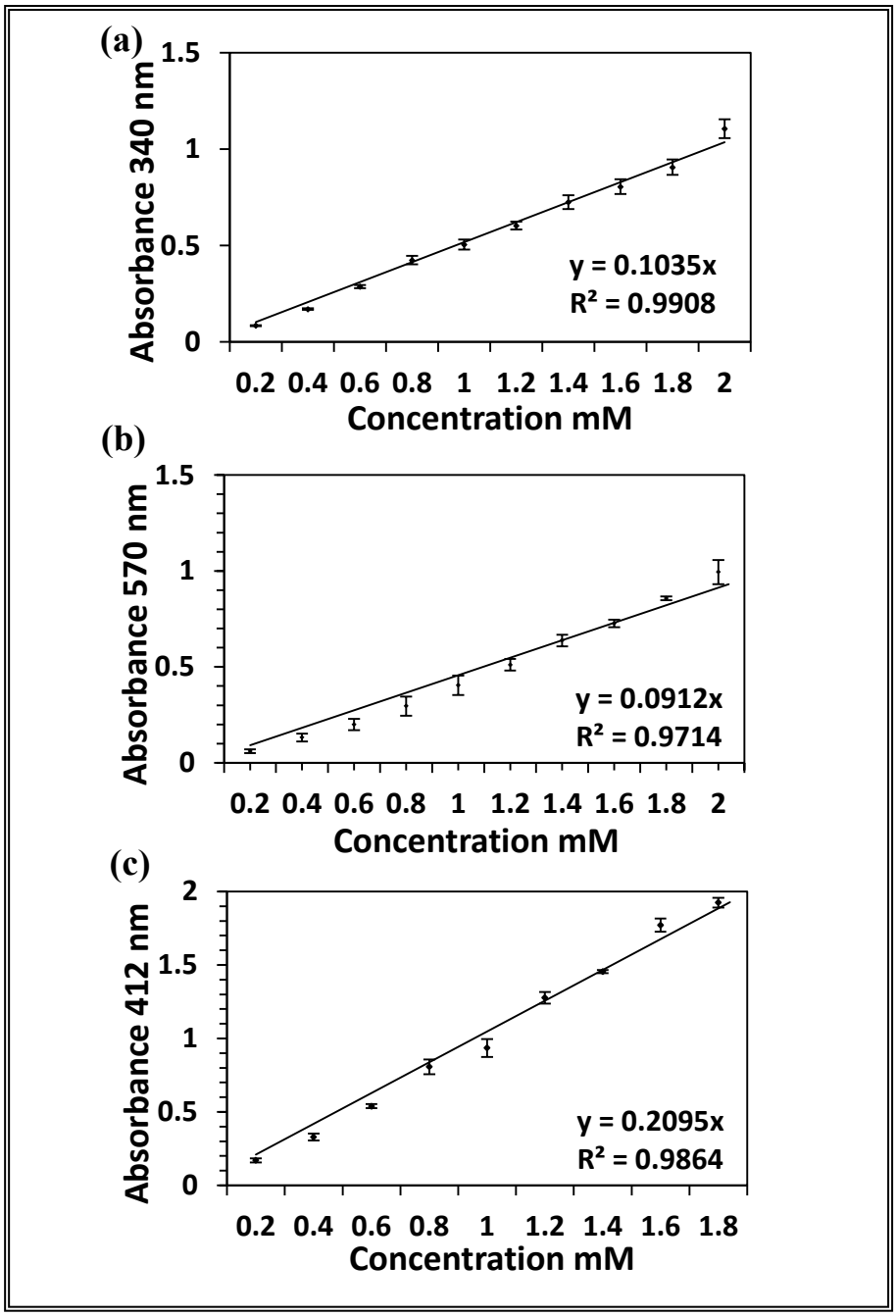

Figure D1. (a) *OPA standard curve for lysine concentrations ranging from 0.2-2.0 mM, absorbance taken at 340 nm.* ***(b)*** *Ninhydrin standard curve for lysine concentrations ranging from 0.2-2.0 mM, absorbance taken at 570 nm.* ***(c)*** *Ellman's standard curve for cysteine concentrations ranging from 0.2-2.0 mM, absorbance taken at 412 nm. Error bars represent the standard deviation of the mean of three replicates.*

Appendix E

α-Amylase activity assay

Both starch-iodide (KI) and DNS assay were done to assess the amount of starch being hydrolysed into sugars by α-amylase immobilised CPNFs. The relative activity (compared to initial amount of starch present) of both free and immobilised sample as determined by the KI assay, and the amount of reducing sugar produced as determined by the DNS assay **(Figure E1)** showed good co-relation, suggesting that immobilised enzyme effectively hydrolysis starch ~ 70 to 80% as compared to 80 to 90% for free amylase.

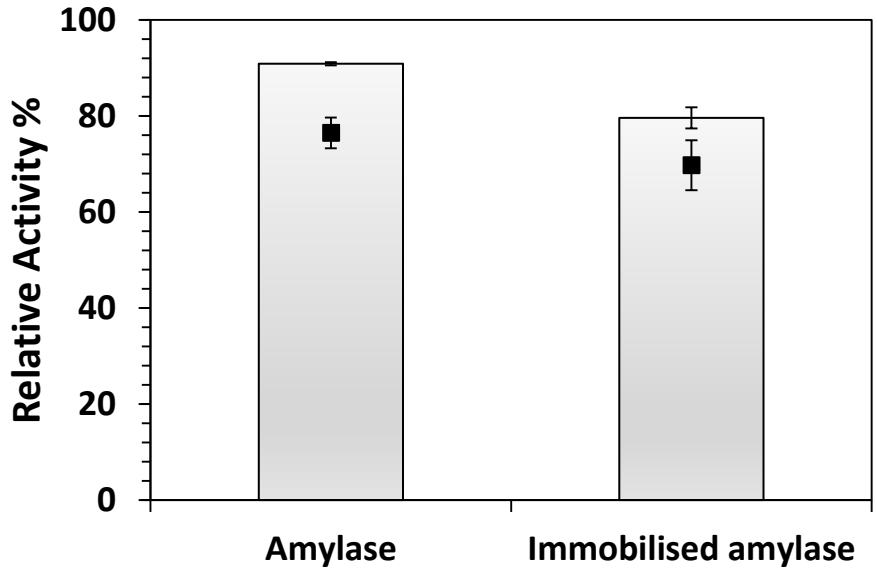

Figure E1. *Activity assay for α-amylase functionalised crystallin PNFs, where grey bars - amount of starch hydrolysed, characterised by KI assay, absorbance measured at 620 nm, and black bars - amount of reducing sugars produced as detected by the DNS assay, absorbance measured at 540 nm. Error bars represent the standard deviation of the mean of three replicates.*

Appendix F

Silk-PNF blend films

Table F1. *Number of cleavage sites for crystallins and whey proteins determined from the available sequence information. The percentage values were calculated from the number of cleavages and the total residue number.*

Proteins	**αA**	**αB**	**βB_2**	**βB_3**	**γB**	**γM_7**	**β-lg**
Representative protein	Zebrafish AlphaA crystallin	Human AlphaB crystallin	Human $BetaB_2$ crystallin	Human $BetaB_3$ crystallin	Bovine GammaB crystallin	Zebrafish $GammaM_7$ crystallin	Bovine Beta lactoglobulin
UniProt file	P02470	P02511	P43320	P26998	P02526	Q5XTN3	P02754
Total residues	173	175	205	211	175	174	178
No. of cleavages	**αA**	**αB**	**βB_2**	**βB_3**	**γB**	**γM7**	**β-lg**
Protease type XIV	48	51	54	60	55	56	31
Chymotrypsin	61	53	51	58	53	46	56
Collagenase	2	2	2	1	-	-	-
% of cleavage	**αA**	**αB**	**βB_2**	**βB_3**	**γB**	**γM7**	**β-lg**
Protease type XIV	27%	29%	26%	28%	31%	32%	17.4%
Chymotrypsin	35%	30%	25%	27%	30%	26%	31%
Collagenase	1%	1%	1%	0.4%	-	-	-

Note*: Where possible, the sequence used was that from Danio rerio (zebrafish), as this is the only fish for which full crystallin sequence information is available. If no structure or sequence information from D. rerio was available, the sequence used was that of the UniProt files available, that had the highest sequence similarity to D. rerio. Previously Domigan (2012), studied various sequence allignments for crystallins and showed that the chosen structures had highest sequence similarity to D.rerio.*

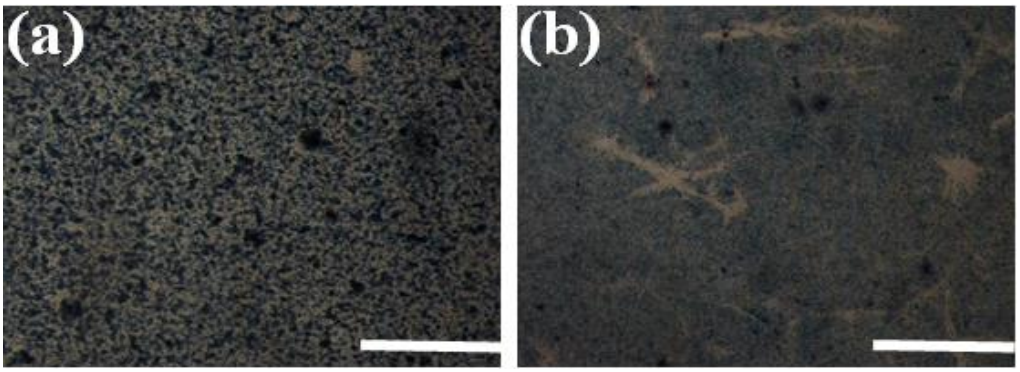

Figure F1. *Images of silk blend films after MTT staining, where (a) silk-only (50:50), and (b) silk:crystallin (50:50) blend films. Scale bar- 100 μm.*

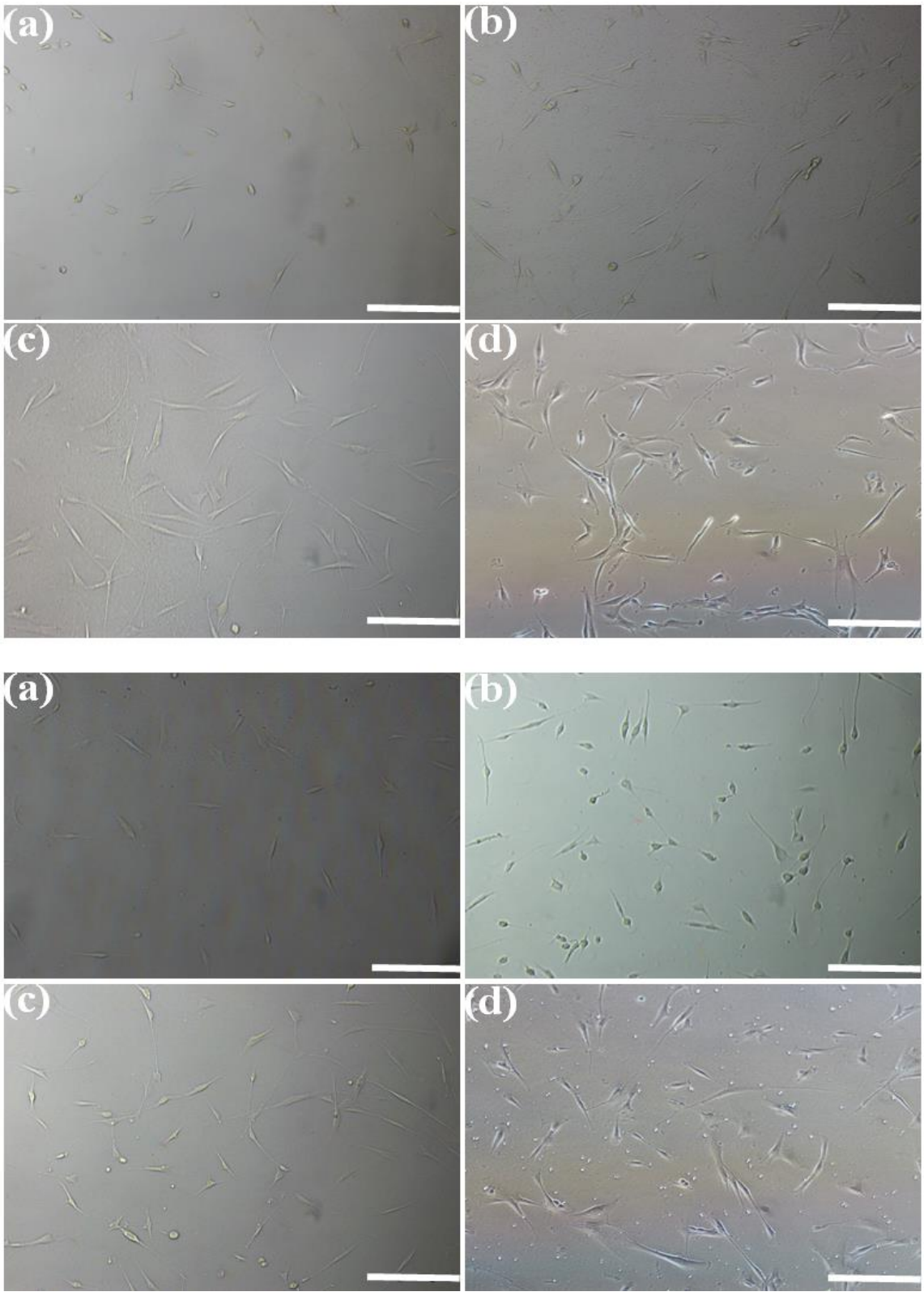

Figure F2. *Images of mouse fibroblast cells cultured for silk:PNF films at different ratios, silk:PNF (75:25) - left panel, and silk:PNF (25:75) - right panel, where top panel - crystallin PNFs and bottom panel - whey PNFs, after 18 h - sample a and b, and after 48 h - sample c and d. Scale bar - 100 µm.*

Appendix G

Crystallin fibrillation process

Fish eye lenses extracted from Hoki (Macruronus novaezelandiae) were obtained from the local fish suppliers, Christchurch, New Zealand. The method established by Kang (2011) as detailed below was then used to obtain high quality crystallin PNFs. The process can be divided into four main steps: **Step 1**: the protein extraction process, **Step 2**: preparation of 10 mg/mL final concentration of crystallin protein homogenate with 25% n-propanol. **Step 3**: heating and centrifugation to remove amorphous aggregate to obtain high quality PNFs, **Step 4**: the self-assembly process at room temperature. Previous work by Kang (2011), has demonstrated that three different PNFs products, based on their quality can be obtained via this PNF self-assembly process: low, medium, and high quality **(Figure G1 and G2)**. The quality of PNFs obtained depends on the presence or absence (removed by centrifugation after incubation for an h) of amorphous aggregates formed during heating.

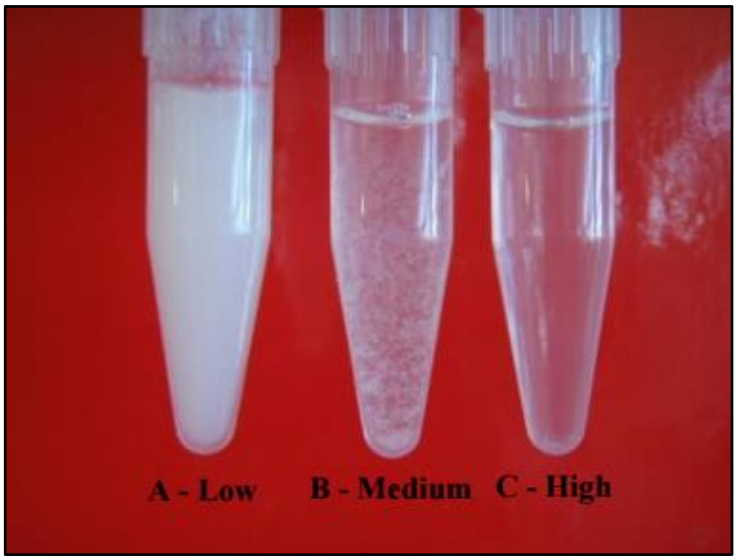

Figure G1. *Three different qualities of the final product contain protein nanofibres. Taken from Kang (2011).*

As the main focus of this work was utilisation of PNFs, therefore it was decided to remove amorphous aggregate formed after 1 h of incubation to obtain high quality PNFs. Briefly, 50 mM Tris base, 5 mM EDTA, 1 mM DTT at a pH 7.5 was prepared and added to the extracted fish eye lenses in the ratio of 2 mL per one gram of fish lens. The lenses were homogenised in the buffer using an IKA ULTRA TURRAX Tube Dispersar set at maximum speed 9 for 20 minutes at room temperature.

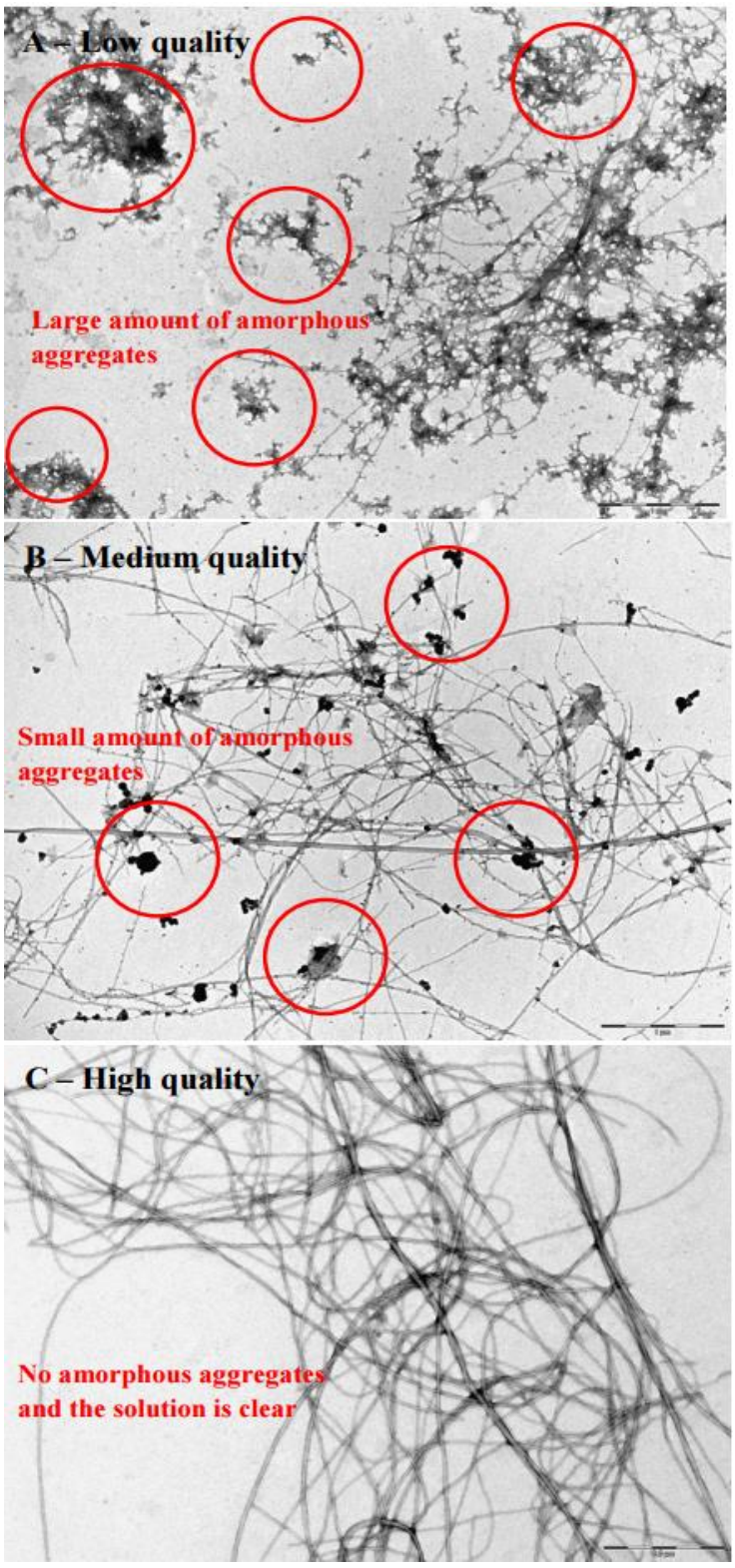

Figure F2. *TEM images showing different types of PNFs obtained, based on their quality. Taken from Kang (2011).*

After the protein extraction step, obtained crude crystalline homogenate was transferred into centrifuge tubes and spun at 12,000 rpm for 30 minutes. The supernatant was then collected into a new tube and diluted 1:100 with extraction buffer and the protein concentration was determined using the NanoDrop (section 7.1.4). For PNF synthesis, the crude crystallin homogenate obtained was further diluted using 25% n-propanol at pH 3.5 to obtain the required final concentration (10 mg/mL). The crystallin protein mixture at 10 mg/mL final concentration was then incubated at 80 °C for an h on a heating block. After 1 h incubation, the sample was removed from the heating block and centrifuged at at 12,000 rpm for 2 min at room temperature to remove the amorphous aggregates formed during heating. The supernatant was collected and incubated at 80 °C on a heating block for 24 h.

After 24 h incubation, sample was then removed from the heating block and left at room temperature for the self-assembly process. The amyloid fibril samples were then analysed for quality and consistency using ThT (section 7.1.2), TEM (section 7.1.3), and Bradford assay (7.1.5).

References

[1] K.Y. Wong, *Scaling up the production of protein nanofibres*, Master's Thesis, University of Canterbury, (2011).